The Pennsylvania State University

The Graduate School

College of Engineering

AN ASSESSMENT OF PHOTOSYNTHETIC BIOFUELS AND ELECTROFUELS TECHNOLOGIES UNDER RATE-LIMITED CONDITIONS

A Thesis in

Chemical Engineering

by

Amalie Tuerk

Submitted in Partial Fulfillment
of the Requirements
for the Degree of

Master of Science

December 2011

The thesis of Amalie Tuerk was reviewed and approved* by the following:

Wayne R. Curtis
Professor of Chemical Engineering
Thesis Advisor

Robert Rioux
Assistant Professor of Chemical Engineering

Andrew Zydney
Professor of Chemical Engineering
Head of the Department of Chemical Engineering

*Signatures are on file in the Graduate School

ABSTRACT

This thesis investigates the yields and system productivities for two different biofuel production processes, where the kinetics of the systems are constrained by rate-limitations expected in commodity-scale systems.

The system that is the subject of the first investigation is an experimental assessment of a photosynthetic algal biofuel production system under light-limited growth, where it is hypothesized that system productivities will be a function of light-limited growth kinetics rather than the intrinsic maximum growth rate of an algal species. Biomass and algal oil productivities were determined for two algal species -- the fast-growing, lipid-producing *Chlorella vulgaris* and the slow-growing, isoprene hydrocarbon-producing *Botryococcus braunii* -- in a continuous high-density, light-limited trickle-screen photobioreactor. In a light-limited system, all light is being utilized to its fullest extent such that the algal growth kinetics are dominated by the rate of light available to them. Despite an order-of-magnitude difference in the growth rates of these two algae, biomass productivities in the system conditions differed only by 10%, and the slower-growing alga (*B. braunii*) actually achieved slightly higher productivities. However, the productivity of energy captured into both algal oils and biomass (determined by bomb calorimetry) were very different: *B. braunii* captured 2.2 times as much light energy into algal oils than *C. vulgaris*, and twice as much light energy into the total algal biomass (oil + non-oil cell mass). **These results highlighted the importance of species selection based on energy conversion efficiency and not intrinsic growth rate.** Because the lipid-synthesis kinetics of *C. vulgaris* are growth dissociated, a loop air-lift batch reactor run was executed to determine if higher lipid productivities could be achieved by the induction of lipid-synthesis under non-growth conditions, at both light-limited and non-light limited conditions. *C. vulgaris* biomass and oil productivity under light-limited conditions far exceeded those in the non-light limited conditions,

which **confirmed the hypothesis that maximum utilization of light (i.e., light-limited growth) was essential for maximal productivities.** *C. vulgaris* productivity in the batch system peaked during light-limited growth, but fell below the performance of the continuous reactor system. While *C. vulgaris* lipid productivity in the light-limited batch system exceeded that found during the continuous growth, it did so by only 25%. Furthermore, the biomass and lipid productivities peaked simultaneously when the lipid content of *C. vulgaris* was still very low (prior to lipid accumulation induction). Although the lipid content of *C. vulgaris* increased from 6-22% by the end of the batch run, lipid productivities during this accumulation phase were still lower than those found during the active growth phase. **This emphasized that lipid productivity and not lipid content is a more important metric for assessing the performance algal fuels technologies.**

The system that is the subject of the second investigation is a theoretical "Electrofuels" process, where gaseous H_2, O_2, and CO_2 are the growth substrates for chemolithoautotrophic production of isoprene hydrocarbons by *Rs. eutropha* or *Rb. capsulatus*. The H_2 and O_2 are generated by abiotic electrolysis, using electricity that could be generated by solar photovoltaic cells, and serve as the electron donor and acceptor to provide energy for microbial metabolism. The yields, productivities, and process economics of such a system were assessed theoretically to provide insight and focus towards research areas with the highest possible impact for process feasibility. This was accomplished through the development of a modified theory of microbial energetics, based heavily upon the 'Electron Balance' approach originally developed by McCarty (1971; 2007); this method predicts maximum yields of microbial growth based on the relative energetics of energy generation (catabolic reactions) and cell synthesis (catabolic reactions). Employing this approach, the maximum theoretical yields of cell and product fuel were established on each of the gaseous substrates; expressions for realistic, net fuel yields for the system were then derived based on an assumption of kinetic limitation by gas-liquid mass-

transfer in a commodity-scale continuous-growth bioprocess. This quantitative theoretical framework was utilized in the calculation of fuel yields, fuel productivities, and minimum operating costs for fuel production in a range of process conditions. The rate of mass-transfer to the bioprocess is a critical process parameter that determines the productivity of the system. Furthermore, it was established that a continuous growth-process siphons metabolic energy that could otherwise be used for fuel synthesis; very little of the energy contained in the H_2 substrate was captured into fuel. **Therefore, high-mass transfer, low-growth perfusion-type process development and genetic manipulation for the metabolic decoupling of fuel and growth processes are important research thrusts for Electrofuels process feasibility in order to maximize the amount of substrate hydrogen utilized towards fuel synthesis.**

TABLE OF CONTENTS

LIST OF SYMBOLS, ACRONYMS, AND ABBREVIATIONS

Symbol	Definition
a_λ	Wave-length λ specific absorbtivity coefficient
A	Ratio of electrons to energy generation / electrons to synthesis
A_λ	Measured absorbance for wavelength λ
α	Molar ratio of fuel production to cell synthesis
b	Pathlength of absorbsion
β	Mass ratio of fuel produced per mass total biomass (cell + fuel) produced
c	Concentration of analyte causing light absorbtion
C_i^*	Equilibrium concentration of *i* (mol *i*/L)
$C_{BPF,out}$	Concentration of BPF in outlet stream (g BPF/L)
$C_{BPF,in}$	Concentration of BPF in inlet stream (g BPF/L)
$C_{BPF,R}$	Concentration of BPF in reactor (g BPF/L)
$C_{i,out}$	Concentration of *i* in outlet stream (mol *i*/L)
$C_{i,in}$	Concentration of *i* in inlet stream (mol *i*/L)
$C_{i,R}$	Concentration of *i* in reactor stream (mol *i*/L)
C_L	Lipid concentration (g lipid/L)
C_L^0	Initial lipid concentration (g lipid/L) for productivity calculation
CF_f, CF_{fuel}	Carbon flux to fuel fraction
CF_C	Carbon flux to cell fraction
D	Dilution rate ($time^{-1}$)
D_i	Diffusivity of species *i* (m^2/s)
E_{anode}	Anode potential (mV)
$E_{applied}$	Applied voltage (mV)
$E_{cathode}$	Cathode potential (mV)
E_{cell}	Electrochemical cell potential (mV)
η_{oil}	Photosynthetic energy capture efficiency into oil
η_{tc}	Photosynthetic energy capture efficiency into total culture
ε	Cellular efficiency factor
ε_{calc}	Calculated cellular efficiency factor based on literature data
ε_{TL}	Cellular efficiency in the thermodynamic limit (=1.0)
f_e	fraction of electrons from donor directed to energy generation (in the net yield scenario)
f_e^0	fraction of electrons from ED directed to energy generation (in the true / maximum yield scenario)
f_s	fraction of electrons from ED directed to cell and fuel synthesis (in the net yield scenario)
f_s^0	fraction of electrons from ED directed to cell and fuel synthesis (in the true / maximum yield scenario)
$f_{S,\text{exp}}$	fraction of electrons from ED directed to cell/fuel synthesis as determined from experimental data
$\bar{F}$	Proportionality factor relating the rate of BPF synthesis to the rate of cell synthesis (g BPF synthesized/g cell synthesized)
$FW_{biomass}$	Formula weight of biomass (weighted average of cell and fuel portions)
FW_{cell}	Formula weight of cell mass

Symbol	Definition
FW_{fuel}	Formula weight of botryococcene product fuel
ΔG^{ex}	Gibbs free energy for an exergonic reaction
ΔG^{end}	Gibbs free energy for an endergonic reaction
ΔG^{0}_{an}	GED Method: Gibbs free energy change for anabolic reactions to form 1 carbon mole of biomass (kJ/C-mol)
ΔG^{0}_{cat}	GED Method: Gibbs free energy change for catabolic reactions required to form 1 carbon mole of biomass (kJ/C-mol)
$\Delta G^{0\prime}_{ea}$	EB Method: Gibbs free energy change for electron acceptor half reaction at standard biological conditions (kJ/eeq)
$\Delta G^{0\prime}_{ed}$	EB Method: Gibbs free energy change for electron acceptor half reaction at standard biological conditions (kJ/eeq)
ΔG_{ENERGY}	EB Method: Gibbs free energy change of the energy generating redox reaction at the system conditions (kJ/eeq)
$\Delta G^{0\prime}_{ENERGY}$	EB Method: Gibbs free energy change of the energy generating redox reaction (between EA and ED) at standard biological conditions (kJ/eeq)
$\Delta G_{H2-NAD+}$	Gibbs free energy change for the reduction NAD^+ at the expense of H_2 (kJ/mol H_2)
ΔG_{H2-O2}	Gibbs free energy change for the reduction of O_2 at the expense of H_2 (kJ/mol H_2)
$\Delta G^{0\prime}_{intermediate}$	Original EB method only: Gibbs free energy change for the half reaction of the selected cellular intermediate (kJ/eeq)
ΔG_{SYNTH}	EB Method: Gibbs free energy change of the overall synthesis redox reaction at system conditions (kJ/eeq)
$\Delta \hat{G}_{SYNTH}$	EB Method: Gibbs free energy change of the overall synthesis redox reaction, corrected for efficiency losses (kJ/eeq)
$\Delta G^{0\prime}_{SYNTH-1}$	Original EB method only: Gibbs free energy change of synthesis step 1 (reduction of at standard biological conditions
$\Delta G_{SYNTH-2}$	Original EB method only: Gibbs energy change associated with the formation of cell mass from the cellular intermediate based on an cellular ATP yield (kJ/eeq)
$\Delta G_{SYNTH,END}$	Modified EB Method: The sum of the Gibbs free energy associated with all endergonic cell synthesis reactions (kJ/eeq)
$\Delta G_{SYNTH,EX}$	Modified EB Method The sum of the Gibbs free energy associated with all exergonic cell synthesis reactions (kJ/eeq)
$\Delta_r G^0_X$	GED Method: Gibbs dissipation energy for 1 carbon mole of cell growth (kJ/C-mol)
γ	Degree of reduction (# electron equivalents for donation per mol of carbon in compound)
ΔH_c	Enthalpy of combustion of cell mass (kJ/g cell)
ΔH_{oil}	Enthalpy of combustion of oil (kJ/g oil)
ΔH_{tc}	Enthalpy of combustion of total culture (kJ/g total culture)
$\Delta_c H^{HHV}_{fuel}$	HHV enthalpy of combustion of botryococcene product fuel (kJ/g)
$\Delta_c H^{HHV}_{H2}$	HHV enthalpy of combustion of H_2 (kJ/g)
I	Light intensity after passing through sample causing absorption
I_0	Initial light intensity
k_i	Henry's Law coefficient for substrate species *i* (L-atm/mol)
$k_{i,T}$	Henry's Law coefficient for substrate species *i* at temperature T (L-atm/mol)
$k_{i,298}$	Henry's Law coefficient for substrate species *i* at 298K (L-atm/mol)

Symbol	Definition
$k_L a$	Gas-liquid mass transfer coefficient for O_2 (hr^{-1})
$(k_L a)_i$	Gas-liquid mass transfer coefficient for species other than O_2 (hr^{-1})
K	Constant overall rate of algal culture mass increase during light-limited growth (g algal biomass/time)
m_i	Maintenance coefficient of species *i* (mol *i*/g cell/hr)
m_L	lipid content of algae (g lipid/g DW algae)
m_L^0	initial lipid content of algae (g lipid / g DW algae)
MTR_i	Mass transfer rate of species *i* (mol *i*/L/hr)
MW_{ED}	Molar weight of electron donor (g/mol)
μ^{NET}	Apparent / observed growth rate (hr^{-1})
μ^T, μ^{TRUE}	True growth rate (that possible if maintenance energy is 0) (hr^{-1})
μ_{exp}	Calculated growth rate during exponential phase growth (hr^{-1})
μ_{max}	Maximum intrinsic growth rate of organism (hr^{-1})
μ_{max}^{obs}	Maximum observed (i.e. net) possible intrinsic growth rate (hr^{-1}) for an organism
μ_{max}^{True}	Maximum true possible intrinsic growth rate (hr^{-1}) ($\mu_{max}^{obs} + b$)
μ_{MTL}^{NET}	Net mass-transfer limited growth rate (hr^{-1})
μ_{MTL}^{T}	True mass-transfer limited growth rate (hr^{-1})
$n_{C,cell}$	Number moles of carbon per mole of cell
$n_{C,fuel}$	Number moles of carbon per mole of fuel
ν_{cell}	Stoichiometric coefficient of cell in the stoichiometric cell growth equation
ν_i	Stoichiometric coefficient of molecular species *i* in the stoichiometric cell growth equation
v_s	superficial gas velocity (m/s)
p	exponential factor for determining effect of cellular inefficiency; -1 for exergonic reactions, +1 for endergonic reactions
P/V	Power per unit volume (W/L)
P_B	Algal biomass productivity (g biomass/L/time)
P_{fuel}, P_{BPF}	Botryococcene product fuel productivity (mass fuel/volume/time)
P_i	Partial pressure of gas substrate *i* (atm)
P_L	Lipid productivity (g lipid/L/hr)
P_{oil}	Oil productivity (g oil/L/hr)
P_{tc}	Total culture productivity (g total culture/L/hr)
P_X	Biomass productivity (g biomass/L/time)
$P_{X,LL}$	Light-limited biomass productivity (g biomass/L/time)
ϕ_i	Parameter specific to species *i* for obtaining temperature dependence of Henry's Law coefficient
$\hat{q}_i$	Specific substrate utilization rate (mol *i*/ g cell/hr)
$\hat{q}_{O2}$	Specific oxygen utilization rate (mol O_2/g cell/hr)
$\hat{q}_L$	Specific utilization rate of light (light energy/g cell/time)
Q	Number of electron equivalents required to synthesize a mole of total biomass (cell + fuel)
Q_i	Number of electron equivalents contained in a mole of species *i*
Q_{in}	Volumetric flow rate into process (L/hr)
Q_{out}	Volumetric flow rate out of process (L/hr)
r_{ea}	Electron acceptor half-reaction

Symbol	Definition
r_{ed}	Electron donor half-reaction
r_F	Specific rate of fuel synthesis (g fuel/g cell/hr)
r_{synth}	Biomass synthesis half reaction synthesis half reaction
R	Ratio of botryococcene Gibbs energy of combustion to cell Gibbs energy of combustion
R_{ENERGY}	Energy generating redox reaction
$R_{OVERALL}$	Overall, stoichiometrically balanced growth reaction
R_{SYNTH}	Cell synthesis redox reaction
$\dot{S}_{prod}$	Entropy production rate (J/mol/time)
V	Volume
X	Cell concentration
X_0	Algal population density at onset of light-limitation (g biomass/L)
X_B	Biomass concentration (g biomass / L)
X_B^0	Initial biomass concentration (g biomass/L)
X_{OUT}	Biomass concentration in outlet stream (g biomass/L)
X_R	Cell concentration in reactor
X_{SS}	Steady-state cell concentration
$\dot{\xi}$	Rate of cell growth (specific to Gibbs energy dissipation theory)
Y^{ATP}	Cell growth yield on ATP
Y_i^{NET}	Net or observed yield on substrate *i*
Y_i^T	True / maximum yield on substrate *i*
Y^{TRUE}	True / maximum yield
Y_i^{MAX}	True / maximum yield on substrate *i*
$Y_{X/_i}$	Yield of cell mass on substrate *i* (g biomass/g *i*)
$Y_{X/_{ED}}$	Yield of cell on electron donor (g cell / g ED)

Acronym/ Abbreviation	Definition
AFDW	Ash-free dry weight
ARPA	Advanced Research Projects Agency
ARPA-e	Advanced Research Projects Agency-Electrofuels division
BEAMR	Biochemically assisted microbial reactor
BPF	Botryococcene Product Fuel
CBB	Calvin Benson Bassham cycle; Calvin cycle; reductive pentose phosphate pathway – pathway of CO_2 fixation
CCS	Carbon capture and storage
COD	Chemical oxygen demand
CS	Carbon source
CTP	Cytidine triphosphate
DMAPP	Dimethylallyl diphosphate
DTE	Direct Transesterification
DW	Dry weight

Acronym/ Abbreviation	Definition
EA	Electron Acceptor
EB	Electron balance methodology
ED	Electron Donor
eeq	electron equivalent
ETC	Electron Transport chain
FAME	Fatty Acid Methyl Ether
FOA	Funding opportunity Announcement
FPP	Farnesyl diphosphate
G3P	Glyceraldehyde-3-phosphate
GC	Gas chromatograph
GC-FID	Gas chromatography Flame Ionization Detector
GED	Gibbs Energy Dissipation theory
GPP	Geranyl diphosphate
HHV	High heating value
IPP	Isopentyl diphosphate
LHV	Low heating value
LL	Light-limited
MBH	Membrane bound hydrogenase
MBL	Maximum biological limit
MEC	Microbial electrolysis cell
MEP	Methyl Ertyhritol Phosphate
MFC	Microbial Fuel cell
MTL	Mass Transfer Limited
MVA	Mevolonate
NETL	National Energy Technology Laboratory
NL	Non-light Limited
NS	Nitrogen Source
OD	Optical Density
OD550	Optical Density at 550nm
PAI	Photosynthetically active irradiance (W/m^2)
PAR	Photosynthetically active radiation
PARF	Photosynthetically active radiant flux (J/s)
PFD	Photon flux density
PMF	Proton motive force
PPFD	Photosynthetic photon flux density (μmol quanta/m^2/s)
PS	Phosphur source for cell synthesis
PSPP	Pre-squalene diphosphate
PV	Photovoltaic
RCF	Relative centrifugal force
RET	Reversed electron transport
SAM	S-adenosyl methionine
SH	Soluble hydrogenase
SMR	Steam methane reforming
SS	Steady-state OR Sulfur source for cell synthesis
TAG	Triacylglyceride

Acronym/ Abbreviation	Definition
SSL	Squalene-synthase-like enzyme
tc	Total culture
TCA	Tricarboxylic acid cycle
TL	Thermodynamic limit (reversible microbial growth)
TS	Trickle screen reactor
UQ	Ubiquinone (oxidized)
UQH2	Ubiquinol (reduced)
UTEX	University of Texas algae culture collection
WFAM	Wayne's freshwater algae medium
WWTP	Wastewater treatment plant

LIST OF FIGURES

LIST OF TABLES

ACKNOWLEDGEMENTS

I extend my thanks to Dr. Perry McCarty, author of the Microbial Energetics theory (referred to as the Electron Balance method in this work) upon which the yield analysis in this work was based, for helping me to clarify some key concepts central to this theory. I would also like to acknowledge the work done by our collaborators at the University of Kentucky (Dr. Chappell's Laboratory; Joe Chappell, Thomas Niehaus, and Stephen Bell); they provided the *Botryococcus braunii* Race B (Showa) algae strain, and performed the hydrocarbon analysis on *B. braunii* samples. I would also like to thank our collaborators at NETL (National Energy Technology Laboratory*;* Brian Kail, Dirk Link, and Douglas Middleton*)* for their development of the Direct Trans-Esterification method of extraction, their analysis of *Chlorella vulgaris* samples for total cellular lipid content, as well as the purity analysis on the *B. braunii* hydrocarbon sample.

I would like to thank the talented undergraduate researchers in the Curtis Lab who have had a large impact on this work. Without Patrick Hillery's motivated efforts in extracting and purifying *B. braunii* hydrocarbon oils, and his perseverance in making calorimetric determinations (even when things did not go as planned), much of the insight of the energy capture characteristics of *B. braunii* would not have been possible. Along these lines, Doug Middleton's work to transfer the extraction and purification protocol to the Curtis Lab from NETL is appreciated. Justin Yoo's *B. braunii* subculturing efforts are commendable, and I am so glad that I have been able to leave the care of my 'babies' in such sure hands. Jackie Guo's willingness to always lend an extra hand and a smile, be it troublesome assay development or help with light measurements, is truly valued; I look forward to learning of her contributions to the lab in the years to come. Thanks to Jessica Bigham and Dilwinderpal Singh for their efforts in reviewing the literature to find microbial composition data. Erik Wolcott's summary of mass-transfer technologies and correlations was incredibly useful in predicting mass-transfer costs. Other undergraduate researchers in 'Team Algae' have had a huge impact in the scope of the experiments this group has been able to undertake, including summer REU researcher Shalini Saxena and IIT intern Lalit Darunte; I was so sad to see you both leave the lab after such a short time! I am very thankful to Robert Hendrix and Adam Nebzydoski for their pioneering work in basic 'bag reactor' construction. And while Manuel Sebastian Escotet did not directly contribute to this thesis, I know that he will be a great leader of the algae work as he transitions into graduate student responsibilities. I would like to call out Matt Curtis as one of the most

selflessly helpful people in the laboratory; while your efforts are not often recognized formally, I know that you have had a huge hand in keeping the lab 'going'. I am indebted to Benjamin Woolston's determination in getting the EPA P3 project off the ground; without him as a teammate in this effort this project would have been much more difficult and a lot less fun to (finally) pull off. Brandon Curtis's efforts in lab IT development have had a huge impact in the organization of the lab; I am additionally grateful for the extensive thesis edits he made, and his assistance in clarifying the botryococcene synthesis metabolic pathways. Finally, I would like to thank all the other undergraduates whose character, intelligence, and motivation on their own projects simply made the Curtis lab an enjoyable and inspiring place to be: John Meyers, Sydney Shaw, and Christine Taylor were among those I interacted with the most, but there are many more.

Next I would to thank the many graduate students in the Curtis Lab with whom I have had the pleasure and privilege or working with and learning from. First, those on 'Team Algae', with whom I've shared so many memories as well as learning experiences: Lisa Grady's determination and consistent technique was something I tried to emulate every day while running the algae trickle screen reactor – I thank her for training me in methods that she had taken so much time to perfect. Waqas Khatri is possibly one of the most enthusiastic idea-generators that I have ever met, and his vision of 'things that could be', in both algae and in life, is one-of-a-kind. I am grateful to the seeds of excitement he sowed all over the Cutis Lab. I am so grateful to Megerle Scherholz and the level of teamwork that she brought to Team Algae – she has always been ready as a sounding board and has provided so much feedback on research ideas, she was always ready to fill in for a data measurement so I could 'take a break', and always ready to give an instant confidence boost with an encouraging word. In development of the microbial energetics theory utilized for ARPA yield calculations, Nymul Khan was invaluable in providing updates of *R. capsulatus* experimental results, as well as in critical discussions of the microbial energetics theory; I also remember and thank him for his help in data collection during the algae bag reactor experimental development. Jeff Larsen is one of the funniest people I have ever met, and definitely the most knowledgeable; he may not have appreciated the "Just go ask Jeff!" easy-card I played from time to time, but I sure did! His work ethic and organization was an inspiration, and his mentorship of myself and many other lab members will have far reaching effects. And to Sergio Florez, Mustafa Erbakan, and Trevor Zuroff, along with my friends in other labs Jason Binz, Eric Moschetta, and Robert Pantazes – I am so thankful for the laughs, ideas, support, feedback, and the camaraderie that you provided.

The level of support from loved ones that I have had in recent months, while juggling PhD coursework simultaneously with thesis writing, has been unprecedented. I am completely indebted to those at the University of Delaware who convinced me I could when I was certain I could not, as well as the other first-year PhD students whose camaraderie and potluck-planning has made the 'first semester' experience that much more enjoyable. I am also so appreciative of Roseanne Hofmann's support of my decision to leave industry to return academia, and the fact that she still makes the time to periodically lend guidance and provide encouragment in the three years since I left! I am so fortunate have Hannah Segrave as my new roommate; meals, hugs, and an understanding ear to listen have been amazing. I am also so thankful for the long time friends whose pep talks and emails of encouragement have never failed to make my day – I cannot wait to have more time to spend with you again: Heather Coletti, Megan Leinen, Sarah Leinen, Tacy Napolillo, Erin Hicks, and Alexandra Archer. Aaron Drew's humor, love, understanding, and unwavering support enhanced every day of my M.S. degree at Penn State, and while I so miss our coffee breaks now, his constant support has continued to give me strength. I am so blessed and do not know how to sufficiently thank him for these gifts, and I so look forward to getting to enjoy his company again on a more regular basis. Finally, I am so blessed to have the family that I do, who have not just accepted, but encouraged me through my changing life trajectories with minimal protest, despite moving me into and out of more apartments more than any of us care to remember. I love you so much and I look forward to spending some quality non-stressed time with you all in the near future. Dad – I aspire to some day give to my own children the love and confidence that you have given me. I promise that your phone calls to check up on me did always make me smile. Mom – while the influx of homecooked meals and groceries in the 11th hour of thesis crunch were, shall I say, 'clutch,' your love and support in the many years before this have been what got me to that 11th hour in the first place. Elissa –I hope you realize how much I try to emulate your work ethic and your perseverance, that I have had the opportunity to witness for so many years. Your support of me has made a huge impact in my life, and I'm so proud to call you my sister!

I would like to extend my gratitude to Dr. Robert Rioux and Dr. Andrew Zydney for agreeing to serve on my M.S. thesis committee. Your comments and insight were extremely valuable in clarifying the focus of the microbial energetics results, and I appreciate your patience in working with me through this extended thesis-writing process. And finally, I cannot thank Dr. Wayne Curtis enough for the many years of his mentorship and guidance – the many ways he has shaped me as a teacher, a researcher, an experimentalist, a naturalist, and a commuter-

biker, throughout both my undergraduate and graduate experiences, are innumerable. I am totally indebted to him for my return to academia from industry; thank you so much for believing in me enough to ask me come back to Penn State to teach ChE 340. I hope that future students find your lab and your work as inspiring and as interesting as I have, since I first set foot in it nearly 10 years ago.

The work in this thesis was supported under the NSF Collaborative grant no. CBET-0828648 entitled **"**Development of a Sustainable Production Platform for Renewable Petroleum Based Oils in Algae" which included a GRDS and a GRS supplement which specifically supported my M.S. work**,** the NSF grant no. DBI-0215923, which supported the installation of the Plant Growth Chambers, and the ARPA-E Electrofuels grant # DE-AR0000092 entitled "Development of *Rhodobacter* as a Versatile Microbial Platform for Fuels Production."

Chapter 1

Introduction – Algae and Electrofuels as Potential Renewable Biofuel Technologies

This introductory chapter presents background on renewable energy development efforts over the past few decades, with a focus on photosynthetic and algal technologies. Then, in the context of the overall renewable energy development efforts, this chapter provides a background and rationale of the approach of two solar bioenergy investigations, which is the work presented in this thesis:

1. An experimental bio-oil productivity comparison of two algal species, *C. vulgaris* and *B. braunii*, in light-limited photobioreactors, and
2. A theoretical investigation into the predicted process yields and productivities for bio-hydrocarbon production in a chemolithoautotrophic "Electrofuels" process.

Finally, feedstock costs critical for the work of this thesis in the context of the renewable energy development efforts

Renewable Energy Development Efforts

While the period of industrial expansion in the 20th century was fueled primarily by fossil resources (coal, oil, and natural gas), it is widely recognized that these energy sources are finite and continued dependence upon them for long-term future growth is unrealistic. Therefore, the threat of dwindling reserves of these energy sources has prompted research efforts into new, renewable technologies across the globe. Within the United States, an additional emphasis has

been placed upon developing technologies that will move us towards energy independence and reduce our reliance on foreign-sourced oil.

A particular focus is on the development of liquid fuels, as their high power density makes them indispensable for many applications. A large fraction of the most technologically tractable approaches for liquid fuel production is the production of bioethanol by microbial fermentation, relying on a source of inexpensive sugars as the feedstock. The distinct disadvantage of this approach is arable-land requirement for growing these feedstock energy crops, which directly competes utilization of this acreage for food supply, prompting concern for future food shortages. Other currently technically viable approaches for producing liquid biofuels have limited capacity (i.e. biodiesel from waste vegetable or animal fat). One nascent bioenergy approach that has been touted for its ability to eliminate issues of food-source competition is cellulosic ethanol processes. However scale-up and commercialization of this technology is hindered by the need for improved pre-treatment technologies (Yan and Wyman 2008).

Algae have been considered a potential source of renewable liquid fuels for several decades; the Department of Energy's Aquatic Species Program (1978-1996) investigated the development of biodiesel from pond culture of high-lipid content algae (Sheehan et al. 1998). However, this research focused heavily on biology and not bioreactor design and operational principles. A major conclusion of the Aquatic Species program was the assumption of deep pond culture as the only feasible photobioreactor design for commercialization of biofuels (Benemann and Oswald 1996), which limits operation to low biomass loadings. One advantage of algal biofuel production over the fermentation of terrestrial biomass feedstocks is their improved productivity: algae pond-culture systems routinely achieve biomass production levels of 25 g dry weight (DW)/m^2/day, with numerous reports achieving up to 100g DW/m^2/day (Pulz and Scheibenbogen 1998). This corresponds to 30 to 100+ tons of biomass a year per acre, which is several-fold greater than terrestrial plant productivity (e.g. 7 tons/year/acre for switchgrass)

(McLaughlin et al. 1999). In addition, algal culture does not require arable land for its production, which eliminates the competition over land for food crops. Algae are also capable of using and recycling waste nutrients such as nitrogen and phosphorous from wastewater and CO_2 / NO_X from power plant emissions (Sheehan et al. 1998).

Many of the commercial designs deployed to data for algal bioprocess systems have obvious or hidden limitations that have a significant impact on both productivity and on the cost of operation (Lundquist et al. 2010). To improve bioprocess economics, achieving high density culture is a well-established means of increasing volumetric productivities and reducing the costs of water handling (pumping, biomass separation, extraction efficiency). Therefore, the development of high density algae culture systems is a requirement for economic feasibility of commodity-scale algae biofuel production.

A fundamental mistake of recent research efforts and algae bioprocess development is the emphasis on developing algae strains with a high intrinsic growth rate. Inherent to these research thrusts is the assumption that the major limitation of an algal production system will be the intrinsic maximum growth rate of the algae species. For this assumption to be applicable, the rate of light energy available to the algal culture must be equal to or above that required to support the maximum growth rate of the algae, such that light in the photobioreactor is in excess; this will occur only in dilute, shallow algae systems. For the reasons articulated above, however, the cell density must be as high as possible for economic reasons; this results in 'self-shading' and extreme light attenuation within the interior of the culture. Consequently this is a rate-limited growth scenario, where light is the limiting factor and the algae cannot grow at their maximum intrinsic growth rate. Furthermore, operation of an algae photobioreactor under light-limited kinetics is required for the fullest extent of photon utilization. Therefore, under the conditions necessary for economic feasibility, dilute exponential growth kinetics become irrelevant.

Each of the biomass-derived renewable energy technologies discussed thus far in this work have a common primary energy source, which is the solar energy used for their photosynthetic growth. Because the efficiency of algal photosynthesis is low, with a theoretical maximum storage potential of 18% (S J Pirt et al. 1980), and because photosynthesis in terrestrial plants is even lower (2% and below), this method of capturing solar energy into useable fuels for human consumption is very inefficient. Therefore, technologies for capturing and directly using solar energy have been widely investigated. Improvements to photovoltaic (PV) technology have increased efficiency of photon capture to greater than 60%, with future projected efficiencies approaching 80% (Ramsden, Steward, and Zuboy 2009). Furthermore, decreases in manufacturing costs have improved their accessibility. However, methods of storing solar energy captured by PV for use at a later time currently remain elusive.

A means for storing the solar energy captured by photovoltaics directly into liquid fuels that are compatible with existing fuel refining and distribution infrastructure would be a transformative breakthrough in alternative energy technologies. A 2010 Funding Opportunity Announcement (FOA) from the Advanced Research Projects Agency (ARPA) challenged researchers across the United States to investigate the potential for this exact type of technology, coined "Electrofuels": liquid biofuels produced from CO_2 and electric energy, which could be derived from light energy by photovoltaics. ARPA stipulated that these 'Electrofuels' must be energy-dense (greater than 32 MJ/kg, such as butanol and C8 hydrocarbons). One possible Electrofuels process permutation is the utilization of PV-captured electricity to perform abiotic electrolysis, splitting water into H_2 and O_2. These species can be utilized as growth substrates by a class of microorganisms capable of 'Knall-gas' growth: aerobic oxidation of hydrogen for metabolic energy generation, coupled with the fixation of carbon dioxide as the carbon source. This growth mode is a type of chemolithoautotrophic growth.

Bioenergy Technologies Investigated in this Thesis

Light-limited productivity of algal oils by *Chlorella vulgaris* and *Botryococcus braunii,* Race B

This thesis presents research towards two of the alternative energy strategies discussed above. Chapter 2 of this thesis investigates algal biomass, oil, and energy productivities in high-density, light-limited systems versus those in low-density, non-light limited systems. Two algal species are compared: the fast-growing, lipid-producing alga *Chlorella vulgaris*, and a slow-growing, hydrocarbon-producing alga, *Botryococcus braunii,* Race B. The isoprene hydrocarbons produced by *B. braunii* are highly reduced compounds, C_{30}-C_{34} called botryococcenes with a very high energy content: 44.8 kJ/g hydrocarbon oil (see Chapter 2 of this thesis). The hypothesis challenged with this comparison was that the intrinsic growth rates of the species would become irrelevant under light-limited production systems. Further specific background to this work is presented at the beginning of Chapter 2. The results of this algal comparison support the theory that in high-density, light-limited culture the biomass productivities of the two species are nearly equivalent; however, it is determined that culture conditions highly favor *B. braunii* in terms of energy capture productivity into useful oils. These results emphasize the need for a photobioreactor design that maximizes light availability under light-limited growth conditions. Furthermore, the results emphasize the need for species selection criteria that look beyond intrinsic growth rate to energy capture efficiency.

"Electrofuels" production of isoprene hydrocarbons by *Rhodobacter* and *Ralstonia*

Chapters 3-6 present an assessment of the theoretically possible yields, productivities, and economics of an Electrofuels production system. The system specifically investigated in this

work is the heterologous production of $C_{34}H_{58}$ isoprene hydrocarbons (botryococcenes) by bacterial species capable growth by autotrophic hydrogen oxidation (a form of chemolithoautotrophic growth): *Rhodobacter capsulatus* and *Ralstonia eutropha*. The development of this system is a current effort in the Dr. Wayne Curtis Laboratory as part of the ARPA-E electrofuels initiative.

The rationale for the selection of *Rb. capsulatus* as the primary host organism for chemolithoautotrophic hydrocarbon production is based on several items. First, *Rb. capsulatus* is a purple-non-sulfur bacterium capable of a diverse array of metabolic modes, including heterotrophic photosynthetic and fermentative modes in addition to autotrophic aerobic hydrogen oxidation. Secondly, the approach of developing molecular genetic manipulation of *Rb. capsulatus* for hydrocarbon fuels production was considered to be a more reasonable technological challenge than moving the required pathways for aerobic hydrogen oxidation into a well-characterized organism such as *E. coli* (H_2 utilization, carbon fixation). The primary disadvantage of working with *Rhodobacter* is that it lacks the highly refined strains and techniques that have been developed for *E. coli*; however, previous work in the Curtis laboratory has included the development of molecular biology tools for the genetic manipulation of another *Rhodobacter* species, *Rb. sphaeroides*.

The enhancement of isoprene metabolism in *Rb. capsulatus* was chosen over the introduction of other biofuel metabolic pathways for the following reasons:

1. Triterpenes have a high utility for generating a complete suite of liquid fuels, from high-octane gasolines to aviation fuels (Hillen et al. 1982).
2. *Rhodobacter* species have demonstrated a high capacity for induction of lipid metabolism, including the rapid accumulation of accessory pigments derived from isoprene metabolism.

3. The laboratory of Dr. Joseph Chappell at the University of Kentucky, collaborators of the Curtis lab, has demonstrated the capability to manipulate the isoprene pathways and has made discoveries around unique biosynthetic capabilities of C_{34} hydrocarbons.

Because the three main substrates for this chemolithoautotrophic growth mode are gasses (H_2, O_2, and CO_2), the likelihood of a system where gas-liquid mass-transfer limits growth and productivity is high. *Rs. eutropha* was selected as a comparative organism in assessing the feasibility of this production system; *Rs. eutropha* is a Knall-gas bacterium with a maximum growth rate significantly higher than *Rb. capsulatus*. Therefore, this enabled the comparison of theoretical yields and productivities of two organisms with different intrinsic growth kinetics in a system rate-limited by the mass-transfer of the gas-phase substrates into the liquid phase.

Chapter 3 is dedicated to a review of the metabolic pathways associated with the autotrophic hydrogen oxidizing *Ralstonia eutropha* and *Rhodobacter capsulatus*; the understanding of these pathways was critical to the proper development of the Energetic model to predict biomass yields.

Chapter 4 describes the Electron Balance method of McCarty (1971; Rittman and McCarty 2001) for assessing microbial energetics. It then processed to discuss the development of modifications to this theory necessary to enable the model to predict chemolithoautotrophic growth and botryococcene fuel synthesis.

Chapter 5 presents the derivation of the mass balances specific to mass-transfer-limited growth of the chemolithoautotrophic growth scenario, which were utilized in making mass-transfer-limited yield and productivity projections.

Finally, Chapter 6 presents the results of an extensive technological and economic feasibility analysis enabled by employing the theory developed in Chapters 4 and 5. Yields of botryococcene product fuel (BPF), BPF productivities, and minimum production costs (based on substrate costs and energy requirements for mass-transfer) are presented.

The goal of this assessment was to identify key aspects of the proposed Electrofuels process which have the largest potential to maximize the likelihood of technical and economic feasibility, and to subsequently focus efforts within the Electrofuels community towards research objectives with the greatest capacity for transformative improvements. The methodology developed in this thesis could be expanded to make similar evaluations of other proposed Electrofuels processes.

Estimates of Substrate and Electricity Costs Relevant to the Electrofuels Process

The key metric for evaluating Electrofuels project success is an assessment of the economic feasibility of the final product fuel cost: $ / kJ in final fuel. In addition to a predicted product fuel yield on the process substrates, which can be determined from a balanced stoichiometric growth equation, substrate cost predictions are required. Realistic costing estimates of CO_2, electricity, and H_2 therefore are key parameters for accurate assessment of electrofuel feasibility; these are explored below.

Carbon Dioxide (CO_2)

The stipulation for autotrophic carbon dioxide (CO_2) as the carbon source in Electrofuels scenarios results from a need for net fixation of CO_2 in the fuel production process, and to align with ongoing co-current CO_2 capture and concentration development efforts. Furthermore, CO_2 is an over-abundant carbon source, and its recycle back into the energy stream is highly desirable. The costs of CO_2 capture and concentration from a waste gas stream was approximated to be $63-87/ton, using current state-of-technology amine-capture (Black and National Energy Technology

Laboratory 2010,1:). For this analysis, the upper value was assumed for a worst-case cost analysis.

Electricity

The electricity costs associated with abiotic water electrolysis for hydrogen are analyzed with the cost analysis of hydrogen; here the cost of electricity is required because the cost of mass-transfer is linked to its energetic requirements.

The assumed price per kwh of electricity depends on the assumed source. According to the U.S. Energy Information Administration, the 2012 projected average pricing per kwh for electricity obtained the industrial sector is 8.72 cents/kwh (U.S. Energy Information Administration 2011). However, the range of pricing over the various US regions is quite wide, ranging at the low end at 5.91 cents/kwh (West South Central) to 22.83 cents/kwh (Hawaii and Alaska – 2011 data). The commercial and residential electricity costs are somewhat higher, with the 2012 projected costings averaging at 11.82 and 13.47 cents/kwh, respectively. A key hope for the implementation of the ARPA Electrofuels program is integration with a renewable means of electricity generation, such as via solar photo-voltaics or wind-powered electricity. While the capital costs of these systems are extensive, envisioning a scenario where a dedicated electricity-generating source (wind farm or field of PV) localized at an Electrofuels production facility provides at least a portion of the power to an electrofuels process could result in diminished electricity costs. As a basement estimate to bracket potential scenarios, ARPA-e estimates an off-grid electricity cost of 2.5 cents / kwh (ARPA, personal communication). In this assessment, an electricity cost of 8.72 cents/kwh as an industrial electrical cost is assumed for the base case.

Hydrogen

H_2 Generated by Abiotic Electrolysis:

Currently, fossil fuels, including natural gas, petroleum, and coal, provide the main source of hydrogen production through steam methane reforming (SMR), a process which co-produces CO_2 (Energy Information Administration 2008). As a key goal for electrofuels production is a reduction in CO_2 emissions, hydrogen production must either be coupled with carbon capture and sequestration or produced by non-CO_2 emitting processes, such as electrolysis using non-coal fired electricity. Furthermore, as fossil fuels are currently the cheapest feedstock, H2 production by SMR is also the most currently economical (Energy Information Administration 2008). Hydrogen production by electrolysis is significantly more expensive, due to the high capital costs associated with the required process equipment. Furthermore, using grid-based electricity is currently the least-carbon neutral method of production, due to the heavy dependence of electricity generation on coal-fired power plants. However, considering that the SMR of natural gas and coal are only 67-73% efficient (Energy Information Administration 2008), resulting in energetic losses, and the fact that these fuels can be independently as fuels on their own, electrofuels technologies should focus on hydrogen production strategies that don't dip into our fossil fuel resources to maximize energy availability. All production methods of hydrogen result in net energy loss, with electrolysis production currently achieving 73.8% efficiency and projected to exceed 88% efficiency in future (Ramsden, Steward, and Zuboy 2009). While typical efficiency calculations are based upon the LHV for the output fuel, the HHV is more applicable here for the assessment of hydrogen as a produce, considering that the end-use of the hydrogen will not be for high-combustion applications (where the LHV is more applicable). Table 1.1 lists the production costs and total projected capacity for a selection of

Table 1.1: Production Costs and Capacity for Selected Hydrogen Generation Technologies

This table provides the relative costs of various abiotic hydrogen production technologies to provide a context for the variation in predicted pricing and projected capacities available.

Technology and Fuel	Capital Cost	Feed-stock Cost	O&M Cost	Total H_2 Cost [1]	Total Possible Capacity	Reference
	[$ / kg H2]				*[10^3 kg / day]*	
Centralized SMR of Natural Gas	$0.18	$1.15	$0.14	**$1.47**	379,387	(Energy Information Administration 2008)
Centralized Coal Gassification w/ CCS	$0.83	$0.56	$0.43	**$1.82**	307,673	(Energy Information Administration 2008)
Centralized Grid-based Electrolysis (Future Case) [2]	$0.47	$2.64	$0.13	**$3.24**	51 [3]	(Ramsden, Steward, and Zuboy 2009)
Centralized Wind-based Electrolysis	$1.48	$1.69	$0.65	**$3.82**	124,474	(Energy Information Administration 2008)
Centralized Grid-based Electrolysis (Current Case) [2]	$1.16	$3.02	$0.32	**$4.50**	51 [3]	(Ramsden, Steward, and Zuboy 2009)
Distributed Grid-based Electrolysis	$0.96	$5.06	$0.73	**$6.75**	1,500	(Energy Information Administration 2008)
Distributed Wind-based Electrolysis	$3.00	$3.51	$0.74	**$7.25**	480	(Energy Information Administration 2008)
Solar PV-based Electrolysis [4]	---	---	---	**$8.00**	----	(Doty 2004,2004:)

SMR = Steam Methane Reforming; CCS = Carbon Capture and Sequestration

Pricing is based on 2007 data, except where otherwise noted

[1] Note: Compression, Storage, Dispensing costs not included

[2] Using 2005$

[3] Capacity is for a single production plant, not total

[4] Projected costs for 2015 based on PV power at $0.10/kWh

Hydrogen technologies. The listed costs do not include transportation, compression, and delivery costs, as the envisioned scenario for interface with an electrofuels process is for hydrogen used in the gas-phase close to the point of production. It should also be noted that the Total Possible Capacity indicated is that which is probable for the entire United States (Energy Information Administration 2008), except where noted otherwise.

H_2, Generated by Biologically Catalyzed Process:

An alternative, bio-catalyzed means of hydrogen production is known as both a Microbial Electrolysis Cell (MEC) as well as a Bioelectrochemically Assisted Microbial Reactor (BEAMR) (Logan 2008). This device utilizes microbial activity to catalyze hydrogen production and reduce the necessary input voltage to split water, and therefore requires reduced electrical energy unit. A schematic of a single-chamber MEC configuration is shown in Figure 1.1. Whereas abiotic electrolysis of water requires a minimum voltage input of approximately +2.0 V input, based on the overpotential required as a driving force for this endergonic process, a MEC can utilize the catalytic activity of microbes on a bioanode to achieve lower required power inputs for electrolysis (Logan 2008). Microorganisms growing in a biofilm on the anode utilize an organic substrate electron donor, using the anode of the MEC as a terminal electron acceptor. This occurs spontaneously, producing a potential at the anode; for the defined substrate of acetate, the anode potential will be E_{anode} = -0.30 V, referenced to a standard hydrogen electrode (Logan 2008). The by-products of the microbial metabolism produced at the anode are CO_2 and H^+; the H^+ is required at the cathode for reduction to hydrogen gas. Therefore, the anode and the cathode must either be enclosed in the same chamber (as shown in Figure 1.1), or in a double-chamber separated by a proton exchange membrane to allow diffusion of H^+ between the two chambers (configuration not shown).

At the cathode, if oxygen is present, the O_2 will be reduced to H_2O, producing a potential of $E_{cathode} \approx$ +0.2 V. Because the total cell potential in this case is +0.5 V (Equation 1.1), and is positive, this will proceed spontaneously (Hong Liu, Grot, and Logan 2005). In this configuration, the cell *generates* electricity, and is termed a Microbial Fuel Cell (MFC).

$$E_{cell} = E_{cathode} - E_{anode} = +0.2\text{ V} - (-0.3\text{ V}) = +0.5\text{ V} \qquad \textbf{Equation 1.1}$$

Figure 1.1: Diagram of a Single Chamber MEC Configuration

This figure shows a schematic of a single-chamber MEC (Microbial Electrolysis Cell) for the production of Hydrogen at the cathode. The microbes on the anode utilize the organic substrate in the chamber anearobically and donate electrons to the anode. AT the cathode, these electrons are used to reduce H^+ to hydrogen gas. The H^+ released at the anode due to microbial metabolism must be transported over the cathode in order to maintain the pH balance of the chamber. $E_{applied}$ = applied voltage; E_{anode} = potential of the anode.

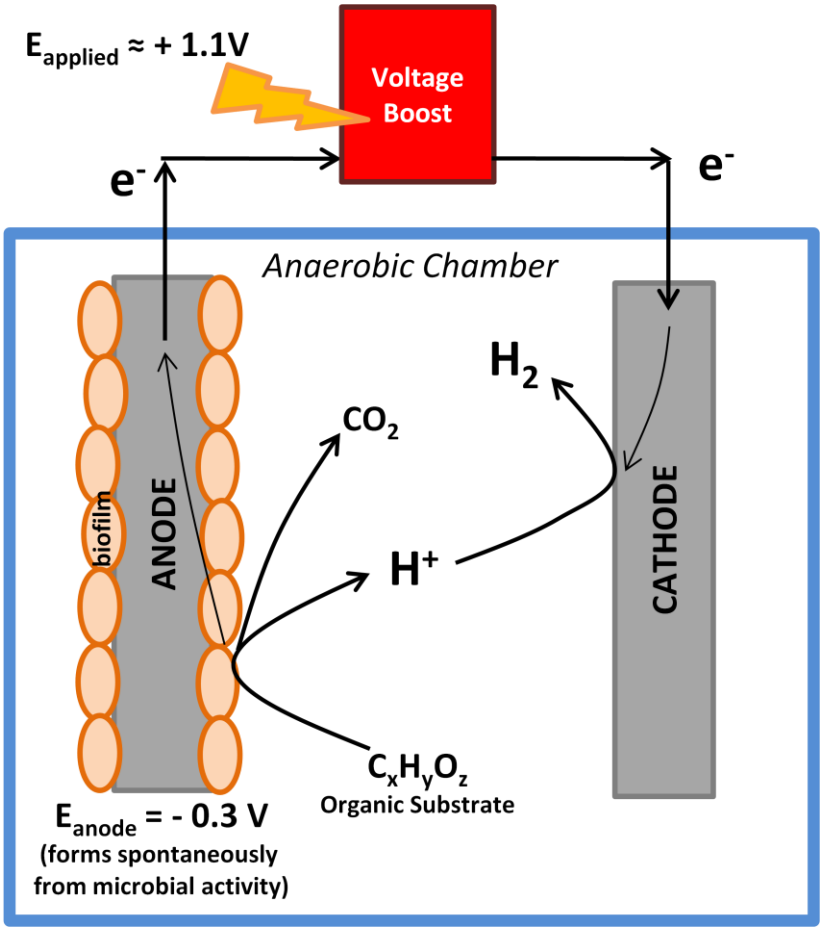

However, in order to generate hydrogen in an MEC configuration, the cathode must be enclosed in an anaerobic chamber to remove the highly electronegative oxygen, which is otherwise reduced preferentially over H^+. H^+ is reduced to H_2 at the cathode at a potential of -0.41 V, resulting in overall cell potential of -0.11V (Equation 1.2). Therefore, reduction of H^+ at the cathode will not proceed spontaneously. In order to drive the production of hydrogen from H^+ at

the cathode, additional electrical voltage must be supplied to the cell; the theoretical minimum applied voltage required for the reaction to proceed spontaneously is +0.11 V (Equation 1.2).

$$E_{cell} = E_{cathode} - E_{anode} = \text{-0.41V - (-0.3 V) = -0.11 V} \quad \textbf{Equation 1.2}$$

$$E_{applied} = -E_{cell} \quad \textbf{Equation 1.3}$$

In reality, at least +0.25V is necessary for the reaction to proceed in order to compensate for inefficiency losses and overpotential at the cathode, and applied voltages of at least +0.8V are required in order for the reaction to proceed at an appreciable rate (Shaoan Cheng and Logan 2011; Cusick et al. 2011; Logan et al. 2008).

Additionally, the substrate species present at the anode for microbial metabolism makes a large difference in the performance of the MEC. If the growth substrate is a single species and is easily metabolized, a more highly negative potential forms at the anode, decreasing the applied voltage required to drive the reaction forward. For example, for acetate, which has an anode potential of E_{anode} = -0.30V at a concentration of 1 g/L, the resulting higher coloumbic efficiencies of the system provide a higher yield of H_2 as well as higher rates of H_2 production compared to using wastewater as a growth substrate (Logan 2008). Use of wastewater resulted in less negative potentials at the anode, particularly when the wastewater was of low strength (Cusick, Kiely, and Logan 2010). The diminished potential at the anode reduces the current density of the system and therefore the yield and production rate of H_2.

However, if the H_2 from the MEC were to be the source of H_2 for an electrofuel production process, the cost of the growth substrate must also be factored into the electrofuel cost, which would be much higher for a single, defined growth substrate. Furthermore, the energetic costs of producing and purifying a single growth substrate would also need to be factored into the overall energy capture efficiency of the process. From this perspective, therefore, wastewater is much more attractive of a substrate for MEC hydrogen generation, as it is 'free' and wastewater requires nutrient removal as a part of its treatment prior to re-release into

the watershed. Thus, in analyzing the input costs of H_2 via an MEC device, two scenarios are considered:

1) acetate obtained at market price is the fuel source

2) wastewater from domestic WWTP is the fuel source.

Data from various literature reports on MEC performance with both acetate and wastewater was surveyed (Hong Liu, Grot, and Logan 2005; Rozendal et al. 2006; Ditzig, Hong Liu, and Logan 2007; Call and Logan 2008; Geelhoed and Stams 2011; Cusick et al. 2011; Shaoan Cheng and Logan 2011), and the best performing examples of each wastewater (Cusick et al. 2011) and acetate (Shaoan Cheng and Logan 2011) as fuels were selected. The data presented in these two literature reports (voltage applied, electricity recovery, volumetric hydrogen production rates, and yield of hydrogen on either acetate or COD (chemical oxygen demand)) were utilized to predict the cost of hydrogen production by the MEC technology, as well as to predict reasonable scales of production. Cost (\$ / kg H_2) for the acetate-feeding scenario were considered to be the sum of the required acetate feed and the electricity required; cost for the wastewater feeding scenario were considered to be the electricity required, reduced by cost-avoidance of electricity costs for the wastewater treatment. The outcome of this analysis is presented in Table 1.2.

Table 1.2: Microbial Electrolysis Cell (MEC) Hydrogen production costs and current possible capacity.

This table demonstrates that current MEC technology either produce hydrogen at costs that are prohibitively expensive to other technologies (acetate feeding scenario) or at volumetric productivities that are economically infeasible based on expected capital costs.

	Electricity Cost	**Substrate Cost** *[\$ / kg H_2]*	**Total Cost**	**Daily Capacity** *kg H_2 / 1000L / day*	**Reference**
Acetate-feeding Scenario	\$3.29	\$7.24	**\$10.53**	1.44	(Shaoan Cheng and Logan 2011)
Wastewater-feeding Scenario	\$3.64	-\$1.92	**\$1.72**	0.023	(Cusick et al. 2011)

The costing presented for the generation of H_2 by MEC is not directly comparable with that for the abiotic electrolysis because the MEC cost analysis did not take into consideration the effects of capital cost and general operating / maintenance costs. Therefore, the costs presented in Table 1.2 for MEC hydrogen production must be compared with only the feedstock costs for the abiotic generation of hydrogen scenario (Table 1.1). Thus, it can rapidly be seen that the feedstock costs for the acetate-feeding scenario will be very cost-ineffective compared to the projected costs for all methods of abiotic electrolysis. Comparing the acetate-MEC feedstock costs with the most expensive feedstock costs for abiotic H_2 generation, those for distributed grid based production, shows a two-fold difference in cost: \$10.53 versus \$5.06 per kg H_2. Even in comparing the overall most expensive abiotic option, that for Solar PV generated electricity, the total cost by solar PV is still less than only the feedstock costs for acetate-MEC. It is expected that the capital costs for MEC construction will not be negligible, especially considering the very small volumetric productivity associated with the technology.

Additionally, while the wastewater-feeding scenario appears to be cost-competitive with feedstock costs for renewable-electricity-driven abiotic electrolysis scenarios (Central Wind and Distributed Wind), it is very clear that the volume of the production process required to generate significant masses of hydrogen is extremely large. This suggests that capital costs for wastewater-fueled generation of H_2 by MEC will rapidly become prohibitive, and that production of H_2 on a scale required for electrofuels production using this technology is simply not feasible at this time.

Hydrogen costs, summary:

For the economic feasibility assessment of the various Electrofuel scenarios presented in this work, the costing associated with the Centralized Wind Electrolysis scenario for hydrogen

production will be considered as the base-case ($3.82 / kg H_2) with an investigation into the effects of economic feasibility if the hydrogen costing shifts to the Solar PV Electrolysis scenario.

Chapter 2

Algal Production of Alternative Fuel Feedstocks

This chapter investigates algal biomass, oil, and energy productivities in high-density, light-limited systems versus those in low-density, non-light limited systems. Two algal species are compared, the fast-growing, lipid-producing alga *Chlorella vulgaris*, and a slow-growing, hydrocarbon-producing alga, *Botryococcus braunii*, Race B. The hypothesis challenged with this comparison was that the intrinsic growth rates of the species would become irrelevant under light-limited production systems.

Introduction and Background

Botryococcus characteristics – oils, lipids, and growth kinetics

The green colonial microalga *Botryococcus braunii* possesses an unusual characteristic in that its individual cells are embedded in a hydrocarbon matrix; the nature of the hydrocarbon matrix has spurred classification of the *B. braunii* species into three races. Race A primarily produces alkadienes and alkatrienes derived from fatty acids, Race L produces linear tetraterpenes, and Race B produces branched triterpene hydrocarbons (Metzger et al., 1985; Wolf, 1985). Race B has attracted attention as a potential renewable resource for the production of liquid biofuels for a variety of reasons.

First, this alga produces isoprene hydrocarbons rather than lipids as an energy storing strategy, and it is capable of producing them to high levels of the biomass composition, typically 25-40% of the dry weight (Wolf 1983). These branched isoprene hydrocarbons, referred to as botryococcenes, have a variety of structures (C_nH_{2n-10}; n = 30-37) (Wolf et al., 1985), all of which

are highly reduced and have a high theoretical enthalpy of combustion (43.8 kJ/g for a $C_{34}H_{58}$ species). Because these oils are highly reduced and non-polar, they are totally insoluble with water, which facilitates the separation of the oils from water. An additional feature of the botryococcene oils is that they accumulate extracellularly, with only 7% of the botryococcenes located intracellularly (Wolf, Nonomura, and Bassham 1985). This reduces the energy input associated with extraction of botryococcene oils from algae, as it is not necessary to break open the algal cell walls to access the oils. Furthermore, the high-level extracellular oil accumulation can often result in colonies that are neutrally buoyant, even floating on the water surface (Wake and Hillen 1980). This would also aid in processing of the algal oils to fuel, because simply allowing the algae to float would result in concentration and dewatering without energetically intensive processes such as centrifugation or filtration.

Another large benefit of producing fuel from the botryococcene hydrocarbons is that they can serve as a drop-in substitute for crude oil in current catalytic cracking processes to gasoline, providing the ability to interface directly into existing energy production and utilization infrastructure. Hillen et al. (1982) demonstrated that hydrocracking of oils extracted from a natural lake-occurring bloom of the algae resulted in a distillate comprising of a 67% gasoline fraction, 15% aviation turbine fuel fraction, and 15% diesel fuel fraction.

B. braunii **growth characteristics compared to lipid producing algae**

The growth characteristics of *B. braunii*, Race B differ markedly from those of other microalgae. As demonstrated by Wolf et al. (1985), the growth rate of *B. braunii* Race B is slow compared to other microalgae; under optimal conditions (aerated with CO_2 supplementation) and at low culture densities, *B. braunii* was observed to double every 40 photohours, a rate of growth which has been replicated in the Curtis laboratory (data not shown). Furthermore, these authors

also demonstrated that the botryococcene hydrocarbon fraction of the biomass was relatively constant through the entire duration of a CO_2-supplemented, aerated batch growth curve, ranging from 24-29% of the total dry weight. Only a culture aerated with ambient air (no CO_2 supplementation) had a botryococcene content that varied over the batch time course, from 29% to 39%, although the productivity of this culture overall through the growth curve was much less than the CO_2 supplemented cultures. Depletion of inorganic nutrients (nitrogen, phosphorus) was not observed to induce accumulation of botryococcenes, as occurs with lipid accumulation in many other algae. These results suggest that the botryococcene is a growth-associated product of *B. braunii*, occurring simultaneously with cell growth (Figure 2.1)

Figure 2.1: Diagram of algal biomass and oil accumulation kinetics of each (A) *B. braunii* and (B) *C. vulgaris.*

The growth associated production of botryococcene oil by *B. braunii* is clearly demonstrated by the constant proportion of oil with the algal biomass. The nongrowth associated production of lipids by *C. vulgaris* is demonstrated by the region of rapid growth without lipid concentration increase, and the onset of lipid concentration increase at the end of the algal growth period.

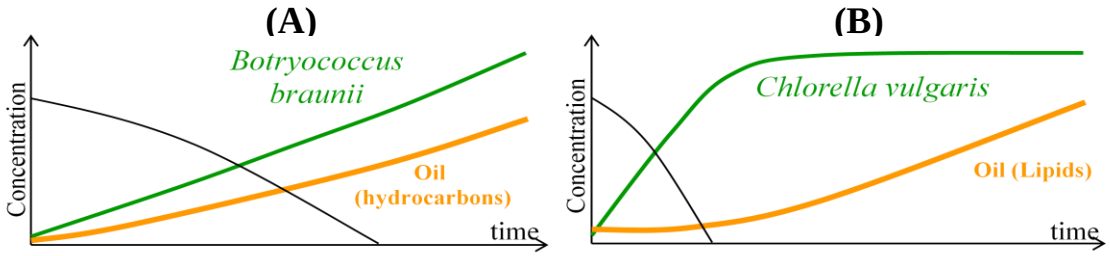

By comparison, the fast-growing, lipid-producing microalgae *Chlorella vulgaris* has doubling times of 5-6 hours under aerated conditions with CO_2 supplementation, as measured in the Curtis Laboratory. This particular alga accumulates lipids, and it is widely demonstrated that accumulation of the lipids occurs under conditions of nutrient deprivation when the cellular growth rate has slowed or ceased (Shifrin and Chisholm 1981; Collyer and Fogg 1955; Illman, Scragg, and Shales 2000). The lipids therefore have tendencies of growth-disassociated product formation (Figure 2.1). These biosynthesis kinetics of *B. braunii* and *C. vulgaris* suggest very different reactor operational schemes for maximum biomass and oil productivity. For *B. braunii*,

because oil production is concurrent with growth, the highest oil productivities will occur roughly when biomass is at its highest productivity, prompting a continuous-type reactor configuration (Metzger et al. 1985). For *C. vulgaris*, oil productivity will be offset from the peak of biomass productivity; the actual maximum point of *C. vulgaris* oil production will be dependent upon the accumulation of lipids once growth has ceased. This type of product formation kinetics is more amenable to a batch-type configuration, where the batch would be terminated upon reaching the maximum productivity.

Interestingly, the slow growth rate of *B. braunii* does not appear to be a symptom of either slow rates of CO_2 diffusion into the cells nor a sluggish metabolism; measured rates of CO_2 assimilation, O_2 generation, and even dark respiration compare to those reported for *C. vulgaris* (Wolf 1985). Rather, because the synthesis of isoprene hydrocarbons is so energetically intensive due to the high level of reduction and the large energy content of these compounds, much more energy must be diverted away from the synthesis of non-oil biomass, thus reducing the overall rate of biomass accumulation.

The lipids produced by *C. vulgaris* and other lipid-producing algae have less-desirable features than the botryococcene hydrocarbons: slightly water soluble thus complicating water removal; intracellular lipid accumulation thus requiring energetically-intensive extraction procedures; lower energy density per mass. However, the slow growth rate of *B. braunii*, nearly an order of magnitude slower than *C. vulgaris* and other faster-growing algae, is considered by many to eliminate the ability of this species to attain productivities competitive with faster-growing algae. Indeed, much of the research into algae-to-fuels is focused on prospecting, selecting, and genetically engineering for the algae strains with the fastest inherent growth rates, presumably because of the assumption that the faster an algae grows, the more productive it will be. However, this emphasis in current research trajectories is based on a significantly flawed assumption; that all nutrients will be available in unlimited quantities to allow the algal species to

grow at their maximum inherent rates. In reality, microorganisms can only grow at their maximum growth rates until some nutrient for growth becomes either yield- or rate-limiting. Much of the research with algae has centered upon nutrient-limited culture conditions, where some inorganic nutrient (nitrogen, phosphorus) runs out after some period of culture duration (yield-limitation), totally restricting further growth of the algae. The nutrient media typically used for algal culture typically have low inorganic nutrient concentrations to prevent toxicity effects to the algae, therefore batch culture cannot achieve high density cultures. For example, the nitrogen concentration in the original formulation of Chu-13 medium had only 6.9 mg of nitrogen per liter (Chu 1942) and later modified versions of the medium contain 27.7 mg of nitrogen per liter, which limit the total possible culture density of the algae to less than 1.5 g/L algae under batch growth conditions. While decreasing the nitrogen content of the media increases the lipid content, reducing nitrogen also limits biomass accumulation in a batch system (Piorreck, Baasch, and Pohl 1984). Therefore, under these growth conditions, growth will typically cease while the algae are still at low culture densities (< 3 g/L) (Shifrin and Chisholm 1981), which is not conducive to high productivities and economically feasible algal production.

This work, instead, focuses on algae grown under a condition of light-limitation, which imposes a rate-limitation rather than a yield-limitation. In a system that has been designed for maximal light utilization, growth under light-limited conditions results in much higher algal productivities, as will be shown in this work.

Algal Growth Kinetics, Mass Balances and the Effect of Light Limited Growth

For economic feasibility of an algae-to-fuels production technology, the system will need to trend towards both high volumetric productivity and low-capital cost reactor systems. Thus, the tendency towards dilute, batch-type systems are inherently less likely to provide economic

feasibility, because larger volume reactors will be required for a more dilute algal culture, and because the down-time between batch runs reduce available processing time. Other disadvantages of dilute systems include higher costs of water removal. Shifting instead towards a high-density, continuous reactor system to minimize reactor costs and maximize volumetric productivity, the limitations on the process change. For a continuous system, where algal biomass and oil are removed at a constant rate (the dilution rate, D), nutrients must be provided constantly to enable algal growth to replace removed biomass; the mass balances presented in Equation 2.1 and Equation 2.2 are for the algal biomass and the yield-limiting substrate, respectively.

General Case (Algal biomass)

$$\frac{d}{dt}(X_R\,V) = \mu^{NET}\,X_R\,V - Q_{out}\,X_{out}$$

Continuous, Steady State Case

$$\rightarrow \quad \mu^{NET} = {}^{Q_{out}}\!/_{V} = D$$

Equation 2.1

General Case (Yield-limiting Substrate *i*)

$$\frac{d}{dt}(C_{L,R}V) = Q_{in}\,C_{i,in} - \frac{1}{Y_{X/L}}\mu^{NET}\,X_R\,V - Q_{out}\,C_{i,out}$$

Continuous, Steady State Case

$$\rightarrow\ X_R = Y_{X/L}(C_{i,in} - C_{i,out})$$

Equation 2.2

It follows from **Equation 2.1** that under continuous, steady-state conditions the net specific growth rate of the algae, defined as $\mu^{NET} = \frac{1}{X}\frac{dX}{dt}$, is equal to the dilution rate (D) of the reactor system:

$$\mu^{NET} = D \qquad \textbf{Equation 2.3}$$

In the above equations, X_R and X_{out} are the concentrations of algal biomass in the reactor and flowing out of the reactor, respectively; V is the reactor culture volume; Q_{in} and Q_{out} are the volumetric flowrates of the process in and out of the reactor, respectively; D is the dilution rate; $C_{i,in}$, $C_{i,R}$ and $C_{i,out}$ are the concentrations of the yield-limiting substrate *i* flowing into, within, and flowing out of the reactor, respectively; $Y_{X/i}$ is the yield of algal biomass growth on the yield-limiting substrate *i*. In going from the general case to the continuous steady state cases, the

following assumptions are applied: the mass of biomass and substrate L in the reactor are constant, and therefore the accumulation terms on the left-hand-sides of the general case equations are set to zero; $X_R = X_{out}$; $Q_{in} = Q_{out}$.

Assuming that both the specific growth rate μ and the yield $Y_{X/L}$ are only very weak functions of the actual substrate concentration within the reactor, then the biomass concentration X_R is independent of the dilution rate (Pipes and Koutsoyannis 1962). Furthermore, the dilution rate of the reactor could, in theory, be run all the way up to the maximum possible growth rate of the organism, μ_{max}, above which wash-out of the reactor system would occur. Combining **Equation 2.3** and **Equation 2.4** results in the following expression for maximum productivity under inorganic nutrient limitation:

$$P_X = D\,X_R = \mu_{max}\,Y_{X/i}\left(C_{i,in} - C_{i,out}\right) \qquad \textbf{Equation 2.4}$$

While, in theory, a system could be run at nitrogen-limited conditions (or limited by some other inorganic nutrient), the algae concentration and therefore the biomass productivity will be directly dependent upon the nutrient concentration fed, as can be observed by **Equation 2.4**. Furthermore, under low concentrations of a yield-limiting inorganic nutrient, the growth rate will actually be restricted by the low concentrations of nutrients according to Monod kinetics, which will reduce the maximum possible growth rate and therefore chip away at the system's potential productivity; this is the classical example of a system's productivity being limited by a sub-maximal growth rate.

In order to increase the culture density, it could be argued that simply providing higher levels of the yield-limiting inorganic nutrient would allow growth of the culture to a higher algae concentration X_R, according to **Equation 2.2**. However, as algae concentration increases, the demand upon all nutrients in the system increases, requiring higher rates of provision of all nutrients to avoid limitation and keep the growth rate at its inherent maximum rate. Providing

sufficient inorganic nutrients for sustained growth of the algae is a comparatively simpler problem than ensuring sufficient provision of light (Pipes and Koutsoyannis 1962). Unlike nutrient limitation, where (in theory) the rate of nutrient feeding could be ramped up with culture density increase (as long as nutrient toxicity or counter-ion accumulation is avoided), there is a definite limit to the amount of light flux that can be provided to a photobioreactor system. It is limited on the supply side by the actual light provided from the source (there are cloudy days and winter months) as well as on the photobioreactor side by the geometry of the system. Furthermore, as the density of the algal culture in the system increases, the ability of light to penetrate into the depths of the culture is inhibited by the algal culture itself; absorption and scattering of the light attenuates light to an extreme degree, especially at high densities. For example, at an algal culture with an optical density of 20 (approximately 10 g DW/L algae), the light is attenuated to only 1% of its original intensity by a depth of 1mm within the culture due to absorbance alone.

In a photosynthetic system, light energy is the entire source of energy for cellular growth due to the absence of an alternative carbon/energy source. As the culture density increases, self-shading of the algae begins to limit the rate of light which is available to any given algal cell (Pipes and Koutsoyannis 1962). The point during algal growth at which the light available to each algae cell is insufficient to continuously sustain photosynthesis is where the culture becomes rate-limited by the light energy (photosynthetically active radiant flux, PARF, J/s) incident on the system. While Pipes and Koutsoyannis (1962) state that this point of light-limitation can be characterized by some population density of the algae in a continuous system, in reality there is not one unique population density at which the onset of light limitation will occur for a given system. In reality, this point is dependent upon two factors resulting from an increased algal population: both the amount of light available to each individual algal cell decreases (due to self-shading of the algal culture), and the overall rate of algae accumulation increases (such that the

demand for light energy at some point exceeds what is available). This is particularly evident in a batch growth system; the actual population density measured at the observed point of light-limitation is dependent upon how fast the algal culture is growing.

The transition from exponential, non-limited growth to light-limited linear growth is characterized by K, the constant overall rate of increase of the culture as a whole (Pipes and Koutsoyannis 1962):

$$V\frac{dX}{dt} = K \qquad \textbf{Equation 2.5}$$

At constant volume, the growth profile of X in a batch system thus results in a linear curve with respect to time. In a continuous system, the algal culture density will approach the steady state algal density, X_{SS}, according to the expression in **Equation 2.6**, where at large *t* X_{SS} is obtained from **Equation 2.7**.

$$X(t) = \frac{K}{V\,D} + \left(X_0 - \frac{K}{V\,D}\right) e^{-D\,t} \qquad \textbf{Equation 2.6}$$

$$X_{SS} = \frac{K}{V\,D} \qquad \textbf{Equation 2.7}$$

X_0 is the population density at the onset of light limitation. From **Equation 2.6**, it is evident that when $X < X_S$, X will approach the equilibrium population density $\frac{K}{V\,D}$ asymptotically from below; thus in light-limited continuous culture, the culture density is inversely proportional to the dilution rate of the continuous system. Thus the productivity for the light-limited system becomes:

$$P_{X,LL} = X\,D = \frac{K}{V\,D}\,D = \frac{K}{V} \qquad \textbf{Equation 2.8}$$

and the productivity of the light-limited system should be only a function of the light-limited growth constant and not of the dilution rate of the system. Therefore, in the light-limited continuous system, the productivity is NOT governed by the algal species' inherent growth rate, but instead by the efficiency of the system at capturing light for algal growth.

This analysis sets the stage for a comparison of the biomass and oil productivities of *B. braunii* and *C. vulgaris* in a high-density, light-limited photobioreactor, where the hypothesis was that under a high-density, light-limited photobioreactor system the productivities of the two species would converge. The head-to-head comparison of *B. braunii* and *C. vulgaris* in a light-limited photobioreactor was the subject of a previous Curtis Lab member's M.S. thesis, Lisa Grady (2010), where the author of this work contributed to the reactor runs. Reference is made to her thesis for the full details of the experimental set-up and conditions, but the major points are summarized in the following section. Furthermore, the author expanded upon the results of the head-to-head comparison with additional quantitative analysis and growth studies, and these results, in the context of the original head-to-head comparison, are the focus of the remainder of this chapter.

Biomass and Oil Productivities of Two Alga in a Light-Limited, Continuous System

B. braunii and *C. vulgaris* were each cultivated in a vertical trickle-screen photobioreactor, where the 0.5L total volume of algal culture was continuously cycled from a reservoir to the top of the screen, allowed to trickle in a thin film down the screen, and then re-collected in the reservoir. The large surface area of the screen and the thin film of the algae flowing over it allowed light penetration even at high culture densities (~ 20 g dry weight (DW) algae/L). The screen was housed within a transparent plastic enclosure to allow continuous provision of humidified air supplemented to 5% v/v with CO_2 to the algae culture at a rate of 6.47 L/min. The entire photobioreactor was located within a controlled environment plant-growth chamber, which provided artificial light measured at a photosynthetic photon flux density (PPFD) of 282 μmol/m^2/s normal to the plane of the trickle-screen for 16 hours a day, with 8 hours/day darkness. During the beginning and final hour of each 16-hour lighted period, the lighting was

reduced to 1/3 of the power to simulate 24-hour diurnal sunlight periods. Supplemental carbon dioxide was turned off during the dark hours, and only ambient humidified air was provided to the system. Ambient temperature in the growth chamber was controlled to 28°C during the day and 25°C at night. Temperature of the algal culture in the photobioreactor was maintained using a heat-exchanger supplied with recirculated cooling water at 25°C from a Fisher Scientific Isotemp Refrigerated Circulator.

For each *C. vulgaris* and *B. braunii*, the system was run at a daily dilution rate of 7.5%, which was previously established to be the optimum for *B. braunii* continuous, light-limited growth (Curtis Lab, unpublished). Thus, 37.5mL of the total culture was removed daily and replaced with inorganic nutrient media sufficient to replenish the estimated amount of nitrogen consumed and allow re-growth in the next 24 hours. Prior to reaching the light-limited steady-state culture density, more nutrients than consumed were provided to allow growth to the higher density.

Figure 2.2 and Table 2.1 present the key results of these studies; following is a summary of the results and discussion presented in Grady (2010), noting that the author contributed both to the experimental work as well as the editing of the material presented in Grady (2010). As can be observed by Figure 2.2 and Table 2.1, the steady-state algal biomass densities and productivities of each *B. braunii* and *C. vulgaris* were quite similar, despite the order of magnitude difference in their inherent growth rates. Although the difference in the actual concentrations between the steady state biomass concentrations was statistically significant, with *Botryococcus* having a steady state biomass concentration 10.8% higher than that of *Chlorella*, this is a rather small difference from process standpoint given the large magnitude of the difference between the organism's inherent maximum growth rate. This demonstrates that under light-limited high-density photobioreactor culture, run under the same dilution rate, the biomass productivities converge as predicted for light-limited growth. The chosen dilution rate of 7.5% for the system

Figure 2.2: Steady-state algal biomass concentrations of each *B. braunii* and *C. vulgaris* in the continuous trickle-screen photobioreactor versus time in the reactor.

The uncertainty associated with the concentrations is the standard deviation of all measured algal biomass concentrations during the steady-state period. Despite order-of-magnitude differences in the growth rate of the two algal species, under light-limited conditions and the same dilution rate (7.5% / day) the biomass concentrations (and therefore the biomass productivities) converged to very similar values. (Adapted from Grady 2010)

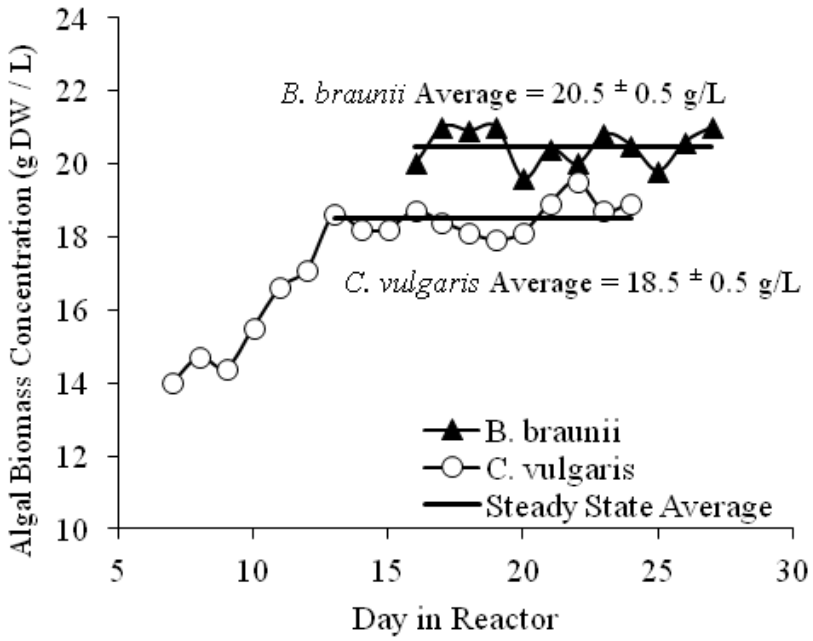

Table 2.1: Algal biomass concentration and biomass productivity observed during the steady-state period of a continuous high-density, trickle-screen photobioreactor run.

(Adapted from Grady 2010)

Algae Strain	Biomass Concentration (g/L)	Biomass Productivity (g/L/day)
Botryococcus	20.5 ± 0.5	1.54 ± 0.04
Chlorella	18.5 ± 0.5	1.39 ± 0.03

was optimized for *B. braunii*; this corresponds to a generation time of 9.2 days (148 photohours), which is significantly slower than *B. braunii'*s maximum inherent growth rate of ~ 40 photohours, preventing the issue of wash-out with this slower growing algae. However, because the minimum doubling time of *C. vulgaris* is only 5-6 hours, the growth of *C. vulgaris* in this system is even more severely attenuated. The 7.5% dilution rate was also chosen as the process

Table 2.2: Lipid concentration in algal culture and lipid productivity observed during the steady-state period of a continuous high-density, trickle-film photobioreactor run.

(Adapted from Grady 2010)

Algae Strain	Oil Lipid Content (g / 100 g cell)	Oil Concentration (g/L)	Oil Productivity (g/L/day)
Botryococcus	17.2 ± 3.6	3.5 ± 0.7	0.27 ± 0.05
Chlorella	6.7 ± 0.7	1.1 ± 0.1	0.085 ± 0.009

condition for *C. vulgaris* for several reasons. First, a direct comparison with the *B. braunii* system was desired. Secondly, this attenuation of the *C. vulgaris* growth rate was a way to force slow growth of the alga and therefore was reasoned to be a way of inducing lipid accumulation. Finally, according to light-limited growth kinetics, the productivity of the system was predicted to be independent of the dilution rate of the system (Equation 2.8).

Although the algal biomass productivities were nearly the same for both *B. braunii* and *C. vulgaris*, the oil productivities between the two species were substantially different, as shown in Table 2.2. The oil productivity for *B. braunii* is one of the highest algal oil productivities reported in the literature, and while the oil productivity for *C. vulgaris* is still appreciable, it is not the highest for this species nor among algal production systems as a whole (see the comparison of these results with literature reports at the end of this chapter). The surprising difference in oil productivity between the two algal species in the work of Grady (2010) indicates that this system is not ideal for oil production by *C. vulgaris*. It appears that repressed growth rate alone is insufficient to trigger lipid accumulation of the algae as long as inorganic nutrients are being provided continuously. In fact, the average steady-state biomass lipid composition observed in this system (6.7%, ranging from 5.40-7.15%) is even lower than a value reported for the lipid content of *C. vulgaris* from membrane lipids only: 9.2% lipid by gravimetric extraction (Northcote et al., 1958). However, the likely difference between these values is attributable to the difference in extraction method, as the method employed in this work is a direct, *in situ* esterification of all lipids in the cell and subsequent quantification by gas chromatography, which

all but eliminates the likelihood of over-estimation of lipid content due to solubility of non-lipid cell components in the extraction liquid. Other reports of batch-grown *C. vulgaris* state much higher observed lipid contents at the end of the batch reactor run; Illman et al. (2000) report *Chlorella* compositions of 40% lipid at the end of a 16-day batch run, and (Z.-Y. Liu et al., 2008) reports 58% lipid at the end of a 25-day batch run; the authors of both of these reports quantified lipid via chloroform/methanol extraction and gravimetric determination. Despite the differences in analytical methods, these results suggest that in the steady-state, continuous light-limited photobioreactor system explored in the work of Grady (2010), primarily membrane/structural lipids were produced and storage lipid production was minimal.

To quantify the energetics of light capture by each *B. braunii* and *C. vulgaris* in the high-density photobioreactor system, bomb calorimetry determinations were made, which is the subject of a later section of this chapter (Results and Discussion: Energy capture in algal biomass and oils by *B. braunii* and *C. vulgaris* in the continuous, high density trickle-screen photobioreactor). To investigate whether *C. vulgaris* productivities could be enhanced by growth in a batch-type operational mode, batch growth experiments were carried out, detailed in a later section of this thesis chapter (Results and Discussion: Batch growth comparison of *C. vulgaris* under both light-limited and non-light limited conditions). A key aspect of these batch growth experiments was to provide sufficient biomass for the quantification of lipids by both DTE (direct *in-situ* trans-esterificaton) as well as extraction and gravimetric determination, to provide a better basis for the comparison of the lipid productivities reported in the work of Grady (2010) with productivities in the literature determined gravimetrically. The significance of these further studies was to enable a deeper understanding of the utilization of light energy by both *C. vulgaris* and *B. braunii* for useable oil production in light-limited and non-light limited systems; this knowledge provides direction for future work in the development of algal biofuel production systems towards economically feasible technologies.

Materials and Methods for Batch Air-Lift Reactor Studies

Algal Cultures:

The algae strain *Chlorella vulgaris* is indexed at UTEX as culture number 2714, and the algae strain *Botryococcus braunii*, race B was obtained from the University of Kentucky (Berkeley, Showa strain) (Nonomura 1988).

Algal Media Formulations

In designing the mediums for algal growth utilized in this work, a key consideration was the need for high-density cultures. Therefore, the medium would need to support growth to 20 g DW/L or higher. Algal growth medium formulations previously described in the literature, such as Chu-13 (Chu 1942) and HS (Sueoka et al., 1967), were formulated for growth to 1-2 g DW/L, as assessed by an analysis of the formula for the yield-limiting inorganic nutrient, which typically was determined to be nitrogen. Furthermore, they clearly had very high levels of some inorganic components (potassium, chlorine, phosphorus, or sulfur) relative to the degree of biomass growth that could be supported by the limiting nutrient. Therefore, attempting to directly scale these imbalanced formulations to support the targeted high-density growth could lead to salt toxicity due to accumulation of unused nutrients. To facilitate growth to high-density culture, a balanced medium (Wayne's Freshwater Algae Medium, WFAM) was developed based on comparison of the existing algae formulations, as well as plant tissue culture media such as MS (Murashige and Skoog 1962) and B5 salts (Gamborg et al., 1968). The rationale for utilizing plant based media is that composition of algae and higher plants should be similar for mineral nutrients and plant

tissue culture has been implemented successfully for decades of serial heterotrophic culture to densities of 10-20 grams dry weight (g DW) without problems of accumulated toxic salts.

The composition of WFAM (Appendix A) was developed based on nitrogen as the reference nutrient for assessing the culture density the medium would support. 0.3 g N/L was chosen as an arbitrary baseline medium strength, which could support biomass growth up to 3 gDW/L assuming 10% nitrogen by weight of the biomass. Therefore, the concentrations of all media used in this work are expressed in terms of their relative concentration to this '1X strength' formulation. The WFAM formulations used specifically for *Botryococcus braunii* culture included both ammonium and nitrate as nitrogen sources, as is used in plant media to provide a balance of pH during nitrogen utilization. The composition of WFAM used for *C. vulgaris* used only nitrate as a nitrogen source, to avoid issues of pH control resulting from the rapid assimilation of ammonium by *C. vulgaris* that could result in the death of the algal culture due to pH shock. In addition, WFAM for Chlorella contained only $1/10^{th}$ the Calcium Chloride as regular WFAM; this change was made to bring the concentration of calcium in the medium closer to that of other *Chlorella* media formulations as well as was a means to reduce the chlorine present in the medium, which is not taken up by the algae and could accumulate in the culture.

Lighting and Temperature

Experiments were carried out in a Conviron BDW120 walk-in incubator equipped with high-intensity lighting supplied by banks of Philips (#36881-1) 400W high-pressure sodium vapor and Philips (#34415-0) 400W metal-halide lamps contained in chilled loft that is constructed of plexiglass to decrease UV radiation by 20%. This environmental chamber allowed for mimicking 24-hr diurnal sunlight periods; the lights would come on at 1/3 power for the first and last hour of the 16-hr lighted photo-period. Local photosynthetically active photon flux

densities (PPFD, μmol quanta/m^2/s) of photosynthetically active radiation (PAR) were measured with a LICOR LI-1400 data logger and LI-190SA quantum sensor. Measurements were made normal to the vertical surfaces of the air-lift bag reactors. Each reactor surface was divided into four quadrants and light measurements were taken at each of the four corners of the quadrants (9 measurements total over the surface of the bag surface). The four measurements for each quadrant were averaged to give an average PPFD for the quadrant, and this was multiplied by the area of the quadrant (m^2) to obtain the photosynthetically active radiant flux (PARF, μmol quanta/s) for the quadrant. The radiant fluxes for all quadrants for a bag reactor were summed to obtain the total PARF for each reactor. The environmental growth chamber temperature was controlled at 28°C during lighted hours and 25°C during dark hours with a linear temperature change during the lighting warm-up and cool down; the selection of temperature control was based on the fact that the chamber was shared with other plant growth, whose needs dictated this diurnal temperature cycling.

Growth Measurements

Optical Density: Optical density measurements were made using 1-cm pathlength cuvettes on a Beckman DU-520 Spectrophotometer at 550nm (OD_{550}). This wavelength was selected because it is insensitive to changes in chlorophyll content, and thus correlates best with actual biomass concentration without interference from chlorophyll absorbance (at 680nm) (Berberoglu, Gomez, and Pilon 2009). The samples were diluted with tap water prior to analysis to bring the measured OD below 0.4 to ensure linearity of the response.

Biomass Concentration Measurements, *Chlorella vulgaris:* Polypropylene microcentrifuge tubes (1.7 mL) were pretared to 4 decimal places (0.0001 g) and handled with clean-room gloves. For each sample replicate, two precise aliquots of 0.750 mL were transferred

to the pre-tared tube using a P1000 Pipetman. The centrifuge tubes were then centrifuged at 14,000 RPM for 5 minutes on a Beckman Coulter Microfuge 18 centrifuge. The supernatant was poured off and each pellet was re-suspended in 1mL of tap water (to decrease osmotic shock and avoid lysing cells), and the centrifuge tubes were re-centrifuged as above. The supernatant was again poured off, and the tubes were stored at -20°C until freeze drying. For freeze-drying, the tubes were transferred to a -80°C freezer for 30 minutes; the tops were popped open, and the samples were freeze dried in a Labcocno freeze dryer for at least 24 hours. After freeze drying, the mass of the cell pellets was determined by difference and the dry weight algae biomass concentration was determined from the initial volume of algal culture placed into the tubes.

Biomass Concentration Measurements, *Botryococcus braunii:* Because *B. braunii* colonies are at times neutrally buoyant, and will not always settle even upon centrifugation, the rinsed-cell pellet method for biomass concentration determinations could not be utilized here. Using clean room gloves, a small hole was punched directly into the tip of a 0.6 mL polypropylene microcentrifuge tube using a thumbtack. Two layers of glass fiber filters (GelmanSciences Extra Thick glass fiber filger, 47mm, P/N 66078) were placed on top of each other, and a small circle was cut out using a P5000 plastic pipetteman tip. This cut-out filter paper piece was transferred into the tip the microcentrifuge tube, and care was taken to clear stray fibers stuck to the outside of the tube. This assembly was pre-tared to 0.00001 g, and was then placed inside of a 2.0-ml polypropylene centrifuge tube with the snap cap cut off (to allow the assembly to fit within the centrifuge). To prime the filter and set the filter in place, 0.3 mL of distilled water was transferred to the top of the filter using a P1000 pipettman, and this liquid was driven through the filter by centrifuging in a mini, single-speed centrifuge (Capsule HF-120, Tomy Seiko Co., LTD.) for 30 seconds; the liquid passed through the filter and collected in the 2.0-mL microfuge tube was discarded. To collect a measurement, a 0.3ml aliquot of well-mixed *B. braunii* culture was transferred to the top of the primed filter, and the liquid was driven

through the filter by centrifuging in the same centrifuge for 2 minutes; the filtrate collected in the 2.0-mL microfuge tube was then discarded. To rinse the cell pellet, 0.3 mL of distilled water was transferred to the top of the filter and algal filter cake/pellet, and this was driven through the filter by centrifuging again for 2 minutes. At the end of each centrifugation step, the liquid collected in the 2.0-mL microfuge tube was inspected for breakthrough of the *B. braunii* colonies; if breakthrough was observed the sample was discarded and the measurement repeated. The samples in the 0.6-mL microfuge tubes were stored at -20°C until they were freeze dried. After freeze drying, the mass of the cell pellets were determined to 0.00001 g on an analytical balance. The dry weight algae biomass concentration was determined from the final freeze dried weight of the cell pellet/filter cake and the initial volume of algal culture placed into the tubes.

Freeze Drying: For freeze-drying, the microfuge tubes containing the biomass samples were transferred to a -80°C freezer for 30 minutes; the snap caps were popped open, and the samples were freeze dried in a Labcocno freeze dryer for 24 hours. After freeze drying, the mass of the cell pellets were determined to either 0.0001 or 0.00001 g on an analytical balance (depending on the precision of the pre-tared weight).

Theoretical Prediction of botryococcne heat of combustion

The enthalpy of combustion of botryococcene hydrocarbons was predicted using bond energies (Hill and Holman 2000) and the balanced reaction for the complete combustion of a representative botryococcene species, selected as a $C_{34}H_{58}$ botryococcene with the structure shown in Appendix B (Anirban Banerjee et al. 2002).

Growth of Botryococcus braunii for obataining oils for calorimetric determinations

B. braunii was grown to generate sufficient triterpene hydrocarbon oil for calorimetric determinations. Flask-grown (100-200ml) *B. braunii* cultures, under a 16-hour light/8-hour dark light cycle were started at low culture density from a parent culture, which was inoculated into 0.5X (1/8xNH_4^+) WFAM (see Appendix A). These cultures were grown at photon flux densities ranging from 50 -150 μmol/m^2/s and the headspace of the flasks was provided air supplemented with CO_2 to 5% (v/v). The inoculum cultures, in shaker flasks, were also supplemented with ~5% CO_2 v/v in air by mixing pure CO_2 from a gas cylinder with compressed building air using rotameters set to achieve the appropriate gas concentration mixtures. Evaporation was minimized by humidifying the gas stream by passing it through sintered glass spargers in a train of three 500-mL flasks containing distilled water. The gas was passed to the flask cultures (arranged as a "daisy chain" of three flasks) through a 0.2 μm Gelman Acro 37TF gas vents at the flask inlets and sterilized non-absorbent cotton at the flask outlet. The flasks were subcultured at a weekly dilution rate of 25%, and were fed based on a nitrogen mass balance in the flasks, using algal biomass measurements and assuming 5% of the total biomass was nitrogen. Various WFAM media formulations varying in overall strength and NH_4^+ / NO_3^- ratios were employed in the feeding, in order to match the total nitrogen feeding requirement as well as to maintain pH in the range of 7.5-8.5 in the flasks. The ratio of inorganic nutrients other than nitrogen were fed in a constant ratio to nitrogen, according to the ratio of WFAM (Appendix A). The cultures were harvested by filtering the culture through a 20 μm mesh, which retained the *Botryococcus* colonies but allowed the media to filter through, and the filter cake was scraped into a plastic tube, where it was frozen at -20°C until ready for extraction.

Botryococcus extraction and purification procedures

Quantitative determination of cellular triterpene (botryococcene) oil content: For determination of triterpene hydrocarbon content of frozen (-20°C) *B. braunii* culture samples from the high-density trickle-screen reactor system, extraction was performed by the laboratory of Joseph Chappell at the University of Kentucky (College of Agriculture, Department of Plan and Soil Sciences, Lexington, KY). 1mL of thawed culture was vortexed in a glass vial with 1mL of acetone for 2 minutes. 1 ml of n-hexane was added and the mixture was vortexed for 2 minutes, then the vial was centrifuged at 750 RCF for 1 minute. The hexane phase was removed to a glass gas chromatography vial and evaporated to dryness with a stream of N_2 gas. The hexane extraction was repeated on the sample by adding another ml of n-hexane and repeating the vortexing, centrifugation, and hexane removal steps. The second hexane extract was pooled with the first in the GC vial, and the hexane was again evaporated under a stream of N_2 gas. The dried oil extract was then re-suspended with exactly 1.000 mL of hexane and was analyzed by GC-FID, as described below.

Oil calorimetric determinations: For extraction of triterpene hydrocarbons for calorimetric determinations, a modified, scaled-up version of this extraction procedure was used. For every 20mg of fresh weight algae sample being extracted, 1mL of distilled water and 1mL of acetone was added to the algae sample in a separatory funnel; the funnel was shaken for 1-2 minutes. The same volume of n-hexane was then added to the separatory funnel and the funnel was again shaken for 1-2 minutes. The contents of the separatory funnel were then added to 15 mL conical bottom glass centrifuge tubes (Kimble Chase, p/n 73802-15415) with Teflon lined caps (Kimble Chase, and the extraction mixture was centrifuged for 3 minutes at 750 RCF using a Beckman-Coulter Allegra X-12R centrifuge and SX4750 rotor to induce separation of the organic (top) and aqueous (bottom) layers. After centrifugation, the organic layer from all centrifuge tubes was

removed and combined into a tared glass vial. The aqueous portions still remaining in the centrifuge tube were then recombined into the separatory funnel, and the same volume of n-hexane was again added, and the extraction and centrifugation steps were repeated. The organic layer was again removed from the centrifuge tubes and was pooled with the previously collected organic layers. Evaporation of hexane was carried out using a Büchi HB-140 Rotovap, set up with a recirculated cooling bath at -14 - -4°C. The apparatus was purged three times with nitrogen gas prior to starting evaporation; evaporation was carried out under vacuum (16-20 in Hg) and the hexane phase was rotated in a heated water bath at 40°C. The residue, which contained the botryococcenes as well as pigments and other hexane-soluble components, was then purified by flash column chromatography: a silica gel column (1.2 cm ID x31 cm) was packed by the slurry method using a silica gel to n-hexane ratio of 1g/2.5 mL. The progression of the column chromatography was monitored by watching the movement of the pigment bands down the column, and the elution was ceased just prior to the elution of the pigments. The collected hexane, containing the triterpene hydrocarbons was then evaporated using the rotovap as described above.

GC-FID Quantification of Triterpene Oils (Botryococcenes)

The hexane extracts were analyzed by the Laboratory of Joseph Chappell at the University of Kentucky (College of Agriculture, Department of Plan and Soil Sciences, Lexington, KY). Quantification was made using an HP 5890 Gas Chromatograph with an Flame Ionization Dector detector and a Restek Rtx®-5ms fused silica column (30m, 0.25 mm ID, 0.25 μm df). The following program was used: initial temperature 220°C, hold for 1 minute; ramp at rate of 20°C/min until 280°C, then ramp at a rate of 3°C/min until 320°C; hold at 320°C for 5 minutes. Using this method, C_{30} botryococcene eluted at 8.7 minutes and C_{30} squalene eluted at

10.3 minutes, as determined by running botryococcene and squalene standards. A typical chromatogram resulting from this analysis is provided in Appendix C. The majority of the oils in the hexane extract were C_{32} and C_{34} botryococcenes, which eluted at 9.2 and 9.5 minutes respectively. Squalene standards were prepared from squalene purchased from Sigma (≥ 98% purity), where 40.0 mg of squalene were dissolved in exactly 20ml of hexane to give a 2μg/μL standard concentration. Standards were run with each analysis to generate a calibration curve for hydrocarbon quantification. The areas of each botryococcene and squalene peak were correlated to a hydrocarbon mass, and the sum of these was determined to a total mass of hydrocarbon in the injection, which was back-calculated to a concentration of triterpene hydrocarbon in the original *B. braunii* culture sample.

Enthalpy of Combustion Determinations by Adiabatic Bomb Calorimetry

The enthalpy of combustion of freeze-dried algae total culture samples, freeze-dried cell pellet samples, and extracted botryococcene hydrocarbon oil were determined using a Parr model 1710 adiabatic bomb calorimeter (Penn State Energy Institute). Because of the small mass of the samples, the samples were combusted concurrently with a benzoic acid tablet of known mass and enthalpy of combustion and the enthalpy of combustion of the algal samples was determined by difference. A correction for the additional heat released due to the formation of aqueous nitric acid oxidized nitrogenous components during combustion was applied: the water remaining in the bomb post-combustion was rinsed out with a methylene orange solution, and then titrated with a 0.03545M sodium carbonate solution until the methylene orange solution turned pink. The volume of titrant required to reach the endpoint is proportional in a 1 mL:1 calorie ratio to the calories of additional energy released due to the nitric acid formation.

Lipid Quantification Methods:

Direct Trans-esterification (DTE) Method: Method development and sample analysis was performed by the National Energy Technology Laboratory (Pittsburgh, PA). Each sample was subjected to direct transesterification and extraction in duplicate with each replicate injected into the GC-FID in triplicate. Direct esterification was performed by reacting 3.5 mg of biomass sample with acidic methanol using an acid: biomass ratio of 6.4:1, at 120 °C for 2 hours. Upon cooling, samples were spiked with known amounts of C_{13} and C_{17} triacylglyceride (TAG) as extraction recovery standards, and an equal volume of 20% $CaCl_2$ (w/w) was added. The mixture was extracted three times with hexane with all extracts were combined and dried over $CaCl_2$ and nitrogen. The resultant FAMEs were dissolved in 100 µl of toluene and analyzed by GC immediately. Spike recoveries as fatty acid methyl esters (FAME) were calculated to both verify the extent of reaction as well as correct for total lipid in the sample.

Bligh-Dyer Extraction and Gravimetric Quantification: Three-100 mg portions of the freeze dried algal cells were each homogenized with 1.875 ml of 2:1 (MeOH:$CHCl_3$) for 2 minutes in glass vials with a PTFE lined caps. Next, an equal volume of $CHCl_3$ was added and the samples were homogenized for an additional 2 minutes. Once complete, 1 ml of a 20% $CaCl_2$ solution was added and the samples were inverted several times prior to centrifugation at 2200 rpm for 10 minutes. After centrifugation, the lower layer was removed by pipette, filtered and transferred to a pre-weighed glass vials with PTFE caps. The samples were re-extracted with a fresh 1.25 ml volume of $CHCl_3$ by vortexing for 60 seconds, followed by centrifugation at 2200 rpm for 10 minutes. The lower layers were removed by pipette, filtered and combined with the first. The total extract solution was weighed and ~525 µl of this solution was transferred into two separate pre-weighed reaction vials, thus generating three portions of extract per sample trial. The mass of the portioned sample was weighed and all extracts were dried to constant mass under a

stream of N_2 gas. Once dried, the gravimetric yield was determined in triplicate for each extract and the sum of triplicate extractions were used for the final yield determination.

Bligh-Dyer Extraction and GC-FID Quantification: The resultant residues that were produced during the Bligh-Dyer extraction were treated in the direct extraction and transesterification reaction as if the extract were an algal sample. Thus each extract was transesterified in duplicate with triplicate GC-FID injections for quantitation. The values for the weight % lipid in the extract and weight percent lipid in the cells (based upon extraction) were determined by averaging the lipid content of all three extractions for each sample (and their duplicate esterifications).

Procedures for Execution of Batch Loop Air-lift Reactor Experiments

Loop Air-lift Bag Reactor Construction: Bag reactors (Figure 2.3 A) were constructed of translucent plastic sheeting (4mil Low Density polyethylene plastic tubing, 18" wide, purchased from U.S. Plastic Corp) heat sealed to form an air-lift loop reactor with a single baffle and with the dimensions indicated (Figure 2.3 B). The bioreactors were fabricated using a W-605A 24-inch Single Impulse heat-sealer with 5mm seal. Settings for sealing the polyethylene were 1.0 for Recycle, 3.8 for Congealing, and 4.0 for Sealing. The baffle was achieved by placing a sheet of paper on either side of the sheeting, above and below the baffle position to prevent sealing. The bag was sandwiched between wire racks for support to give a thickness of approximately 3/4". Total volume of the bag at the start of the experiment was 1.5L, which provided an initial working volume height of 12.5" from the riser bottom. At the start of the experiment, the exposed area of the reactor bag (0.162 m^2) received an average light flux of 274 $\mu mol/m^2/s$, measured perpendicularly to the reactor bag surface. Throughout the experiment, the reactor bag was sparged at 0.2 vvm with air supplemented with CO_2 to give a total volumetric CO_2

Figure 2.3: Loop Airlift Bag Reactor, Photograph of reactor filled with water (A) and schematic with dimensions (B).

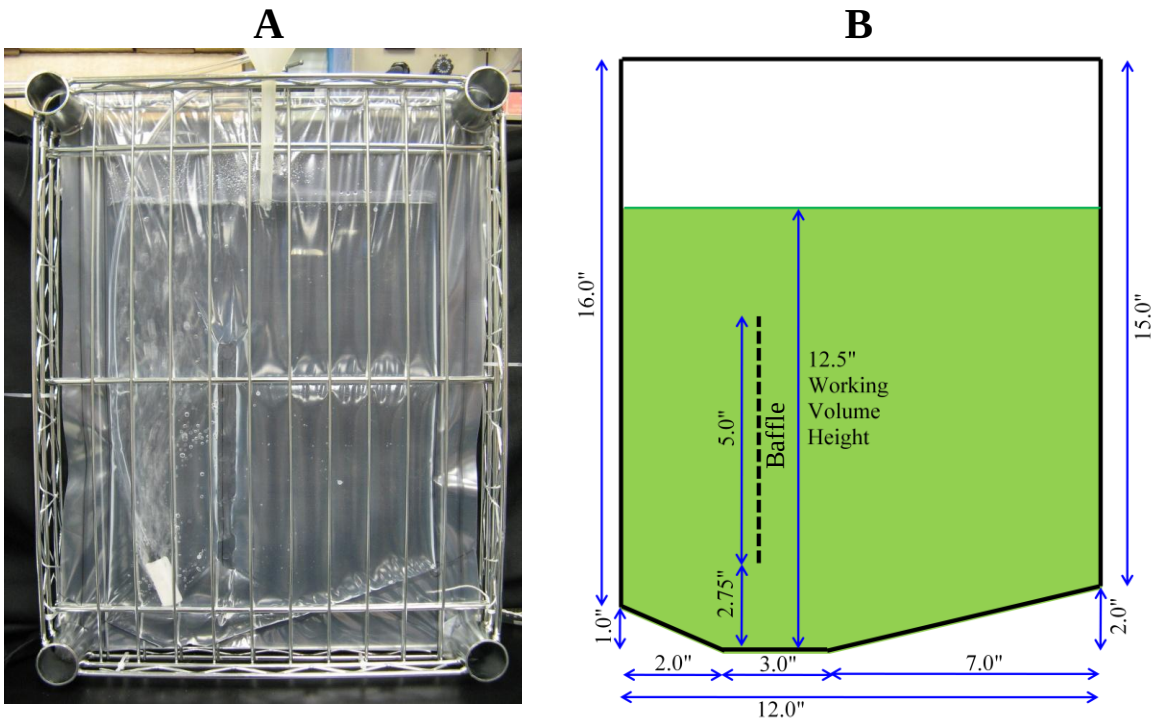

concentration of 5%. The gas concentration was obtained by mixing pure CO_2 from a gas cylinder and building compressed air using rotameters set to achieve the appropriate volumetric flow rates of each gas (Sho-Rate Model 1355E Rib Guided Tubes, Spherical Floats).

Inoculum Preparation: Inoculum cultures for the batch airlift-loop bag photobioreactors ("Bag Reactors") were midlog cultures of *Chlorella vulgaris*, UTEX 2714, grown in 100 mL of 1X nitrate-only (0 NH_4^+) WFAM media with only $1/10^{th}$ the calcium solution as 1X WFAM (see Appendix A), as per the standard *Chlorella* medium preparation. The inoculum was cultivated in 250 mL Erlenmyer flasks on a shaker at 132 rpm; cultivation time was approximately 24 photohours on a 16 hour light / 8 hour dark cycle at an approximate light intensity of 500-550 $\mu mol/m^2/s$. The inoculum cultures, in shaker flasks, were also supplemented with ~5% CO_2 v/v in air by mixing pure CO_2 from a gas cylinder with compressed building air using rotameters set

to achieve the appropriate gas concentration mixtures. Evaporation was minimized by humidifying the gas stream by passing it through sintered glass spargers in a train of three 500-mL flasks containing distilled water. The gas was passed to the flask cultures (arranged as a daisy chain of three flasks) through a 0.2 μm Gelman Acro 37TF gas vents at the flask inlets and sterilized non-absorbent cotton at the flask outlet.

Prior to inoculation, the optical density (OD) of the inoculum culture was measured at 550nm in triplicate (Beckman DU-520 Spectrophotometer); the culture was diluted in order to bring the OD in the cuvette to less than 0.4 to avoid non-linearity. Using the measured OD, the inoculum volume required to obtain a final OD of 0.1 in each of the bag reactors was determined. This volume of inoculum was centrifuged for 5 minutes at 2,000 RCF (Beckman Coulter Avanti JE Centrifuge, JA-14 Rotor), and the supernatant medium was decanted to remove remaining extracellular nitrogen from the inoculums. The culture was re-suspended in 1X WFAM without any nitrogen source and with $1/10^{th}$ the calcium as WFAM, re-centrifuged as above, and re-suspended in 20.5 ml of the same nitrogen free medium so that a 5ml aliquot of concentrated algal culture would be inoculated into each of the four bag reactors.

Media Formulations: The concentration of inorganic nutrients for the batch bag reactor treatments are provided in Table 2.3 below; the rationale for the nutrient concentrations utilized in the treatments is explained later in the results section. The initial doses of nutrients (both treatments) were provided at the start of the experiment; the second dose of inorganic nutrients for the light-limited treatment was provided after 21.8 photohours of growth.

Table 2.3: Inorganic Nutrient concentrations in the Batch Bag Reactors

	Non-Light Limited Treatment (NL)			Light-Limited Treatment (LL)		
	Nitrogen (as KNO_3) (g N / L)	**Calcium (as $CaCl_2$) (g Ca/L)**	**All other inorganic nutrients**	**Nitrogen (as KNO_3) (g N / L)**	**Calcium (as $CaCl_2$) (g Ca/L)**	**All other inorganic nutrients**
Initial Nutrients	0.031	0.00153	At 0.425X WFAM conc.	0.070	0.00343	At 0.953X WFAM conc.
2^{nd} Feeding	n/a	n/a	n/a	0.070	0.00343	At 0.953X WFAM conc.

Growth Measurements – Optical Density: Optical density was monitored with triplicate determinations throughout the duration of the batch bag reactor cultures; measurements were made on a Beckman DU-520 Spectrophotometer at 550nm with a 1cm cuvette. The samples were diluted with tap water prior to analysis to bring the measured OD below 0.4 to ensure linearity of the response.

Growth Measurements – Biomass Concentration: Biomass concentration was monitored in triplicate at various timepoints throughout the duration of the batch bag reactor cultures; for each replicate, two aliquots of 0.750 mL were transferred to a pre-tared 1.7 mL centrifuge tube using a P1000 Pipetman. Gloves were worn whenever the dry weight samples were handled to minimize weight added to the tubes from skin oils. The centrifuge tubes were centrifuged at 14,000 RPM for 5 minutes on a Beckman Coulter Microfuge 18 centrifuge; the supernatant was poured off and each pellet was re-suspended in 1mL of tap water, and the centrifuge tubes were re-centrifuged as above. The supernatant was again poured off, and the tubes were stored at -20°C until freeze drying.

Results and Discussion: Energy Captured into Algal Biomass and Oils by *B. braunii* and *C. vulgaris* in the Continuous, High Density Trickle-screen Bioreactor

The energy captured by the algae during culture in the continuous, high-density trickle-screen bioreactor was assessed by the use of Adiabatic Bomb Calorimetry determinations; this

work was greatly enabled by the assistance of undergraduate researcher Patrick Hillery, who was responsible for the extraction and purification of the associated Botryococcus biomass samples, as well as the heat of combustion determinations.

Because the heat of combustion associated with triterpene oils (botryococcenes) from *B. braunii* are not thermodynamically characterized in the current literature, an experimental value for this property was sought. Six adiabatic heat of combustion determinations from a single sample of extracted oils from Botryococcus, presumed to be comprised primarily of triterpene hydrocarbons (botryococcenes) were made over two separate days; on the first day four determinations were made (Table 2.3). However, it turned out that the hot water supply to the external water bath was malfunctioning, resulting in non-equilibrium temperature conditions between the outer water bath and the bath immediately surrounding the calorimetric bomb. This would have resulted in heat transfer from the bomb bath to the surrounding supposedly isothermal external bath, because the external bath would have been at a lower temperature than the than the bomb bath, leading to under-estimates of the actual heat of combustion of each sample.

The remaining two determinations were made on a separate day when the hot water supply was confirmed to be functioning properly (Table 2.4). As can be seen by the results, the mean Enthalpy of Combustion (ΔH_c) value determined from the overall average of all determinations is markedly lower than the value predicted by the bond energy method (7.14%); after splitting the values determined each on the day with the malfunctioning hot water (determinations 1-4) and the day when the problem was corrected (determinations 5-6), it can be seen that the mean ΔH_c determined was very different between the two analysis dates. Furthermore, the results from 6/10/2011 are much lower than the theoretical value (by 11.74%) and lower than the values determined on 6/22/2011 (by 13.6%). An unpaired, 1-tailed student T-test on the two data sets, assuming unequal variances and a confidence interval of 95%, results in

Table 2.4: A comparison of the enthalpy of combustion data obtained over three separate analysis events for botryococcene oils extracted from *B. braunii*.

This data provides evidence that the heat of combustion determined from data collected on the first day of analysis (Set 1) was artificially depressed by a malfunctioning hot water system, which prompted additional oil collection and calorimetric determinations.

Theoretical ΔH_c:		43.86 kJ/g			**Separated by Day of Analysis**			
Determination #		**Day of Analysis** [2]	**Oil Sample Mass (g)**	**Measured ΔHc kJ/g**	**Mean kJ/g**	**std dev kJ/g**	**% CV**	**% Error**[1]
Set 1	1	6/10/2011	0.1103	39.71	38.71	1.46	3.76%	-11.74%
	2	6/10/2011	0.1077	39.96				
	3	6/10/2011	0.1152	38.36				
	4	6/10/2011	0.1164	36.80				
Set 2	5	6/22/2011	0.1114	44.99	44.8	0.3	0.740%	2.04%
	6	6/22/2011	0.0130	44.5				
Set 3	7	11/9/2011	0.0587	46.6	44.8	1.7	3.7	2.10%
	8	11/9/2011	0.0614	45.6				
	9	11/9/2011	0.0471	44.2				
	10	11/9/2011	0.0309	42.8				
		Overall:	Mean:	42.3				
			Std. Dev:	3.38				
			%CV:	7.99%				
			% Error[1]:	-3.45%				

[1] Calculated with respect to the theoretically estimated Heat of Combustion.
[2] Measurements were made over three separate days; on 6/10/2011 (Set 1) the hot water supply to the bomb calorimeter bath was malfunctioning, resulting in non-equilibrium conditions; the anticipated impact is that there was heat loss from the bomb that was not accounted for, resulting in artificially depressed combustion energies from the true value. Oil from the same original sample was analyzed on 6/22/2011 (Set 2), resulting in values significantly higher than those found in the initial analysis, providing evidence that the initial determinations were depressed due to the malfunctioning water system, and this prompted a desire for further measurements. In order to allow further determinations, additional *B. braunii* samples had to be collected, their botryococcene oils extracted, and purified; the determinations on this second, separate sample of *B. braunii* oils correspond to the Set 3 data.

a T_{test} value of -3.803; compared to the t_{crit} value of 2.920 for 2 degrees of freedom and 95% confidence interval.

This provides sufficient evidence to reject the null hypothesis that the two averages are the same, and lends support for the hypothesis that the determinations made during the faulty hot-water delivery were in fact artificially low due to heat transfer from the bomb bath to the external

bath. In order to obtain more conclusive evidence than which only two samples could supply, a second round of *B. braunii* algae was collected over the period of XX-XX; these samples were subjected to extraction and the oils purified, and a final round of bomb calorimetry on these samples was undertaken on 11/9/2011. The value of ΔH_C from this final set of samples (Set 3) agreed very closely with the Set 2 data, even though the determinations were made on oil collected from a different collection of *B. braunii* algae samples. This provides strong evidence that the hot water system was malfunctioning during the Set 1 calorimetry determinations, and that the true experimental value for the heat of combustion of botryococcene oils is the average of the Set 2 and Set 3 data: 44.8±1.3 kJ/g oil.

Table 2.5: Botryococcene content of oil extracted for bomb calorimetry determinations.

The purpose of this analysis was to rule out the possibility that significant amounts of impurities in the oil extract had artificially lowered the determined enthalpy of combustion.

Overall % Botryococcenes in Oil Sample			
Mean		**Std. Dev.**	
98.00		1.69	
Distribution of Botryococcene Species in Oil Sample			
Peak #	**ID**	**% of Total Oil**	
		Mean	**Std. Dev**
1	C_{34}	0.68	0.01
2	C_{26}	6.06	0.11
3	C_{34}	1.71	0.01
4	C_{31}	25.9	0.52
5	C_{34}	3.07	0.03
6	C_{32}	36.23	0.96
7	C_{32}	16.65	0.85
8	C_{26}	0.98	0.11
9	unknown mass	4.61	0.07
10	tetraterpenoid	2.04	0.01
*	Squalene	NA	NA

Another possibility for the low values compared to the theoretically calculated values is that significant amounts of low-energy impurities existed in the oil sample, leading to a depressed enthalpy of combustion value (on a mass basis) for the sample. In order to test this, a portion of the oil from the same sample was tested by GC-FID for botryococcene oil content. The results of this analysis are shown below in Table 2.5 and Figure 2.4.

As can be observed, the overall purity of the oil sample with respect to botryococcene content was very high, 98.00±1.69%. Of the oil positively identified as the triterpene botryococcene hydrocarbons, only 3.75% of these were identified as

C_{34} botryococcenes which was the structure utilized for the theoretical calculation. The distribution of the botryococcene species in the extracted and purified oil was diverse, with identities ranging from C_{26}-C_{34} species. Two small fractions of the botryococcenes in the oil were unable to be definitely identified; one species at peak 9 was not able to be assigned a definite mass, and the peaks labeled as '10' are likely tetraterpenoid species more similar to the structure of squalene. It is likely that the heat of combustion of each of these individual species varies, but because these are all highly reduced hydrocarbon species it is unlikely that this variation alone resulted in the depressed value for the heat of combustion observed in the first four

Figure 2.4: GC-FID Chromatograms of extracted and purified *Botryococcus* oils used for bomb calorimetry determinations.

The purpose of this analysis was to rule out the possibility that significant amounts of impurities in the oil extract had artificially lowered the measured enthalpy of combustion. Curves are with (grey) and without (black) squalene internal standard spike; the numbers correspond to the species associated with for each peak (inset).

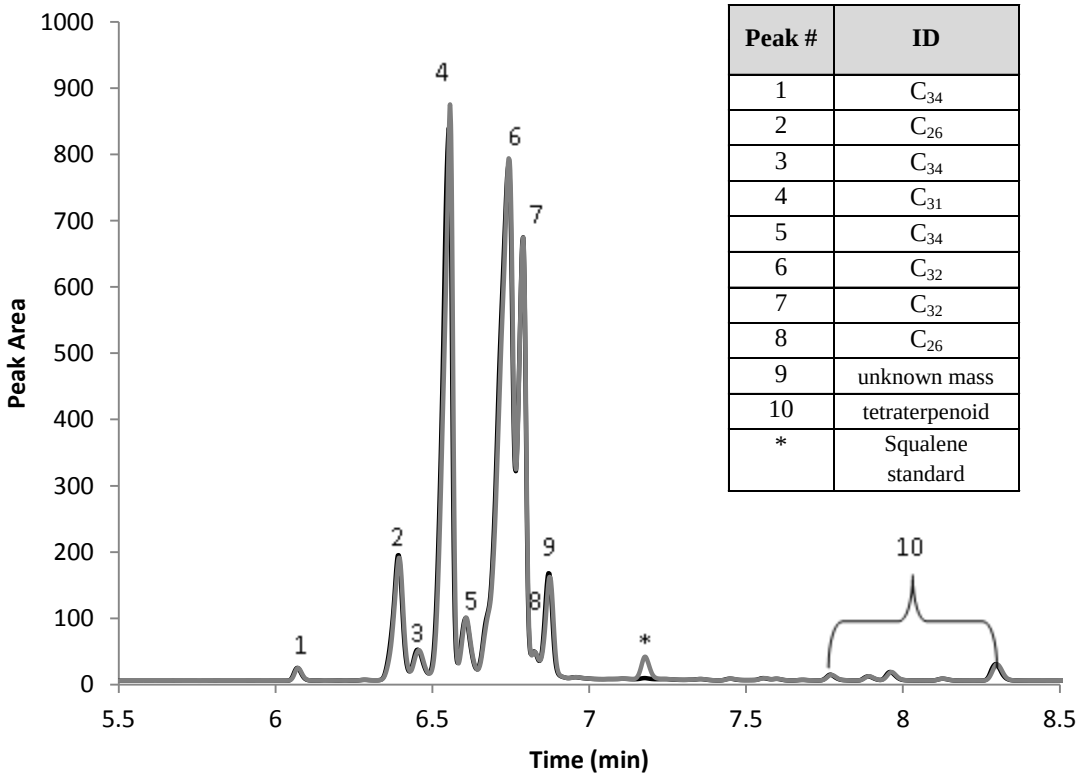

Peak #	ID
1	C_{34}
2	C_{26}
3	C_{34}
4	C_{31}
5	C_{34}
6	C_{32}
7	C_{32}
8	C_{26}
9	unknown mass
10	tetraterpenoid
*	Squalene standard

determinations. Furthermore, it is unlikely that the 2.00% of the oil not identified as botryococcenes resulted in a 7.14% depression in heat of combustion value from the theoretical value. Because the exact structural determination of each triterpene present in the oil is outside the scope of this work, this will not be taken further to estimate the heat of combustion of each individual species and use the weighted average of the values as a comparator to the actual experimental value.

Therefore, for the remainder of the energetic analysis, the average heat of combustion determined from determinations 5 and 6 was used as the value for botryococcene oils (44.8±0.3 kJ/g). Because it is from only two data points, this is motivation for further oil samples to be collected and their enthalpy of combustion to be measured, and preparations for this work are currently underway to generate more *Botryococcus braunii* cultures for this purpose.

To quantify the total energy captured by the algae into each biomass (cell mass only) as well as the total culture (inclusive of extracellular secreted organics), calorimetric determinations were made on each dried biomass and total culture. From this data, the extent of energy captured each into oil (triterpene botryococcene hydrocarbons by *B. braunii* or lipids by *C. vulgaris*), non-oil cell mass, and extracellular (excreted) organics was determined on a volumetric basis for the steady-state periods of *B. braunii* and *C. vulgaris*. The results are shown below in Figure 2.5. It is clearly seen that *B. braunii* captured a greater amount of energy into oil than *C. vulgaris*, which was expected based on the higher oil productivity of *B. braunii*. However, it is also observed that energy captured per liter of culture by *B. braunii* (838±24 kJ/L) exceeds *C. vulgaris* (456±40 kJ/L) by nearly two times. While *C. vulgaris* does appear to capture slightly more energy into *B. braunii* captured more energy into non-oil biomass than *C. vulgaris*, and therefore the total extracellular secreted organics (top layer in Figure 2.5) than *B. braunii*, the error associated with these calculated values (explained below) eliminates the ability to make conclusions about the significance of the difference. The large error associated with the energy of the secreted organics

Figure 2.5: Breakdown of the energy captured per liter total culture into Oil, Biomass, and extracellular secreted organics by each *B. braunii* and *C. vulgaris*, as determined by adiabatic bomb calorimetry.

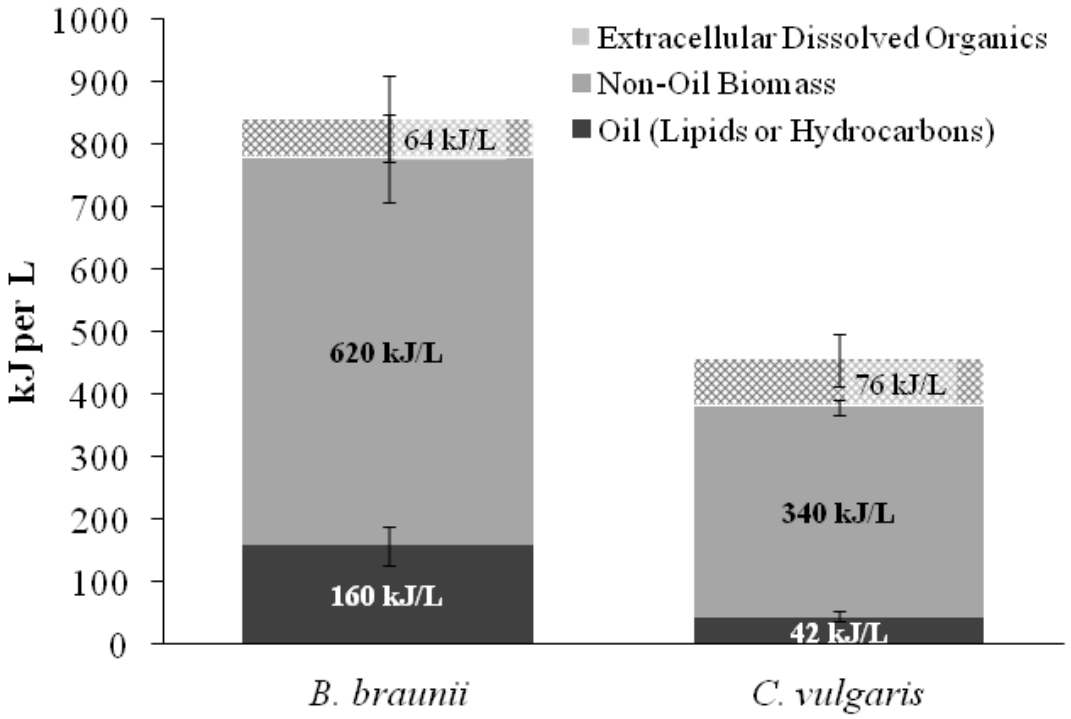

is due to the method of calculation; the amount of energy captured per liter into the biomass and oil was subtracted from the total energy captured per liter of total culture. Though the variability associated with each the energy contained in the total culture and the biomass is small relative to those values, the small magnitude of energy captured into excreted soluble organics (as determined by difference) means that the error of the calculation is large compared to this value.

Therefore, on a mass basis the energy contained in non-oil biomass of *B. braunii* is significantly higher than *C. vulgaris*: 36.5±8.0 kJ/g non-oil DW biomass for *B. braunii* versus 19.4±2.3 kJ/g non-oil DW biomass for *C. vulgaris*, respectively. There are several possible reasons for this difference. It could partially be attributed to the fact that most lipids contained in *B. braunii* biomass are not soluble with the extraction solvent for botryococcene hydrocarbons (hexanes) and would therefore were not accounted for in the oil portion of the biomass.

Therefore, the energy content of any lipids in *B. braunii* is therefore 'counted' in the non-oil biomass rather than in the oil. However, *B. braunii* biomass from a separate sample of culture, drawn from maintenance flasks, was determined to be only 2.2±0.2% lipid by mass by a separate determination via the DTE method, which would not make up the difference in measured energy content of the biomass between these two species. This lipid content is on par with that expected when only membrane lipids are present in a species, and not storage lipids. Therefore, unless significant storage lipids were present in the *B. braunii* derived from the continuous trickle-screen run, this is an unlikely explanation for the higher energy content between the two species. Another possible explanation is that there are significant amounts of other high-energy compounds manufactured by *B. braunii* that are not detected by either the hydrocarbon extraction method or the lipid determination method. For example, in the separate sample mentioned above, 10.6% of the cell mass was determined to be pigments (composed of Chlorophyll A and Chlorophyll B).

Another consideration is that while the total energy captured by each species per mass of each total culture sample and per mass of biomass is directly determined, the breakdown among the sub-components is then dependent upon the determination methods of each the total culture and biomass concentrations; the oil concentrations / content, etc. It has been recently identified by our Chappell lab collaborators that the determinations made on the *B. braunii* samples corresponding to this data may have been compared against a standard curve made using an overly concentrated standard. The standard curve for GC analysis of botryococcenes is a squalene standard, diluted into n-hexane. Hexane is inherently volatile, and it has been theorized that the standard used for this analysis had become overly concentrated due to evaporation. The evidence for this is that the slope of the standard curve from this analysis is ~50% steeper than a standard curve constructed when the standard had been recently prepared (6 months prior to the determinations made on these *B. braunii* samples). Furthermore, in a later analysis, *B. braunii* oil

samples were analyzed using this same questionable squalene standard, but were also analyzed independently by another laboratory (National Energy Technology Laboratory) using the same method developed by the Chappell lab. The botryococcene content of the oil samples as analyzed by NETL on this occasion were much higher than the values determined by the Chappell lab; ~3X higher. While this particular difference was not conclusively resolved, I worked with both labs to perform additional comparative runs of *B. braunii* samples and ultimately comparative results between the two labs were obtained, although whether these original samples had an underestimated botryococcene content remains an open question.

If the oil concentration determination for *B. braunii* was underestimated, this would result in a lower portion of the biomass energy being accounted for as oil, inflating the energetic content of the biomass on a mass basis. To assess the effect that this would have, I applied the slope of the standard curve associated with the freshly prepared squalene standard, and recalculated the weight percent of botryococcenes in the biomass, and then recalculated the energy captured into oil and that captured into non-oil biomass. With the adjusted slope, the calculated botryococcene -content of the biomass increased from 17% to 27%, which is closer to the botryococcene content of this *B. braunii* strain as reported in the literature (24-29% by mass, Wolf et al., 1985). The effect of this correction on the botryococcene oil productivity was to increase it from 0.27 to 0.41 g oil/L/day. Then carrying this correction through to calculate the energy captured per liter of algal culture, the effect was a calculated increase from 160 kJ/L to 250 kJ/L energy capture in oil, and a corresponding decrease in the total energy captured into non-oil biomass per L of culture. However, the calculated value of the energy content of non-oil *B. braunii* biomass did not change significantly; even though the total energy captured in non-oil biomass was calculated to have decreased, the amount of non-oil biomass decreased correspondingly, resulting in similar values for the energy content. This indicates that there is some other contribution to the high-energy content of *B. braunii* non-oil biomass.

Results and Discussion: Batch Growth Comparison of *C. vulgaris* under both Light-Limited and Non-light Limited conditions

Batch growth experiments were carried out as described in the Materials and Methods section with *C. vulgaris.* The purpose of the experiments was to:

- Determine whether higher productivities could be achieved during batch growth of *C. vulgaris,* due to its tendency to accumulate lipids only when growth has ceased;
- Explore whether non-light-limited growth conditions resulted in higher biomass and lipid productivities than growth under light-limited conditions.

Two treatments with two replicates of each treatment were investigated:

1. A Non-Light-Limited culture (NL), where the rate of light energy available to the culture is able to support non-limited growth rates over the entire culture duration (until another nutrient became yield-limiting). The anticipated result is a culture which remains exponential growth over the entirety of its growth phase.
2. A Light-Limited (LL) culture, where the rate of light energy supplied to the culture at some point becomes rate-limiting with respect to the inherent maximum growth rate prior to yield-limitation by another nutrient. The apparent result is a culture which transitions from exponential growth to linear growth prior to yield-limitation by another nutrient.

Algae in both treatments were grown in identical air-lift loop bag bioreactors constructed of transparent plastic sheeting and sandwiched between wire racks to obtain a maximum thickness of ¾" (1.905 cm) (Figure 2.6). Areal light intensity (irradiance, μmol/m^2/s) and the exposed area (m^2) of the reactors was controlled such that the total rate of light energy (μmol/s) incident on each treatment was the same; see Table 2.6. With a constant rate of light energy available to each treatment and in the absence of rate-limitations by any other nutrients, light

becomes rate-limiting when the inherent growth rate of the alga exceeds the rate of growth possible from the rate of light energy provided.

Figure 2.6: Photograph of *C. vulgaris* cultured in the Loop Airlift Batch Bag Photobioreactors.

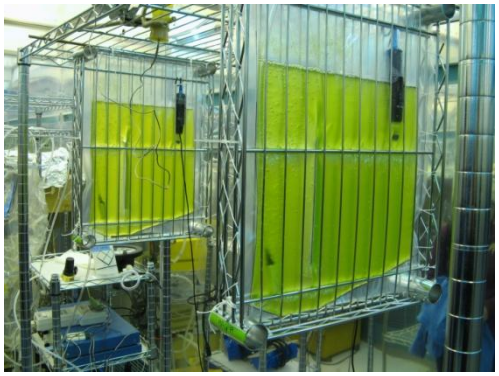

Table 2.6: Photosynthetically Active Radiant Flux (PARF, µmol quanta/s) incident upon each bag reactor replicate.

NL = non-light limited treatment; LL = light-limited treatment. PARF for each treatment was targeted to be equivalent while minimizing variations in PARF for each replicate.

Overall Average, All Treatments µmol/s	**NL-1**		**NL-2**		**LL-1**		**LL-2**	
	TOTAL µmol/s	**% off from avg**	**TOTAL µmol/s**	**% off from avg**	**TOTAL µmol/s**	**% off from avg**	**TOTAL µmol/s**	**% off from avg**
41.0	41.0	0.1%	40.6	-0.9%	44.5	8.6%	37.8	-7.7%
Average for Each Treatment (µmol/s):	40.8				41.1			

Two interrelated effects associated with the growth of algae will cause this to happen: as algae grow exponentially, where µ is the specific growth rate of the alga and is a constant ($dX/dt = \mu X$), the cell density X increases, and at some point the rate of growth, dX/dt, becomes larger than what the light power can support. In addition, as X (the cell concentration) increases, absorption and scattering effects in the culture cause light attenuation with depth of culture. Therefore, as cell density increases, the cells 'self-shade' each other, diminishing the average amount of light available to each cell in the culture. These compounded effects result in a point

of light-limitation that is dependent both upon the culture density of the algae at a given time as well as the rate of growth of the algae culture.

Therefore, in this experiment, the cell density was chosen as the control for triggering light-limited growth conditions (or not); the NL culture was restricted to a lower ultimate cell density than the LL culture. A simple yield-limitation was imposed on the cultures to control the ultimate cell density, which was imposed in the form of nitrogen limitation. Therefore, the amount of nitrogen provided to the NL culture (as nitrate) was less than that provided to the LL culture (Table 2.7), ensuring that the NL culture would stop growing prior to the onset of light-limitation. The use of nitrogen as a means for limiting the ultimate cell density also serves to trigger lipid accumulation by *C. vulgaris*.

Table 2.7: The use of nitrogen limitation as a means of inducing light-limitation in the batch bag reactors.

Nitrogen provided to each treatment and the targeted and actual OD_{550} at growth cessation are indicated.

Treatment	**Nitrogen Fed per L culture (as nitrate)**	**Targeted OD_{550} at growth cessation**	**Actual OD_{550} at growth cessation**
Non-Light Limited (NL)	0.031 gN/L	2.70	2.6 ± 0.2
Light-Limited (LL)	0.141 gN/L (two doses of 0.070 gN/L)	10.8	9.5 ± 0.2

All other inorganic nutrients were supplied in stoichiometric excess with respect to the nitrogen supplied. To prevent osmotic shock to the LL culture, which had overall higher amounts of nutrents provided, the nutrients were provided in two doses to these cultures, with the second dose being fed when the culture had grown to an OD_{550} of approximately 1.4 (~0.7 g DW/L); this culture density represents when the nitrogen from the first feeding dose is approximately depleted from the extracellular media, assuming a constant nitrogen content of the biomass as 10.6% nitrogen/g dry weight. This ensured that the culture did not run out of nitrogen prior to the ultimate culture density as well as minimized the chances for nutrient toxicity or osmotic shock effects.

Growth was monitored over the course of the experiment by optical density determinations, taken at 550nm. As can be seen by below in Figure 2.7, the LL cultures attained much higher biomass densities than the NL cultures due to the higher level of nitrogen provided, enabling the stoichiometrically higher degree of growth.

The growth phases of each treatment are indicated in more detail in Figure 2.8 A and B. For the NL treatment, a clear exponential growth phase is observed. The specific growth rate, μ, was determined by fitting the data to an exponential curve and was calculated as 0.11 hr^{-1}. This exponential growth phase continued all the way until 1.78 photodays of growth, which corresponds to when the cellular nitrogen content can be calculated as 4.9%, based upon the optical density, the measured average DW concentration/OD ratio for the experimental treatment (0.462 g DW/OD_{550}), and the nitrogen provided to the cultures in the initial media. After this

Figure 2.7: Time-course of optical density measurements of *C. vulgaris* versus time over the batch experiment.

Time is reported in 16 hour photodays. The timing of the second dose of nutrients fed to the Light-Limited treatment is indicated. Each timepoint is the average of two replicate cultures with triplicate determinations on each culture; error bars represent the standard deviation associated with the six measurements.

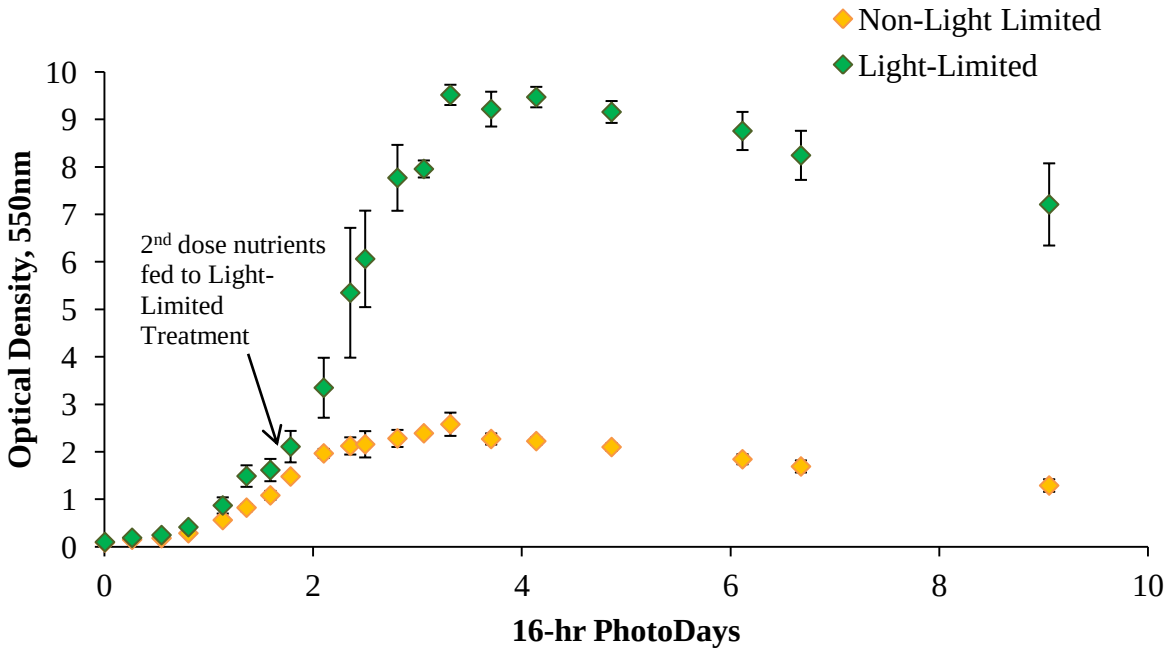

Figure 2.8: Timecourse of the batch experimental data showing the exponential, linear/post-exponential, and declining phase of each culture. (A) Non Light-Limited (NL) Treatment; (B) Light-Limited (LL) Treatment

Each timepoint is the average of two replicate cultures with triplicate determinations on each culture; error bars represent the standard deviation associated with the six measurements.

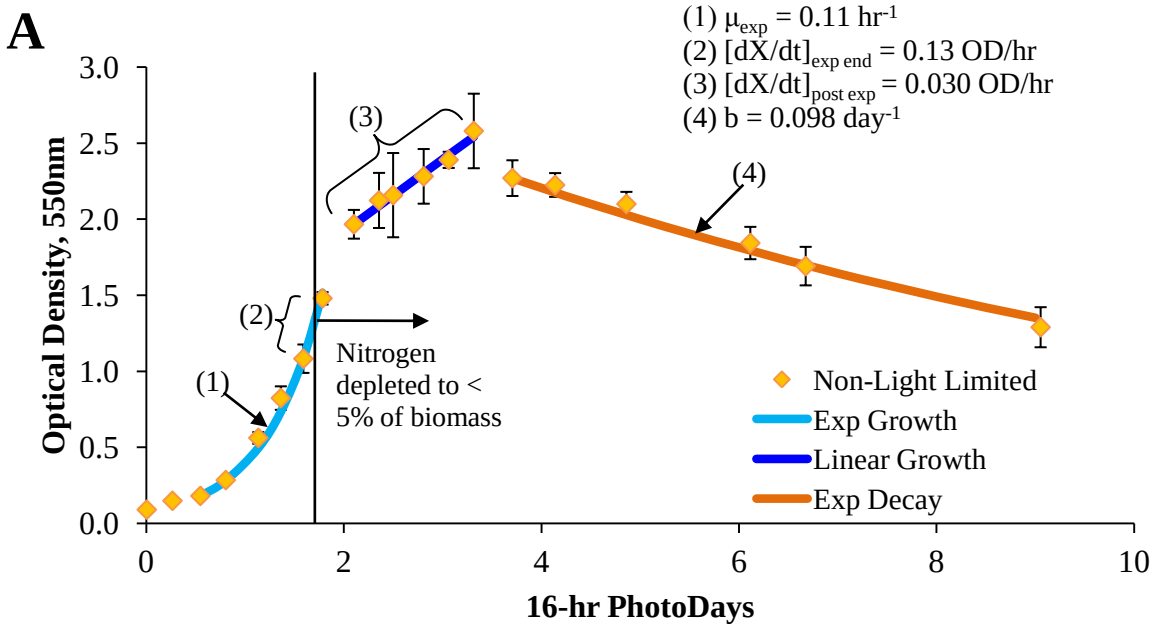

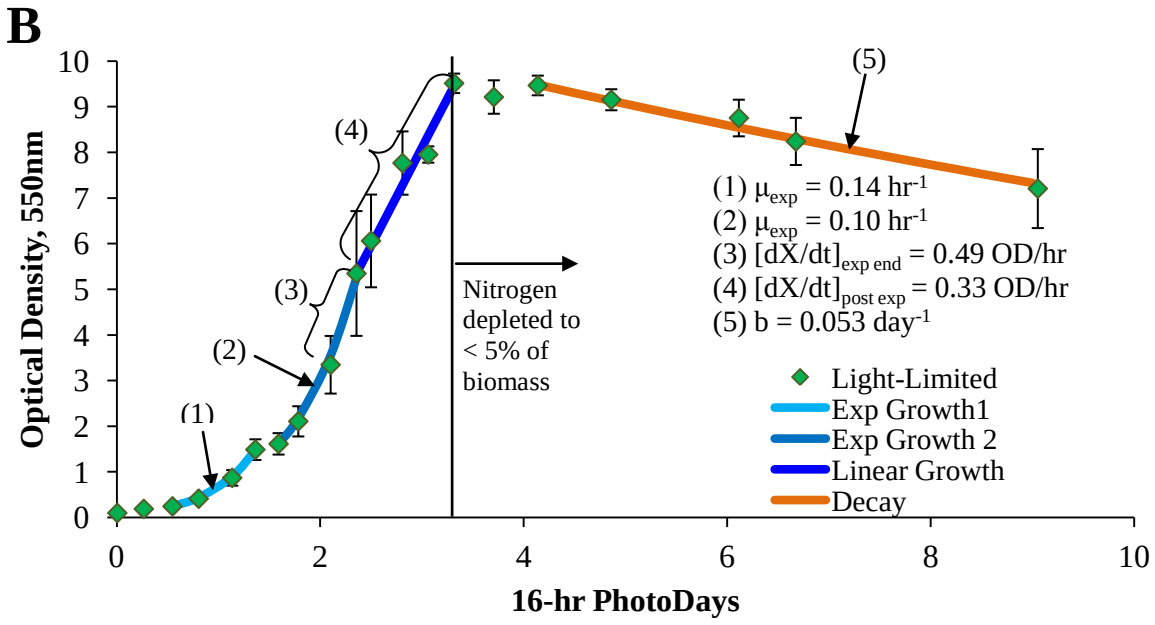

exponential growth phase, the culture enters into a declining phase, eventually leveling out at a maximum OD of approximately 2.6. Prior to attaining the maximum OD, it appears that the cultures do enter into a phase characterized by a slow linear growth rate; it is unlikely this phase is due to rate-limitation by light flux for several reasons. First, the expectation of light-limitation is that the absolute rate of growth at the point of light-limitation (dOD/dt) should remain constant into the light-limited phase; the rate of light is sufficient only to maintain the growth rate at the point of limitation. What is observed in the case of the NL treatment is a rate of growth slower than that observed at the end of the exponential phase. This suggests instead that the slower rate of growth is due to the nitrogen limitation, where the dwindling internal nitrogen stores increasingly limit protein synthesis within the cell. Furthermore, the overall growth rate (dOD/dt) at the end of exponential growth for the NL treatment (dOD/dt = 0.13 OD/hr) is nearly three-fold slower than the dOD/dt observed during linear growth in the LL treatment (0.33 OD/hr); because the treatments experienced nearly equivalent rates of light energy, it is very unlikely that the linear growth phase in the NL culture was due to light-limitation.

For the LL treatment two different exponential growth phases are observed; they are separated by a 'night' period of 8 hours of darkness, and when exponential growth resumes the next day the calculated specific growth rate of the second exponential period is slower than the first: 0.10 hr^{-1} versus 0.14 hr^{-1}. The exact reason for this break in the exponential growth period and the slower specific growth rate during the second day of exponential growth is unknown, although this observation has been repeated whenever exponential growth during a batch culture has extended over a 2-day period. It is not likely to have anything to do with nitrogen availability because the second dose of nitrogen feeding was provided at the end of the first exponential growth period, and so the algae should not have been experiencing nitrogen limitation during this time. However, this step-change in the specific rate of growth is similar to that which would be associated with a decrease in the yield on the energy-providing substrate. Assuming that the

substrate in question is light, and the culture is growing in the non-light limited regime, the utilization rate of light per mass of algae should be roughly constant at the maximum rate of utilization over the duration of non-light limited growth (excess light will be dissipated by the culture as heat). The specific substrate utilization rate of an organism (in this case light, $\hat{q}_L$) is equivalent to the ratio between the net (i.e. observed) growth rate (μ^{APP}) and the net (observed) yield (Y^{NET}) on light, as shown in Equation 2.9.

$$\hat{q}_L = \frac{\mu^{NET}}{Y^{NET}} = \frac{\mu^{TRUE}}{Y^{TRUE}} \qquad \textbf{Equation 2.9}$$

Therefore, an observed decrease in μ^{NET} could be due to a decrease in the yield on light energy; this could occur if the *efficiency* of the light utilization into biomass decreased as culture density increased.

The overall rate of increase of the culture as a whole ($\frac{d}{dt}(X_R V)$, Equation 2.1) at the end of the exponential growth period was calculated to be 0.49 OD/hr; $\frac{d}{dt}(X_R V)$ entering into the light-limited linear growth phase (Equation 2.5) was approximately 33% slower. This is a deviation from the expectation that the light-limited growth phase would be characterized by a growth rate similar to the rate at the end of exponential growth. A possible explanation for this difference is that under light-limited conditions, further increases in cell density result in an increasingly lower rate of light energy being available to each cell, further decreasing the efficiency of light utilization and therefore the yield and the specific rate of growth.

To qualitatively demonstrate the effect of culture density on light limitation (and therefore possible growth rate), Figure 2.9 shows the profile of Photon Flux Density (PFD) through the thickest portion (3/4" = 1.905 cm) of the culture in the bag reactor. The profiles were constructed using Beer-Lamberts Law, neglecting the effects of light scattering by the algae cells and assuming absorbance is the main mechanism of light attenuation.

$$A_\lambda = a_\lambda\, b\, c = -\log\frac{I}{I_0}$$ **Equation 2.10**

In Equation 2.10, A_λ is the measured absorbance for wavelength λ; a_λ is the absorbtivity coefficient (wavelength-specific); *b* is the pathlength; c is the concentration of the analyte (in this case, the algae cells); I is the light intensity after it has passed through the sample, and I_0 is the initial light intensity. Using optical density measurements over the duration of the experiment at timepoints where cell dry weight concentration was measured concurrently, an average a_λ was estimated for each batch reactor culture. This value was then utilized along with the measured average irradiance at the front and back surfaces of the bag reactors to calculate the light intensity profiles (or Photon Flux Density) through the culture depth at two different timepoints during the batch run when the dry weight cell density was also measured. The results are shown in Figure 2.9. Several major assumptions were made in order to simplify the problem for this qualitative assessment:

1. The Photon Flux Density from both sides of the bag reactor was assumed to be completely additive within the culture;
2. Light entering the culture through the vertical surface of the culture was neglected due to its small area compared to the flat sides of the bag reactor.

In Figure 2.9, the PFD profile is plotted as a function of distance from the front surface of the bag reactor for both the NL and LL treatments. Curves portray the irradiance profiles at three different points in the algal growth curves: exponential growth (solid lines), where the PFD is above the light compensation point at all points through the culture volume. The light compensation point is the irradiance where oxygen production is balanced by oxygen uptake (net gas exchange is zero) because the rates of photosynthesis and respiration are in balance (Geider and Osborne 1992). Here, is taken to be 7.5 μmol/m^2/s for *C. vulgaris*, as determined by (Degen et al. 2001). At the exponential growth point (time of 1.1 photodays), the minimum PFD for each the NL and the LL cultures are 103 and 38.3 μmol/m^2/s. The next time point for which curves are

shown is just after the end of exponential growth (dotted lines, t = 2.4 photodays). At this point, the PFD profile for the NL cultures remains largely above the light compensation point (87% of the culture volume is above the light compensation point), and the minimum PFD at the center of the culture is 6.8 μmol/m^2/s. This provides evidence that the end of exponential growth for the NL culture was due to nitrogen limitation and not light limitation. It is possible that the cells experienced light limitation for transient periods of time while circulating through the bag reactor, but the majority of the time would have been spent in irradiance levels above the light compensation point. For the LL culture, however, this timepoint corresponded to the transition from exponential to linear growth, as can be seen in Figure 2.9, and only 40% of the culture

Figure 2.9: Photon Flux Density (PFD) within the bag reactor culture as a function of the distance from the front surface of the bag reactor.

PFD profiles are shown at three different points in the batch growth curve of the cultures: During exponential growth both the LL and NL treatments experience PFD above the Light Compensation Point at all points within the culture volume; the NL culture has the majority of its culture volume experiencing PFD above the light compensation point at both subsequent timepoints (post-exponential growth and after growth has ceased); the LL culture has only a small fraction of its culture volume experiencing PFD above the light compensation point at the subsequent timepoints. Light incident onto both sides of the bag reactor was assumed to be additive within the culture so that the minimum PFD occurred at the middle of the culture volume. NL = non-light limited treatment; LL = light limited treatment.

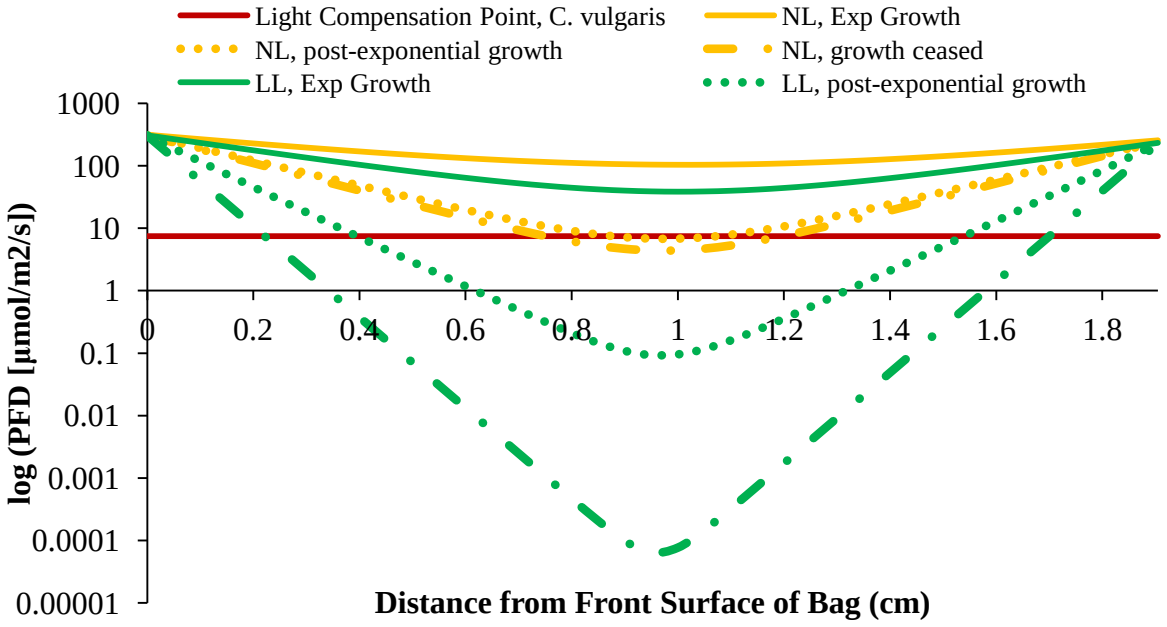

volume experienced irradiance above the light compensation point at any given time. Furthermore, the minimum irradiance at the center of the culture was calculated to be on 0.09 $\mu mol/m^2/s$, well below the light compensation point. In fact, 40% of the total culture volume was calculated to have experienced irradiance levels of less than 1 $\mu mol/m^2/s$ at this timepoint. This provides evidence for the light-limited culture conditions of the LL treatment.

Finally, the PFD profiles after growth has ceased are also shown to demonstrate that while the LL treatment continued to grow past the point of light limitation, evidenced by the further increase in light-limited culture volume (now at 79% of the total volume), there was little further growth by the NL culture, and 76% of the culture volume remained at irradiance levels above the light-compensation point. Minimum calculated irradiances for the NL and LL cultures were calculated to be 4.4 and $6x10^{-5}$ $\mu mol/m^2/s$, respectively, and 66% of the LL culture experienced irradiance levels less than 1 $\mu mol/m^2/s$.

Algae biomass concentration (X_b, g DW/L) in the photobioreactor was monitored concurrently with optical density; the two indicators of cell density in the photobioreactor demonstrated very similar trends, although the ratio of dry weight cell density to optical density (X/OD) was not constant throughout the batch runs, ranging from 0.34 to 0.71 for all treatments. The higher ratios occurred during the most actively growing growth phase for all treatments, and the lower ratios occurred during the stationary phase of growth. Interestingly, the ratio X/OD was lower for the light-limited treatments than for the non-light limited treatments; the reason for this is not immediately clear.

Lipid content in the algae (m_L, g lipid / g DW algae) was also measured at various points over the course of the batch run, and this value was used to calculate a lipid concentration (C_L, g lipid / L culture) in the photobioreactor using Equation 2.11. The results of biomass and lipid concentration over the course of the batch experiment, as well as the lipid content, are shown in Figure 2.10 and Figure 2.11.

Figure 2.10: Timecourse of lipid concentration (g lipid/L, primary Y-axis) and biomass algae concentration (g algae/L, secondary Y-axis) n the batch bag reactors plotted versus culture time.

The biomass concentration initially increases more quickly and reaches its maximum earlier in the batch culture than the lipid concentration. Each biomass concentration datapoint is the average of two replicate cultures with triplicate determinations on each culture; error bars represent the standard deviation associated with the six measurements. Each lipid concentration datapoint is the average value of independently determined lipid concentrations (Equation 2.11) for each replicate photobioreactors within each treatment; error bars represent the standard deviation between the two independent determinations.

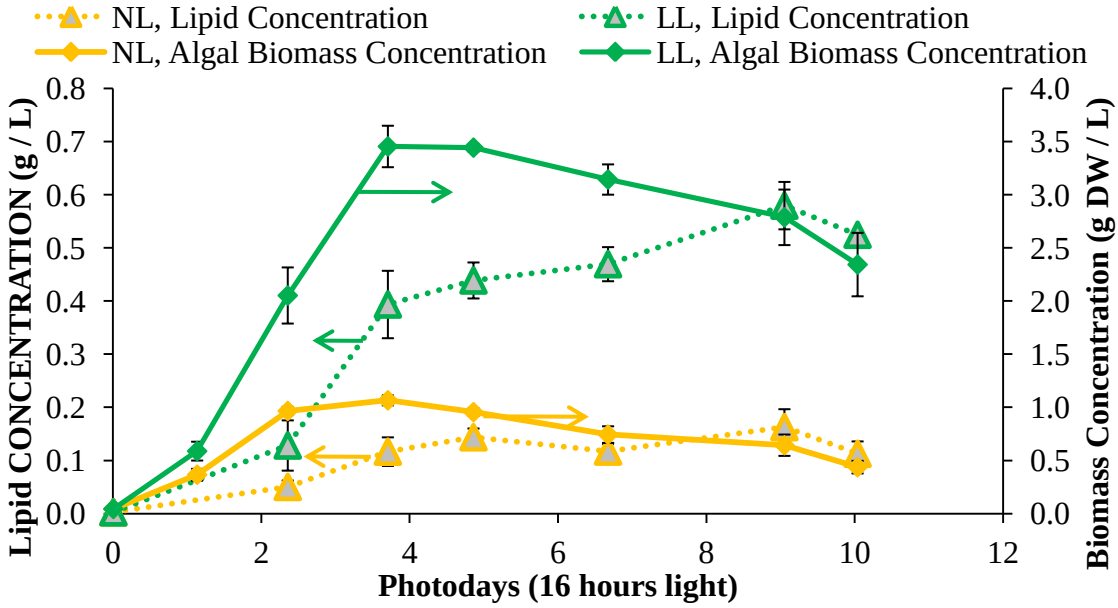

Figure 2.11: Lipid content (g lipid/g biomass) plotted versus batch culture time in 16-hour photodays.

The lipid content of the biomass remains essentially constant during the exponential growth phase but begins to increase in the linear and stationary phases of growth. Each lipid content data point is the average of two replicate treatment samples with triplicate determinations on each sample; error bars represent the standard deviation associated with the six measurements.

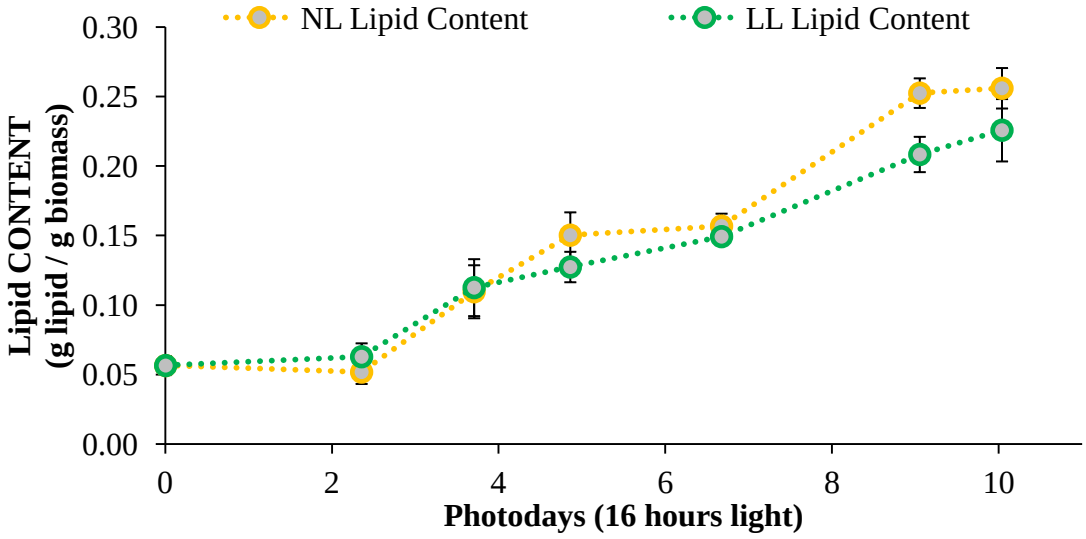

$$C_L = X_b\, m_L$$ **Equation 2.11**

As expected, the biomass concentration attained by the non-light limited (NL) treatment was ultimately lower than the light-limited (LL) treatment due to the lower amount of nitrogen that it received: 1.07 versus 3.46 grams dry weight algae/L. Because of the higher biomass concentration, the overall lipid concentration attained by the light-limited treatment also exceeded the NL treatment; the overall lipid content (g lipid / g biomass) between the two treatments trended very similarly throughout the duration of the experiment despite the large difference in light limitation between the two treatments. This result of similar lipid accumulation kinetics between both the NL and LL treatments is quite different than the stated result of Pruvost et al. (2009), who found the kinetics of total lipid accumulation between a high and low nitrogen treatment (0.047 g NO_3-N/L and 0.020 g NO_3-N) to be quite different. However, numerous inconsistencies in their work made it impossible to reconcile this statement quantitatively.

In this work, the lipid concentration increase occurred over a longer duration than the increase of biomass concentration, as seen in Figure 2.10 A; biomass concentration peaks at 3.71 days for both the NL and LL treatments before it begins to gradually decrease, but lipid concentration does not reach a maximum until 9.05 days. The delayed peak in the lipid concentration is due to the distinctly different profile of lipid content of the algal culture compared to the biomass concentration; as can be seen in Figure 2.10, the lipid content of the algae increased over the entire duration of the batch experiment. This was sufficient to lead to increasing overall lipid concentration up to 9.05 days even though the algal biomass concentration begins decreasing after 3.91 days. After this point the decrease of overall algae concentration outweighs the increase in the lipid content of the algal biomass, and so the concentration began decreasing. While it is possible and likely the actual maximum lipid content of the algae was not captured in this experiment because the algal cultures were terminated prior

to that point, as will be shown later the maximum lipid productivity occurs well in advance of the point of maximum lipid content.

The delayed accumulation of lipid with respect to biomass accumulation is a result of the nongrowth-associated production of lipid, where lipid accumulates above the baseline content only at low or no cellular growth, which is triggered in these results by a depletion of the available nitrogen in the culture medium. To show this in more clarity, the instantaneous net specific growth rate of the algal culture was estimated from the dry weight data by Equation 2.12 and Equation 2.13. The two different equations were used to calculate the specific algal growth rate based on whether the growth between the two time points (as determined by the optical density data) was better approximated by an exponential function or a linear function. X_2 refers to the algal biomass concentration at an arbitrary timepoint t_2; X_1 refers to the algal biomass concentration at earlier, arbitrary timepoint t_1. In the non-exponential equation, the quantity $\frac{X_2+X_1}{2}$ is the approximate average biomass concentration over the time period t_1 to t_2. The error of this approximation is minimized when the timepoints are selected as close to each other as possible, particularly during exponential growth.

$$\mu^{NET} = \frac{\ln \frac{X_2}{X_1}}{t_2 - t_1} \quad \text{(During exponential growth)} \qquad \textbf{Equation 2.12}$$

$$\mu^{NET} = \frac{X_2 - X_1}{t_2 - t_1} \frac{1}{\left(\frac{X_2 + X_1}{2}\right)} \quad \text{(During non-exponential growth)} \qquad \textbf{Equation 2.13}$$

In Figure 2.12 A, the increase in measured cellular lipid content (g lipid / g DW cell) and the calculated (approximate) average net specific cellular growth rate over the time-period are both plotted versus time in the bioreactors. Lipid accumulation above the baseline lipid content of 5-6% during active growth does not occur until after exponential growth phase has ended, which is also concurrent with the total depletion of nitrate in the culture medium, as shown in Figure 2.12

Figure 2.12: Relationship of lipid content and to algal growth rate and growth phase.

(A) Lipid content and μ (net specific growth rate) plotted versus photodays. Lipid content begins to increase once the exponential growth phase is completed. (B) Nitrate-nitrogen (NO_3-N) concentration versus time. By comparing plots A and B it is clear that lipid accumulation begins concurrently with the depletion of extracellular nitrogen. (C) Lipid content plotted versus specific algal growth rate; as the algal growth rate decreases the lipid content increases.

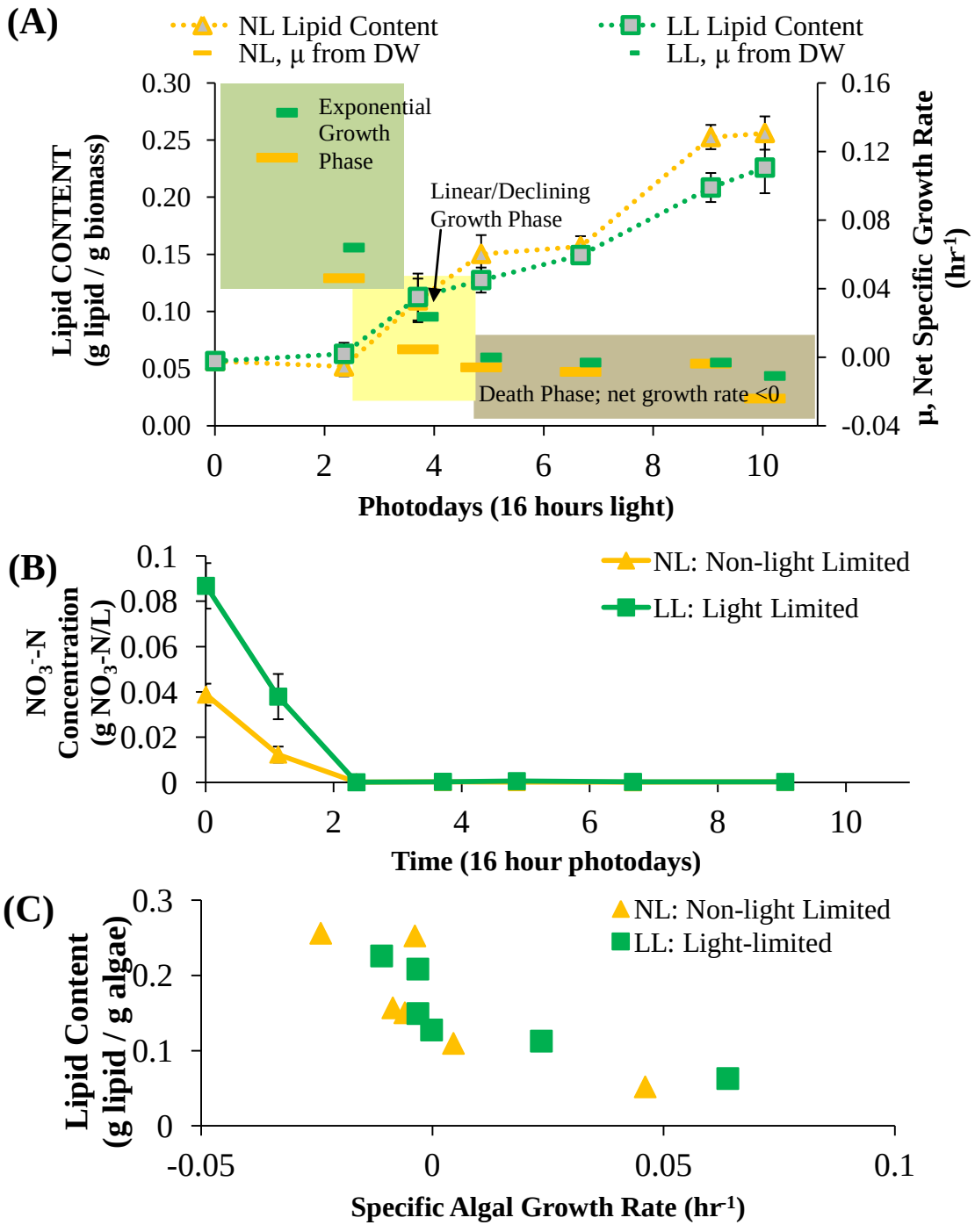

B. During the time when growth is in the linear and stationary phases, and when nitrate is depleted, the lipid content of the algal cells increases from approximately 6% to 22% (for the light-limited treatment) and to 25% (for the non-light limited treatment). While the lipid content of the non-light limited culture did slightly exceed the light-limited treatment, the overall lipid concentration of the light-limited culture far exceeded the NL treatment at the end of the experiment (0.52 g lipid/L versus 0.11 g lipid/L). Obviously, this difference is due to the much larger algal biomass concentration attained by the non-light limited culture. It should be noted that the method of lipid determination employed in this work directly quantifies the total lipid content independently of the lipid's individual solubilities in various solvents, and thus is considered to be highly accurate (Link and Kail, NETL, personal communication). The inverse relationship between specific growth rate and lipid content is clarified further by Figure 2.12 C. Here the lipid content of the alga biomass is plotted versus the apparent growth rate μ. It is clearly observed that the highest lipid content levels occur when the μ is at a minimum, and even less than zero.

While the confirmation of the lipid product formation mode for *Chlorella vulgaris* is interesting from a physiological standpoint, these results confirm previously demonstrated results, and therefore a more interesting analysis of this batch, airlift photobioreactor system is its batch lipid productivity, P_L (g lipid/L culture/day), calculated from any point for the entire batch growth period by **Equation 2.14**. For comparison, the batch biomass productivity (P_B) can be calculated by a similar method, by **Equation 2.15**.

$$P_L = \frac{C_L - C_L^0}{t - t^0} = \frac{m_L X_B - m_L^0 X_B^0}{t - t^0} \qquad \textbf{Equation 2.14}$$

$$P_B = \frac{X_B - X_B^0}{t - t^0} \qquad \textbf{Equation 2.15}$$

The calculated biomass and lipid productivity for the batch, airlift photobioreactor system are shown in Figure 2.13 A and B. It is evident that the light-limited treatment out-performed the

Figure 2.13: Biomass Productivity (A) and Lipid Oil Productivity (B) of *C. vulgaris* over the batch run in the bag photobioreactors.

The maximum biomass productivity and oil productivity is indicated, along with the productivities obtained in the continuous trickle-screen photobioreactor for *C. vulgaris*. The NL treatment consistently performed below the light-limited treatment. The biomass productivity of the LL bag reactor was 34% lower than the trickle-screen (TS) reactor, but the oil productivity was 25% higher than the trickle-screen reactor. This suggests that a batch growth mode of *C. vulgaris* for oil production is more suited to triggering oil production mechanisms.

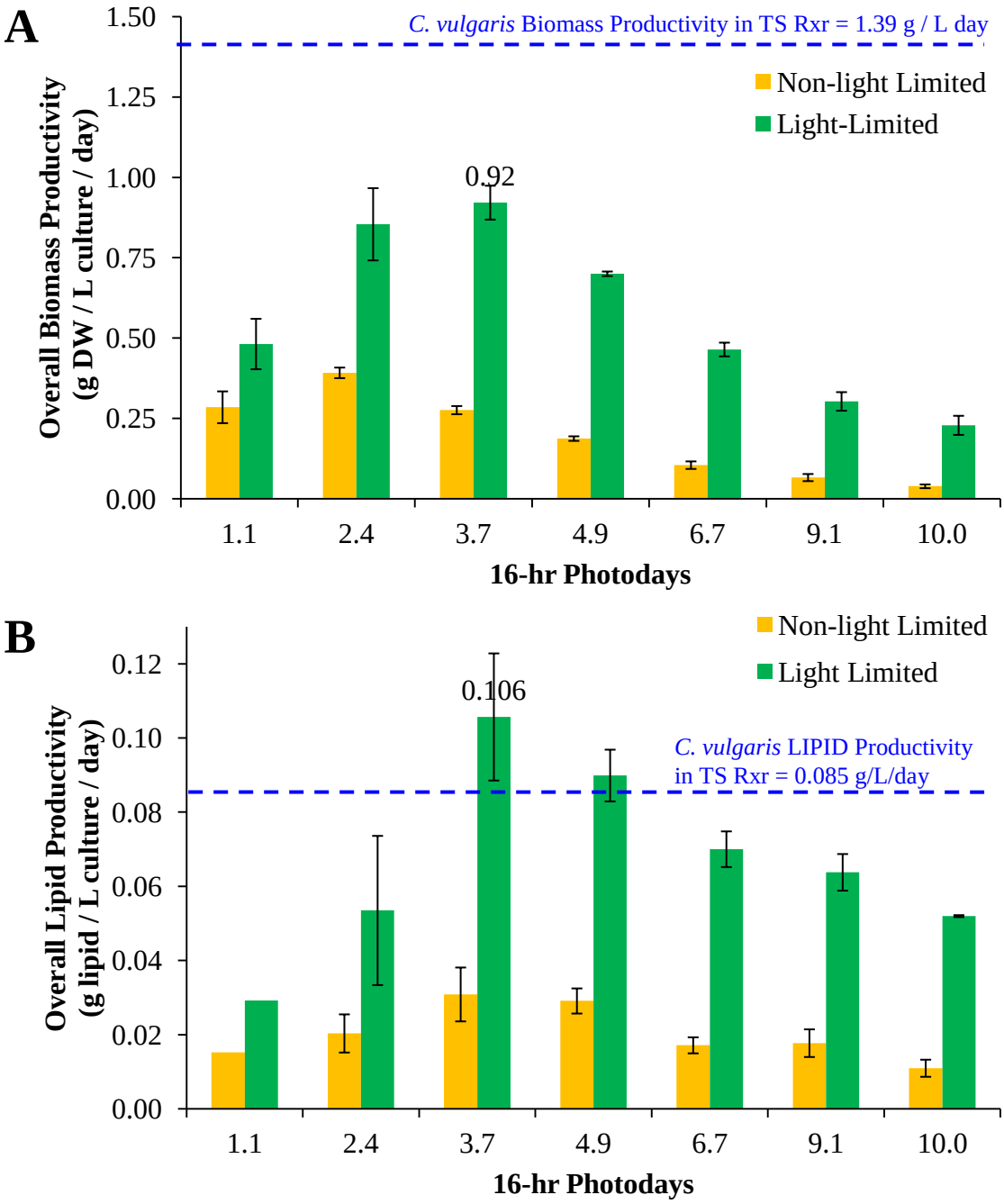

non-light limited system in both algal biomass productivity and lipid productivity at all points during the batch reactor system. Furthermore, while the peak of biomass productivity for the NL treatment occurred at 2.4 days, at the end of the exponential growth period, the peak of biomass productivity for the LL system occurred between 2.4 and 3.7 days, well into the light-limited growth phase of the light-limited (LL) treatment. Furthermore, the attained level of overall algal biomass productivity even of the LL system is significantly lower than that attained by the light-limited trickle-screen reactor system: 0.92 versus 1.39 g DW biomass/L/day. Although it is acknowledged that the light distribution and utilization characteristics of this particular batch photobioreactor system are not fully optimized for batch production system of *Chlorella vulgaris*, the results are fully consistent with the logic that running algal photobioreactor systems at any mode other than at light-limitation inherently restricts their productivity to sub-maximal levels. Furthermore, this also presents evidence towards the observation that it is not the inherent growth rate of which the algal species is capable that determines a system's productivity, but rather the light-distribution characteristics of the system and photon use efficiency of the algae. By increasing the photosynthetically active radiant flux provided per liter of culture in these systems, the overall productivity of the algal biomass would likely have been increased.

Interestingly, overall biomass productivity and overall lipid productivity peak at nearly the same point in the batch culture, despite the fact that the relative rate of lipid production to cellular biomass growth increases significantly once the specific biomass growth rate has dropped below zero. For both treatments, lipid productivity peaks somewhere between 3.7 and 4.9 days, past the end of exponential growth and just before the onset of the biomass growth stationary phase. Therefore, the peak of lipid productivity occurred at a lipid content of approximately 11-15% (for the NL treatment) and 11-13% for the LL treatment. While allowing the batch culture to continue for a longer duration certainly results in a culture with higher lipid concentrations, and

a higher lipid content in the biomass, the actual productivity of the system decreases after 4.9 days.

Productivity and Photosynthetic Efficiency Comparison of Air-lift Batch System with Continuous Trickle-Screen Reactor

An objective of executing the *C. vulgaris* batch air-lift experiments was to obtain productivity data in a batch system (biomass and oil productivity) to compare versus the *C. vulgaris* continuous trickle-screen system. It is interesting to observe that the maximum overall lipid productivity of the light limited air-lift batch system is 25% higher than that of the high-density continuous trickle-screen photobioreactor: 0.106 g lipid / L / day versus 0.085 g lipid / L /day. The overall average PARF (photosynthetically active radiative flux, μmol/s) per Liter of culture volume of the light-limited treatment in this photobioreactor system is approximately 27.4 μmol/s/L; for the light-distribution optimized continuous trickle-screen reactor the PPFD (photosynthetically active photon flux density, $\mu mol/m^2/s$) was measured as 282 $\mu mol/m^2/s$ parallel to the vertical screen, and using the total area of both sides of the trickle-screen reactor screen (0.649 m^2) and the culture volume (0.500 mL), the PARF per L of culture volume was approximately 366 μmol/s/L. Qualitatively, it is evident that the batch system captured light energy into lipid oils much more efficiently than the continuous system; this effect is quantified below. However, it is noteworthy to consider that the continuous trickle-screen system operated at an optical density of 36-39 whereas the batch bag reactors had a maximum OD of only 9.5. Therefore, even despite the thin film arrangement of the trickle-screen reactor, the high OD combined with the cycling of the culture down the screen then through a reservoir meant that a large portion of the algal culture's time in the trickle-screen reactor was in the dark.

A metric that explicitly compares the ability of the different systems to effectively capture photosynthetic energy is to determine a photosynthetic efficiency. A variety of methods of calculating the photosynthetic efficiency have been presented elsewhere (Kirk 1994). For the purposes of this work, two photosynthetic efficiencies are defined:

1. η_{oil} : efficiency of light energy captured into oil energy, where P_{oil} is the oil productivity (g oil/L/day), ΔH_{oil} is the heat of combustion of oil (kJ/g), PAI is the photosynthetically active irradiance (W/m^2), A is the lighted area of the reactor, and V is the total volume of the culture in the reactor (**Equation 2.16**).

$$\eta_{oil} = \frac{P_{oil}\Delta H_{oil}}{PAI\ (A)}V \qquad \textbf{Equation 2.16}$$

2. η_{tc} : efficiency of light energy captured into total culture (tc) organic compounds (algal biomass, algal oils, and extracellular organic compounds such as polysaccharides), where P_{tc} is the total culture productivity (g/L/day) and ΔH_{tc} is the heat of combustion of dry total culture solids (kJ/g) (**Equation 2.17**).

$$\eta_{tc} = \frac{P_{tc}\Delta H_{tc}}{PAI\ (A)}V \qquad \textbf{Equation 2.17}$$

The energy available from the incident photosynthetically active photon flux density (μmol/m^2/s) will vary with the exact wavelength of the light, but an average value of underwater light energy for a range of water types is 0.24MJ per mole of quanta (Kirk 1994), which enables photosynthetically active irradiance (PAI, W/m^2) to a system to be calculated from the PPFD. The rate of energy captured into oils can be calculated from the oil productivity and the energy content of the oil species (37.3 kJ/g for lipid oils and 44.8 kJ/g for botryococcene hydrocarbon oils). Similarly, the rate of energy captured into total culture organic compounds can be calculated from the total culture productivity and the total culture heat of combustion (reported in Appendix B). Table 2.8 provides a summary of the photosynthetically active irradiance (W/m^2),

the incident PAR power per liter culture (W/L), η_{oil}, and η_{tc} for each the Light Limited Trickle Screen (TS) reactor systems, and the Light Limited and Non Light Limited batch reactor systems.

Table 2.8: Comparison of available light energy and efficiency of energy capture into each oil and total culture organic compounds among the four algal growth systems discussed in this work: high-density light-limited trickle-screen reactors of *B. braunii* and *C. vulgaris* and the batch bag reactors of *C. vulgaris* (non-light limited and light-limited).

PAI = Photosynthetically Active Irradiance; PAR = Photosynthetically Active Radiation; HD = High Density; TS = Trickle Screen; LL = Light-Limited; NL = non-light limited

	PAI *(W/m^2)*	**Incident PAR Power per L culture** *(W/L)*	**η_{oil}: Efficiency of Energy Capture into Oil**	**η_{tc}: Efficiency of Energy Capture into Total Culture**
HD LL Continuous TS, *B. braunii*	68	88	0.23%	1.2%
HD LL Continuous TS, *C. vulgaris*	68	88	0.062%	0.68%
NL Batch, *C. vulgaris*	65	6.53	0.31%	1.9%
LL Batch, *C. vulgaris*	64	6.58	1.0%	5.3%

The slightly higher lipid productivity of the light-limited batch system, despite a much lower PARF per unit culture volume indicates a more efficient utilization of the light into oil by *C. vulgaris* in the batch system, and this is verified by the calculated η_{oil} of 1.0% for the batch system. By comparison, the η_{oil} in the trickle-screen reactor system was only 0.062% for *C. vulgaris* and 0.23% for *B. braunii*. Obviously, the photosynthetic efficiency of energy capture into oils is very low for all of these systems; in addition to the energy being dissipated as heat, the energy is also being captured into algal biomass and into extracellular excreted compounds such as polysaccharides. When the energy captured into non-oil algal biomass and secreted organic compounds is considered (η_{tc}), the calculated efficiencies all rise as expected. The largest increase is for the high-density continuous *C. vulgaris* system, since very little energy was partitioned into oil production but energy was put into biomass and extracellular organics

production. However, in comparing the systems the overall trends remain the same; the most efficient user of light energy was the Light-Limited batch system. Because both the non-light limited batch system and the high-density systems were all lower in efficiency, it is speculated that the efficiency penalty experienced by each of the other systems is for different reasons. For the non-light limited system, it is likely that the algal concentration was not sufficient to capture all the light incident on the system, and therefore significant light energy simply either passed through the system or was dissipated as heat. For the high-density systems, which were extremely light-limited, the culture density was such that very little light was able to penetrate into the system; in this case, much of the algae would have been living using dark respiration, living off stores of energy created during times of photosynthesis and therefore decreasing the overall efficiency of the light energy captured into useful compounds.

In the case of the continuous trickle-screen reactor systems, the daily removal of 7.5% of the algal mass in the system forces the system to be continuously growing to replace that lost biomass. While *B. braunii* also synthesizes the botryococcene hydrocarbons concurrently with growth, in the TS system the majority of the energy of *C. vulgaris* was utilized for the production of biomass and not lipids, as evidenced by the very low lipid content of *C. vulgaris* in that system. Conversely, in the batch system the cessation of growth enabled the switch of *C. vulgaris'* metabolism over to lipid production, which resulted in a large increase in the photosynthetic efficiency of *C. vulgaris* in the batch system compared to the continuous system. Whether it was the requirement of daily growth by *C. vulgaris* in the continuous system or the constant presence nitrogen that suppressed the accumulation of lipids in the trickle-screen reactor system is not distinguished in these studies.

Some characteristics of the trickle-screen system that could have contributed to its lower efficiency compared to the batch system are listed and briefly discussed here. First, the illuminated area of the trickle-screen was not entirely covered by algal culture; in fact, the algae

culture tended to coalesce together into rivulets running down the screen, rather than spreading out over the entire surface of the screen. Though the efficiency calculations used the entire exposed area of the screen, in reality it is likely that only a much smaller area of algae was actually effectively illuminated because of this issue. Furthermore, the collection of the algae into rivulets also meant that the thickness of the algal culture through which the light must pass through is significantly greater. This would have lead to additional attenuation compared to a culture in which the algae had been fully spread out over the screen. In subsequent reactor runs, with different experimental purposes, the algal culture was manually spread out over the entire surface of the screen at the beginning of the run to better utilize the illuminated area. In subsequent continuous TS reactor runs, where the operating conditions were sufficiently different from the original runs to exclude the ability to make a direct comparison between the results, *C. vulgaris* biomass and oil productivities of 2.5 and 0.12 g/L/day, respectively, were achieved. These productivities are 80% and 41% higher, respectively, than those obtained in the continuous trickle-screen reactor system described in this work. These occurred under similar PPFD lighting conditions and with *lower* rates of carbon dioxide supplementation, confirming that light and not CO_2 is the rate-limiting factor for algal productivity in these systems. These results indicate that the poor spreading of the algal culture in the TS runs discussed in this work could have contributed to the low efficiency.

Another characteristic of the trickle-screen reactor system that varied significantly is the rate of cycling of the algae from light to dark. In the trickle-screen reactor system, there are two rates of cycling that would occur; first, as the algae traveled down the trickle-screen, the algal cells would cycle from light to dark due to the eddies formed by the trickling motion. The exact intensities of light experienced in both the ‘light’ and ‘dark’ regions and the residence time in each is a function of the thickness of a rivulet, the viscosity of the algal culture, the overall optical density of the algal culture, and a variety of other factors, and the calculation of this cycle is

beyond the scope of this current work. A secondary light-dark cycling arises from the fact that after the algae's trip down the screen, the culture was collected into a vessel at the base of the screen where it would reside for a short time until its trip back up through tubing to the top of the screen again. The approximate length of time for the algae to cycle through the whole system was about 45 seconds. Various researchers have studied the effects of the length of cycling between the light and the dark on photosynthesis; Grobbelaar (2010) provides a summary. In early work, Kok (1953) concluded that for photosynthesis to proceed at maximal efficiency, the amount of time the algae are exposed to light should be at most $1/10^{th}$ the time they are exposed to the dark, and this was interpreted as the utilization of 'residual' light every in the dark in the time between when the next dose of light was received. However, for this enhancement to be realized, relatively high photon flux densities are required due to the dilution of the light in high-density algal culture (Terry 1986). Furthermore, the duration of the light periods must be sufficiently short to match the time required to turn-over the primary electron acceptor of Photo System II from its reduced to oxidized state, which is approximately 1 ms (Grobbelaar 2010). Periods of light duration in excess of this will be dissipated, while periods of light duration shorter than this will result in rate-limitation by light. Laws *et al.* (1983) has observed that light fluctuations on the order of this time-scale have an enhancing effect to productivities, but fluctuations of increasing duration lead to decreased productivities (Grobbelaar 2010).

Intermittent light falls into three ranges: low frequency cycles are on the order of hours to days; medium frequency fluctuations occur on the order of seconds to minutes, and the productivity-enhancing high frequency fluctuations occur on the order of 100ms or shorter (Grobbelaar 2010). The light-dark fluctuations imposed upon algae traveling down the turbulent trickle-screen should fall well within the range of high-frequency fluctuations and could have an enhancing effect on algal productivity. However, the periodic cycling of algae through the trickle-screen reactor reservoir and tubing back to the top of the screen would result in medium

frequency fluctuations in light, which would not be expected to enhance productivity, and could actually detract from the productivity of the trickle-screen system. The vertical bag reactor system, however, would be expected to have fluctuations falling somewhere between the high- and medium-frequency fluctuations, (the exact calculation of these frequencies is beyond the scope of this thesis). The absence of true medium-frequency fluctuations (order of minutes) in the case of the vertical bag reactor could be a contributing factor to the increased light utilization efficiency of this system.

Despite the fact that the *C. vulgaris* culture grown under light-limited conditions in a batch configuration resulted in the most efficient utilization of the light energy, the overall energy productivity of this system (the rate at which every was captured into oils) was still only 34% of that of the *B.braunii* continuous reactor system, as can be observed by Figure 2.14.

Figure 2.14: Productivity of Oil Energy (kJ oil / L / day) for each of the four algal systems discussed in this work.

HD = High-Density; TS = Trickle-screen; LL = Light-Limited; NL = non-light limited

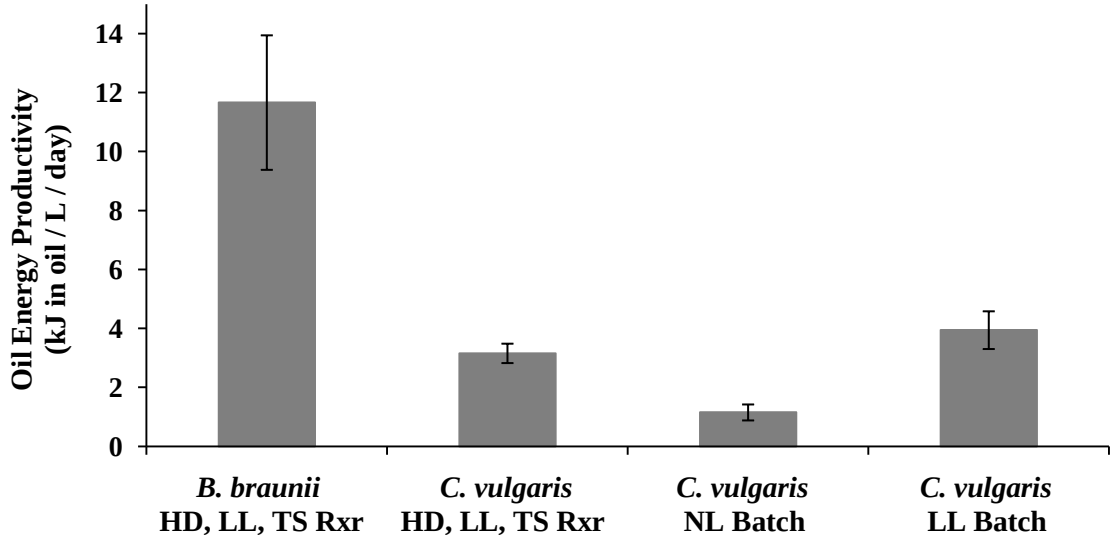

Comparison of Biomass and Oil Productivities with Literature Reports

The productivities of each the continuous trickle-screen reactor systems and the batch reactor systems presented in this work are compared to other algal productivities in the literature in Table 2.9-Table 2.11. While the emphasis of this work is upon *B. braunii* (Table 2.9) and *C. vulgaris* (Table 2.10), in order to enable direct comparison to the species in this work some other species have also been included in this comparison (Table 2.11). Within each grouping they are ordered by the lipid productivity, reported from highest to lowest. Because of the range of lighting strategies employed by the different works, all results are normalized to the photohour to decrease the effect of continuous lighting scenarios versus day/night sequences.

The continuous trickle-screen systems of Grady (2010) described in the introduction to this work are numbered as 1 (Table 2.9) and 11 (Table 2.10), and the LL treatment of the batch system described extensively in the batch system of this work is number 10 in Table 2.10.

B. braunii in the continuous trickle-screen photobioreactor (Number 1, Grady, 2010) is the most productive system in terms of algal biomass productivity, not just among *B. braunii* but across the entire spectrum of reviewed systems in the literature. It is noted here that the oil content of this system has been called into question based on the potential use of an over-concentrated squalene standard in the analysis of these samples, as discussed previously. The values shown in parentheses are those that would result if a prior calibration curve was used to correct the values. (The investigation into this is currently on-going). Obviously, if the correct values were utilized, the productivity of this system would exceed all other systems by an even greater magnitude; however, this cannot be decisively established at this time. Even using the originally calculated oil content and productivity, the *B. braunii* continuous trickle-screen system of (Grady 2010) system also has the highest oil productivity across all systems except for one; this outlier (Number 18, Table 2.11, Kong et al., 2010) has a very high productivity (21 mg

oil/L/hr) but is from the alga *Chlamydomonas reinhardtii*. This alga is not known for high level lipid production, although it is known to produce lipids under conditions of nitrogen limitation (Moellering & Benning, 2010; Wang et al., 2009). The biocoil photobioreactor system employed by Kong et al. (2010) is a continuous system, such that the algae are continuously growing and being supplied with nutrients for their growth. Based on the daily dilution rate utilized (56%) and the reported biomass productivity (2.0 g/L/day), the biomass density in the photobioreactor system can be estimated as 3.54 g/L. The growth medium for the experiments with this reported

Table 2.9: Comparison of *B. braunii* biomass productivities and oil productivities in the literature

(1) Productivities have been normalized to the photohour because of the different lighting phases utilized in the various works cited. In the case of batch-mode reactors the productivity reported is the maximum value attained from the beginning of the batch run
(2) Converted from Klux using conversion factor of 14 μmol/m^2/s per Klux for halogen lamps (Biggs)
(3) Value not explicitly reported in original manuscript; estimated from data presented in tables, figures, or text
(4) Not explicitly stated; assumed continuous
(5) Values based on potential correction to the *B. braunii* oil content, due to underestimated determinations resulting from a potentially over-concentrated standard. Whether this adjustment can be considered more accurate remains to be determined.

***Botryococcus braunii* Strains**									
Strain (Race)		**Mode**	**Reactor Type**	**Lighting Intensity (μmol/ m^2/s) and Phase (light/dark)**	**Biomass Prod. (1) (mg/L/ photo hr)**	**Extraction Solvent / Quant. Method**	**Determined Oil Content (% of biomass)**	**Oil Prod (1) (mg/L/ photo hr)**	**Reference**
1	*Showa* (Race B)	Continuous (7.5% DR)	Turbulent Trickle Screen	282 16 / 8	96.3	Hexane / GC-MS	17.7% *(26.8%)*(5)	17 *(26)*(5)	(Grady 2010)
2	unknown (Race A)	Batch	Cylindrical Airlift	119 14 / 10	19	Hexane / GC-MS	44.2%	9.3	(Casadevall et al. 1985)
3		Continuous (30% DR)			29		27.0%	7.8	
4	unknown (Race B)	Batch	Bubble Column	140 (2) 24 / 0 (4)	14 (3)	Hexane / Gravimetric	50%	7.5 (3)	(Kojima and K Zhang 1999)
5	UTEX 572 (Race A)	Batch	Bubble Column	100 24 / 0	32 (3)	Hexane / GC-FID	13%	3.8	(An et al., 2003)
6	*Showa* Race B)	Batch	Flask	250 24 / 0	7.5 (3)	Hexane / GLC-FID	24-29%	2.0 (3)	(Wolf, Nonomura, and Bassham 1985)
7	*Showa* (Race B)	Continuous Perfusion (5.7% DR)	Cylindrical Airlift	68 24 / 0	1.2	Hexane / gravimetric	49%	0.57	(Sawayama, Inoue, and Yokoyama 1994)
8	UTEX 572 (Race A)	Batch	unknown	150 24 / 0 (4)	1.1	Bligh and Dyer / gravimetric	25.8%	0.21	(Yoo et al., 2010)

biomass productivity and the lipid productivity of 21mg/L/hr was wastewater, specifically centrate, which is the wastewater that results from centrifugation of activated sludge. Centrate is rich in nutrients, particularly ammonia nitrogen and phosphorus. The centrate employed in the work of Kong et al. (2010) was reported to have an ammonia content of 67 mg/L, a total phosphorus content of 121 mg/L, and a total Kjeldahl nitrogen (ammonia-nitrogen plus organic

Table 2.10: Comparison of *C. vulgaris* biomass productivities and oil productivities in the literature

(1) Productivities have been normalized to the photohour because of the different lighting phases utilized in the various works cited. In the case of batch-mode reactors the productivity reported is the maximum value attained from the beginning of the batch run

(2) Converted from Klux using conversion factor of 14 μmol/m^2/s per Klux for halogen lamps (Biggs)

(3) Value not explicitly reported in original manuscript; estimated from data presented in tables, figures, or text

***Chlorella* Species**									
Species (Strain)		**Mode**	**Reactor Type**	**Lighting Intensity (μmol/ m^2/s) and Phase (light/dark)**	**Biomass Prod. (1) (mg/L/ photo hr)**	**Extraction Solvent / Quant. Method**	**Determined Oil Content (% of biomass)**	**Oil Prod (1) (mg/L/ photo hr)**	**Reference**
9	*Chlorella* spp. (multiple)	Semi-cont. (50% DR)	Cylindrical Airlift	300 24 / 0	44	Sonication + Chloroform-MeOH / Gravimetric	33.9%	15	(Chiu et al. 2008)
10	*C. vulgaris* (UTEX 2714)	Batch	Air-lift loop bag	268 16 / 8	58	DTE / GC-FID	11.0%	6.6	This Work
11		Continuous (7.5% DR)	Trickle Screen	282 16 / 8	87	DTE / GC-FID	6.7%	5.3	(Grady 2010)
12	*C. emersoni* (CCAP 211/11N)	Batch	2L Stirred Bioreactor	25 24 / 0 (2)	3.3	Bligh-Dyer / Gravimetric	63%	2.1	(Illman, Scragg, and Shales 2000)
13	*C. vulgaris* (not stated)	Batch	Cylindrical Airlift	60 24 / 0	8.3 (3)	FT-IR Spectrometry	20%	1.7	(Lv et al., 2010)
14	*C. vulgaris* (CCAP 211)	Batch	2L Erlenmyer Flasks	70 24 / 0	5.9	Ultraound + Chloroform-MeOH / Gravimetric	14.4%	0.85	(Converti et al., 2009)
15	*C. vulgaris* (CCAP 211/11B)	Batch	2L Stirred Bioreactor	25 24 / 0 (2)	1.5	Bligh-Dyer / Gravimetric	40%	0.62	(Illman, Scragg, and Shales 2000)
16	*C. vulgaris* (KCTC AG10032)	Batch	unknown	150 24 / 0 (2)	4.4	Bligh-Dyer / Gravimetric	6-10%	0.29	(Yoo et al., 2010)
17	*C. protothe-coides* (CCAP 211/8D)	Batch	2L Stirred Bioreactor	25 24 / 0 (2)	0.96	Bligh-Dyer / Gravimetric	23%	0.22	(Illman, Scragg, and Shales 2000)

nitrogen) content of 128 mg/L. The content of any nitrate-nitrogen is not reported but typically the levels of nitrate are low in activated sludge if there is no nitrification step in conjunction with the activated sludge. Assuming that the algae were not able to utilize any of the organic nitrogen compounds, and based on the estimated biomass concentration of 3.54 g/L, the 67 mg/L NH_3 is sufficient to ensure a minimal content of1.9% nitrogen in the biomass. Based on work undertaken in the Curtis Lab, this low of a nitrogen content in the biomass is likely to trigger lipid accumulation, but only after the cessation of growth. Because the algae were fed daily, the duration of time when external nitrogen levels would be fully depleted would have been short. In the batch experiments described in the work reported here, it took a full 123 photohours for the light-limited treatment (provided 0.070 g nitrogen/L) to increase its lipid content from 5.7% to

Table 2.11: Comparison of biomass productivities and oil productivities in the literature for other species

(1) Productivities have been normalized to the photohour because of the different lighting phases utilized in the various works cited. In the case of batch-mode reactors the productivity reported is the maximum value attained from the beginning of the batch run

(2) Converted from Klux using conversion factor of 14 μmol/m^2/s per Klux for halogen lamps (Biggs)

(3) Value not explicitly reported in original manuscript; estimated from data presented in tables, figures, or text

Other Species

	Species (Strain)	Mode	Reactor Type	Lighting Intensity (μmol/ m^2/s) and Phase (light/dark)	Biomass Prod. (1) (mg/L/ photo hr)	Extraction Solvent / Quant. Method	Determined Oil Content (% of biomass)	Oil Prod (1) (mg/L/ photo hr)	Reference
18	*Chlamydo-monas reinhardtii* (not stated)	Continuous (27% DR)	Biocoil Reactor	220 24 / 0	83	Acetone / Gravimetric	25%	21	(Kong et al. 2010)
19	*Neochloris oleoabundans* (UTEX 1185)	Batch	Flasks	360 24 / 0	17	Ethyl Ether / Gravimetric	34%	5.5	(Y. Li et al., 2008)
20	*Neochloris oleoabundans* (UTEX 1185)	Continuous (55% DR)	Flat panel airlift	270 24 / 0	23	Methanol & chloroform) / Gravimetric (Total) Hexane / Gravimetric (TAG)	23% (total) 3% (TAG)	5.3 (total) 0.69 (TAG)	(Pruvost et al. 2009)
21	*Scenedesmus sp.* (KCTC AG20831)	Batch	unknown	150 24 / 0 (2)	9.1 (3)	Bligh Dyer / Gravimetric	10-12%	0.88	(Yoo et al., 2010)
22	*Nannochlor-opsis oculata* (not stated)	Batch	2L Erlenmyer Flasks	70 24 / 0	4.3	Ultraound + Chloroform-MeOH / Gravimetric	15.9%	0.68	(Converti et al., 2009)

22.6%; it took less than 107 photohours for the non-light limited treatment to increase its lipid from 5.7% to 25%. Therefore, it seems unlikely with the continuous growth of this system that the algae would have had sufficient nitrogen-deplete time periods to have the 25.25% lipid content reported in the work of (Kong et al. 2010). Furthermore, the method of lipid determination utilized, acetone extraction and gravimetric quantification, is not at all specific to lipids suitable for fuel production. It is very likely that the lipid productivity observed in the Kong et al. (2010) work is overestimated.

Thus, except for the Kong et al. (2010) report, whose results are somewhat questionable, the oil productivity by the *B. braunii* continuous trickle-screen system is the highest among all the literature reports surveyed. Among the *Chlorella* oil productivities reported, the light-limited batch airlift system described in this thesis (Number 10, Table 2.10, 6.6 mg oil/L/hr) is second only to the productivity reported by a continuous airlift system described by Chiu et al. (2008) (Number 9, Table 2.10, 15 mg lipid/L/hr). The oil productivity of the light-limited batch system reported in this work however is only 44% of the oil productivity reported by Chiu et al. (2008) for their continuous system. While the biomass productivity of the batch system and the continuous *C. vulgaris* trickle-screen system were actually higher than the continuous system of Chiu, the lipid content (33%) reported by Chiu made the very large difference in the lipid productivities.

The level of nitrogen and phosphorus used in the nutrient medium of Chiu et al. (2008) were extremely low, reported to be only 0.14 mg NO_3-N/L and 0.016 mg phosphorus/L. Based on the reported productivity of 1.055 g/L/day and this nutrient concentration, the nitrogen content of the biomass would have only been approximately 0.01%, which is not enough to support sustained growth of the biomass. It is questioned as to whether there is an error in the reported nutrient concentrations fed to the algal production system. However, if these nutrient concentrations are correct, then the nutrient feeding to the system of Chiu et al. was much lower

than either that for the batch or continuous systems described for *C. vulgaris* in this work. The higher nutrient concentrations employed in this work could have suppressed lipid accumulation leading to the lower productivities.

A major aspect to consider in the comparison of the productivities reported in this work with literature productivities is the method of lipid quantification employed. Because much of the reported data in the literature used gravimetric analysis to assess lipid content, and the method utilized for quantification of lipids in this work utilized a very specific method called a direct-transesterification to assessing the lipid content, these values cannot reasonably be compared. A gravimetric analysis involves simple extraction of cellular biomass with a selected solvent, evaporation of the solvent, and weighing of the residue to approximate lipid content. A large assumption in using this method for lipid content analysis is that the majority of the residue is itself lipid; however without further species identification this assumption cannot be confirmed. A refined approach is to subsequently use a species identification method, such as GC-FID, to identify and quantify the actual species in the residue; this provides information on what extent of the actual mass of the extracted residue is itself various lipid species. However, this method yields very solvent-specific results, as various solvents and solvent combinations will extract a wide variety of compounds with varying efficiency. For example, the cellular components that are extracted using a very non-polar solvent such as hexane compared to a polar solvent such as methanol are quite different. Because lipid species run the gamut of long and short chain fatty acids with a varying degree of saturation, the lipid composition of a cell will determine the extent of the total lipids that are removed by a particular solvent.

By contrast, the method utilized by in this work, developed and executed by our collaborators at the National Energy Technology Laboratory (NETL) involves direct transesterification (DTE) of lipid species (free fatty acids, di-, and tri-acyl glycerides) to their Fatty Acid Methyl Ether counterparts (FAMEs); the FAMEs are subsequently extracted with

hexane, and quantified by GC-FID. Because the FAMEs of all lipid species are comparatively comparable in hexane, the solvent specificity issue is eliminated in this method. The use of GC-FID also has the benefit of directly quantifying only the species of interest, and so other compounds (such as pigments) which are not useful as biofuel feedstock are not considered in the oil content result.

Therefore, the methods of lipid determination employed to quantify the oil production in each this work (DTE) and Chiu et al. (methanol/chloroform extraction with gravimetric quantification) are quite different. The lipid productivity determination of (Chiu et al. 2008) was made with a methanol/chloroform (2:1) extraction of the algae biomass assisted with sonication. After one hour of extraction, the mixture was adjusted with additional chloroform and a 1% NaCl solution to obtain a final ration of methanol:chloroform:water of 2:2:1. Finally, the chloroform phase was removed, the chloroform was evaporated, and the residue weighed for to quantify the lipids. This method is similar to a common lipid determination method called the Bligh-Dyer method. To enable a better comparison of the results of this work for the batch air-lift production of lipid by *C. vulgaris* with the rest of the literature reports of lipid productivities, at the end of the batch production run the remaining algal biomass was collected and subjected to lipid quantification by a Bligh Dyer extraction and gravimetric quantification.

The expectation was that the results of the Bligh-Dyer (BD) extraction and gravimetric quantification would greatly exceed those found by the DTE method; however the opposite was true. In Table 2.12 below, the first column presents the cellular lipid composition as determined by a BD extraction and gravimetric quantification, which were very similar for both treatments (13.6% for NL and 13.9% for LL); a GC-FID quantification was then made on the raw extract, and the percentage of actual lipid species in the residue were determined to be only 56.2% and 54.7% for the NL and LL treatments, respectively. Thus, the second column provides the corrected cellular lipid content based on the GC-FID quantification. It is readily observed that the

gravimetric method provided a cellular oil content that is approximately half of that determined by the DTE method; the BD extraction coupled with a GC-FID quantification provided results only about 28-34% of the DTE determination method. These results confirm the expectation that a gravimetric determination will overestimate the lipid content of the residue due to co-extracted components other than actual lipid species; however, it appeared that the extraction efficiency of the Bligh-Dyer method for extracting all lipid species relative to the DTE method is actually quite inefficient.

Table 2.12: Comparison of lipid contents determined on the batch reactor harvests by three different methods

DTE = direct *in situ* transesterification; FID = flame ionization detection (method for quantifying actual lipid content in a residue)

	Lipid Oil Content (% of Algal Biomass)		
	Bligh-Dyer, Gravimetric	Bligh-Dyer + FID	DTE + FID
NL Treatment	13.6%	7.2%	25.6%
LL Treatment	13.9%	7.6%	22.6%

Several of the cited works used a means of physical disruption, ultrasound or sonication, in order to increase the extent of the lipid species able to be removed and quantified from the algal cells (numbers 9 and 14 in Table 2.10, and 22 in Table 2.11). While 14 (*Chlorella*, Converti et al., 2009) had a much lower lipid productivity than the *Chlorella* systems described in this work, this is primarily because the biomass productivity was so much lower; the gravimetric lipid content of 14 was on the same order as that determined gravimetrically in this work for the Batch system. Number 9 (Chiu et al. 2008), however, had a much higher determined lipid content (by sonication assisted gravimetric determination) than the batch system of this work on the day of the highest lipid productivity. This raises a point of ambiguity in comparing the results; because the batch system Bligh-Dyer gravimetric results were actually lower than the DTE-determined lipid contents, it is possible that the productivities of the number 9 system could have been found to be even higher using a DTE-determination method for lipid content; however it is also possible that the Bligh-Dyer extraction method was simply more effective at extracting lipids from the

number 9 system than for the batch system in this work, possibly because of the sonication-assisted extraction.

While this does little to resolve the matter of what lipid productivity system is 'the best' it does make the case for the necessity for standardized and species-specific quantification methods of lipid and oil content determination for making projections of biofuel feasibility. It also makes clear that great strides are required for bringing algal-produced oils to the point of an economically-feasible alternative energy technology. Even without considering operating costs but just the mere scale of the system required for production of a significant volume of oil, massively large systems would be required. For a modest production of only 1000 L (m^3) of feedstock oil per day, Table 2.13 below provides a perspective on the process volumes that would be required for the top four most productive systems (as listed in Table 2.12).

As can be seen in Table 2.13, for even this very modest rate of oil feedstock production, equivalent to 10 barrels of oil/day, the system volumes required are extremely large.

Table 2.13: Process Volumes required for production of 1000L per day of feedstock oil.
Values are calculated using the assumptions listed in the furthest right column of the table

Number and Reference	Species	P_{oil} (mg/L/hr)	Required Process Volume (m^3)	Assumptions (apply to all systems in this table)
, (Grady 2010)	*B. braunii* (Race B)	17	9,991	Oil production: 10 barrels /day
2, (Casadevall et al. 1985)	*B. braunii* (Race A)	9.3	18,264	12 hours/day light
9, (Chiu et al. 2008)	*Chlorella* spp.	15	11,850	10% downtime
10, (This Work)	*Chlorella vulgaris*	6.6	26,933	25% cloudy day penalty

Conclusions and Future Work

In this work, several advances were made in elucidating the design aspects of algal production systems that will provide enhanced productivity. The most significant aspects are the

need to maximize the light utilization of the photobioreactor system and the screening and selection of algal species for maximal conversion of light energy into oil energy. This was demonstrated by comparing the productivities (biomass and oil) of two very different algal species, *B. braunii* and *C. vulgaris*, in two types of reactor systems. The synthesis of botryococcene hydrocarbon oil by *B. braunii* is a growth-associated process, where the oil synthesis rate scales with overall algal growth rate. By contrast, the synthesis of lipids by *C. vulgars* is not growth-associated; storage lipid synthesis increases when biomass synthesis stops. *C. vulgaris* has a biomass growth rate that is nearly an order of magnitude faster than *B. braunii*, but the energy content of *B. braunii* botryococcene hydrocarbons (on a mass basis) is higher than that of lipids.

The productivity of *B. braunii* and *C. vulgaris* were challenged head-to-head in a high-density, light-limited continuous trickle-screen (TS) reactor system, run at a 7.5% dilution rate. Two key findings were made as a result of this comparison. First, the biomass productivities determined for each species were very similar, despite the large difference in the growth-rate capacity of these organisms. This was a direct result of the light-limited nature of the system, where the rate of light-energy available to the system limited the growth rate rather than the intrinsic growth rate of the organisms. Because the system was designed for maximum light utilization, the algal cultures grew to high density, and the rate-limiting factor for additional growth was the rate at which light could 'get' to the algae. In any large-scale algae system, the rate at which light can be provided to the culture will be the limiting factor for algal productivity, and therefore this finding establishes that algal growth rate is <u>not</u> the ultimate factor in establishing potential productivities. In an algal production system that is rate-limited by an external factor, i.e. the rate at which light energy can be provided, the intrinsic growth rate of the algal species will never be achieved unless that rate-limiting factor is less rate-limiting than the intrinsic growth rate.

The second key finding was that the oil productivity of *B. braunii* was three times higher than *C. vulgaris* on a mass basis, and four times higher on an energy basis, indicating that under the conditions of the continuous reactor the ability of *B. braunii* to effectively capture light energy into oils is much greater. However, the lipid contents of *C. vulgaris* remained very low throughout the entire duration of the continuous TS run, indicating that the system conditions were not optimal for inducing lipid accumulation. The trigger for lipid accumulation by *C. vulgaris* and other lipid-producing algae is low-growth triggered by inorganic nutrient depletion (nitrogen and/or phosphorus). Because growing algae continuously requires constant feeding of necessary inorganic nutrients, lipid accumulation by *C. vulgaris* was not triggered. By contrast, the continuous growth scenario for *B. braunii* was ideal for botryococcene hydrocarbon synthesis. These results confirm the need to take into consideration the product formation kinetics when designing algal production systems and their operational strategies.

Because *C. vulgaris* oil content remained so low in the TS reactor system, air-lift batch reactor runs of *C. vulgaris* were executed to see if a production system better matched to the product formation kinetics would result in higher oil productivities. Two treatments were tested – a non-light limited batch culture (more dilute algal culture) and a light-limited batch that became light-limited due to increased density of the culture and self-shading of the algae. Biomass and oil productivities in the light-limited culture exceeded those achieved by the non-light limited culture at all points through the duration of the reactor run. This supported the theory that maximal algal productivities will always be obtained when light is the limiting factor, rather than the intrinsic growth rate of the algae. When the biomass and oil productivities of the light-limited batch system were compared to those of *C. vulgaris* in the continuous TS reactor, it was found that the oil productivity of the batch system did slightly exceed that of the continuous system up to day 4 of the batch system (0.106 g/L/day versus 0.085 g/L/day); the most productive days for oil occurred when the algae were most rapidly growing even though the lipid content remained

low during this time. However, at durations of batch culture longer than this, the oil productivity declined, even though lipid content of the algae increased dramatically (from ~5% to 22-25%). Therefore, the peak of biomass and lipid productivity, even under batch growth for *C. vulgaris*, occurred almost simultaneously. The oil productivities of *C. vulgaris* in the batch system still fell far below those for *B. braunii* in the continuous trickle-screen system.

The areal efficiency of light utilization can be calculated as the rate that energy is captured into oil or into total culture (biomass, oil, and extracellular secreted organic compounds), divided by the rate of light energy impingent on the reactor illuminated (η_{oil} or η_{TC}, respectively). This parameter was determined for each the *C. vulgaris* and *B. braunii* trickle-screen systems, as well as both the light-limited and non-light limited *C. vulgaris* batch systems. Despite similar photosynthetically active irradiance (W/m^2) incident on each system, the incident photosynthetically active radiation (W) available per liter of culture was much greater for the trickle-screen systems: 88 W/L versus 6.5 W/L (Table 2.8). Therefore, the calculated energy capture efficiency was much lower for the trickle-screen systems, even for *B. braunii*, despite the fact that the volumetric energy productivity of the *B. braunii* trickle-screen reactor was much greater than the batch reactors. This is an interesting result which can potentially be explained by the fact that the algal culture flowing over the trickle-screen formed rivulets rather than covering the entire screen, which would have served to greatly decrease the actually area of illumination for the culture. However, it also needs to be considered that even though the areal efficiency of light utilization was greater for the batch systems, these systems are much more dilute; greater energy would need to be spent in the downstream process for dewatering than in a higher-density system.

The biomass and oil productivities for the reactor systems described in this work were compared against literature reports; at 0.27 g oil/L/day, the productivity of the *B. braunii* continuous high-density trickle-screen reactor, to the best of my knowledge, has the highest oil

productivity reported in the literature. The *C. vulgaris* light-limited batch process and the high-density trickle-screen reactor systems had the second and third highest oil productivities reported for *C. vulgaris*; they fell behind a report which claimed oil productivities 2.5 times higher than the LL batch (Chiu et al. 2008). However, the method utilized for lipid quantification by Chiu et al. (2008) was a chloroform-methanol extraction with gravimetric determination, where there is no assurance that the final mass of the extracted oil residue only contained trans-esterifiable lipids that could be converted to fuel in a biodiesel process. The specificity of the direct-transesterification method utilized in this work quantifies only lipids which can be esterified, and therefore is extremely quantitative and specific. It is possible that the report of Chiu et al. (2008) over-estimated the actual lipid content of the algae. However, this cannot be conclusively resolved, highlighting the need for to develop standard quantification methods for algal lipid and hydrocarbon contents in the assessment of algal biofuel system productivities and performance.

However, even for the high-density *B. braunii* TS photobioreactor system, with the highest reported oil productivity in the literature, the scale of the process that would be required for reasonable rates of oil production is staggering. In order to produce an extremely modest 10 barrels (1000 L) of oil/day, the process volume required for this is nearly 10,000 m^3 (10^7 L). This emphasizes the need for even higher-density, higher-volumetrically productive systems for economic and technical feasibility.

A final outcome of this work was the experimental determination of the heat of combustion of extracted botryococcene hydrocarbons and the comparison of the result with a theoretically calculated value. The experimental determination was slightly higher (+2.0% difference) than the theoretically calculated result, which could be due to an incorrect selection of the exact hydrocarbon structure used in the theoretical calculation. To my knowledge, this is the first report of a measured heat of combustion value for botryococcene hydrocarbons.

Chapter 3

Metabolic Pathways of *Ralstonia eutropha* and *Rhodobacter capsulatus*

This chapter is dedicated to describing the electron transport chains, energy generating pathways, and carbon fixation pathways specific to *Ralstonia eutropha* (formerly *Alcaligenes eutrophus*) and *Rhodobacter capsulatus* undergoing *chemolithoautotrophic* growth. This growth mode is characterized by the utilization of exogenous chemical compounds as the primary energy source, as opposed to light energy from photosynthesis (*chemo-),* the use of only inorganic chemical species in energy generation, in this case H_2 and O_2 (-*litho*-), and the use of inorganic carbon as the sole carbon source (-*auto*-). A detailed, stoichiometric understanding of each the carbon fixation and energy generating pathways was necessary for accurate implementation of microbial energetics theory in yield calculations.

This chapter opens by briefly discussing the carbon fixation pathway active in *Rs. eutropha* and *Rb. capsulatus,* then continues on to describe the electron transport pathways utilized by each organism for energy capture in the form of ATP and reductant power captured into NADH. Finally, the chapter concludes with an overview of the triterpene hydrocarbon biosynthesis pathways from *Botryococcus braunii* which will be engineered into *Rb. capsulatus* in the Curtis Lab.

Carbon Fixation

Under chemolithoautotrophic growth, both *Rs. Eutropha* and *Rb. capsulatus* fix carbon dioxide (CO_2) via the energetically-demanding Calvin-Benson-Bassham (CBB) Pathway (Bowien and Kusian 2002; Paoli and F Robert Tabita 1998). Energy for carbon fixation is required in the

form of ATP and reducing equivalents are provided by the electron carrier NADH: 3 ATP and 2 NADPH (4 electrons) are stoichiometrically required to fix a molecule of CO_2 via the CBB pathway (Lengeler, Drews, and Schlegel 1999). Therefore, carbon fixation in both *Rs.* eutropha and *Rb. capsulatus* serves as the electron sink for the reducing equivalents generated from the oxidation of hydrogen under chemolithoautotrophic growth, requiring complex regulatory links between carbon fixation and energy generation in order to maintain redox homeostasis (Dubbs and F Robert Tabita 2004). Under chemolithoautotrophic growth, reducing energy from the oxidation of H_2 by the electron transport chain is captured into NADH, and the electrons contained in NADH are available for cellular pathways. NADH is known as the electron carrier for catabolic (i.e. energy generating pathways); the electron carrier for anabolic/synthesis pathways, such as the CBB cycle for carbon fixation and the mevolonate pathway to generate botryococcene precursors, is NADPH. The mechanism for NADPH production under the chemolithoautotrophic growth of *Rs. eutropha* and *Rb. capsulatus* is not clear, but possible pathways for its generation are through a NADPH-NAD+ oxidoreductase, which transfers electrons between NADPH and NADH, through a malate-NAD^+ oxidoreductase, or by a similar reversed electron transport mechanism as for NADH generation. For the purpose of this analysis, it was assumed that electrons available as reducing power in the form of NADH would be able to be shuttled to anabolic pathways as needed through an appropriate means.

The ATP required for cellular processes is formed as a result of the proton motive force generated by the capture of the energy in the electron transport chain. Details of these interrelated processes are provided in the following section.

Hydrogen Oxidation, Electron Transport, and Energy Generation

During respirative growth, the electron transport chain is responsible for capturing energy generated from the oxidation of the electron donor and reduction of the electron acceptor (the 'energy-generating reaction') into the cellular energy currency, ATP. Specifically, in the case of chemolithoautotrophic growth by *Rs. eutropha* and *Rb. capsulatus*, the electron transport chain is responsible for capturing the energy released from H_2 oxidation and O_2 reduction. It should be noted that the electron transport chain is not involved with fermentative processes. In prokaryotes, the electron transport chain is physically located in the cytoplasmic membrane. Electrons are removed from H_2 by enzymes called hydrogenases, which catalyze the reaction $H_2 \leftrightarrow 2\ H^+ + 2\ e^-$. These electrons enter into the electron transport chain, and move down their potential gradient until finally reducing oxygen, and the energy released as the electrons move down this gradient is captured in the form of a electrochemical gradient across the cytoplasmic membrane, the 'Proton Motive Force' (PMF).

Because the electron donor hydrogen is also the primary source of reducing power for growth, the electrons from hydrogen must also be transferred to the cellular electron donor NADH. The mechanism by which this occurs and the energy demands associated with this process differ between *Rs. eutropha* and *Rb. capsulatus.* Several other specifics of the electron transport chain also differ, including the exact hydrogenases associated with H_2 oxidation and the number of protons translocated per molecule of H_2 oxidized. Each organism-specific pathway is described in the two following sections. However, the following elements are common:

- Electron flow through the electron transport chain (ETC) generates an electrochemical gradient across the cytoplasmic membrane, also known as the proton motive force, through both passive and active translocation of protons from the cytoplasmic side to the periplasmic side of the membrane (Kleihues et al. 2000; Zannoni, Schoepp-Cothenet, and

Hosler 2008; Gray and Daldal 1995). Active translocation occurs when a charge-separation event occurs as a result of the 'pumping' of H^+ across the membrane; this event is always coupled to the energy released by moving an electron at a higher potential to a lower potential. Passive translocation occurs when a charge-separation event occurs as a result of the uptake of an H^+ on the cytoplasmic side of the membrane (i.e. in the formation of H_2O frm H^+ and O_2), or the release of an H^+ on the periplasmic side of the membrane (i.e. in the oxidation of H_2 to 2 H^+) (Zannoni, Schoepp-Cothenet, and Hosler 2008). These details are clarified in the following sections.

- The Proton Motive Force (PMF) is responsible for the generation of ATP via an ATP synthase (Bowien and Schlegel 1981; Zannoni, Schoepp-Cothenet, and Hosler 2008), and therefore electron transport is coupled to ATP generation.
- Electrons from the electron donor required for cellular processes must be transferred to NADH, the cellular electron carrier (Forrest and Walker 1971).

Electron transport in *Ralstonia eutropha*

Rs. eutropha utilizes hydrogen as an electron donor and oxygen as electron acceptor in chemolithoautotrophic growth, with an overall Gibbs free energy release of $\Delta G_{H2/O2} = -237$ kJ/mol H_2. It possesses two distinct hydrogenases: a membrane-bound hydrogenase (MBH) (Schink and Schlegel 1979) and a soluble, NAD^+-reducing hydrogenase (SH - E.C. 1.12.1.2) (Schneider and Schlegel 1976). The MBH is responsible for shuttling electrons from H_2 into the electron transport chain, but is incapable of directly reducing NAD^+. The SH, on the other hand, is not directly associated with the electron transport chain and does not deliver electrons into the ETC. *Rs. eutropha* is one of only a few species identified to possess both types of hydrogenases; most hydrogen oxidizing bacteria possess only the membrane bound type, which is incapable of

reducing NAD^+. One species, *Norcadia opaca*, has been determined to possess only a SH (Schneider and Schlegel 1976). Whereas the MBH is responsible for initiating the electron transport chain and therefore energy generation, the role of the SH is to generate NADH for CO_2 fixation and other biosynthesis processes (Forrest and Walker 1971). This unique characteristic of *Rs. eutropha* enables it to utilize the energy possessed in hydrogen more efficiently over other hydrogen-oxidizing bacteria. The two hydrogenases and their relevant electron pathways are shown above in Figure 3.1 and Figure 3.2.

Electron transport through the Membrane Bound Hydrogenase:

Molecular H_2 is initially oxidized by the MBH, and electrons are believed to enter the electron transport chain at the level of the ubiquinone/ubiquinol pool (Friedrich and Schwartz 1993). Ubiquinone is an electron carrier that operates within the electron transport chain in both its oxidized form as ubiquinone (UQ) and its reduced form as ubiquinol (UQH_2). The putative pathway from UQH_2 is then the reduction of a Quinol-Cytochrome c Oxidoreductase (cytochrome bc_1, also known as respiratory Complex III), and subsequent reduction of cytochrome c_2 or cytochrome c_y (Kömen et al. 1991; Kömen, Zannoni, and Schmidt 1991; Cramm 2009). The ultimate destination of the electrons is the terminal electron acceptor oxygen, which is reduced to water via various terminal oxidases (Kömen, Schmidt, and Friedrich 1992). Hydrogen has a redox potential of -0.414 V, and once electrons enter the electron transport chain, they step down in potential until they reach oxygen, which has a redox potential of +0.818V. Thus, as the electrons move through the electron transport chain, energy is released at each step, and this energy is partially conserved in an electropotential gradient formed by translocation of protons across the cytoplasmic membrane from the cytoplasmic side to the periplasmic side. The cytochrome bc_1 and the terminal oxidase proteins act as proton pumps, coupling the energy

Figure 3.1: *Rs. eutropha* Energy Generating electron transport chain

Electrons are removed from the electron donor, H_2 by the membrane bound hydrogenase and passed into the electron transport chain at the level of ubiquinone. From there, the electrons travel through the ETC until they are finally transferred to O_2, the terminal electron acceptor. Along the pathway, charge separation events create an electromotive force across the cytoplasmic membrane, which drives the production of ATP. Because charge separation stoichiometry for *Rs. eutropha* could not be found in the literature, the stoichiometry in the figure below is proposed in this work based on the stoichiometry suggested for *Rb. capsulatus* (Zannoni, Schoepp-Cothenet, and Hosler 2008). UQ = oxidized ubiquinone; UQH_2 = reduced ubiquinol

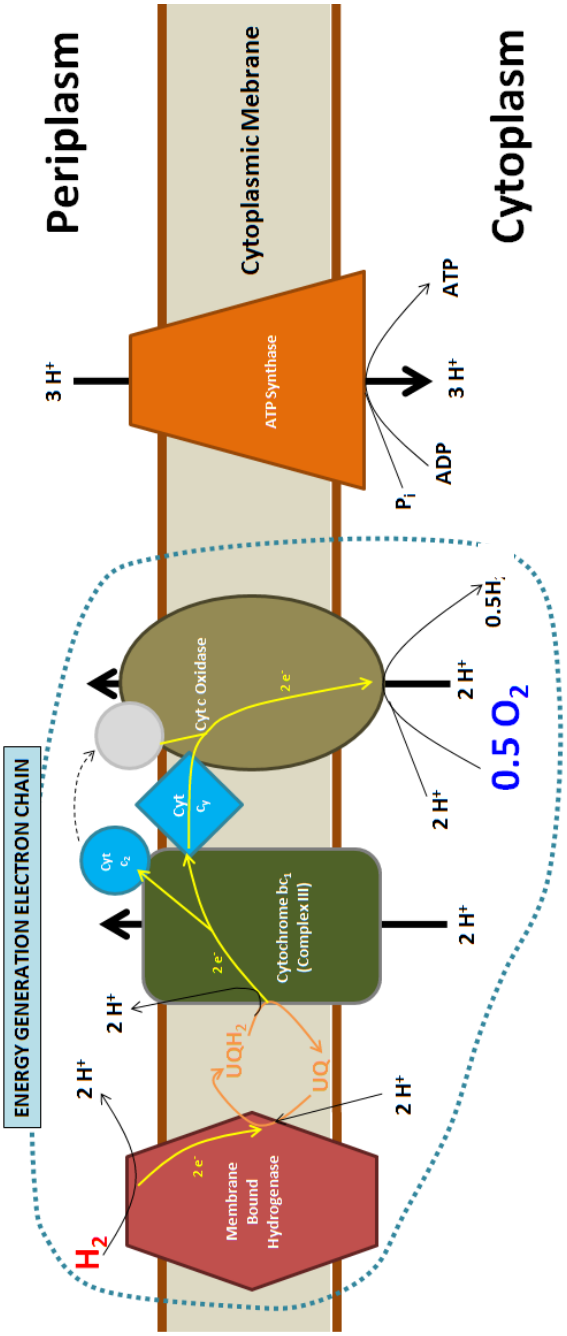

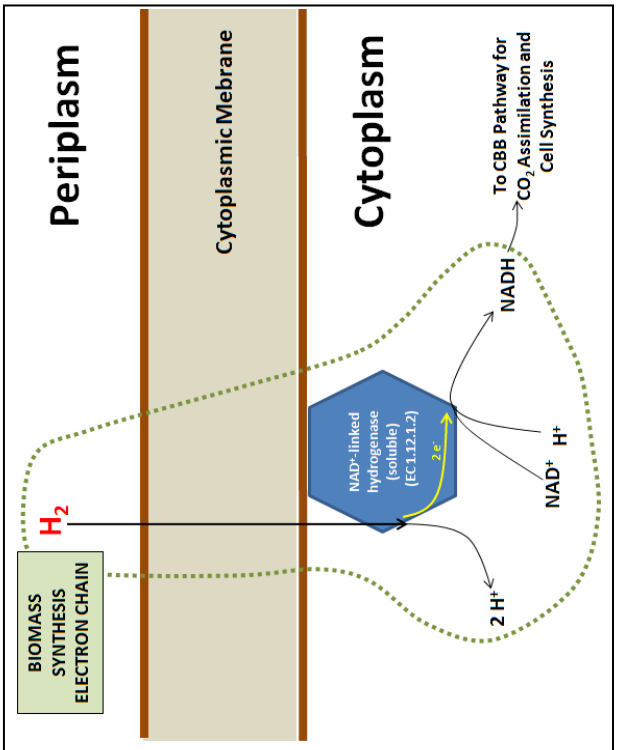

Figure 3.2: *Rs. eutropha* NADH reduction by H_2

Electrons are removed from H_2 by the soluble hydrogenase, and are transferred directly to the cellular electron carrier NADH. This process may dissipate H^+ into the cytoplasm, which would diminish the PMF, or there could potentially be a mechanism for conserving the energy released in this process in the PMF. This aspect of H_2 oxidation to form NADH is not currently clear. NADH is then utilized in various cellular processes including carbon fixation via the CBB cycle.

provided by moving electrons down the potential gradient of the ETC with actively pumping H^+ up against a concentration gradient from the cytoplasm to the periplasm (see Figure 3.1). The MBH and the cytochrome c oxidase translocate protons passively (i.e. this process occurs without energetic coupling) by uptaking H^+ in reactions on the cytoplasmic side and releasing them in reactions on the periplasmic side. Stoichiometry for the charge separation events accompanying electron flow through the ETC in *Rs. eutropha* could not be found in the literature, so the stoichiometry presented in Figure 3.1 is the same as that which was found for *Rb. capsulatus* (described below). Finally, this electropotential gradient (the PMF) drives the formation of ATP by an ATP synthase, where one ATP is formed from each 3 H^+ passed back to the cytoplasmic side (http://www.genome.jp/kegg/pathway/map/ map00190.html).

Electron pathways from the Soluble Hydrogenase:

Hydrogen that is oxidized by the SH transfers its electrons directly to NAD^+ to produce NADH, which has a redox potential of -0.320V; the change in Gibbs free energy associated with this exchange is $\Delta G_{H2/NAD+} = -18$ kJ/mol H_2. The amount of energy released from this reaction is low compared to the total energy released in the transfer of electrons from H_2 to O_2 catalyzed by the ETC (-237 kJ/mol H_2), and it is not clear whether there is a mechanism for conservation of this energy in the electropotential gradient/PMF. Either way, the direct delivery of electrons from hydrogen to reduce NAD^+ has a significant energetic benefit for *Rs. eutropha* compared to a situation without this soluble hydrogenase: *Rs. eutropha* knockouts without the soluble hydrogenase have been observed to grow more slowly than wild-type strains, with a doubling time increase from 3.6 hours to more than 12 hours (Hogrefe, Römermann, and Friedrich 1984; Friedrich and Schwartz 1993). *Rs. eutropha* mutants deficient in the membrane bound hydrogenase, however, showed only a slight decrease in their growth rate compared to the wild-

type, indicating that NADH production via reverse electron is a rate-limiting step for growth in the absence of the soluble hydrogenase (Kömen, Zannoni, and Schmidt 1991).

Electron Transport: *Rhodobacter capsulatus*

Rb. capsulatus also utilizes H_2 as an electron donor and O_2 as the electron acceptor, with an overall Gibbs free energy release of $\Delta G_{H2/O2}$ = -237 kJ/mol H2, and the capture of this energy into an electropotential gradient for the generation of ATP by ATP synthase. Electron flow through the ETC is shown below in Figure 3.3and Figure 3.4. A key difference between *Rb. capsulatus* and *Rs. eutropha* is the fact that *Rb. capsulatus* possesses only a membrane bound hydrogenase, and not a SH. All electrons from the oxidation of H_2 enter directly into the respiratory electron transport chain, likely at the level of the UQ/UQH_2 pool (Gray and Daldal 1995). A second key difference in the ETC is the presence of two different paths along which electrons can travel through the ETC to form the PMF, which is illustrated in Figure 3.3:

- Primary path: UQH_2 reduces cytochrome bc_1, which in turn reduces either cytochrome c_2 or cyt c_y, which in turn reduces the cytochrome c terminal oxidase, and O_2 is reduced to H_2O. Along this path ten charge separation events (translocation of protons from cytoplasm to periplasm) occur for every two electrons removed from an H_2 molecule, equivalent to pumping ten protons from the cytoplasmic to the periplasmic side of the membrane (Zannoni, Schoepp-Cothenet, and Hosler 2008). This path is open for electron flow for all degrees of reduction of the ubiquinone pool (Zannoni 1995).
- Secondary Path: UQH_2 directly reduces a Cytochrome bd-type Terminal Oxidase, which reduces O_2 to H_2O. Along this path only six charge separation events per two electrons removed from an H_2 molecule, potentially suggesting that this pathway is less efficient at energy generation per mole of H_2 oxidized (Zannoni, Schoepp-Cothenet, and Hosler 2008).

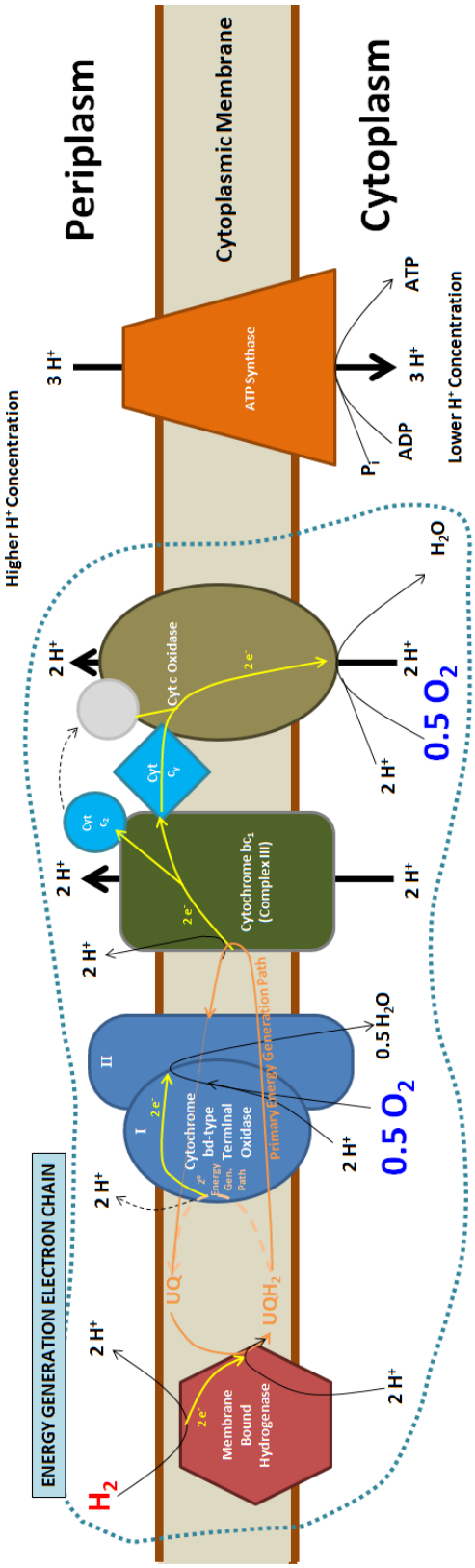

Figure 3.3: *Rb. capsulatus* Energy generating electron transport chain (Left)

Electrons are removed from hydrogen by the membrane bound hydrogenase and enter the ETC at the level of ubiquinone. The electrons can follow two paths through the ETC to oxygen, one that results in 10 charge separation events (the main path) and one that only results in 6 events. The second path only becomes available when the level of reduction of the ubiquinone pool exceeds 25%.

Figure 3.4: *Rb. capsulatus* NADH reduction by reversed electron transport (Below)

Electrons must be obtained from the reduced ubiquinone pool, which is at a lower potential than NADH. Therefore, the production of NADH is coupled with energy consumption. The energy is obtained from the proton motive force, which is used to run the NADH Dehydrogenase 'backwards', taking electrons up the potential gradient from ubiquinone to NADH.

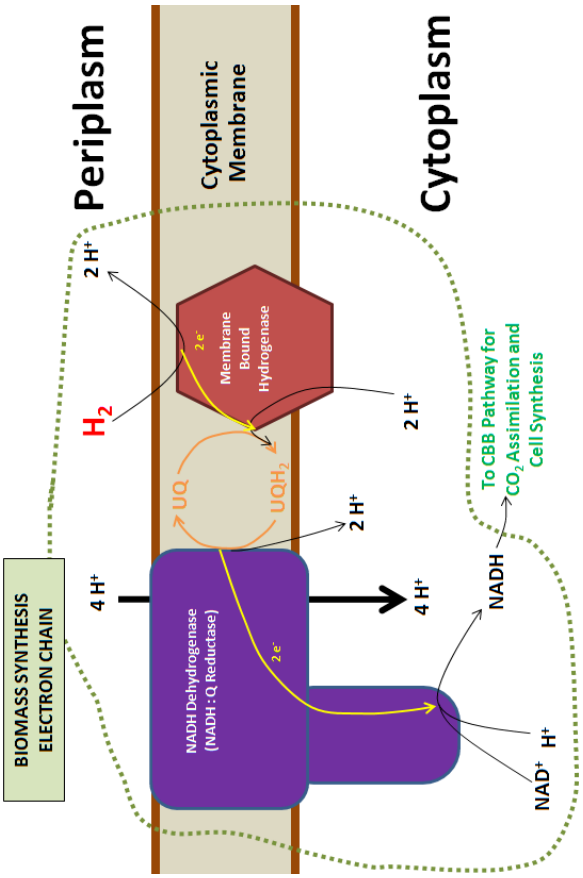

This path does not appear to become active and open to electron flow until the ubiquinone pool is at a degree of reduction of 25% (Zannoni 1995).

A major consequence of the lack of a soluble hydrogenase is the inability of *Rb. capsulatus* to directly couple hydrogen oxidation to NAD^+ reduction, as the MBH is not capable of this. Therefore, in *Rb. capsulatus* H_2 cannot be used to directly reduce NAD^+ via the same mechanism as *Rs. eutropha*. Instead, electrons for the reduction of NAD^+ must come from within the ETC after they have already reduced ubiquinone. However, in order to transfer electrons from within the ETC to the cellular electron donor NADH, energy is required because electrons present at the potential of UQH_2 (and at all subsequent steps in the ETC) are at a lower potential than NADH (-0.320V). Ubiquinone has the highest potential at +0.113V, but this is still below the potential of NADH.

The pathway proposed by Kömen *et al.* (1992) for the production of NADH is via reversed electron flow through the NADH-Ubiqinone Dehydrogenase enzyme, also known as respiratory Complex I (shown in Figure 3.4). This is the same mechanism by which the dissipation of reducing power from an overly-reduced ubiquinone pool to NAD^+ under phototrophic growth of *Rb. capsulatus* would occur (Dupuis et al. 1997; Tichi, Meijer, and F.R. Tabita 2001). In the forward direction, Complex I catalyzes the oxidization of NADH produced from cytoplasmic reactions, subsequently reducing UQ and capturing the liberated energy by pumping protons up their electrochemical gradient to the periplasm. In the reverse direction, this enzyme would need to utilizes the energy contained in the proton motive force to reverse electron flow up the potential gradient from UQH_2 to NADH. This mechanism for NADH production would therefore diminish the energy stored in the electrochemical gradient and subsequently reduces the amount of ATP that can be produced as a result of the energy generating electron transport chain.

Furthermore, the lack of the SH couples the rate of NADH generation directly to the rate at which reversed electron transport through Complex I can proceed; because NADH is required for reducing CO_2 in the CBB pathway, the rate of carbon fixation is also coupled to the kinetics of reversed electron transport. A study by Kömen *et al*. (1992) showed that a soluble hydrogenase-deficient mutant of *Rs. eutropha* had a doubling time of greater than 8 hours, corresponding to a growth rate of 0.087 hr^{-1}, whereas the wild type strain had an observed growth rate of 0.19 hr^{-1} in this study. In other studies, *Rs. eutropha* has been observed to have growth rates ranging from 0.3-0.42 hr^{-1} (Repaske and Mayer 1976; Bongers 1970; Siegel and Ollis 1984). Comparatively, a maximum observed growth rate ranging from only 0.0772-0.12 hr^{-1} has been observed for *Rb. capsulatus* (Madigan and Gest 1979; Siefert and Pfennig 1979). The reduced rate of growth of both the SH-deficient mutant of *Rs. eutropha* and of *Rb. capsulatus* indicates that production of NADH in the absence of a SH could impose a rate-limitation on CO_2-fixation and growth, which has been proposed by Kömen et al. (1992).

Biofuel Production Pathways: Isoprene Biosynthesis

This section will briefly describe the isoprene biosynthesis pathways required specifically for the triterpene hydrocarbons (Botryococcenes) produced by *Botryococcus braunii*, Race B. Neither *Ralstonia eutropha* nor *Rhodobacter capsulatus* natively possess these pathways, and therefore this capability must be engineered into the organisms. Therefore, the yields predicted as the outcome of this work is currently only theoretical, and cannot be verified against an experimental system until the pathway engineering in *Rb. capsulatus* has been accomplished; this work is currently in progress in the Curtis Lab.

Many compounds produced by living organisms, such as carotenoids, cholesterol and steroids, and plant essential oils, fall into a class of compounds termed ‘isoprenoids’. Isoprenoids

are constructed from the basic building block isopentyl diphosphate (IPP), a five carbon compound, by a polymerization reaction catalyzed by prenyltransferase. Isoprenoids are polymers of IPP, and the nomenclature is such that C_{10} compounds (two IPP monomers) are termed 'monoterpenes'. The triterpenoid compounds under which the botryococcene hydrocarbons are classified are compounds with 30+ carbons; the additional carbons are obtained from methyl addition to the C_{30} triterpenoid backbone.

Isoprenoid precursors are derived from the the key cellular metabolite Acetyl-CoA by two possible pathways: the Mevolonate pathway (MVA), which is found in higher organisms including *B. braunii*, or the non-mevolonate/Methyl Erythirol Phosphate (MEP) pathway, which is found in many bacteria including *Rb. capsulatus*. Therefore, two parallel strategies are being employed for the genetic engineering of isoprenoid biosynthesis into *Rb. capsulatus* in the Curtis Lab:

1. Insertion of the entire MVA pathway into *Rb. capsulatus*, based on the hypothesis that heterologous, eukaryotic pathways will be unregulated in prokaryotic *Rb. capsulatus*, therefore maximizing isoprenoid precursor flux.
2. Removal of rate-limiting steps in the existing MEP pathway by heterologous over-expression of key enzymes.

MVA Pathway: Acetyl-CoA to IPP via Mevolonate

The intermediate mevolonate is produced from three Acetyl-CoA molecules via a three step process that requires two NADPH or NADH. Mevolonate is then phosphorylated twice to produce mevolonate diphosphate, and a third ATP molecule is required for the final reaction to IPP, from which higher order terpenoids can be produced.

Non-Mevalonate/Methyl-erythritol Phosphate Pathway: Acetyl-CoA to IPP via MEP

The non-mevolonate pathway does not begin with Aceyl-CoA, but instead from glyceraldehyde-3-phosphate (G3P) and pyruvate; both of these metabolites are products of glycolysis, where G3P is produced upstream of pyruvate and pyruvate is the final product. The typical route for conversion of pyruvate to Acetyl-CoA is pyruvate decarboxylase, which produces a molecule of NADH and occurs as the link between glycolysis and the Krebbs cycle (Citric Acid or TCA cycle) in aerobic organisms. G3P and pyruvate are combined in a 2-step mechanism which requires oxidation of one NADPH to produce 2-C-methyl-D-erythritol-4-phosphate (MEP). A series of five subsequent reactions converts MEP to IPP, which require one CTP (cytidine triphosphate), one ATP, oxidation of one reduced ferredoxin, and oxidation of an additional NADPH.

Terpenoid Polymerization: IPP to FPP

IPP (five carbon hemiterpenoid) is isomerized to dimethylallyl diphosphate (DMAPP), and then a second IPP molecule is combined with IPP to yield the 10-carbon geranyl diphosphate (GPP), a monoterpenoid. GPP is then combined with an additional IPP to yield the 15-carbon (sesquiterpenoid) farnesyl diphosphate (FPP). Each of these reactions is a polymerization step that results in the release of a diphosphate group, but no further ATP or NADH cofactors are required for these steps (http://biocyc.org/META/NEW-IMAGE?type=PATHWAY&object=PWY-5123&detail-level=3).

Botryococcene Synthesis from FPP: Two possible mechanisms

The mechanism for botryococcene synthesis initially proposed was for the polymerization of two FPP molecules to produce C_{30} botryococcene via botryococcene synthase, requiring the oxidation of a single NADPH molecule (Okada 2004). More recently, Niehaus *et al.* (2011) have described the mechanism of botryococcene synthesis as occurring in two steps from FPP. First, two FPP molecules are combined by squalene-synthase-like enzyme 1 (SSL-1) to produce pre-squalene diphosphate (PSPP); the reductive rearrangement of PSPP by squalene synthase-like enzyme 3 (SSL-3) then occurs to produce C_{30} botryococcene by the oxidation of a single NADPH (Niehaus et al. 2011). By either mechanism, the pathway from IPP to C_{30} botryococcene requires only a single additional NADPH, which is involved in either the combination of two FPP directly to botryococcene (mechanism 1) or the reductive rearrangement of pre-squalene diphosphate into botryococcene (mechanism 2).

Botryococcene Synthesis: Energetics Overview

Assuming that the MVA pathway is utilized for botryococcene synthesis, the total cofactor requirements for one molecule of C_{30} botryococcene, starting from Acetyl-CoA, are 13 molecules of NADPH and 18 molecules of ATP. The synthesis of higher-order botryococcenes proceeds by methyl addition using S-adenosyl methionine (SAM) (Okada, T P Devarenne, and Chappell 2000). Because SAM is made from ATP and methionine, methylation to create higher-order botryococcenes has additional energetic requirements of one ATP for each methylation. Therefore, for C_{34} botryococcene, the total ATP requirement from Acetyl-CoA is 22 ATP.

Chapter 4

Microbial Energetics as a Method for Development of Balanced Growth Equations and Theoretical Prediction of Maximum (True) Biomass Yields

In the 20th century, a variety of methods for the prediction of biomass yields and a balanced growth equation were developed and tested; Battley provides an extensive review (Battley 1987). The Electron Balance (EB) theory of McCarty (McCarty 1971; Rittman and McCarty 2001; McCarty 2007) was used here as the basic framework predicting true yields of cell growth and botryococcene product fuel (BPF) production as a function of process conditions and the characteristics of *Rs. eutropha* and *Rb. capsulatus*. In this work, a number of modifications and refinements were implemented to the EB method, based on the detailed knowledge known of the metabolic pathways of the organisms under investigation, as presented in Chapter 2. A key parameter of the EB method, the cellular efficiency factor ε, cannot be directly known but is critical for accurate predictions. A method for estimating ε for each *Rs. eutropha* and *Rb. capsulatus*, based on growth data, was developed using insight provided from an alternative theory for making theoretical yield predictions, the Gibbs Energy Dissipation (GED) theory (Heijnen and van Dijken 1992; Tijhuis, van Loosdrecht, and Heijnen 1993; Heijnen, van Loosdrecht, and Tijhuis 1992; von Stockar et al. 2006; Jingsong Liu et al. 2007). The relationship between this alternative theory and the method for estimating ε is briefly discussed.

Yield and Stoichiometry Predictions by the Original Electron Balance (EB) Method of McCarty

The foundation for the yields predicted in this work is based upon the Electron Balance (**EB**) method of McCarty for constructing stoichiometric growth and botryococcene fuel synthesis (McCarty 1971; Rittman and McCarty 2001; McCarty 2007). While this theory is summarized here, the reader is referred to the originally referenced works for the intricate details of this theory. The EB method compartmentalizes microbial metabolism into two coupled redox reactions, which are diagrammed in Figure 4.1.

- In the energy generating/catabolic reaction, the Electron Donor (ED) reduces the Electron Acceptor (EA). This provides energy and electrons to the cell for synthesis and cellular processes;
- In the synthesis/anabolic reaction, the ED reduces the Carbon Source (CS) and Nitrogen Source (NS) to form biomass and the botryococcene fuel product. This consumes energy in the building of complex cellular material from the substrates provided for growth.

An electron balance on the available electrons from the electron donor is performed, where it is assumed that the electrons must be conserved. We define the fraction of electrons from the electron donor partitioned to energy generation as f_e^0; f_s^0 denotes the electrons partitioned to cellular synthesis. f_s^0 and f_e^0 must always sum to 1 due to the requirement that the electrons are conserved. The ^{0} subscript indicates that these parameters are associated with the electron portioning for the true yield of the cell; the true yield is defined as the growth and/or synthesis that could occur in the absence of cellular maintenance. The electron partitioning associated with the net yield, the yield which is actually observed and is less than the true yield, has an f_e that will always be greater than f_e^0 because more equivalents of the ED must be oxidized to supply sufficient energy for both growth and maintenance. By the same reasoning, the

Figure 4.1: Schematic of the microbial energetics theory and the electron balance, specific to the chemolithoautotrophic growth of *Rs. eutropha* and *Rb. capsulatus*.

Electrons from the electron donor can either go to energy production or cell synthesis; the fraction of each are designated f_E^0 or f_S^0. The degree of electrons sent to energy generation versus those that can be used for cell synthesis is dependent upon the relative energetics of the energy generating reaction and the cell synthesis reaction.

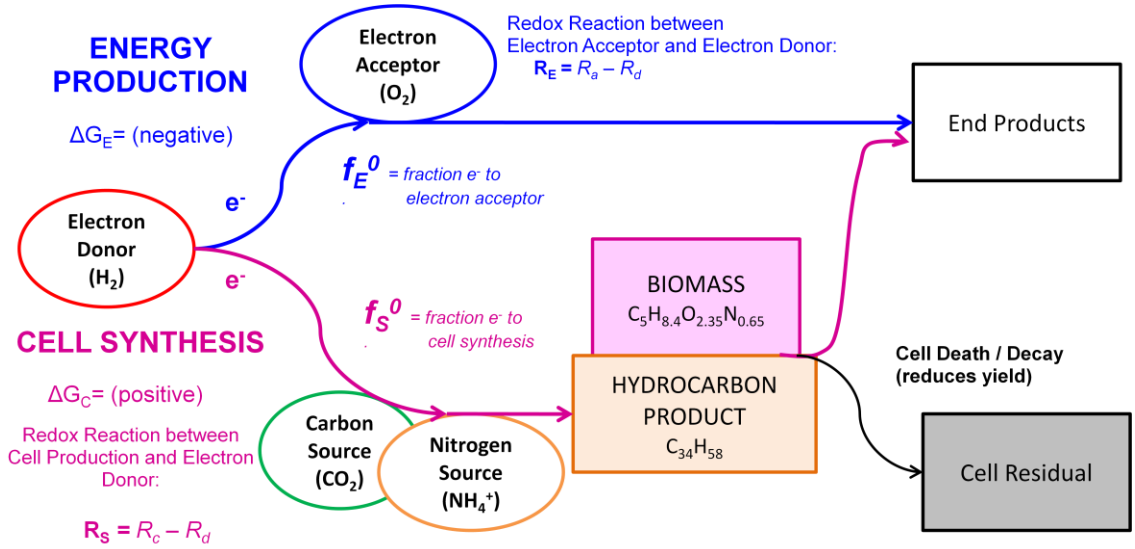

partitioning of electrons to cell synthesis that is associated with the net yield, f_e, will always be less than f_s^0. However, f_s and f_e must always still sum to unity because of the assumption of electron conservation. While the electron partitioning associated with the net yield is that which is of interest for calculating expected yields in real bioprocesses, it cannot be directly calculated from the energetics of cellular metabolism. Instead, f_e and f_s must first be determined from f_s^0 and f_e^0, and the method for the pre-requisite determination of f_s^0 and f_e^0 is the focus of this chapter; the method of calculating f_e and f_s is covered in CHAPTER 5. Once f_s^0 and f_e^0 have been determined, these are used to directly calculate the true yield of the bioprocess, and therefore the true yield is directly related to the relative energetics of the catabolic and anabolic reactions. It is briefly noted here that the net/apparent yields from any process will always be less than the true yields, due to the cost of maintenance energy demands by the cell. These effects are amplified in the scenario of external limitations to the microbe's growth rate, such as by mass-transfer limitations of the electron donor or electron acceptor substrate. This is discussed further in CHAPTER 5.

The **EB** method was selected over other approaches for a number of reasons. First, the method delineates the portion of the electrons from the electron donor utilized for energy generation versus those used for cell synthesis in a manner consistent with the pathways actually present in microbial metabolism. This has the 'downside' of requiring knowledge of the intricate details of a particular microbe's pathways, but knowledge of metabolic pathways for many organisms is advancing at exponential rates, and this information is now readily available. Therefore, this is not as large of an obstacle to model development as it would have been when microbial energetics theories were initially developed. Secondly, this method is readily adaptable to varying microbial compositions and degrees of reduction. This was an advantage in this work, where the botryococcene product fuel was modeled as another "cell compartment" where energy and substrates could be utilized for either cell synthesis or fuel synthesis. This conceptualization allowed assessment of systems where the extent of microbial metabolism devoted to fuel synthesis was an adjustable variable.

One aspect of microbial energetics clearly addressed in other methods is the irreversibility of microbial growth (i.e. the 2^{nd} law of thermodynamics). One prominent alternative theory to the **EB** method, the Gibbs Free Energy Dissipation (GED) theory, accounts for the generation of entropy in inherent to microbial metabolism by considering the dissipation of Gibbs free energy that occurs during growth. As will be showed in this chapter, while not described as explicitly in the original presentation of the **EB** method, this aspect is introduced implicitly in the form of an assumed cellular efficiency factor ε. This factor 'contains' the difficult-to-quantify irreversibility and the less-than-unity efficiency of cellular processes; ε accounts for these phenomena by diminishing the energy available from exergonic reactions and increasing the energy required for endergonic reactions. The approach for accounting for irreversibility and inefficiency in microbial metabolism between the GED and EB theories is

quite different, however, they are conceptually the same, and this is explored at the end of this chapter.

The procedure for yield determinations in the original EB method

The basic steps to the McCarty method, as originally presented by McCarty (McCarty 1971; Rittman and McCarty 2001) are as follows:

1. Identify the electron donor (ED), the electron acceptor (EA), the carbon source (CS), and the nitrogen, phosphorus and sulfur sources (NS, PS, SS) for microbial growth:
    - For heterotrophic growth, the electron donor and the carbon source are the same compound. For autotrophic growth (which is the mode of growth considered in this work), inorganic carbon (CO_2) is the carbon source. This necessitates that the carbon source and the electron donor be different compounds, because CO_2 is the most oxidized form of carbon and therefore cannot donate electrons (i.e. serve as the ED). CO_2 can, however, be both the carbon source and the electron acceptor, as in methanogenesis.
    - The element nitrogen makes up a non-trivial portion of microbial biomass, in the range of 5-15% by mass. For the species of interest in this work, *Rs. eutropha* is composed of 11% nitrogen by mass (Ishizaki and Tanaka 1990) and *Rb. capsulatus* contains 8% nitrogen by mass (Hoekema et al. 2006). Furthermore, according to Rittman and McCarty (2001), the degree of reduction of the nitrogen source affects the electrons required from the ED for cell synthesis. Therefore, the inclusion of the nitrogen source as one of the growth substrates in a microbial energetics assessment is required for the most accurate determination of the electron equivalents required to synthesize cell mass, and therefore the stoichiometric yield. McCarty did not include

the phosphorus or sulfur sources in his assessment because their proportion of the biomass is smaller. In this work, these sources were included, even though phosphorus and sulfur were only considered to be 3% and 0.3% respectively. The rationale for the choice of these values is discussed in Chapter 6.

2. Identify an empirical formula for the cell composition ($C_aH_bO_cN_dP_eS_f$).
3. Identify the half reactions (designated by a lowercase *r*) for the electron donor (r_{ed}) and the electron acceptor (r_{ea}). A list of the half reactions specific to this work are provided in Appendix D.
4. Construct a balanced half-reaction for cell synthesis (r_{synth}), with CO_2 as the oxidized carbon species and using appropriate species for the nitrogen, phosphorus and sulfur sources required for cell synthesis. Normalize the equation to a single mole of electrons transferred ("electron equivalent" or eeq) by dividing through by *Q*, the number of electrons transferred in synthesizing one mole of cell mass. This procedure is detailed in Appendix E, and will result in an equation resembling.

The balanced half reaction for cell synthesis: **Equation 4.1**

$$\frac{a}{Q}CO_2 + \frac{h}{Q}H^+ + 1\,e^- + \frac{d}{Q}NH_4^+ + \frac{e}{Q}PO_4^{3-} + \frac{f}{Q}SO_4^{2-} = \frac{1}{Q}C_aH_bO_cN_dP_eS_f + \frac{g}{Q}H_2O$$

Where *g*, *h*, and *Q* are defined below:

$$g = (2\cdot a + 4\cdot e + 4\cdot f - c) \quad \textbf{Equation 4.2}$$

$$h = (b + 2\cdot g - 4\cdot d) \quad \textbf{Equation 4.3}$$

$$Q = (d + h - 3\cdot e - 2\cdot f) \quad \textbf{Equation 4.4}$$

5. Determine the overall redox reaction for energy generation (R_{ENERGY}) by subtracting the half reaction for the electron donor, r_{ed}, from the half reaction for the electron acceptor, r_{ea} (Equation 4.5). Overall redox reactions are designated by uppercase *R*, and the subtraction of the two reactions results from the convention that half reactions are written with the oxidized form of the species reacting to make the reduced form.

Redox rxn for energy generation

$$R_{\mathrm{ENERGY}} = r_{\mathrm{ea}} - r_{\mathrm{ed}}$$

Equation 4.5

6. Calculate the Gibbs free energy released (per eeq) by the energy generating reaction R_{ENERGY} via Equation 4.6.

ΔG released by energy generating reaction, standard conditions

$$\Delta G^{0\prime}_{ENERGY} = \Delta G^{0\prime}_{ea} - \Delta G^{0\prime}_{ed}$$

Equation 4.6

For this calculation, the $\Delta G^{0\prime}$ for each half reaction at standard physiological conditions (298K, 1 atm., unit activities a_i for all metabolites except H^+, $a_{H+} = 10^{-7}$, pH of 7) is employed. Standard physiological conditions are designated by the superscript ^{0} for temperature, pressure, and metabolite activity, and $'$ for pH. Values for the half reactions used in this work are provided in Appendix D.

7. Correct the Gibbs free energy released by the energy generating reaction, $\Delta G^{0\prime}_{\mathrm{ENERGY}}$, from standard conditions to the actual biological process conditions using Equation 4.7.

Correction to non-standard conditions

$$\Delta G_{Rxn} = \Delta G^{0\prime}_{Rxn} + \left(RT\sum_{i=1}^{n} \nu_i ln[a_i]\right) + \left(RT\nu_i ln\left[\frac{10^{-(pH)}}{10^{-7}}\right]\right)$$

Equation 4.7

Because the microbe is assumed to be a dilute system, the activities of each species is approximated as the intracellular concentration of that species. The pH is assumed in this work to be the pH of the microbial culture.

8. Determine the overall biomass synthesis reaction, R_{SYNTH}, by subtracting the half reaction of the electron donor from the half reaction for the cell synthesis reaction, as shown in Equation 4.8.

Redox rxn for cell synthesis, original EB method

$$R_{\mathrm{SYNTH}} = r_{\mathrm{synth}} - r_{\mathrm{ed}}$$

Equation 4.8

9. Determine the free energy change for R_{SYNTH} per electron mole, $\Delta G_{\mathrm{SYNTH}}$, by a two step method described in detail (Rittman and McCarty 2001; McCarty 2007).

    a) First, the carbon source is reduced to a cellular intermediate at the expense of electrons from the electron donor ($\Delta G_{\mathrm{SYNTH\text{-}1}}$) (Equation 4.9).

ΔG (at std. cond.) for oxidation of electron donor to cellular intermediate

$$\Delta G^{0\prime}_{\mathrm{SYNTH}-1} = \Delta G^{0\prime}_{intermediate} - \Delta G^{0\prime}_{ed} \qquad \textbf{Equation 4.9}$$

This reaction may be exergonic or endergonic. The cellular intermediate assumed in this work is Acetyl-CoA (C_2H_3O-CoA), as recommended by McCarty (2007) as a more theoretically suitable intermediate than the pyruvate used originally; the degree of reduction of acetyl-CoA is closer to that of cellular biomass.

b) Energy in the form of ATP is spent to synthesize cellular biomass and products from the intermediate acetyl-CoA. The EB method employs a constant value of 3.32 kJ per gram cell synthesized (Rittman and McCarty 2001), which is converted to eeq by Equation 4.10 ($\Delta G_{\mathrm{SYNTH\text{-}2}}$). This reaction is always endergonic.

ΔG for biomass synthesis from acetyl-CoA

$$\Delta G_{SYNTH-2} = \frac{\left(3.32\ {}^{kJ}/_{g\ cell}\right) FW_{cell}}{Q} \qquad \textbf{Equation 4.10}$$

Here, $FW_{biomass}$ is the formula weight (g/mol) for the cell empirical formula $C_aH_bO_cN_dP_eS_f$ and Q is the number of electrons required to synthesize a mol of cell (see Appendix E).

The energetics associated with each of the two cell synthesis steps are determined independently by Equation 4.9 and Equation 4.10 and adjusted to the conditions of the cell using Equation 4.7 above. Then, the overall Gibbs free energy for cell synthesis can be determined using Equation 4.11, where the ˆ on $\Delta G_{\mathrm{SYNTH}}$ indicates that this value has been adjusted to include efficiency losses.

Overall ΔG for biomass synthesis

$$\Delta \widehat{G}_{SYNTH} = \frac{\Delta G_{SYNTH-1}}{\varepsilon^p} + \frac{\Delta G_{SYNTH-2}}{\varepsilon} \qquad \textbf{Equation 4.11}$$

The energetic losses due to heat generation and cellular inefficiency are accounted for Equation 4.11 by incorporating the cellular efficiency factor mentioned previously (ε). The cellular efficiency factor ε accounts for the fact that inefficiency in cellular processes and non-reversible/non-equilibrium processes result in incomplete capture of all energy from the energy generating reaction into useful work by the cell. Therefore, for endergonic reactions

greater than 100% of the energy required for endergonic reactions will be required to drive the reaction in the cell. Therefore, in Equation 4.11, the endergonic Gibbs free energy associated with synthesis step 2 is divided by ε. For exergonic reactions, there is less than 100% of the energy available to the cell, and therefore the Gibbs free energy associated with exergonic steps should be multiplied by ε. In Equation 4.11, $\Delta G_{SYNTH\text{-}1}$ can either be exergonic or endergonic, depending upon the electron donor and the carbon source. Thus, the factor *p* depends on whether $\Delta G_{SYNTH\text{-}1}$ is exergonic (p = -1) or endergonic (p = 1).

Also note that the lack of the $^{0\prime}$ superscript in Equation 4.11, indicating that the values have been determined for the actual conditions (temperature and metabolite concentrations) of the microbial process using Equation 4.7.

The selection of the value of ε employed in the calculations of this work is discussed in more detail in the final section of this chapter.

10. Construct an overall Gibbs free energy balance for the creation of one electron equivalent of cell mass, now accounting for energetic losses in the energy-generating reactions as well by multiplying ΔG_{ENERGY} by ε (Equation 4.12):

Gibbs free energy balance on one eeq of cell

$$f_e^0(\varepsilon\,\Delta G_{ENERGY}) + f_s^0\Delta\hat{G}_{SYNTH} = 0 = \frac{dG}{dt} \qquad \textbf{Equation 4.12}$$

Equation 4.12 has been formed under the assumption of steady state conditions, such that Gibbs free energy does not accumulate in the cell (dG/dt = 0), which is the rationale for the RHS of this equation being set to 0. To simplify this equation, Equation 4.12 is divided through by f_s^0, and the parameter *A* (Equation 4.13) is introduced into the Gibbs free energy balance (Equation 4.14):

Definition of A

$$A \equiv \frac{f_e^0}{f_s^0} \qquad \textbf{Equation 4.13}$$

Gibbs free energy balance on one eeq of cell

$$A\,(\varepsilon\,\Delta G_{ENERGY}) + \Delta\hat{G}_{SYNTH} = 0 \qquad \textbf{Equation 4.14}$$

A can be conceptualized as the number of electron donor eeq that must be oxidized to provide sufficient energy to meet the energetic demands of cell synthesis, keeping in mind that an additional eeq of donor is being oxidized to provide the electrons for cell synthesis (recall Step 8 and Equation 4.8). Another way of stating this is to say that *A* is the number of turnovers required of the energy-generating reaction to provide the energy required for one eeq of cell synthesis. Equation 4.14 can be rearranged to solve for A (Equation 4.15):

Electron equivalents of ED that must be oxidized to supply energy requirements

$$A = -\frac{\Delta\hat{G}_{SYNTH}}{\varepsilon\Delta G_{ENERGY}} \qquad \textbf{Equation 4.15}$$

As this equation accounts only for cell growth, and not the energetic requirements of cellular maintenance, A is therefore an expression for the inverse of the true yield of the cell, $^{1}/_{Y^{T}}$, with units of eeq electron donor oxidized/eeq cells synthesized.

11. Calculate A using the values determined for ΔG_{SYNTH} and ΔG_{ENERGY} above, and the selected value of ε.

12. In order to construct a balanced growth equation, we need to know how the electrons from the electron donor are partitioned between cell synthesis and energy generation. To determine f_s^0 and f_e^0, we recall Equation 4.13, and rearrange to solve for f_s^0 and f_e^0 in Equation 4.16 and Equation 4.17.

Relationship of f_s^0 and f_e^0 to A, the energy generating reaction turnover number

$$f_s^0 = \frac{1}{1+A} \qquad \textbf{Equation 4.16}$$

$$f_e^0 = \frac{A}{1+A} \qquad \textbf{Equation 4.17}$$

Conceptually the relationship for f_s^0 makes sense: the fraction of electrons to cell synthesis is the number of donor equivalents used for synthesis (1) divided by the donor equivalents oxidized in the energy generating reaction (1+A), and because *A* equivalents of the donor used were specified to be used for energy, and one equivalent of the donor is being utilized

for providing electrons to cell synthesis, the total donor consumed for to generate one eeq of cell is 1+A.

13. Finally, the overall balanced synthesis reaction (R_{OVERALL}) is generated from the coupled electron-donor/ electron-acceptor redox reaction (R_{ENERGY}) and the coupled electron-donor/biomass-synthesis redox reaction ($R_{\mathrm{SYNTHESIS}}$) by Equation 4.18:

Overall stoichiometric growth reaction

$$R_{\mathrm{OVERALL}} = f_e^0 R_{\mathrm{ENERGY}} + f_s^0 R_{\mathrm{SYNTHESIS}} = f_e^0(r_{\mathrm{ea}} - R_{\mathrm{ed}}) + f_s^0(r_{\mathrm{synth}} - r_{\mathrm{ed}}) \quad \textbf{Equation 4.18}$$

From this balanced overall synthesis equation the true yield of cell production on any of the input species can be determined by comparing the stoichiometric ratios of cell and product production to input substrates. Note that net yields, which account for cellular maintenance, will be lower than the true yields calculated here, and these will be more representative of the yields that can be expected in a real bioprocess. The method for calculating net yields from true yields is presented in CHAPTER 5.

Modifications to the Electron Balance Method

Modifications were made to the EB method, specifically in calculating the overall value for the Gibbs free energy of cell synthesis, $\Delta\hat{G}_{SYNTH}$; the calculations for the energy available from the ED-EA reaction (Equation 4.5 - Equation 4.6) and the overall energy balance approach were not altered (Equation 4.14 -Equation 4.18). In this work, the two-step method for calculating the cellular synthesis energetics (described in Step 9 in the original EB method) is broken down into multiple substeps in order to capture the following aspects of the metabolic pathways:

- To more accurately deal with the metabolic pathways of non-photosynthetic, chemolitho-autoautotrophic growth by hydrogen oxidation and the reduction of carbon dioxide to biomass;
- To account for the energy-demanding process of reversed electron transport for NADH generation in *Rb. capsulatus*;
- To account for botryococcene product fuel synthesis in addition to cell growth, which changes the overall energy requirements of synthesis and degree of reduction of the biomass (product + cells) produced.

The breakdown of cellular synthesis into steps, utilized for the calculation of the ΔG_{SYNTH} in the modified EB method are:

Synthesis Step 1a: Electron transfer from the ED (H_2) to NAD^+ to produce NADH

Synthesis Step 1a-i: Electron transfer from the ED to the ubiquinone pool (RET only)

Synthesis Step 1a-ii: Electron transfer from reduced ubiquinone to NAD^+ (RET only)

Synthesis Step 1b: Electron transfer from NADH to CO_2 to produce acetyl-CoA intermediate

Synthesis Step 1c: Electron transfer from acetyl-CoA to cellular biomass

Synthesis Step 2: Utilization of ATP to drive the formation of biomass and fuel products from the acetyl-CoA intermediate

The original EB method is displayed side-by-side with the Modified EB method Figure 4.2; this figure most clearly outlines the changes made to the method, although the details of the changes and the rationale are provided in the sections which follow.

The net result of the modified procedure for the calculation of ΔG_{SYNTH} results in a change to how the Gibbs free energy is -calculated for cellular synthesis, but it does not result in a change to the stoichiometry of the step. Equation 4.19 and Equation 4.20 provide expressions for calculating ΔG_{SYNTH} under the modified EB method; these can be compared to their equivalent in the original method, Equation 4.11. The reader is referred to Figure 4.2 for the

Figure 4.2: Comparison of EB (Electron Balance) and Modified EB Method for calculating ΔG_{SYNTH}

A step-by-step comparison of ΔG_{SYNTH} calculation by the original McCarty Electron Balance method, and the modified version of the method developed in this work specifically for Electrofuels process calculations. Further details of the steps are provided in the text.

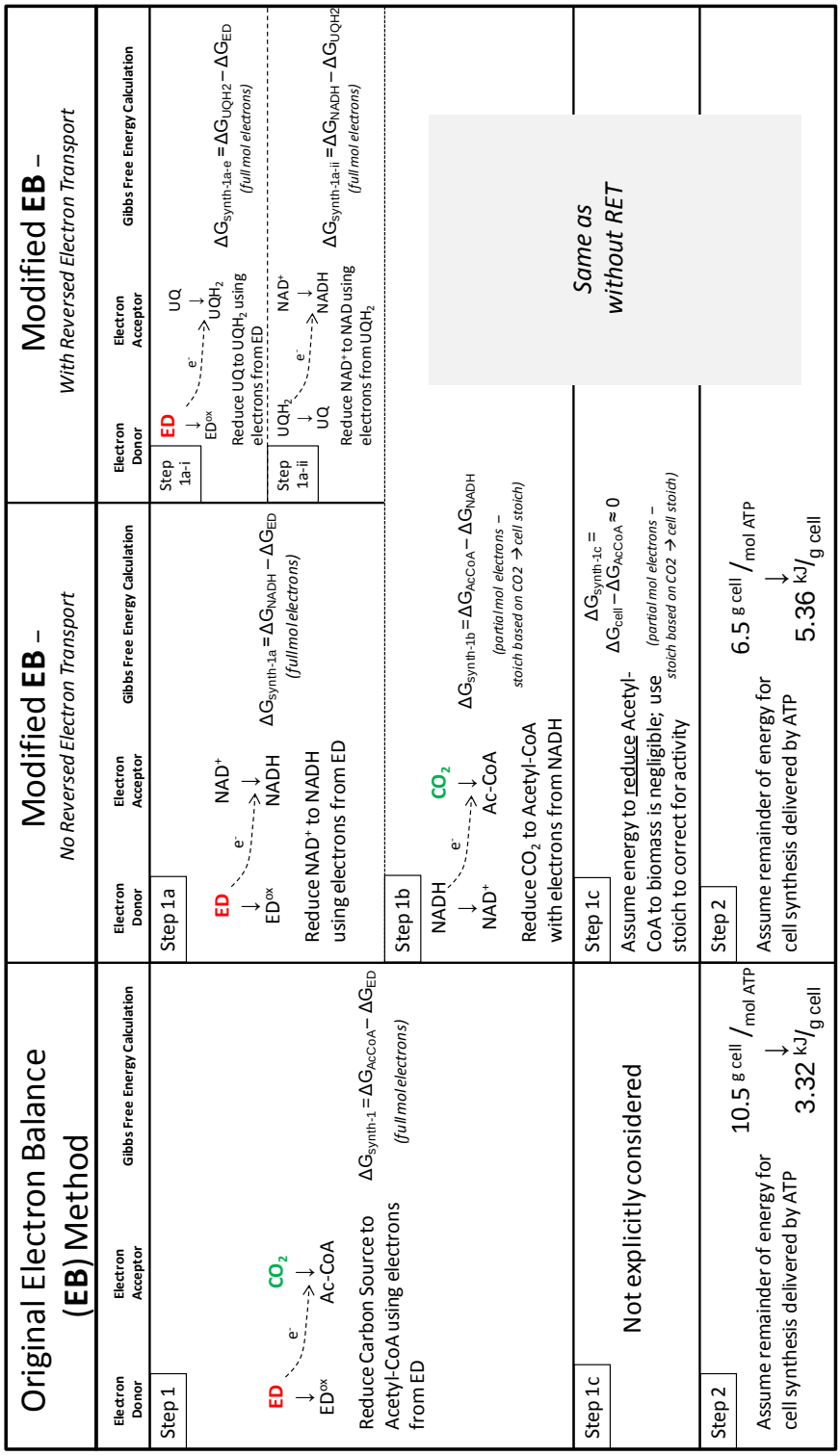

$\Delta\widehat{G}_{SYNTH}$ for *Rs. eutropha* (without Reversed Electron Transport): **Equation 4.19**

$\Delta\widehat{G}_{SYNTH} = \frac{\Delta G_{SYNTH-1a}}{\varepsilon^p} + \frac{\Delta G_{SYNTH-1b}}{\varepsilon^p} + \frac{\Delta G_{SYNTH-1c}}{\varepsilon^p} + \frac{\Delta G_{SYNTH-2}}{\varepsilon^p}$				
Step:	**e^- from H_2 to NADH**	**e^- from NADH to acetyl-coA**	**e^- from acetyl-coA cell and BPF**	**utilization of ATP for cell and BPF synth.**

$\Delta\widehat{G}_{SYNTH}$ for *Rb. capsulatus* (with Reversed Electron Transport): **Equation 4.20**

$\Delta\widehat{G}_{SYNTH} = \left(\frac{\Delta G_{SYNTH-1a-i}}{\varepsilon^p} + \frac{\Delta G_{SYNTH-1a-ii}}{\varepsilon^p}\right) + \frac{\Delta G_{SYNTH-1b}}{\varepsilon^p} + \frac{\Delta G_{SYNTH-1c}}{\varepsilon^p} + \frac{\Delta G_{SYNTH-2}}{\varepsilon^p}$					
Step:	**e^- from H_2 to ubiquinone pool**	**e^- from ubiquinone pool to NADH**	**e^- from NADH to acetyl-coA**	**e^- from acetyl-coA cell and BPF**	**utilization of ATP for cell and BPF synth.**

explanation of the metabolic steps corresponding to each term in the expressions of Equation 4.19 and Equation 4.20, as well as the following sections. In these equations, the cellular efficiency factor is utilized at each step to account for the lack of complete conservation of energy into useful work; *p* is equal to 1 when the reaction is endergonic, so that the cellular efficiency factor increases the amount of energy required for the step; *p* is equal to -1 when the reaction is exergonic, therefore decreasing the amount of energy available from the reaction. In reality, the efficiency of various metabolic steps will not have identical efficiencies, as they are assumed to do so here. The choice of a single cellular efficiency factor for each species is largely a choice of convenience, since it enables only a single parameter to be fit in calibrating the model for a given species. Furthermore, obtaining and including precise knowledge of the exact efficiency associated with step in these metabolic pathways is unrealistic. It is reiterated here what the purpose of including the cellular efficiency factor is: to account for the incomplete capture of energy from hydrogen oxidation into useful work by the cell; losses of energy to heat production, excess ATP hydrolysis, and incomplete energy conservation are difficult to quantify precisely.

SYNTHESIS STEP 1: The carbon source is reduced to a cellular intermediate (Acetyl-CoA) by electrons from the electron donor (Equation 4.21).

Applying the method of the original EB method, the overall reaction for the first step can be considered as the oxidation of the electron donor (H_2), and the use of the electrons to reduce CO_2 to the intermediate acetyl-CoA (Equation 4.21); the energetics of the first step would be determined from the ΔG of the half reactions for each the electron donor ($\Delta G^{0\prime}_{\mathrm{H2}}$ = 39.9 kJ/eeq) and acetyl-coA ($\Delta G^{0\prime}_{\mathrm{AcCoA}}$ = 33.3 kJ/eeq) (Equation 4.22).

Original EB: Overall Reaction for Step 1

$$R_{\mathrm{SYNTH-1}} = R_{\mathrm{acetyl-CoA}} - R_{\mathrm{H2}} \qquad \textbf{Equation 4.21}$$

Original EB: Overall Energetics for Step 1

$$\Delta G^{0\prime}_{\mathrm{SYNTH-1}} = \Delta G^{0\prime}_{\mathrm{acetyl-CoA}} - \Delta G^{0\prime}_{\mathrm{H2}} \qquad \textbf{Equation 4.22}$$

As stated previously, the metabolism being evaluated in this work for *Rs. eutropha* and *Rb. capsulatus* is chemolithoautotrophic growth, where CO_2 is the carbon source and hydrogen is oxidized aerobically to provide energy for metabolism. CO_2 is present in the half reaction for Acetyl-CoA formation, and so the stoichiometry of this first step works out to be a redox reaction between the ED and the carbon source to form the cellular intermediate acetyl-CoA. For the case of photosynthetic autotrophic growth, McCarty (McCarty 1971) reasoned that the true electron donor is water, as it is split into H^+ and O_2 by the energy of the sun. He then concluded that the ΔG associated with the electron donor half reaction for *all* autotrophic growth should always be that for the H_2O / O_2 half reaction ($\Delta G^{0\prime}_{\mathrm{O2}}$ = -78.82 kJ/eeq) (McCarty 1971). This results in a highly endergonic result for the overall Gibbs free energy of synthesis: $\Delta G^{0\prime}_{\mathrm{SYNTH-1}}$ = + 112.0 kJ/eeq. Although the use of water as the electron donor for all autotrophs is not a realistic representation for the vast majority of autotrophic metabolism, McCarty found that this method resulted in yield predictions that matched experimental data better than using the true electron donor in calculating $\Delta G_{\mathrm{SYNTH}}$ (personal communication). In the case of autotrophic growth by aerobic hydrogen oxidation, using the Gibbs free energy of hydrogen (the actual electron donor,

$\Delta G_{H2}^{0\prime}$= 39.9 kJ/eeq) in the calculation of ΔG_{SYNTH} results in a less endergonic result: $\Delta G_{SYNTH-1}^{0\prime}$ = + 38.9 kJ/eeq. Using H_2 as the electron donor therefore results in higher predicted yields than using water as the electron donor, all other factors kept the same (i.e. selection of the same ε): the magnitude of A in Equation 4.15 decreases, thus increasing the fraction of electrons sent to cellular synthesis (Equation 4.16).

However, for autotrophs other than phototrophs, the electrons for cellular synthesis are not derived directly from water. Furthermore if H_2O is always selected as the electron donor in reaction $R_{SYNTH-1}$, the stoichiometry of the equations does not work out correctly. It is possible that the experimental yields matched well for the original method of calculation utilized by McCarty because many autotrophs utilize reversed electron transport in order to generate the cellular electron carrier NADH, a process which requires a significant investment of cellular energy. Therefore, it is possible that the use of water as the electron donor acted as a proxy in inflating the magnitude of $\Delta G_{SYNTH-1}^{0\prime}$ such that the end result was decreased yields that matched experimental results.

In this analysis, I chose a more rigorous approach towards developing an expression for ΔG_{SYNTH} by accounting for the utilization of the actual ED (H_2) and the reversed electron transport (RET) of the biomass. This required investigation into the electron transport pathways for each organism, as described in Chapter 3. In the actual autotrophic metabolism of *Rs. eutropha* and *Rb. capsulatus*, the transfer of electrons from H_2 to CO_2 does not occur directly. Instead, to supply electrons to cellular processes such as carbon fixation, the electrons are transferred first from H_2 to NADH, a cellular electron carrier. In the case of *Rs. eutropha* this transfer is made directly; in the case of *Rb. capsulatus* reversed electron transport must be utilized for this transfer, as explained in Chapter 3. Then, NADH is used to deliver electrons to the CBB cycle and subsequent pathways for the fixation of carbon dioxide into the intermediate species Acetyl-CoA. Thus, in this modified approach to the EB method for calculating Gibbs free energy

of synthesis, Synthesis Step 1 is necessarily broken down into the following sub-steps (which were outlined above, but are repeated here for clarity):

Synthesis Step 1a: Electron transfer from the ED (H_2) to NAD^+ to produce NADH

Synthesis Step 1a-i: Electron transfer from the ED to the ubiquinone pool (RET only)

Synthesis Step 1a-ii: Electron transfer from reduced ubiquinone to NAD^+ (RET only)

Synthesis Step 1b: Electron transfer from NADH to CO_2 to produce acetyl-CoA intermediate

Synthesis Step 1c: Electron transfer from acetyl-CoA to cellular biomass

While the overall stoichiometry is maintained for Step 1 compared to the original EB method, the breakdown into the sub-steps results in a much different value for $\Delta G^{0\prime}_{\mathrm{SYNTH-1}}$.

SYNTHESIS STEP 1a, Modified EB Method: Transfer of electrons from the electron donor to the cellular electron carrier NADH.

This step is only applicable for *Rs. eutropha*, where the transfer of electrons to NADH from H_2 occurs in a single step via the soluble NAD^+-reducing hydrogenase. For *Rb. capsulatus,* RET requires that cell synthesis step 1a be broken down further, and the reader is referenced to the next section. For this one-step transfer, Gibbs energy change is calculated by Equation 4.23:

Modified EB (non-RET): Overall ΔG for Step 1a

$$\Delta G^{0\prime}_{\mathrm{SYNTH-1A}} = \Delta G^{0\prime}_{\mathrm{NADH}} - \Delta G^{0\prime}_{\mathrm{H2}} \qquad \textbf{Equation 4.23}$$

The energy calculated here is used in the first term in Equation 4.19, the overall energy of synthesis calculation for *Rs. eutropha*. A small amount of energy is released in association with this reaction: $\Delta G^{0\prime}_{\mathrm{SYNTH-1A}}$ = -8.99 kJ/eeq, and so *p* for this term (Equation 4.19) is -1. Whether this energy is conserved within the cell, in the electrochemical gradient or by another means, is not clear from the literature, but in this model it was assumed that the energy was indeed conserved. Because the magnitude of this energy transfer is small compared to that of the

reduction of O_2 by H_2, the effect of this assumption will not be large; however, this aspect of the model is something that could be further investigated for future model improvement.

Rb. capsulatus, however, is unable to directly catalyze the transfer of electrons from H_2 to NADH, and instead the electrons must first enter the electron transport chain at the level of ubiquinone (Friedrich and Schwartz 1993). Because ubiquinone has a lower potential than NADH (+0.133 V versus -0.320 V), an input of energy is required in order to transfer electrons from ubiquinol back up to the potential of NADH, as described in CHAPTER 3. Because electrons move in the 'reversed' direction (ie. up the potential gradient from ubiquinol to NADH) this is termed Reversed Electron Transport (RET). Therefore, for organisms with RET, Step 1a must be broken down further into STEP 1a-i and STEP 1a-ii.

STEP 1a-i, Modified EB Method with RET: Transfer of electrons from ED to the ubiquinone pool

A large amount of energy is released in this step, and through the action of the electron transport chain this energy is converted into a chemical potential – the proton motive force (Kleihues et al. 2000; Zannoni, Schoepp-Cothenet, and Hosler 2008; Gray and Daldal 1995) The Gibbs free energy associated with this transfer can be calculated by Equation 4.24:

Modified EB (RET): ΔG for Step 1a-i

$$\Delta G^{0\prime}_{\mathrm{SYNTH-1A-i}} = \Delta G^{0\prime}_{\mathrm{UQ}} - \Delta G^{0\prime}_{\mathrm{H2}} \qquad \textbf{Equation 4.24}$$

The energy calculated here is used in the first term in Equation 4.20, the overall energy of synthesis calculation for *Rs. eutropha*. Because this reaction is exergonic, *p* for this term (Equation 4.20) is -1.

STEP 1a-ii, Modified EB Method with RET: Transfer of electrons from reduced ubiquione to NAD$^+$

The transfer of electrons up the potential gradient from reduced ubiquinone to NADH is catalyzed by the NADH-UQ dehydrogenase in *Rb. capsulatus* (Kömen, Schmidt, and Friedrich 1992). A large amount of energy is required in this step, which is obtained from the proton motive force, therefore decreasing the energy available for ATP generation. The magnitude of the Gibbs free energy associated with this step is calculated by Equation 4.25:

Modified EB (RET): ΔG for Step 1a-ii

$$\Delta G^{0\prime}_{\mathrm{SYNTH-1A-ii}} = \Delta G^{0\prime}_{\mathrm{NADH}} - \Delta G^{0\prime}_{\mathrm{UQ}} \qquad \textbf{Equation 4.25}$$

The energy calculated here is used in the second term in Equation 4.20, the overall energy of synthesis calculation for *Rs. eutropha*. Because this reaction is endergonic, *p* for this term (Equation 4.20) is +1.

The effect of accounting for reversed electron transport on the calculation of the Gibbs free energy for the overall cell synthesis step 1A is illustrated in Table 4.1, where the energy for reduction of NAD^+ to NADH, at the expense of H_2, is significantly endergonic in the case of RET, but slightly exergonic without RET. This result is due to the presence of the cellular efficiency factor, ε, as shown in the final row of Table 4.1: to account for diminished energy availability (without RET), the exergonic reaction is multiplied by ε (reducing the available energy released). However, to account for the need for increased energy to drive the endergonic process of driving electrons from ubiquinone up their potential gradient to reduce NAD^+, the ΔG for this process is divided by ε, increasing the energy required. For any two-step process, neglecting to account for the energy exchange at each step separately, where one step is endergonic and the next step is exergonic, will result in an artificially low calculated value for the energy of the combined steps. Thus, neglecting this key feature of the microbial metabolism in the case of RET would lead to a significant overestimation of the energy available for cell synthesis processes.

Table 4.1: Effect of Reversed Electron Transport (RET) on $\Delta G_{SYNTH-1A}$ Calculation.

This table demonstrates that the ΔG calculated for Step 1A is strongly affected by RET. Without RET, the energetics of this step are found to be mildly exergonic (as for *Rs. eutropha*); when RET is accounted for, this step becomes significantly endergonic (as for *Rb. capsulatus*). For this illustration, ε was assumed to be 0.6, which is a 'typical' value utilized by Rittman & McCarty (2001).

	Calculated value of $\Delta G_{SYNTH-1A}$ (kJ/eeq)	
	Direct reduction of NAD^+ by H_2 (*Rs. eutropha*)	**RET mechanism for NAD^+ reduction (*Rb. capsulatus*)**
	-5.4 kJ/eeq	39.2 kJ/eeq
Expression for calculation of $\Delta G_{SYNTH-1A}$	$\varepsilon\left(\Delta G^{0\prime}_{\mathrm{NADH}} - \Delta G^{0\prime}_{\mathrm{H2}}\right)$	$\varepsilon\left(\Delta G^{0\prime}_{\mathrm{UQ}} - \Delta G^{0\prime}_{\mathrm{H2}}\right) + \frac{\left(\Delta G^{0\prime}_{\mathrm{NADH}} - \Delta G^{0\prime}_{\mathrm{UQ}}\right)}{\varepsilon}$

STEP 1b: Transfer of electrons from the cellular electron carrier NADH to the carbon source (CO_2) to produce acetyl-CoA.

As mentioned previously, the carbon source in chemolithoauthotropic growth is carbon dioxide, which has a degree of reduction of 0; therefore, carbon in CO_2 is in its most oxidized form. The half reaction for acetyl-CoA ($r_{\text{Ac-CoA}}$) from CO_2 is readily developed assuming that the metabolite CoA is conserved and that only the acetyl group is involved in the half reaction (Equation 4.26):

Acetyl-CoA half reaction $0.25\ CO_2 + 0.125\ CoA\text{-}H + H^+ + e^- = 0.125\ C_2H_3O\text{-}CoA + 0.375\ H_2O$ **Equation 4.26**

However, it should be noted that the $r_{\text{AcCo-A}}$ shown in Equation 4.26 is for the transfer of a <u>full mole</u> of electrons in reducing CO_2 to acetyl-CoA. Electrons, carried by NADH, are required at further steps in cellular synthesis besides just in the reduction of CO_2 to acetyl-CoA. Therefore, for a full mole of electrons available in NADH, part will be utilized in reducing CO_2 to acetyl-CoA, but not the full mole.

To determine the fraction of electrons from NADH which are required at downstream metabolic steps for converting acetyl-CoA to cell mass and botryococcene product fuel, we need to first develop the overall half reaction for CO_2 to cell and fuel; this can be developed as described in Appendix E from the known empirical formula for cell mass ($C_aH_bO_cN_dP_eS_f$), the known molecular formula for botryococcene fuel product ($C_{34}H_{58}$), and the molar ratio of fuel synthesized per cell mass synthesized (designated by α).

Definition of α

$$\alpha \equiv \frac{\text{moles fuel synthesized}}{\text{moles cell mass synthesized}} = \frac{\left(\frac{dBPF}{dt}\right)\frac{1}{FW_{fuel}}}{\left(\frac{dX}{dt}\right)\frac{1}{FW_{cell}}} \qquad \textbf{Equation 4.27}$$

In this work, it is assumed that botryococcene product fuel synthesis is growth associated, and that its synthesis is directly proportional to the net rate of growth of the organism by $\left(\alpha * \frac{FW_{fuel}}{FW_{cell}}\right)$, where FW stands for formula weight. Because it is assumed that cell and fuel are synthesized at a constant proportion to each other, we can assume that the fraction of fuel in overall biomass (cell + fuel) is a constant. Thus, using α, the composition of the biomass can be weighted according to the extent of fuel production.

This ratio α is a function of another parameter, CF_f – Carbon Flux to Fuel, which is the fraction of the carbon metabolism which is directed to botryococcene synthesis versus that directed to cell synthesis. By analogy, the fraction of carbon metabolism devoted to cell synthesis is designated CF_C - Carbon Flux to Cell. These quantities sum to unity, as we assume that metabolic carbon flux is directed only towards either fuel production or cell synthesis.

CF_f and CF_C sum to unity

$$CF_f + CF_C = 1 \qquad \textbf{Equation 4.28}$$

The quantitative relationship between α and CF_f these parameters is presented below; $n_{C,cell}$ and $n_{C,fuel}$ are the number of moles of carbon in a mole of cell and fuel, respectively.

Relationship between α and CF_{fuel}

$$\alpha = \frac{CF_f}{CF_C}\frac{n_{C,cell}}{n_{C,fuel}} = \frac{CF_f}{(1-CF_f)}\frac{n_{C,cell}}{n_{C,fuel}} \qquad \textbf{Equation 4.29}$$

This then allows for adjustment of the cell synthesis half reaction according to the weighted composition of anabolic products of cell mass and botryococcene fuel, and using this molar ratio between fuel and cell (α), the half reaction for synthesis of cell and fuel can determined.

From this overall half reaction, we obtain the number of moles of CO_2 which are required for the production of one eeq of biomass ($^{a}/_{Q}$), and then normalize $r_{\text{Ac-CoA}}$ to this number of moles of CO_2. This results in a modified half reaction: r^{N}_{AcCoA} (Equation 4.30 below), where only $\frac{a}{0.25 \cdot Q}$ moles of electrons are required. The factors 0.25 and Q in the denominator are the coefficient for CO_2 in the original half reaction for acetyl-CoA (Equation 4.26), and the number of electrons required for a mole of biomass (fuel + cell) synthesis:

Modified half reaction for acetyl-CoA: r'_{AcCoA}

$$\frac{\boldsymbol{a}}{\boldsymbol{0.25 \cdot Q}}(\boldsymbol{0.25\,CO_2 + \ 0.125\,CoA \cdot H \ + \ H^+ \ + \ e^-} = \boldsymbol{0.125\,C_2H_3O \cdot CoA \ + \ 0.375\,H_2O}) \qquad \textbf{Equation 4.30}$$

Therefore, the half reaction for NADH, $r_{\text{NADH}'}$ must also be normalized, and the overall reaction for Step 1b becomes Equation 4.31; the energy associated with this transfer is calculated from the Gibbs energy of the redox half reactions for Acetyl-CoA and NADH (Appendix C), and is normalized by the same factor as the reaction, resulting in Equation 4.32:

Normalization of Step 1b stoichiometry for a partial equivalent of electrons

$$\boldsymbol{R_{SYNTH-1b} = \frac{a}{0.25 \cdot Q}(r_{AcCoA} - r_{NADH})} \qquad \textbf{Equation 4.31}$$

Normalization of Step 1b Gibbs energy for a partial equivalent of electrons

$$\boldsymbol{\Delta G'^{0}_{SYNTH-1b} = \frac{a}{0.25 \cdot Q}(\Delta G'^{0}_{Ac-CoA} - \Delta G'^{0}_{NADH})} \qquad \textbf{Equation 4.32}$$

While an element/metabolite other than carbon could have been chosen as basis for characterizing the extent of botryococcene fuel synthesis, carbon was a convenient choice, for the reasons listed below:

- In chemolithoautotrophic growth of *Rs. eutropha* and *Rb. capsulatus*, CO_2 is not part of the cellular energy generating process and so it is independent of maintenance; CO_2 is only taken up for growth and synthesis of biomolecules. Because it is assumed in this work that all carbon assimilated by the cells is directed either to cell synthesis or to botryococcene fuel synthesis (a simplification), CF_f and CF_C must sum to unity: $CF_f + CF_C = 1$.
- In a physiological sense, carbon dioxide is fixed through the Calvin-Benson-Bassham pathway, arriving at the same intermediate used in the microbial energetics calculations, acetyl-CoA. From this point, the conceptual model partitions the carbon contained in acetyl-CoA as destined for either cell mass synthesis (through a variety of pathways), or to botryococcene fuel production via the Mevolanate pathway; acetyl-CoA is a precursor for both processes.

STEP 1c: Transfer of electrons from the intermediate acetyl-CoA to cell mass and botryococcene product fuel.

The half reaction for cell mass from Acetyl-CoA ($r_{\mathrm{AcCoA}\rightarrow\mathrm{cell}}$) can now be developed, first for a full mol of electrons (using the process described in Appendix E, but using acetyl-CoA on the left side of the equation rather than CO_2). This half reaction is then normalized by $(1 - \frac{a}{0.25 \cdot Q})$, such that now a full mole of electrons in NADH have been utilized for cell and fuel synthesis – part were utilized in the reduction of CO_2 to acetyl-CoA, and the remainder were utilized in reducing CO_2 to cell mass and botryococcene fuel. (The sum of the normalized half reactions for $CO_2 \rightarrow$ Acetyl-CoA and then Acetyl-CoA $\rightarrow$ biomass ($r'_{AcCoA}, r'_{AcCoA\rightarrow cell}$) will be equivalent to the overall half reaction for CO_2 to biomass, Equation 4.1) The overall reaction for Step 1c is (Equation 4.33):

Normalization of Step 1c stoichiometry for a partial equivalent of electrons

$$\boldsymbol{R_{\mathrm{SYNTH-1c}} = \left(1 - \frac{a}{0.25 \cdot Q}\right)(r_{\mathrm{AcCoA\rightarrow cell}} - r_{\mathrm{NADH}})} \qquad \textbf{Equation 4.33}$$

The energetics of the half reaction between Acetyl-CoA and cellular biomass are inherently undefined because biomass does not have a single chemically defined formula. However, the degree of reduction of Acetyl-CoA (γ = 4.17) is similar to the range of reduction for cellular biomass (γ = 4.4 - 5.7). Therefore, it is assumed that the energy exchange associated with the *reduction* of Acetyl-CoA to biomass is negligible compared to the energy required in the form of ATP. (Note that the electrons required to further reduce acetyl-CoA to biomass are accounted for due to the stoichiometry). Therefore, it is assumed that the energy of this exchange at standard conditions is approximately zero (Equation 4.34).

Gibbs energy for Step 1c

$$\boldsymbol{\Delta G^{0\prime}_{\mathrm{SYNTH-1c}} = \left(1 - \frac{a}{0.25 \cdot Q}\right)\left(\Delta G^{0\prime}_{\mathrm{AcCoA\rightarrow cell}} - \Delta G^{0\prime}_{\mathrm{NADH}}\right) \approx 0} \qquad \textbf{Equation 4.34}$$

In adjusting the value of $\Delta G^{0\prime}_{\mathrm{SYNTH-1c}}$ for non-standard conditions using Equation 4.7, the stoichiometric coefficients from the normalized equations are used.

STEP 2: Energy generated by hydrogen oxidation and conserved in the form of ATP, is spent for cell and botryococcene product fuel synthesis from the cellular intermediate acetyl-CoA.

For the second step in calculating the Gibbs free energy exchange associated with biomass synthesis, McCarty (McCarty 1971; Rittman and McCarty 2001) utilized an average microbial growth yield on ATP (Y^{ATP} = 10.5 g cell/mol ATP) and the energy associated with the hydrolysis of ATP at physiological conditions ($\Delta G^{0\prime}_{ATP\ hydrolysis}$ = 52.3 kJ/mol ATP). These were utilized calculate the Gibbs free energy requirement in ATP energy per gram of cells ($\Delta G^{0\prime}_{synth-2\ /g\ cell}$, Equation 4.35):

Gibbs energy in ATP for cell and synthesis (on a cell mass basis)

$$\Delta G^{0\prime}_{synth-2\ /g\ cell} = \frac{\Delta G^{0\prime}_{ATP,hydrolysis}}{(Y^{\mathrm{ATP}}/\varepsilon)\ \cdot\ f_{deg}} \qquad \textbf{Equation 4.35}$$

As an experimentally determined yield value, the value of Y^{ATP} (in units of g cell/mol ATP) inherently 'contains' the inefficiency of cells from which it was calculated. In Equation 4.35, McCarty corrected for this inefficiency of the cells by dividing Y^{ATP} by ε, set to the value of 0.6. This corrects the experimentally determined yield value to that attainable if there were no cellular inefficiency; this is necessary because the cellular efficiency factor specific to the metabolism being evaluated is accounted for separately in subsequent calculations. Therefore the value of $\Delta G^{0\prime}_{synth-2/g\ cell}$ calculated above has been corrected to the value of the 'true' energy required for cell synthesis if the efficiency was 100%. The factor f_{deg}, set to 0.9, accounts for the assumption that the measured yield value was based on cells that were 90% 'degradable', or in other words that they contained 10% by mass inorganic compounds for which ATP was not spent in synthesizing. As described previously in this chapter, Equation 4.10 then converts the $\Delta G^{0\prime}_{synth-2/g\ cell}$ from units of [kJ/g cell] to units of [kJ/eeq cell] using Q, the number of electron equivalents contained in a gram of cell mass. Using the parameter values detailed in Table 4.2, McCarty determined values of 3.32 kJ/g cell for $\Delta G^{0\prime}_{synth-2/g\ cell}$ and 18.8 kJ/eeq cell for $\Delta G_{synth\text{-}2}$ (Rittman and McCarty 2001).

McCarty obtained the value used for Y^{ATP} (10.5 g cell/mol ATP) from Bauchop and Elsden 1960, which was based on anaerobic heterotrophic growth (fermentations) of *Streptococcus faecalis*, *Propiionibacterium pentosaceum*, and *Saccharomyces cerevisiae* on complex medium with various carbon substrates. Under these conditions, Bauchop and Elsden found that the Y^{ATP} only varied from 8.3-12.6 g cell/mol ATP, averaging at 10.5 g cell/mol ATP. Forrest and Walker (1971) expanded upon this work, and published yields for 47 different determinations of this yield for heterotrophic fermentations, arriving at a very similar average of 10.6 g cell/mol ATP (range 8.5 - 13.1 g cell/mol ATP). While these values are remarkably

Table 4.2: Comparison of the $\Delta G_{SYNTH-2}$ Values calculated by the original Electron Balance (EB) method of McCarty and the modified method presented in this work for the range of CF_{fuel} values assessed. Y^{ATP} = Yield of cell on ATP; Q = mass of fuel + cell produced per electron equivalent (eeq).

	EB Method	**Modified EB Method**		**Equation Reference**
species:	*not specified*	*Rs. eutropha*	*Rb. capsulatus*	
product fuel:	none	$C_{34}H_{58}$	$C_{34}H_{58}$	
Y^{ATP} [g cell/mol ATP]	10.5 (1)	6.5 (2)	6.5 (2)	(1) (McCarty 1971) (2) (Kelly 1990)
$\Delta G^{0'}_{ATP\text{-}hydrolysis}$ [kJ/mol ATP]	52.3	52.3	52.3	
$\Delta G^{0'}_{synth\text{-}2/g\ cell}$ [kJ/g cell]	3.32	5.36	5.36	Equation 4.35
$\Delta G^{0'}_{synth\text{-}2/g\ biofuel}$ [kJ/g biofuel]	n/a	13.0	13.0	Equation 4.38
Q [(g fuel + g cell)/ eeq]	5.65	5.59 - 2.53	5.32 - 2.52	Equation 4.1- Equation 4.4
$\Delta G^{0'}_{synth\text{-}2}$ [kJ/eeq]	18.8	30.0 - 31.3	28.5 - 31.0	Equation 4.10
% Carbon Flux to Fuel (CF_f):		**0% 95%**	**0% 95%**	

similar despite the variation in the taxonomy of the organisms, the growth mode (fermentation) is the same, and quite different than the aerobic lithoautotrophic growth examined in this work. Furthermore, the growth in complex medium means that monomers for cellular synthesis (eg amino acids and nucleotides) are already present, which greatly decrease the energetic demands of the cell. Therefore the 10.5 g cell/mol ATP should be considered an upper limit for cells of average composition growing in scenarios where biomolecules (amino acids, nucleotides) are plentifully available (Forrest and Walker 1971). In this same work, the authors discussed values for other modes of metabolism, and found that while the yields increased for aerobic growth, they also had a greater degree of variability. Furthermore, the theoretical amount of ATP required for cell material synthesis is much greater when the carbon source is carbon dioxide, due to the highly energy demanding Calvin-Benson-Bassham pathway. Therefore, the yield of cells on ATP cannot be considered a constant (Stouthamer 1973).

For the present analysis, a value for Y^{ATP} was sought for the hydrogen-oxidizing, chemolithoautotrophic modes of metabolism utilized by *Rs. eutropha* and *Rb. capsulatus*. A value of 5 g cell/ mol ATP for autotrophic growth has been suggested by Battley (1987) based on a calculation method presented by Forrest and Walker (1971). However, *Rb. capsulatus* utilizes reversed electron transport to generate NADH at the expense of the proton motive force, and therefore at the expense of ATP production; *Rs. eutropha* does not utilize RET and therefore it is expected that the ATP yields between these two organisms would not be the same. Kelly (1990) provides rough calculations for autotrophic growth both with and without RET. The value quoted for autotrophs without RET, Y^{ATP} = 6.5 g cell/mol ATP, aligns with an independent calculation by (Harder and van Dijken 1976). For autotrophs with RET Kelly provides an estimated value of 2.5 g cell/mol ATP. In this work, the value for autotrophic growth without RET (Kelly 1990) is utilized for all organisms, including *Rb. capsulatus*, because the energy utilized to generate NADH via RET is accounted for elsewhere in the calculations – specifically in how the energy for NADH production is calculated (cell synthesis step 1a for *Rs. eutropha* and steps 1a-i and 1a-ii for *Rb. capsulatus*). Therefore, while the diminished cellular yield on ATP due to the need for the energy demands of inorganic carbon fixation is valid, using a value that includes the energy required for NADH generation would essentially be double-counting its contribution. The values used in the present analysis are presented in Table 4.2, and are compared with the original presentation of the EB method, along with the resulting values of $\Delta G^{0\prime}_{\mathrm{synth-2/g\,cell}}$ calculated from these values for each organism. Because it was assumed that the yields on ATP actually formed between the two organisms would be similar, the values calculated for each species very close in the modified EB method; the differences are due to the slightly difference cell composition for each species.

Furthermore, I considered that the energy associated with biomass synthesis would also be dependent on the extent to which the metabolic flux of the organism was directed towards

either cell synthesis or botryococcene biofuel synthesis. In order to assess this factor's effect on the energetics of cell synthesis, I again utilized the Carbon Flux to Fuel parameter (CF_f). At high CF_f (low CF_c), a greater amount of energy would be required for synthesis per mass of overall biomass product (cell + botryococcene fuel) produced. Therefore, in addition to the value of $\Delta G^{0\prime}_{\text{synth}-2/\text{g cell}}$ calculated as described above for non-fuel biomass, a value must be determined for the Gibbs energy for synthesis of botryococcene biofuel, $\Delta G^{0\prime}_{\text{synth}-2/\text{g biofuel}}$. Then, these values together are utilized to calculate the overall Gibbs energy for biomass synthesis from acetyl-CoA, $\Delta G^{0\prime}_{\text{synth}-2/\text{overall}}$, as the weighted average (based on CF_{fuel}) of Gibbs free energy for synthesizing cell and fuel (Equation 4.36). The quantity β is a function of CF_f, and is a mass ratio of fuel produced per total (fuel + cell) produced (Equation 4.37).

Gibbs energy for overall biomass (cell + fuel) synthesis from acetyl-CoA **Equation 4.36**

$$\Delta \boldsymbol{G^{0\prime}_{synth-2/g\ overall}} = \Delta \boldsymbol{G^{0\prime}_{synth-2/g\ cell}} * (\mathbf{1} - \boldsymbol{\beta}) + \Delta \boldsymbol{G^{0\prime}_{synth-2/g\ biofuel}} * \boldsymbol{\beta}$$

Mass ratio of fuel produced per total biomass (cell + fuel) **Equation 4.37**

$$\boldsymbol{\beta} = \frac{\boldsymbol{CF_c}\dfrac{\boldsymbol{FW_{fuel}}}{\boldsymbol{a_{fuel}}}}{\boldsymbol{CF_c}\dfrac{\boldsymbol{FW_{fuel}}}{\boldsymbol{a_{fuel}}} + (\mathbf{1} - \boldsymbol{CF_c})\dfrac{\boldsymbol{FW_{cell}}}{\boldsymbol{a_{cell}}}}$$

To estimate a value for the $\Delta G^{0}_{\text{synth}-2/\text{g biofuel}}$ for the biofuel portion in the absence of published yields of botryococcenes on ATP, I considered that the Gibbs free energy of formation of a given mass of botryococcene would be proportionally greater than the energy required for the same mass of cell by a ratio (R); R is the ratio of the Gibbs energy of combustion of botryococcene to that of cell mass. Therefore, the $\Delta G^{0}_{\text{synth}-2/\text{g biofuel}}$ can be approximated by Equation 4.38:

Approximation for Gibbs energy of biofuel synthesis **Equation 4.38**

$$\Delta \boldsymbol{G^{0\prime}_{synth-2/g\ biofuel}} = \Delta \boldsymbol{G^{0\prime}_{synth-2/g\ cell}} * \boldsymbol{R}$$

R is defined by Equation 4.39:

R, Ratio of botryococcene to cell Gibbs combustion energies

$$\boldsymbol{R \equiv \frac{\Delta G_{combustion,biofuel}}{\Delta G_{combustion,cell}}} \qquad \textbf{Equation 4.39}$$

In Equation 4.39, the Gibbs free energy for the combustion of botryococcene was calculated to be 44.94 kJ/g by the group contribution method as presented by Mavrovouniotis (1990); the $C_{34}H_{58}$ compound structure described in Anirban Banerjee et al. (2002) as 'structure 9' was utilized, which is displayed in Appendix B. The Gibbs free energy for the combustion of cell mass was determined from its enthalpy and entropy of combustion, according to Equation 4.40.

Gibbs energy of combustion for cell mass

$$\boldsymbol{\Delta G_{combustion,cell} = \Delta H_{combustion,cell} - T\Delta S_{combustion,cell}} \qquad \textbf{Equation 4.40}$$

The enthalpy of combustion of cell mass, $\Delta H_{combustion,cell}$, used in Equation 4.40 above was determined experimentally for freeze-dried *Rb. capsulatus* cell mass as -16.7 kJ/g cell. The entropy of combustion ($\Delta S_{combustion,cell}$) at 298K was determined from the stoichiometry of biomass combustion, assuming the empirical formula for cell mass excluding the contribution of P and S (see in Table 6.3), and assuming complete combustion to CO_2, H_2O, and HNO_3. The entropy values for CO_2, H_2O, HNO_3 and O_2 were obtained from http://physics-of-molecules.odessit.org /library/db/thermodata_2400.pdf. The entropy value for biomass was obtained from Battley (1999) and converted to molar cell units.

Finally, to determine the energy required per electron equivalent of (fuel + cell) produced, Equation 4.41 was used in place of Equation 4.10, the difference being the use of $\Delta G^0_{\text{synth}-2/\text{overall}}$ rather than $\Delta G^0_{\text{synth}-2/\text{g cell}}$ and the use of β to obtain a weighted overall formula weight for the cell and fuel produced:

Overall Gibbs energy for synthesis step 2, in kJ/eeq

$$\boldsymbol{\Delta G^{0\prime}_{synth-2} = \frac{\Delta G^{0\prime}_{synth-2/g\ overall}\left(\beta\, FW_{fuel} + (1-\beta) FW_{cell}\right)}{Q}} \qquad \textbf{Equation 4.41}$$

The value of Q, the number of electron equivalents required to synthesize a mole of total biomass, depends on the CF_f assumed; therefore, the value of Q varies in this work, as shown in Table 4.2. At low CF_f, Q will be at a maximum, because it will take fewer electron equivalents to

synthesize cells than highly reduced biofuels. Conversely, at high CF_f, Q will be at a minimum. Consequently, the $\Delta G_{synth\text{-}2}$ value calculated from Equation 4.41 employed in the calculations varies as well.

Modified EB Method: Summary

With the modified value for the $\Delta\widehat{G}_{SYNTH}$ now determined, the true-yield partitioning of electrons to cellular synthesis (f_S^0) can now be calculated from Equation 4.15-Equation 4.17 using ΔG_{ENERGY} and ε, as described for the original McCarty EB method. From f_S^0, the true yield can be calculated by determining the overall true-yield stoichiometric growth equation (Equation 4.18) and calculating the ratio of the coefficient for cell or botryococcene fuel production to the coefficient of the input substrate of interest. Note that net yields, which account for cellular maintenance, will be lower than the true yields calculated here, and these will be more representative of the yields that can be expected in a real bioprocess. The method for calculating net yields from true yields is presented in Chapter 5.

A Thermodynamic Perspective on the Selection of the Cellular Efficiency Factor, ε

Intuitively, it should be obvious that ε cannot be greater than one; for any exergonic reaction, where the energy captured by the cell is $\varepsilon\Delta G^{ex}$, the amount of energy actually captured must always be less than ΔG^{ex}; for any endergonic reaction, where the energy required to be spent by the cell to drive the reaction forward is $\Delta G^{end}/\varepsilon$, the amount of energy required must always be *greater* than ΔG^{end}. In this way, ε places a thermodynamic limit upon cellular growth yields, stipulating that energy available from each transfer is not fully converted into useful work, and that some is lost as heat; this is the realization of the second law of thermodynamics. The

application of the energy balance equation (Equation 4.14) stipulates that the Gibbs free energy *available* from the energy generating reactions, and the Gibbs free energy *required* by the cell synthesis reactions (including the inefficiency) balance each other out. By taking the ratio of these two values for a given efficiency value ε (Equation 4.15), this enables determination of the fraction of electron donor electrons required for energy and the fraction able to be spent on cell synthesis (f_s^0, f_e^0). From these values, the balanced growth and synthesis equation is constructed, and therefore the selection of ε is directly coupled to the outcome of the analysis. While there is inherent value in establishing the thermodynamic maximum of a biofuel process for economic analysis, the use of ε = 1 does not provide *realistic* yield values for this process, but rather an unrealistic ceiling for yields that could never be achieved in reality. Therefore, the real value of the thermodynamic maximum would be to identify processes that have a low likelihood of ever being economically infeasible; if the economics of the unrealistic thermodynamic maximum are not feasible, than obviously the real process will not be either.

However, the effect of the selection of ε is drastic, and the predicted yields are highly sensitive to the ε selected. This sensitivity increases as the magnitudes of the energy changes increase. The sensitivity of the predictions to the selected ε is explored further in Chapter 6. Thus, obtaining a realistic prediction for the cellular efficiency is key to the accurate prediction of biofuel system productivities; essentially, ε is the factor by which the theoretical prediction must be correlated with actual data. While this value cannot be determined directly, experimental data and thermodynamic theory can help guide the selection of an appropriate value for realistic predictions.

Comparison of experimental data with the yields predicted by the McCarty method has shown that there is a wide range in the cellular inefficiency factor ε associated with various types of metabolism (McCarty 1971). For aerobic heterotrophic growth, efficiencies from 32-81% were calculated; for anaerobic heterotrophic growth, efficiencies from 40-85% were determined;

for autotrophic bacterial growth efficiencies of 39-66% (aerobic) and 63-83% (anaerobic) were determined. As mentioned above, however, a range that spans from 39-66% efficiency has a rather large effect on the predicted yield. For illustration, the predicted theoretical maximum yield on H_2 for *Rb. capsulatus*, assuming no biofuel product, is 1.41 g biomass/mol H_2 for ε = 0.39 and 3.41 g biomass/mol H_2 for ε = 0.66; a 242% increase in yield from the low to high efficiency estimate. Furthermore, as mentioned above, the calculation method utilized by McCarty differed from the method used here for autotrophic growth, and so the efficiency range found in his work may not necessarily correspond with a reasonable choice in this case due to the difference in calculation method.

Because a reasonable value for the cellular efficiency method is critical to utilize the EB method for theoretical yield predictions, growth yield data from the literature was employed to estimate cellular efficiency factors for *Rs. eutropha* and *Rb. capsulatus*; this procedure is discussed in the next section.

Estimation of the Cellular Efficiency Factor

To make a reasonable estimation of the cellular efficiency factor (ε) for both *Rs. eutropha* and *Rb. capsulatus*, the approach was to first calculate electron partitioning to synthesis in experimental growth results ($f_{S,exp}$). If the assumption that under the experimental conditions referenced $f_{S,exp} \approx f_S^0$ can be considered valid, then a value for the cellular efficiency factor can be derived by manipulating Equation 4.13 and Equation 4.15 to solve for ε. The following sections describe this approach in more detail.

Calculation of f_S^0 from experimental yield data

As mentioned previously, the fraction of electrons from the electron donor partitioned to cell synthesis is directly proportional to the true yield of the organism growth on the electron donor. In the absence of fuel production, this can be directly quantified using Equation 4.42:

Relationship between true yield on H_2 and f_S^0

$$Y_{X,H2}^{T} = f_s^0 \left(FW_{cell} \frac{Q_{H2}}{Q_{cell}} \right) \qquad \textbf{Equation 4.42}$$

FW_{cell} is the formula weight for the empirical cell formula (g / mol), Q_{H2} is the number of electron equivalents contained in a mole of H_2 (2 eeq/mol H_2), and Q_{cell} is the number of electron equivalents required for the synthesis of one mole of cell matter. Yields directly calculated from experimental growth data, however, are net/observed growth yields which are less than true yields; part of the electrons from the electron donor are spent generating energy for maintenance demands. Because the rate of energy demand to meet cellular maintenance needs is relatively constant, maintenance puts a proportionally larger drain on microbial metabolism when the growth rate of the organism is low. Therefore in searching for reported growth yield data, it was considered that higher growth yields paired with high growth rates would be most representative of giving an estimate of an organism's true yield; these were the values sought for calculating f_S^0.

In the case of *Rs. eutropha*, Bongers (1970) used the method of Pirt (1965) to estimate a true yield estimate (6.2-6.6 g cell/mol H_2), and therefore an estimated true yield of 6.4 g cell/mol H_2 was utilized here in determining the cellular efficiency factor. This yield value was the highest reported yield found in the literature for *Rs. eutropha* growth on H_2 Bongers (1970). Other authors reported net yields ranging from 3.8 - 4.8 g cell/mol H_2 (Siegel and Ollis 1984; Y et al. 1978; Miura et al. 1981). Furthermore, the growth rate of 0.42 hr^{-1} reported in Bongers (1970) was greater than the growth rates reported in the other works, which ranged from 0.29-0.35 hr^{-1}. Therefore, it was reasoned that the reported true yield in Bongers (1970) would be a good

representative estimate of a true growth yield, and would provide a reasonable value for f_S^0. Equation 4.42 was utilized and for *Rs. eutropha* f_S^0 was determined to be 0.57.

In the case of *Rb. capsulatus,* the amount of growth data available in the literature was much less sufficient, particularly under chemolithoautotrophic growth. For this work, the data of Siefert & Pfennig (1979) was utilized; these authors reported a specific consumption rate (153 nmol/mg cell/min) of O_2 and a net growth rate (0.072 hr^{-1}) of *Rb. capsulatus* under chemolithoautotrophic growth. This data was utilized to calculate the net yield on O_2 as 7.8 g cell/mol O_2 using Equation 4.43.

Calculation of net yield on O_2 based on net growth rate and specific O_2 utilization rate

$$Y_{X/O2}^{NET} = \frac{\mu_{NET}}{\hat{q}_{O2}} \qquad \textbf{Equation 4.43}$$

The growth yield of O_2 is can be considered proportional to the electrons sent to cell synthesis divided by the electrons sent to energy generating reaction, because O_2 only participates as the electron acceptor for energy generation under chemolithoautotrophic growth of *Rb. capsulatus*: $Y_{X/O2}^{NET} \propto \frac{f_s}{f_e}$. Therefore,

Relationship between net yield on O_2 and f_S/f_e

$$Y_{X/O2}^{NET} = \frac{f_s}{f_e}\left(FW_{cell}\frac{Q_{O2}}{Q_{cell}}\right) = \frac{f_s}{1-f_s}\left(FW_{cell}\frac{Q_{O2}}{Q_{cell}}\right) \qquad \textbf{Equation 4.44}$$

where this time Q_{O2} is defined as the number of electrons that can be accepted by oxygen (4 e^-/mol O_2), and FW_{cell} and Q_{cell} are defined as previous. By rearranging Equation 4.44 to Equation 4.45, f_S can be calculated as 0.27.

Calculation of f_S from net yield on O_2

$$f_s = \frac{Y_{X/O2}^{NET}}{\left(Y_{X/O2}^{NET} + FW_{cell}\frac{Q_{O2}}{Q_{cell}}\right)} \qquad \textbf{Equation 4.45}$$

In the next chapter, it will be shown that a relationship between f_S and f_S^0 can be expressed in terms of the growth rate and the maintenance rate, *b*; the derivation of this expression will be addressed at that time. However, this relationship, shown below in Equation 4.46, was used to estimate f_S^0 based on the reported growth rate of 0.072 hr^{-1} (Siefert and Pfennig 1979) and a maintenance rate of 0.0095 hr^{-1}, which was calculated based on data in Hoekema et al. (2006).

Calculation of f_S^0 from f_S

$$f_s^0 = f_s \frac{\mu_{NET} + b}{\mu_{NET}}$$ **Equation 4.46**

From this procedure, the f_S for *Rb. capsulatus* was estimated as 0.31.

For each *Rs. eutropha* and *Rb. capsulatus*, the calculation of Q_{cell}, the number of electron equivalents required for the synthesis of one mole of biomass (fuel + cell), was performed by the method described in Appendix E. Empirical cell formulas reported specific to the species and the nitrogen source specific to the work from which the yield data was taken were used. The parameters and their sources utilized in the estimation of f_S^0 values from the literature are Table 4.3 below.

Table 4.3: Parameters from the literature used to estimate f_S^0 for *Rs. eutropha* and *Rb. capsulatus*

	Rs. eutropha		***Rb. capsulatus***	
Method of determining f_S^0	$Y_{X,H2}^T \rightarrow f_S^0$	Yield from (Bongers 1970)	μ_{NET}, $\hat{q}_{O2} \rightarrow Y_{X/O2}^{NET} \rightarrow f_S \rightarrow f_S^0$	μ_{NET} and f_S^0 from (Siegel and Ollis 1984)
b	n/a	n/a	0.0095	(Hoekema et al. 2006)
FW_{Cell}	$C_{4.09}H_{7.13}O_{1.89}N_{0.76}$	(Ishizaki and Tanaka 1990)	$C_5H_{8.4}O_{2.35}N_{0.65}$	(Hoekema et al. 2006)
Q_{Cell}	17 eeq/mol cell	calc'd	21.75 eeq/mol cell	calc'd
Nitrogen Source	NH_4^+	(Bongers 1970)	NH_4^+	(Siegel and Ollis 1984)
f_S^0	0.57		0.31	

Calculation of ε from f_S^0

After calculating an estimate of f_S^0 from yield data for each *Rs. eutropha* and *Rb. capsulatus*, a relationship between f_S^0 and ε was derived in order to estimate ε for each species. Starting from Equation 4.15 (repeated here for clarity):

Electron equivalents of ED that must be oxidized to supply energy requirements

$$A = -\frac{\Delta \hat{G}_{SYNTH}}{\varepsilon \Delta G_{ENERGY}}$$ **Equation 4.15**

$\Delta\hat{G}_{SYNTH}$ was broken back into its constituent energetic terms (such as in Equation 4.19 for *Rs. eutropha* and Equation 4.20 *Rb. capsulatus*) so that the dependence of $\Delta\hat{G}_{SYNTH}$ upon ε was explicit. Collecting all the endergonic and the exergonic energy exchanges of $\Delta\hat{G}_{SYNTH}$ together, and substituting back into Equation 4.15 results in Equation 4.47:

A as an explicit function of ε

$$A = -\frac{\left[\varepsilon \sum \Delta G_{SYNTH,EX} + \frac{1}{\varepsilon}\sum \Delta G_{SYNTH,END}\right]}{\varepsilon \Delta G_{ENERGY}} \qquad \textbf{Equation 4.47}$$

Recalling from Equation 4.13 that $A = \frac{f_e^0}{f_s^0}$, Equation 4.47 can be rearranged to solve for ε:

ε as a function of f_S

$$\varepsilon^2 = -\frac{\sum \Delta G_{SYNTH,END}}{\Delta G_{ENERGY}\left(\frac{1-f_s}{f_s}\right) + \sum \Delta G_{SYNTH,EX}} \qquad \textbf{Equation 4.48}$$

In order to calculate ε, the Gibbs energy exchange associated with the energy generating reaction (Equation 4.6) and that for each step of cell synthesis (Equation 4.23, Equation 4.24, Equation 4.25, Equation 4.32, Equation 4.34, and Equation 4.35) was calculated. Then each of these values were adjusted from the standard conditions to the conditions of the experimental system, using Equation 4.7, as described in Bongers (1970) for *Rs. eutropha* and that of Siefert & Pfennig (1979) for *Rb. capsulatus*). These values were then utilized in Equation 4.48 to calculate ε.

Table 4.4: Values used in the calculation of ε by Equation 4.48 for *Rs. eutropha* and *Rb. capsulatus*

	Rs. eutropha	***Rb. capsulatus***
Experimental conditions	T = 33°C; P_{H2} = 720 mmHg, P_{O2} = 135 mmHg, P_{CO2} = 45 mmHg; cell conc. = 3.5 g DW/L, NH^+ = 1.4e-02 M; PO_4^{3-} = 0.03 M; SO_4^{2-} @ 0.00085 M; pH = 7.0	T = 30°C, H_2 = 75%, CO_2 = 5%, O_2 = 20%; cell conc. estimated to be 3.3 g/L; 0.5 g KH_2PO_4/L, 0.4 g MgSO4-$7H_2O$/L; 1 g NH_4Cl/L; pH = 6.9
ΔG_{ENERGY}	-103.9	-103.9
$\Delta G_{SYNTH,EX}$	-1.67	-43.1
$\Delta G_{SYNTH,END}$	37.9	77.8
ε_{calc}	**0.69**	**0.53**

The values resulting from this analysis are summarized in Table 4.4. Based on this analysis, the cellular efficiency of *Rb. capsulatus* appears to be inherently lower than that of *Rs. eutropha*. Based on *Rb. capsulatus'* utilization of RET for NADH generation, this would suggest

a less inherently efficient cellular growth process for this organism. From this point forward in this work, these calculated values of ε for each *Rs. eutropha* and *Rb. capsulatus* are the ones utilized in calculations for yield predictions, as will be shown in Chapter 6.

Relationship of cellular efficiency factor ε in EB method to the Gibbs Energy Dissipation Theory

The Gibbs energy dissipation theory (Heijnen and van Dijken 1992; Tijhuis, van Loosdrecht, and Heijnen 1993; Jingsong Liu et al. 2007; von Stockar et al. 2006) is an alternative theory for the prediction of biological growth yields based on experimental data. A more detailed description of this method is presented in Appendix G of this thesis, however a few points are worth noting here in the context of the cellular efficiency factor calculation.

First, the Gibbs energy dissipation theory works by correlating growth data for a particular organism to a parameter termed the Gibbs Energy of Dissipation, ΔrG_x^0 (kJ/C-mol cell growth). The calculation for this parameter takes a strikingly similar form to the steady-state Gibbs energy balance (on the cells in the EB method:

Energy Balance, Gibbs Energy Dissipation Theory **Equation 4.49**

$$-\Delta_r G_X^0 = \frac{1}{Y_{X,ED}} \Delta G_{cat}^0 + \Delta G_{an}^0 \quad [= \text{kJ / carbon mol cell formed}]$$

Energy Balance, Gibbs Energy Dissipation Theory **Equation 4.14**

$$0 = A\,\varepsilon \quad \Delta G_{ENERGY} + \Delta \hat{G}_{SYNTH} \quad [= \text{kJ / eeq cell formed}]$$

Comparing Equation 4.49 and Equation 4.14 term-by-term:

- ΔG_{cat}^0 and ΔG_{ENERGY} each correspond to the Gibbs energy change associated with catabolic/energy generating reactions, i.e. the oxidation of the electron donor (ED) by the electron acceptor. The units of these quantities are different; ΔG_{cat}^0 is kJ/mol ED and ΔG_{ENERGY} has units of kJ/eeq ED.

- $\frac{1}{Y_{X,ED}}$ normalizes ΔG^0_{cat} to a single mole of cell, and also converts this quantity from units of [kJ/mol ED] to [kJ/C-mol biomass]. A (= f_e / f_S) normalizes ΔG_{ENERGY} to a single electron equivalent of cell, and converts this quantity from units of [kJ/eeq ED] to [kJ/eeq cell].
- ΔG^0_{an} and $\Delta \hat{G}_{SYNTH}$ each correspond to the Gibbs energy change associated with anabolic/synthesis reactions, and these have the units associated with those of each overall reaction (kJ/carbon mole cell and kJ/eeq cell, respectively).
- Note however that $\Delta \hat{G}_{SYNTH}$ (of Equation 4.14) is a function of the cellular efficiency factor ε; $\Delta \hat{G}_{SYNTH} = \varepsilon \sum \Delta G_{SYNTH,EX} + \frac{1}{\varepsilon} \sum \Delta G_{SYNTH,END}$, whereas ΔG^0_{an} is calculated directly without accounting for energetic losses. Furthermore, the cellular efficiency factor appears in Equation 4.14 in front of ΔG_{ENERGY}.
- Most notably, the right hand side of Equation 4.49 is equal to the Gibbs dissipation energy, $-\Delta_r G^0_X$, whereas Equation 4.14 is equal to 0.

This final difference is worth further discussion. The Gibbs dissipation energy, $-\Delta_r G^0_X$, is defined as the overall change in the molar Gibbs energy for the growth reaction, and is also related to entropy production by the cells:

$$-\Delta_r G_x \equiv \frac{T\, \dot{S}_{prod}}{\dot{\xi}}$$

where $\dot{\xi}$ is the rate of the growth reaction. The Gibbs energy dissipation theory correlates growth data for a particular organism or class of organism with the Gibbs dissipation energy of the overall growth reaction. Revisiting Equation 4.14, we can 'add back' the energy 'lost' to cellular inefficiency to both sides of the equation:

1. $0 = \varepsilon\, A\, \Delta G_E + \varepsilon \sum \Delta G_{S,EX} + \frac{1}{\varepsilon} \sum \Delta G_{S,END}$
2. $\left[(1-\varepsilon) A\, \Delta G_E + (1-\varepsilon) \sum \Delta G_{S,EX} + \frac{\varepsilon - 1}{\varepsilon} \sum \Delta G_{S,END}\right] =$

$$\varepsilon\, A\, \Delta G_E + \varepsilon\, \sum \Delta G_{S,EX} + \frac{1}{\varepsilon}\sum \Delta G_{S,END} + \left[(1-\varepsilon) A\, \Delta G_E + (1-\varepsilon)\sum \Delta G_{S,EX} + \frac{\varepsilon-1}{\varepsilon}\sum \Delta G_{S,END}\right]$$

3. $$\left[(1-\varepsilon) A\, \Delta G_E + (1-\varepsilon)\sum \Delta G_{S,EX} + \frac{\varepsilon-1}{\varepsilon}\sum \Delta G_{S,END}\right] = A\, \Delta G_E + \sum \Delta G_{S,EX} + \sum \Delta G_{S,END}$$

4. $$\left[(1-\varepsilon) A\, \Delta G_E + (1-\varepsilon)\sum \Delta G_{S,EX} + \frac{\varepsilon-1}{\varepsilon}\sum \Delta G_{S,END}\right] = A\, \Delta G_E + \Delta G_{SYNTH}$$ **Equation 4.50**

What results is an equation with all the energy not captured into useful work by the cell, i.e. that lost to entropy losses, heat generation, and incomplete energy capture, is set to the left-hand side of the energy balance equation and is a function of the cellular efficiency factor ε. The right hand-side of the equation is now qualitatively identical to the right-hand-size of the Gibbs energy dissipation theory, neglecting the difference in units. Thus, this establishes the similarities between these two alternative theories – both predict that a gradient of Gibbs free energy exists for the cellular growth reaction. The authors of the Gibbs energy dissipation theory have conceptually related this gradient to the driving force for microbial growth; in the limit of a value of 0 for $-\Delta_r G_x$, entropy generation would also be equal to zero, indicating a completely reversible cellular growth process. However, this growth would proceed at an infinitesimally slow rate (von Stockar et al. 2006). In the EB theory, this would correspond to an ε = 1.0, where the energetic loss term on the RHS of Equation 4.50 would be equal to zero. The behavior of the yield predictions in this limit, termed the 'Thermodynamic Limit' in this work, are discussed in CHAPTER 6.

Some important differences prevented the quantitative equating of these two theories, however:

- The two theories assume different reference states, which makes it challenging to quantitatively compare the $-\Delta_r G_x$ values determined with the EB energetic loss term.

- Furthermore, the Gibbs energy dissipation theory does not currently have a mechanism for adjusting the Gibbs energy for biomass (in the reference state of that theory) for varying biomass compositions.

For further discussion of the Gibbs Energy dissipation theory, see Appendix G to this thesis.

Chapter 5

Derivation of Growth Kinetics and Yields under Gas-Liquid Mass Transfer Limitation for Autotrophic Aerobic Hydrogen Oxidation

In Chapter 4 an Electron Balance (EB) methodology was presented for developing stoichiometrically balanced growth equations, which was modified specifically enable yield predictions for botryococcene product fuel synthesis by chemolithoautotrophic microbes. The resulting growth equations from this methodology provide a means to calculate the true yields of cell growth and botryococcene product fuel (BPF), yields which do not account for any maintenance energy demands of the organism. Maintenance energy is the amount of energy required by the organism to sustain life in addition to energy demands for growth and product synthesis. Therefore, the net yields actually achievable in a process are necessarily lower than the true yields predicted by the EB methodology, as some portion of the energy made available from the energy generating reactions is siphoned off for maintenance. This chapter provides a means by which to determine net yields in a process where conditions do not allow an organism to achieve its intrinsic maximum growth.

The relative degree to which a microbes energy-generating metabolism can shuttle that energy to growth processes versus that which is required by maintenance processes is dependent upon the rate of growth. In a system where there are no external kinetic constraints on an organism's growth rate, and growth proceeds at the intrinsic maximum rate of the organism, maintenance demands will be a minimum relative to the energy demands from growth – an organisms' maintenance rate can roughly be assumed as constant. However, non-limited rates of growth are rarely attained in practice except transiently, at small production scales, and at very low biomass densities. Instead, the organism's growth rate is typically dictated by the supply

rate of one or more growth substrates. Identifying and predicting kinetic rate limitations on microbial growth is important for several reasons:

- The degree that the actual growth rate of the organism is diminished from its maximum has a large effect on both the net yield, as well as the productivity of the process.
- Process yields are proportional to the observed/net rate of growth of the organism.
- Whatever growth substrate is dictating the rate limitation will have a very low concentration within the system because it is utilized as soon as it enters the cells. Particularly if the rate-limiting substrate is the electron donor or the electron acceptor, a low concentration of this substrate will have unfavorable thermodynamic effects on the Gibbs energy associated with the energy-generating process (ΔG_{ENERGY}). For example, in addition to kinetic constraints associated with H_2 mass transfer, the energy-generating reactions would provide less energy for cell growth per mass of hydrogen oxidized.
- For any system where the volumetric productivity (product produced per volume per time) is dependent upon the rate of cell growth, obtaining an accurate rate of cell growth under rate-limited conditions is critically important for realistic productivity projections. Furthermore, volumetric productivity is also a function of the product yield, which itself is a function of the growth rate of the organism.

Reflecting back on the algal work described in Chapter 2 of this thesis, the rate-limiting factor for algal growth in high-density, trickle-screen photobioreactor was the rate of light energy available to the algal culture. As shown with algae, assessing rate-limitations requires looking critically at the overall kinetics of the bioprocess, and the effect of rate-limitations resulted in large deviations in the growth rate of an organism compared to a non-limited scenario (*C. vulgaris*). For the non-photosynthetic growth of *Rs. eutropha* and *Rb. capsulatus*, we will be concerned with a different cause of rate limitation – that of gas-liquid mass transfer limitation. Gas-liquid mass transfer has long been a challenge for the biotechnology industry due to the low

solubility of O_2 gas in aqueous media – the driving force for gas-liquid mass transfer is the difference in the culture concentration and the liquid concentration. When the solubility is low, so will be the driving force for mass transfer. Typically the problem is the supply of oxygen to an aerobic process at a rate sufficient to prevent oxygen limitation. Ensuring rates of mass transfer high enough to keep up with the demand without causing damage to delicate mammalian cells is particularly challenging, because the traditional means of achieving mass transfer result in high shear rates from sparging and impellers. This becomes even more challenging at large production scales with large liquid volumes. In the case of a microbial process like *Rs. eutropha* and *Rb. capsulatus,* high shear rates are less of a concern because of the smaller size of prokaryotic cells. However, all three of the electron donor, the electron acceptor, and the carbon source for the chemolithotrophic growth of *Rs. eutropha* and *Rb. capsulatus* must be delivered from the gas phase to the liquid phase in order to be available for microbial growth. Therefore, without sufficient rates of mass transfer there will be no substrate available for metabolism to occur; this suggests that mass-transfer limitations will be the most likely rate-limiting step for this autotrophic growth mode. Another aspect of gas-liquid mass transfer to consider is that in traditional aerobic bioreactors, low conversions of oxygen from the gas phase to the liquid phase are acceptable because air as a feedstock is 'free'. By contrast, the chemolithoautotrophic growth of *Rs. eutropha* and *Rb. capsulatus* will have gaseous feedstock dominated by the cost of hydrogen generation by abiotic electrolysis (\$3.82/kg H_2 versus \$0.02/kg CO_2 from CCS). Therefore, low conversion of the gaseous hydrogen substrate will be unacceptable for financial feasibility, requiring efficient utilization of H_2 via effective mass transfer.

The rest of this chapter describes the methodology for assessing the rate-limiting factor and the resulting growth rate restriction, and then using this information to adjust the true yields to net yields for calculating of cell growth productivities. This general theory is adapted to the specific case of interest in this work: a mass-transfer limited process for cell growth and

botryococcene hydrocarbon production by aerobic hydrogen oxidation. First a background on microbial growth and product formation kinetics are described. Then, the parameters necessary for assessing values of growth and product formation rates are presented, along with a context for their relevance in the chemolithoautotrophic fuel production. Fundamentals of gas-liquid mass transfer are then discussed, and finally the procedure for obtaining a mass-transfer-limited growth rate and corrected product yields and productivities is presented.

Kinetics of Microbial Growth and Product Formation

The rate of microbial growth is characterized by the specific growth rate μ [hr^{-1}] , which is defined as the rate of cell accumulation normalized to the cell concentration present:

Growth rate definition $$\mu \equiv \frac{1}{X}\frac{dX}{dt}$$ **Equation 5.1**

where X is the concentration of cells [g dry weight (DW) cell / L]. Under non-limited conditions, microbial growth follows exponential growth kinetics, where the constant volume total rate of cell synthesis [g DW cell/hr], is proportional to the cell mass present and μ is constant:

Rate of cell synthesis for exponential growth kinetics $$\left[\frac{dX}{dt}\right]_{synth} \equiv \mu X$$ **Equation 5.2**

Non-limited growth conditions require that all growth substrates are provided to the cell at a rate greater than the rate at which the cells are able to utilize them. A quantity called the yield ($Y_{X/i}$) relates the specific rate of substrate utilization ($\hat{q}_i$) to the specific rate of growth μ. The yield is the quantity of cell growth possible provided a certain amount of substrate:

Definition of specific substrate utilization rate $$\hat{q}_i \equiv -\frac{1}{X}\frac{dCi}{dt} = \mu\frac{1}{Y_{X/i}}$$ **Equation 5.3**

$\hat{q}_i$ has units of [mol i / g cell / hr], C_i is the concentration of substrate i [mol / L] and $Y_{X/i}$ is the yield of cell growth on substrate i [g cell / mol i]. From here forward, the X will be dropped from the subscript of the yield and will be considered to be implied, so that the yield of cell on substrate i becomes Y_i.

$\hat{q}_i$ is the total rate of substrate utilization by the cells, and accounts for substrate used for growth as well as for any maintenance demands; $\hat{q}_i$ can be measured directly. $\hat{q}_i$ can be expressed as a function of the true growth rate and the true yield for each substrate, as shown in Equation 5.4. The true, or maximum yield (as it will be referred to in this chapter, $Y_i^T = Y_i^{MAX}$) is always greater than the net yield Y_i^{NET}. Associated with this true yield then is a true growth rate (μ^T), a growth rate that would be possible if the maintenance needs were zero; μ^T is always greater than μ^{NET}.

Substrate utilization effect as a function of true yields

$$\hat{q}_i = \mu^T \frac{1}{Y_i^{MAX}} \qquad \textbf{Equation 5.4}$$

The relationship between the true rate of growth, μ^T, and the net rate of growth, μ^{NET}, is defined below in Equation 5.5, where b is a maintenance rate [hr^{-1}], conceptualized as the specific rate at which the cell's metabolism is diverted to maintenance needs rather than growth processes.

Relationship between net and true growth rate

$$\mu^{NET} = \mu^T - b \qquad \textbf{Equation 5.5}$$

Rearranging Equation 5.5 to solve for μ^T and then substituting the resulting expression for μ^T in the Equation 5.4 results in the following equality:

Substrate utilization as a function of net growth rate and maximum (true) yield

$$\hat{q}_i = \frac{\mu^{NET}}{Y_i^{MAX}} + \frac{b}{Y_i^{MAX}} \qquad \textbf{Equation 5.6}$$

From Equation 5.6, the specific rates of substrate utilization associated with growth and maintenance can each be defined:

Substrate utilization associated with growth

$$\left[\hat{q}_i\right]_{growth} \equiv \frac{\mu^{NET}}{Y_i^{MAX}} \qquad \textbf{Equation 5.7}$$

Substrate utilization associated with maintenance

$$\left[\hat{q}_i\right]_{maint} \equiv \frac{b}{Y_i^{MAX}} \qquad \textbf{Equation 5.8}$$

The specific substrate utilization rate for maintenance itself is defined as the maintenance coefficient m_i, with units of [mol i / g cell / hr]:

Definition of maintenance coefficient

$$\left[\hat{q}_i\right]_{maint} \equiv m_i \equiv \frac{1}{X}\left(\frac{dC_i}{dt}\right)_{maint} \qquad \textbf{Equation 5.9}$$

and so m_i, can be related to the maintenance rate b by:

Relationship of maintenance rate to maintenance coefficient

$$m_i = \frac{b}{Y_i^{MAX}} \qquad \textbf{Equation 5.10}$$

The distinction between the maintenance coefficient m_i and the maintenance rate b are emphasized here: the maintenance coefficient is specific to a particular substrate and a specific organism, whereas b is always applicable for a particular organism, and therefore is a more general expression of the maintenance needs of the organism. The maintenance rate and maintenance coefficients are generally considered to be constants associated with a particular microbial species.

The kinetics of botryococcene product fuel formation (designated BPF) must also be considered. From a microbial standpoint, several types of BPF formation kinetics are possible; in this work the product fuel was assumed to be growth-associated, occurring concurrently with microbial growth. Thus, the specific rate of BPF formation (r_F, [g BPF/g cell/hr]) was modeled as being directly proportional to the net growth rate by a factor $\bar{F}$ [g BPF synthesized/g cell synthesized]:

Definition of specific rate of BPF formation and relation to net growth rate

$$r_{BPF} \equiv \frac{1}{X}\frac{d(C_{BPF})}{dt} = \bar{F}\frac{1}{X}\frac{dX}{dt} = \bar{F}\mu^{NET} \qquad \textbf{Equation 5.11}$$

Although growth-associated product formation kinetics were assumed, in Chapter 6 $\bar{F}$ is examined over a full range of hypothetical values, and therefore one can examine high product formation under conditions with very little growth.

Relationship of Growth Kinetics to Yield through f_S^0

The EB theory provides a relationship between the net electron partitioning to cell synthesis (f_S) and the true/maximum electron partitioning to cell synthesis (f_S^0) as a function of the net and true growth rates, which is presented here (Rittman and McCarty 2001):

f_S as a function of f_S^0, μ^{NET}, and μ^T

$$f_s = f_s^0\left(\frac{\mu^{NET}}{\mu^{NET}+b}\right) = f_s^0\left(\frac{\mu^T - b}{\mu^T}\right) \qquad \textbf{Equation 5.12}$$

To obtain the stoichiometric growth equation in which the energy cost of maintenance has been accounted for, f_S is used in place of f_S^0 in Equation 4.18, resulting in:

$$R_{OVERALL} = f_S\, R_{SYNTH} + \ (1 - f_S)R_{ENERGY} = f_S\, R_{SYNTH} + \ f_E R_{ENERGY}$$

This enables calculation of net yields for cell growth and fuel synthesis on each substrate using the stoichiometric coefficients for each species.

To allow derivation of a slightly more intuitive relationship for the effect of diminished growth rates on net yields, we can consider that f_S^0 and f_S are themselves yields – the fraction of the total electrons in the electron donor able to be sent to cell and fuel synthesis. These quantities can be converted into mass yields on the electron donor (g biomass / g ED) by utilizing the molar weights of the ED and the overall formula weight of biomass synthesis, which is the average of the formula weights of the cell mass and the BPF, weighted according to the molar ratio fuel synthesis (α, defined in Chapter 4):

Formula weight for overall cell and fuel synthesis

$$FW_{overall-synth} = (1-\alpha)FW_{cell} + \alpha\, FW_{BPF} \qquad \textbf{Equation 5.13}$$

Using this quantity in addition to the number of electron equivalents required per mole of cell and of BPF allows direct conversion between mass yields and the electron-yields:

Relationship between maximum yield and f_S^0

$$f_S^0 \frac{FW_{biomass}}{MW_{ED}} \frac{Q_{ED}}{Q_{cell}} = Y_{X/ED}^{MAX} \qquad \textbf{Equation 5.14}$$

Relationship between net yield and f_S

$$f_S \frac{MW_{biomass}}{FW_{ED}} \frac{Q_{ED}}{Q_{cell}} = Y_{X/ED}^{NET} \qquad \textbf{Equation 5.15}$$

Substituting these into Equation 5.12 provides a similar relationship between the net and true yields on electron donor:

Relationship between Y^{NET} and Y^{MAX} for the electron donor

$$Y_{X/ED}^{NET} = Y_{X/ED}^{MAX} \frac{\mu^{NET}}{\mu^{NET} + b} = Y_{ED}^{MAX} \frac{\mu^{T} - b}{\mu^{T}} \qquad \textbf{Equation 5.16}$$

While this relationship was not employed directly for calculations, it provides a good platform for understanding the coupling between yield and kinetic constraints on microbial growth. First, it can be clearly seen that at a low net growth rate, the relative importance of b is high, so that the net yield on the electron donor is more severely diminished with respect to the true yield on the electron donor. A distinction is required here to clarify two scenarios resulting in a rate-limited system with the same observed impact to the net yield, but with different causes:

1. Low net yields as a result a limited rate of energy generation: this would occur when either the electron donor or electron acceptor is rate-limiting. The rate of energy available from oxidation of the electron donor must be partitioned between cellular maintenance, which is assumed to require a constant rate of energy, growth, and BPF synthesis. Because satisfying cellular maintenance needs is essential for survival, these energetic needs will be fulfilled at a priority, and only the 'remaining' energy available after satisfying maintenance costs will be available for growth and synthesis. Thus, when the rate of energy generation is small, only a small rate of energy is 'left over' for growth, resulting in low growth rates. The slow rate of energy generation (cause) results in slow growth rates, and therefore low net yield on the electron donor (effect) according to Equation 5.16). As this same relationship is that which links f_S and f_S^0 (Equation 5.12), the growth and synthesis yields will be diminished for all substrates. Conversely, when the rate of energy generation is non-limiting, plenty of energy above that required to satisfy maintenances needs is available, which can be utilized for cell growth; thus and the net yield approaches the maximum (true) yield.

2. Low net yields as a result of growth rate-limitations not directly linked to energy generation; as an example, this would occur if the rate of CO_2 transport was slow enough that it could not provide carbon at a rate sufficient to enable the organism's maximum growth rate. However, in this case, the energy generation would not be limiting, and so the previous argument is invalid. Instead, consider that the imposed slow growth rate now utilizes energy at a small rate compared to the maintenance rate; extra energy being generated over that required to satisfy maintenance and the slow rate of growth would need to be dissipated through heat or other means, and would not result in an observed accumulation of cellular mass, resulting in a slow observed (net) growth rate. The limited growth rate (cause) will be proportionally smaller compared to the maintenance rate, resulting in a diminished net yield (effect) according to Equation 5.12 and Equation 5.16). Conversely, if the rate of CO_2 supply is non-limiting, the cell growth rate will proceed at the maximum rate possible for the organism (assuming no other factor is limiting). In this case, the contribution of b to Equation 5.12 and Equation 5.16 is small, and so the yet yield approaches the maximum (true) yield.

Because maintenance needs must be satisfied, for any net growth to occur, the rate of energy available from oxidation of the electron donor must be greater than that required for maintenance. If this is not the case, the lack of energy availability results in no net growth, and the net yield and the net growth rate are both zero.

Obtaining values for μ^{MAX}, m_i, and b

As described in the previous section, to quantify the net growth yields, values for μ^T and b are required. As will be shown in following sections, μ^T can be directly calculated by rearrangement of the substrate mass balance; however, even at high rates of substrate availability

Table 5.1: Growth, maintenance, and yield parameters of *Rs. eutropha* and *Rb. capsulatus* from the literature.

The parameters obtained from the literature review are stated in the table below; the values used in the mathematical calculations in this analysis are shaded, and were selected as the values most likely to represent μ^{MAX} (under non-limited conditions), Y^{MAX} and m_i. Further details on the rationale used for selection are in the text.

Parameter	Value		Ref	Conditions	
Rs. eutropha					
μ^{MAX}	0.31	h^{-1}	Siegel & Ollis, 1984	O_2-limited Chemo-autotrophic chemostat	31°C, pH = 6.5-6.7
Y_{H2}^{MAX}	4.1	g cell/mol H_2			
m_{H2}	0.0010	mol H_2/g/hr			
μ^{MAX}	0.29	h^{-1}		H_2-limited Chemo-autotrophic chemostat	
Y_{H2}^{MAX}	4.5	g cell/mol H_2			
m_{H2}	0.025	mol H_2/g/hr			
μ^{MAX}	0.42	h^{-1}	Bongers, 1970	Chemo-autotrophic, continuous	33°C, pH = 7, H_2:O_2:CO_2 = 720:135: 45 mmHg, X = 3.5 g/L
Y_{H2}^{MAX}	6.4	g cell/mol H_2			
m_{H2}	0.0070	mol H_2/g/hr			
b	0.045	h^{-1}			Calc'd from m_i and Y_i using Equation 5.10
Rb. capsulatus					
μ^{NET}	0.116	h^{-1}	Madigan & Gest, 1979	Chemo-autotrophic, batch	32-34°C, pH = 7.2, H_2:O_2:CO_2 = 85:10:5 (%)
μ^{NET}	0.072	h^{-1}	Siefert & Pfennig, 1979	Chemo-autotrophic, batch	30°C, pH = 6.9, H_2:O_2:CO_2 = 75:20:5 (%), X = 3.3 g/L
Y_{O2}^{NET}	7.84	g cell/mol O_2			
Y_{H2}^{NET}	2.86	g cell/mol H_2			Calc'd from Y_{O2}^{NET} using electron equivalents and and $f_S^0 + f_S^0 = 1$
Y_{light}	2.58E-08	kg cell/J	Hoekema et al., 2006	Continuous Photo-heterotrophic	
m_{light}	102	W/kg cell			
b	0.00947	h^{-1}			Calc'd from m_i and Y_i using Equation 5.10

μ^T will be capped by the intrinsic maximum growth rate of the organism, μ^{MAX}; μ^{MAX} will occur only under non-limited conditions. Note that μ^{MAX} and μ^T are not equivalent; μ^T is the rate of growth possible if the maintenance demands were zero. Therefore, while μ^{MAX} is considered a constant for an organism, μ^T is a function of the process conditions and can be restricted by mass-transfer limitations. Knowledge of μ^{MAX} is required in order to predict when additional increases to substrate availability will not result in further increases in yield.

From the literature, values for each μ^{MAX} was obtained directly. To obtain b, m_i (a maintenance coefficient for substrate i), and literature value of Y_i^{MAX} were obtained, and b was calculated according to Equation 5.10. These values are presented in Table 5.1. For both *Rs. eutropha* and *Rb. capsulatus*, the largest growth rate obtained from the literature was utilized as the μ^{MAX} value, and for *Rb. capsulatus* this value was verified in the Curtis Lab under chemoautotrophic growth conditions (Nymul Khan, personal communication; data not shown). This approach is justified because of the likelihood of mass transfer limitation in chemoautotrophic growth bioreactors, and so therefore it was reasoned that the highest observed growth rate was more likely to be more representative of the true μ^{MAX} than to be due to experimental error. Because the method (typically that of Pirt (1965)) of determining Y_i^{MAX} and m_i is not independent, care was taken to ensure that both the Y_i^{MAX} and m_i used to calculate b was taken from the same dataset. For *Rs. eutropha*, there was sufficient literature data available such that the approach of several authors in obtaining the values could be compared and the 'best' values selected; rather than averaging the data, I assessed the conditions under which the literature values were obtained, and the values used in this analysis were selected based on the dataset assessed to be closest to a non-rate-limited growth scenario (and so the best approximation of true yields and maintenance). For *Rb. capsulatus*, only a single report of a yield under chemoautotrophic growth conditions was found (Siefert and Pfennig 1979). Furthermore this literature value appears to be a net yield, and no maintenance coefficient was simultaneously reported. However, a yield and a maintenance coefficient on light energy was obtained for *Rb. capsulatus* growing photoheterotrophically (Hoekema et al., 2006), and b was calculated from this data. Because chemolithoautrophic and photoheterotrophic growth are very different in nature, it cannot at this time be definitively known whether the maintenance rate under both conditions is the same. However, as this was the only value available at the time of this analysis,

this was the value used; measuring the chemolithoautotrophic maintenance rate for *Rb. capsulatus* is future work planned in the Curtis lab.

Mass Balances in the Mass-Transfer Limited Growth Scenario

Under mass-transfer limited conditions, the rate of growth will be determined both by the mass transfer rate of the limiting substrate as well as the operational configuration of the reactor. Therefore, the most general cases of each the cell, fuel, and substrate balance will be developed, and then the assumptions, restrictions, applicable to the assumed configuration for this work will be applied. For the analysis of botryococcene hydrocarbon production by *Rs. eutropha* and *Rb. capsulatus* presented in Chpater 6, the assumed configuration is a continuous-growth, steady-steady state (chemostat) reactor system with a constant liquid volume.

Cell Balance

The rate of accumulation of cell mass in a control volume V, where V is the liquid phase volume of the control volume, is given by Equation 5.17:

General mass balance on cell

$$\frac{d}{dt}(X_R V) = Q_{in}X_{in} - Q_{out}X_{out} + V\left[\frac{dX}{dt}\right]_{synth} \qquad \textbf{Equation 5.17}$$

where $\left[\frac{dX}{dt}\right]_{synth}$ is the rate of cell growth in the reactor. Assuming that the rate of cell growth in the reactor is defined by the constant growth of the cells (Equation 5.2), the cell mass balance becomes:

Cell Mass balance for exponential growth

$$\frac{d}{dt}(X_R V) = Q_{in}X_{in} - Q_{out}X_{out} + \mu^{NET}X_R V \qquad \textbf{Equation 5.18}$$

In these equations, the variables are defined as follows:

X_R, X_{in}, X_{out} = Concentration of cell in the reactor, inlet flow, and outlet flow, respectively (g dry weight / L)

Q_{in}, Q_{out} = Liquid phase volumetric flow rate in and out of the reactor control volume, respectively (L/time)

μ^{NET} = The net specific growth rate of cell mass (hr^{-1}); this was selected as the growth rate since for the mass balance we are concerned with is the net (apparent) accumulation of cell mass in the reactor

Applying the continuous, steady-state assumption, the accumulation term $\frac{d}{dt}(X_R V)$ on the left-hand side goes to zero. It is assumed that there is no cell mass in the inlet stream, and that the concentration of cell mass in the outlet stream is equal to the concentration in the reactor; thus $X_{in} = 0$ and $X_R = X_{out} = X$. For a reactor system other than continuous, steady state, such as a perfusion reactor or fed-batch, these assumptions and simplifications may no longer apply. Applying these simplifications results in:

Steady-state cell balance

$$\frac{Q_{out}}{V} X = \mu^{NET} X \qquad \textbf{Equation 5.19}$$

Q_{out}/V is called the dilution rate (D), which depends upon X and μ^{NET} as it must be set such that the cell concentration in the reactor remains at steady state. Dividing through by X, it becomes clear that the dilution rate is equivalent to the net rate of growth, which is a defining characteristic of an ideal chemostat; this is a useful equality that will be applied later.

Dilution rate is equivalent to the cell growth rate

$$D = \frac{Q_{out}}{V} = \mu^{NET} \qquad \textbf{Equation 5.20}$$

Botryococcene Product Fuel (BPF) Balance

The botryococcene product fuel balance is constructed similarly to the cell balance, where the rate of accumulation of the product fuel within the reactor liquid control volume V is:

General BPF mass balance

$$\frac{d}{dt}\left(C_{BPF,R}V\right) = Q_{in}C_{BPF,in} - Q_{out}C_{BPF,in} + V\left[\frac{d(C_{BPF})}{dt}\right]_{synthesis} \qquad \textbf{Equation 5.21}$$

$\left[\frac{dBPF}{dt}\right]_{synthesis}$ = rate of fuel synthesis

$C_{BPF,R}$, $C_{BPF,in}$, $C_{BPF,out}$ = Concentration of botryococcene product fuel in the reactor, inlet flow, and outlet flow, respectively (g fuel / L)

V, Q_{in}, Q_{out}, = as defined above under the Cell Balance.

If the fuel being synthesized was volatile (such as ethanol or another solvent with a high vapor pressure), the rate of the evaporation of the fuel from the liquid phase would be significant; this would require including a term in Equation 5.21 to account for the evaporation, and would require a gas-phase mass balance as well. However, for the $C_{34}H_{58}$ botryococcene product assumed in this work, the vapor pressure of this oil is extremely low due to the high molecular weight, and can be neglected.

In this work, the cells are the catalysts for the production of botryococcene from the gas-phase substrates. Once substrate utilization for cellular maintenance requirements are satisfied, the remaining substrate can be utilized for cell synthesis and BPF synthesis. Because the cells must 'decide' whether substrates are used to generate more cell mass or to synthesize BPF, we assume that the specific rate of BPF formation r_{BPF} is proportional to the specific growth rate of the cells in the reactor by a proportionality factor $\bar{F}$, the mass ratio of fuel produced to cells synthesized. This method of modeling BPF synthesis is also aligned with the assumption of growth-associated product formation kinetics, and yet allows for a broad range of cellular productivities even at greatly reduced growth rates:

Definition of specific rate of BPF formation

$$r_{BPF} \equiv \frac{1}{X}\left[\frac{dC_{BPF}}{dt}\right]_{synth} = \left(\frac{1}{X}\frac{dX}{dt}\right)\bar{F} = \mu^{NET}\bar{F} \qquad \textbf{Equation 5.22}$$

Where $\bar{F}$ is defined as:

Fuel synthesis proportionality factor

$$\bar{F} \equiv \frac{\text{specific rate fuel production}}{\text{specific rate cell growth}} \equiv \frac{\left(\frac{1}{X}\frac{dC_{BPR}}{dt}\right)}{\left(\frac{1}{X}\frac{dX}{dt}\right)} = \frac{dC_{BPF}}{dX} \qquad \textbf{Equation 5.23}$$

The overall mass balance on BPF then becomes:

BPF mass balance for growth-associated fuel synthesis kinetics

$$\frac{d}{dt}\left(C_{BPF,R}V\right) = Q_{in}C_{BPF,in} - Q_{out}C_{BPF,out} + VX_R r_{BPF} = Q_{in}C_{BPF,in} - Q_{out}C_{BPF,out} + VX_R(\mu^{NET}\bar{F}) \qquad \textbf{Equation 5.24}$$

Applying the assumption that the concentration of cell and BPF in the reactor is the same as the concentration in the outlet ($X_R = X_{out} = X$; $C_{BPF,R} = C_{BPF,out} = C_{BPF}$), that there is no fuel in the inlet stream ($BPF_{in} = 0$), the fuel mass balance simplifies to:

Steady-state BPF mass balance

$$\frac{Q_{out}}{V}C_{BPF} = \mu^{NET} X \bar{F} \qquad \textbf{Equation 5.25}$$

Applying Equation 5.20, this further simplifies to the expression in Equation 5.26, which shows the relationship of BPF concentration to cell concentration at steady state.

Relationship of BPF concentration to cell concentration at steady-state

$$C_{BPF} = X\bar{F} \qquad \textbf{Equation 5.26}$$

When $\bar{F}$ is constant, the concentration of BPF within the system is directly proportional to the concentration of cell in the reactor; if the BPF were an intracellular product, the composition of BPF in the cell would be constant

In this work, $\bar{F}$ is conceptualized as a function of the parameter CF_f, which was presented in Chapter 4 as the fraction of metabolic carbon flux directed towards fuel production; by analogy CF_C is the fraction of metabolic carbon flux directed towards cell synthesis, and CF_f and CF_C sum to unity (Equation 4.28). The parameter CF_f answers the question: to what extent is fixed CO_2 shuttled to making botryococcene product fuel versus generating more cell mass? To obtain a relationship between $\bar{F}$ and CF_f, we must first utilize another parameter defined in Chapter 4, which is the molar ratio of fuel produced to cell synthesized (α, Equation 4.27). $\bar{F}$ is related to α directly using the formula weights (FW) for the fuel and the non-fuel cell mass:

Relationship between the mass and molar ratios of fuel-to-cell synthesis

$$\bar{F} = \alpha \frac{FW_{fuel}}{FW_{cell}}$$ **Equation 5.27**

Because α is directly related to CF_{fuel} by EQUATION 4.29, we can relate $\bar{F}$ to CF_{fuel}:

Relationship of $\bar{F}$ to CF_f

$$\bar{F} = \frac{CF_f}{1 - CF_f} \frac{n_{C,cell}}{n_{C,cell}} \frac{FW_{fuel}}{FW_{cell}}$$ **Equation 5.28**

where $n_{C,fuel}$ and $n_{C,cell}$ are the moles of carbon per mole of fuel and cell, respectively.

Substrate Balance

The accumulation of the any gas-phase substrate i is calculated from the following substrate balance on the liquid control volume V:

General mass balance on substrate *i*

$$\frac{d}{dt}\left(C_{i,R}V\right) = Q_{in}\, C_{i,in} - Q_{out}\, C_{i,out} + MTR_i\, V - \hat{q}_i\, X_R\, V$$ **Equation 5.29**

The terms of this equation are defined as:

$C_{i,R}$, $C_{i,in}$, $C_{i,out}$ are the concentrations of substrate *i* in each the reactor liquid, the inlet stream, and the outlet stream.(mol *i* / L)

MTR_i is the rate of mass transfer of substrate *i* from the gas phase to the liquid phase (mol *i* / L / hr)

$\hat{q}_i$ is the specific utilization rate of i (mol *i* / g cell / time)

V, Q_{in}, Q_{out}, = as defined above under the Cell Balance.

Both MTR_i and $\hat{q}_i$ warrant some further attention, and so they are discussed in further detail here.

Gas-Liquid Mass Transfer

The mass transfer rate (MTR) for a gas phase substance into a body of liquid is proportional to the difference in liquid phase concentration difference between the equilibrium concentration of i, C_i^*, and the actual concentration in the reactor, $C_{i,R}$:

Definition of gas-liquid mass-transfer rate

$$MTR_i \equiv (k_L a)_i \left(C_i^* - C_{i,R}\right) \qquad \textbf{Equation 5.30}$$

Here, $(k_L a)_i$ is the species-specific mass-transfer coefficient (in hr^{-1}). The equilibrium concentration C_i^* is the concentration of i in the liquid phase that is in equilibrium with the gas-phase partial pressure of the substrate (P_i) by the gas phase. This is obtained by Henry's Law using the proportionality factor k_i, also referred to as the Henry's Law coefficient (L-atm/mol).

Equilibrium concentration of *i* by Henry's Law

$$C_i^* = \frac{P_i}{k_i} \qquad \textbf{Equation 5.31}$$

Henry's Law coefficient is specific to each gaseous species, and is not a constant but varies with temperature. An expression for the temperature dependence of k_i is provided in Equation 5.32 as a function of the value of k_i at 298K:

Temperature dependence of Henry's Law coefficient

$$k_{i,T} = k_{i,298}\, exp\left(\varphi_i \left(\frac{1}{T} - \frac{1}{298}\right)\right) \qquad \textbf{Equation 5.32}$$

In this equation, $k_{i,T}$ and $k_{i,298}$ are the values of the Henry's Law coefficient at the actual temperature T and 298K, respectively; φ_i is a constant specific to the substrate, and T is the temperature in degrees Kelvin. Values utilized for $k_{i,298}$ and φ_i are listed in Appendix F.

$k_L a$ is the gas-liquid mass transfer coefficient for oxygen mass transfer, and the vast majority of correlations for $k_L a$ report only this value for oxygen. However, the $k_L a$ for any other species is related to the oxygen $k_L a$ by the following expression (Ho, Baddour, and Stalker 1987):

Species-specific gas-liquid mass-transfer coefficient

$$(k_L a)_i = (k_L a)_{O2} \left(\frac{D_{O2}}{D_i}\right)^{\frac{2}{3}} \qquad \textbf{Equation 5.33}$$

D_{O2} and D_i are the diffusivities of oxygen and substrate i in liquid water, respectively; the values of the diffusivities for each gas-phase species are listed in Appendix F.

The Specific Utilization Rate of Substrate i

The specific utilization rate of substrate *i*, $\hat{q}_i$, is obtained from Equation 5.4 using the true rate of cell growth (μ^T) and the true yield of cell on substrate *i* (Y_i^T, in units of gram cell / mol i). Y_i^T is obtained from the overall balanced stoichiometric growth equation developed using the EB method described in Chapter 4 by applying the following equation:

True yield, calculated from stoichiometric coefficients of balanced true growth equation

$$Y_i^{MAX} = \frac{\nu_{cell}}{\nu_i}\,(FW_{cell}) \qquad \textbf{Equation 5.34}$$

In Equation 5.34, ν_{cell} and ν_i are the stoichiometric coefficients of cell and species *i* from the balanced growth equation, respectively. Because the Carbon Flux to Fuel fraction fixes the ratio of fuel to cell produced, and because the CF_f is factored in when developing the balanced growth equation, the amount of substrate required for fuel synthesis as well as cell synthesis is inherently captured in the cell yield on substrate i.

The Steady-State, Continuous-Growth Substrate Balance

The substrate balance (Equation 5.29) can now be reformulated with expressions for the mass transfer rate (Equation 5.30) and specific substrate utilization rate (Equation 5.4), resulting in the following equation:

Substrate Mass balance

$$\frac{d}{dt}\left(C_{i,R}V\right) = Q_{in}\,C_{i,in} - Q_{out}\,C_{i,out} + \left[(k_L a)_i\left(C_i^* - C_{i,R}\right)\right]V - \frac{\mu^T X_R V}{Y_i^{MAX}} \qquad \textbf{Equation 5.35}$$

where $(k_L a)_i$ and C_i^*, are obtained using, respectively, Equation 5.33, Equation 5.31 and Equation 5.32, and Y_i^{MAX} is obtained from the application of the EB method described in Chapter 4.

For the continuous, steady state reactor system assumed in this work, similar assumptions as applied can be employed here ($X_R = X_{out}$; $C_{i,out} = C_{i,R} = C_i$; accumulation term $\frac{d}{dt}\left(C_{i,R}\,V\right) = 0$).

A simplification was made in that the volumetric flow of the inlet and outlet streams (Q_{in} and Q_{out}) were assumed to be equal. Note that Q_{in} did not contribute to either the final form of the cell mass balance or the fuel mass balance. Because the operational mode is a dead-end fermentation, where all the gas-phase substrates transferred into the liquid phase culture are converted into either cell mass, botryococcene fuel, or water (as can be seen from the overall balanced growth equation). In reality, due to the nature of the dead end fermentation, the volume of the liquid phase must increase with an increase in the mass at a constant density. Therefore, the inlet and outlet flow rates will not be identical; at low rates of net growth (under low rates of mass-transfer), the difference between Q_{in} and Q_{out} does becomes significant, which is explained by briefly examining the overall steady-state mass balance on the system; it is observed that at low μ^{NET} the effect of the sum of the substrate entering the system due to mass transfer will greatly affect Q_{in}:

$$0 = \rho(Q_{in} - Q_{out}) + V\left(\sum_i MTR_i\right) \quad \rightarrow \frac{Q_{in}}{V} = \frac{Q_{out}}{V} - \frac{\sum_i MTR_i}{\rho} = \mu^{NET} - \frac{\sum_i MTR_i}{\rho}$$

However, the only place where Q_{in} is used in these calculations is the inlet flow term in the substrate mass balance. Because it is assumed that the concentrations of the gas phase substrates in the inlet stream are the equilibrium concentrations of O_2 and CO_2 based on the composition of atmospheric air, the inlet substrate concentrations are very small. Therefore the magnitude of the rate of substrate supply due to the inlet stream ($Q_{in}\ C_{i,in}$ in Equation 5.35) is very small ($\ll 0.01\%$) compared to the rate of substrate supply due to mass transfer ($\left[(k_L a)_i\left(C_i^* - C_{i,R}\right)\right]V$). Even at very low net growth rates, the difference in the ultimate productivity calculation as a result of this simplification is <0.05% (even though the low growth rates force the real value of Q_{in} to be only 10% of the Q_{out} required to maintain the steady-state cell concentration. The value of this simplification is that without it Q_{in} is a function of the substrate concentrations in the reactor, and therefore another layer of iteration is required for the

complete convergence of the overall mass balance, which significantly increased the overall computational time for these iterative calculations.

Therefore, the substrate balance becomes:

Steady-state substrate mass balance

$$\frac{Q_{out}}{V}\left(C_{i,in} - C_i\right) + \left(k_L a\right)_i \left(C_i^* - C_i\right) = \frac{\mu^T}{Y_i^{MAX}} X \qquad \textbf{Equation 5.36}$$

Making the substitution provided by Equation 5.20 for Q_{out}/V, and then converting μ^{NET} to $\mu^T - b$, Equation 5.36 can now be solved for μ^T or μ^{NET}:

True mass-transfer limited growth rate

$$\mu^T = \frac{Y_i^{MAX}\left(k_L a\right)_i \left(C_i^* - C_i\right) - bX}{X - \left(C_{i,in} - C_i\right)Y_i^{MAX}} + b \qquad \textbf{Equation 5.37}$$

Net mass-transfer limited growth rate

$$\mu^{NET} = \mu^T - b = \frac{Y_i^{MAX}\left(k_L a\right)_i \left(C_i^* - C_i\right) - bX}{X - \left(C_{i,in} - C_i\right)Y_i^{MAX}} \qquad \textbf{Equation 5.38}$$

Finally, f_S can be calculated as a function of f_S^0, μ^{NET}, and μ^T using , which allows calculation of the balanced overall growth equation accounting for maintenance and mass transfer limited growth:

Overall stoichiometrically balanced growth equation based on net yields

$$\begin{aligned} R_{\text{OVERALL}} &= f_e R_{\text{ENERGY}} + f_s R_{\text{SYNTHESIS}} \\ &= f_e\left(r_{\text{ea}} - r_{\text{ed}}\right) + f_s\left(r_{\text{synth}} - r_{\text{ed}}\right) \end{aligned} \qquad \textbf{Equation 5.39}$$

Procedure for Calculating μ^T and Fuel Productivity

The procedure described below for the calculation of μ^T and fuel productivity (P_f) in this work is specific to the assumptions around the process system selected. Therefore, this procedure is only applicable to the continuous steady state reactor described as the assumed production system in this work. The algorithm outlined below required iterative calculations, which were performed using a Microsoft® Excel spreadsheet and Visual Basic-coded macros. The assumptions made in this work are listed in Table 5.2.

Table 5.2: List of Assumptions employed in making mass-transfer limited yield and productivity predictions			
Continuous Flow Reactor System at Steady State Gas Phase is completely mixed; composition is unchanging and known in terms of partial pressures Liquid Phase is completely mixed			
$C_{i,min}$ for each substrate (mol *i* / L)	H_2	4.60E-07	10% of K_i as reported in Siegel & Ollis, 1984. K_i is a Monod parameter that corresponds to the inverse of an organism's substrate affinity.
	O_2	3.70E-07	
	CO_2	5.23E-06	Calculated from C^*_{CO2} using the same ratio as $C_{O2,min}/C^*_{O2}$

Calculation of μ^T and μ^{NET}

1. First, the rate limiting substrate must be identified. This is done by assuming that the concentration of each substrate is at some very small minimum level ($C_{i,min}$), which will enable the largest driving force for mass transfer for each substrate. The values selected for $C_{i,min}$ in this work are listed in Table 5.2 above. Using $C_{i,min}$ in place of C_i in Equation 5.37 as well as:
    - values for C_i^* and $(k_La)_i$ calculated for each substrate by Equation 5.31, Equation 5.32, and Equation 5.33;
    - an assumed concentration of cell (X);
    - Y_i^T calculated from the overall true-yield balanced growth equation;

    the maximum possible true growth rate on each substrate species is calculated. If all of the calculated possible growth rates are greater than the maximum growth rate inherent to the species, then μ^T is considered to be μ^{MAX}.
2. The possible true growth rates based on the rate of mass transfer for each substrate (as calculated in Step 1) are compared, and the substrate providing the slowest rate of growth is considered to be rate limiting; the associated μ^T with this substrate is now considered

the correct μ^T. Therefore, the true concentration of C_i for the limiting substrate is now set to $C_{i,min}$; as the limiting substrate, the concentration will be at its minimum.

3. Updated substrate concentrations C_i are now calculated for the non-limiting substrates, using the following rearranged version of Equation 5.37 to solve for C_i:

Computing updated values for substrate concentrations C_i

$$C_i = \frac{(\mu^T - b)C_{i,in} + (k_L a)_i C_i^* - \frac{\mu^T}{y_i^{MAX}} X}{\mu^T - b + k_L a} \qquad \textbf{Equation 5.40}$$

The same values of C_i^*, Y_i^{MAX}, and $(k_La)_i$ used in Step 1, and the value of μ^T determined in Step 2 are employed in this step.

4. The newly calculated C_i for each substrate is now compared with the concentrations of C_i that were used in the microbial energetics calculations to obtain the true-yield balanced growth equation and Y_i^{MAX} used in Step 1 and Step 3. If the values match within a tolerance (set to 10% of $C_{i,min}$ for each species), then the calculations move on to Step 5. Otherwise, the updated values of C_i are used to re-calculate the true-yield balanced growth equation, Y_i^{MAX} is updated according, and the calculation sequence is repeated from step 3. This calculation sequence is iterated until the substrate concentrations C_i calculated at the end of the sequence match those used in the Microbial Energetics calculations within the specified tolerance.

5. Once the solution has converged, the value for μ^T is used to calculate μ^{NET} by Equation 5.5, and f_s is calculated by Equation 5.12. f_S is then used to calculate the overall balanced growth equation by Equation 5.39, and the net yields can be calculated from the stoichiometric coefficients of the growth equation.

Cell and Botryococcene Product Fuel Productivity Calculations

The calculation of BPF productivity (P_{BPF}) is accomplished by going back to Equation 5.25 the fuel balance in the continuous steady-state reactor assumption, repeated here for convenience:

Steady-state BPF mass balance

$$\frac{Q_{out}}{V} C_{BPF} = \mu^{NET} X \overline{F} \qquad \textbf{Equation 5.25}$$

The productivity of the product fuel in a continuous system is the dilution rate (Q_{out}/V) multiplied by the concentration of the product fuel in the system, which is the left hand side of Equation 5.25. Therefore P_f can be calculated using either expression in the following equation:

BPF Productivity Calculation

$$P_f = \mu^{NET} C_{BPF,R} = \mu^{NET} X_R \bar{F} \qquad \textbf{Equation 5.41}$$

Cell productivity is obtained by a similar procedure, this time starting with the steady-state cell mass balance Equation 5.19. The resulting expression for cell productivity is:

Cell Productivity Calculation

$$P_X = \mu^{NET} X_R \qquad \textbf{Equation 5.42}$$

Chapter 6

Results of the Energetic Analysis: Predicted Botryococcene Product Yields and Process Feasibility Assessment

In this chapter, the microbial energetics theory developed in Chapter 4 and the continuous bioreactor model developed in Chapter 5 are applied to predict the yields and productivities of botryococcene hydrocarbon ($C_{34}H_{58}$) production by both *Ralstonia eutropha* and *Rhodobacter capsulatus* growing chemolithoautotrophically. As described in Chapter 5, the system envisioned for the purpose of these calculations is a continuous, steady-state process, where a constant rate of cell mass and product fuel is removed; this system encompasses the assumptions previously described (Table 5.2). Various performance metrics were determined as a function of the mass transfer rate, gas phase composition, and metabolic carbon flux to fuel ratio (CF_{fuel}): yields of cell mass and botryococcene product fuel (BPF) on each gas-phase substrate (hydrogen, oxygen, and carbon dioxide), system productivities (L BPF / L process / day), and operating costs on both a BPF volume and BPF energy basis (feedstock costs and power input costs per L BPF and per MJ of energy captured in botryococcenes). The calculations were accomplished with the use of an Excel spreadsheet, coded to make iterative calculations using Visual Basic.

The first section of this chapter describes the approach towards analyzing this wide range of potential process conditions and assessing the effects of varying different parameters. The following four sections then describe the effects of the various scenarios on yields, productivities, and processing costs for the continuous bioreactor system. The final section of this chapter discusses alternative bioprocessing configurations that could produce improved productivities and yields.

Analysis Approach: Summary of Scenarios Examined, Parameters Varied, and Assumptions Challenged

Because there were many possible permutations of parameter values and assumptions that could be applied to analyze the yields and productivities possible for the Electrofuels production system, the approach to assessing the effect of all the factors was to first select a 'Base Case Scenario.' In this 'Base Case', realistic initial estimates of values for the parameters of CF_f (Carbon Flux to Fuel), gas phase composition, and k_La (oxygen mass transfer coefficient) were selected. The values of these parameters as well as the rationale for their selection are presented in Table 6.1. Within the Base Case, yields, productivities, and operating costs of the Electrofuels process were determined.

Table 6.1: Parameter Values Utilized in the Base Case.

CF_f = Carbon Flux to Fuel; P_{H2}, P_{O2}, P_{CO2} = partial pressure of each gas; k_La = the O_2 gas-liquid mass transfer coefficient

Parameter	Description	Value	Rationale
CF_f	Carbon Flux to Fuel: (mol C to fuel/ mol C utilized)	0.25	25% botryococcene product fuel was selected as an attainable extent to which metabolic flux could be directed to fuel production, based upon the observed oil weight fractions in the native host for production of botryococcenes, *Botryococcus braunii*
P_{H2}:P_{O2}:P_{CO2}	Gas Phase Composition (atm)	75:16:9	Composition selected so that rate of oxygen supply through mass-transfer O_2 is rate-limiting for growth. It was important in the base case for a composition that would not lead to O_2 toxicity to be selected. as long as O_2 is limiting, it cannot accumulate in the system to induce toxic effects.
$(k_La)_{O2}$	O_2 Mass Transfer Coefficient (hr^{-1})	250	A typical oxygen transfer coefficient in an aerated, stirred reactor (Ho, Baddour, and Stalker 1987)

Then, to examine the effect of each of these parameters on the calculated yields, productivities, and operating costs, one of each of the parameters listed in Table 6.2 was varied individually in one of five different scenarios; these scenarios are summarized in Table 6.2. One of the parameters not varied in this analysis was the dilution rate of the continuous process, which is based on the following rationale. In a steady-state, continuous bioreactor process, the dilution

rate of the process must match the net growth rate of the organism under the conditions of the system for the cell concentration in the process to remain constant (Equation 5.20). Because the substrate limiting the rate of growth is not provided in the liquid feed stream and is instead provided through gas-liquid mass transfer, the dilution rate of the system is not an independent variable in this system model. Rather the mass-transfer rate and the yield of the process sets the possible growth rate of the organism, which then fixes the dilution rate.

Table 6.2: Description of scenarios analyzed in this work for each *Rs. eutropha* and *Rb. capsulatus* making botryococcene hydrocarbon fuel

Scenario	Description (variation from the base case)
Base Case	Yields of Biomass and botryococcene product fuel are compared for each species in the base case, exploring the assumptions relating to the cellular efficiency and mass transfer limitations on growth as described in Table 6.4.
I	CF_{fuel} varied; Yields and Feedstock costs predicted according to several sub-cases were examined:
II	P_{H2} and P_{CO2} varied while P_{O2} held constant
III	P_{H2} and P_{O2} varied while P_{CO2} held constant
IV	k_La varied; productivities and total operating costs examined

A variety of other parameters of the model were held constant throughout all the scenarios, either because it was expected that their values would have a negligible impact on the resulting yield and productivity calculations (e.g. the concentration of the sulfur source in the inorganic medium) or because changing their values would result in unrealistic scenarios (i.e. changing the assumed composition/empirical formula of the biomass, except for the composition changes associated with increased botryococcene production). The rationale for the selection of values for the critical parameters of biomass composition, calculated innate cellular efficiency factor, and operating conditions (temperature, active cell concentration, and total gas-phase pressure) are detailed in Table 6.3.

Table 6.3: Parameters held constant in the Energetic Analysis

This table provides the species-specific values of cellular elemental composition, the calculated intrinsic cellular growth efficiency (ε_{calc}), and the operating conditions selected (active cell concentration, temperature, and total operating gas-phase pressure)

	Ralstonia eutropha		***Rhodobacter capsulatus***	
Parameter	**Value**	**Reference**	**Value**	**Reference**
Empirical Cell Formula (for Carbon, Nitrogen, Oxygen, and Hydrogen)	$C_{4.09}H_{7.13}O_{1.89}N_{0.76}$	(Ishizaki and Tanaka 1990)	$C_5H_{8.4}O_{2.35}N_{0.65}$	(Hoekema et al. 2006)
Phosphorus Content [(1)]	984 μmol P/g DW	(Curtis 1988)	same as *Rs. eutropha*	
Sulfur Content [(2)]	1.50% by mass	(Mandalam and Palsson 1998)	same as *Rs. eutropha*	
Empirical Cell Formula (Adjusted to contain Phosphorus and Sulfur)	$C_{4.09}H_{7.13}O_{1.89}N_{0.76}P_{0.097}S_{0.008}$		$C_5H_{8.4}O_{2.35}N_{0.65}P_{0.118}S_{0.01}$	
ε_{calc}, Calculated Innate Cellular Efficiency [(3)]	0.69	(Bongers 1970)	0.53	(Siefert and Pfennig 1979)
μ_{max}^{True}, intrinsic maximum possible growth rate: $\mu_{max}^{obs} + b$	0.465 hr^{-1}	Calc'd using data from Hoekema et al., 2006; Madigan & Gest, 1979	0.125 hr^{-1}	Calc'd using data from Bongers, 1970)
Cellular Maintenance Rate, b	0.045 hr^{-1}	Calc'd from Hoekema et al., 2006;	0.009 hr^{-1}	Bongers, 1970
Operating Temperature [(4)]	32°C	(Ishizaki and Tanaka 1990)	32°C	(Madigan and Gest 1979)
Operating Active Cell Concentration	10 g DW/L	n/a	10 g DW/L	n/a
Operating Total Gas-Phase Pressure	1 atm	n/a	1 atm	n/a
pH	7.0	n/a	7.0	n/a

[(1)] The phosphorus content of *Pseudomonas aeruginosa* was utilized as an approximate bacterial value, as values for *Rs. eutropha* and *Rb. capsulatus* could not be found

[(2)] The sulfur content for *Chlorella vulgaris* was utilized as an approximate content, as values for *Rs. eutropha* and *Rb. capsulatus* could not be found

[(3)] Calculated as per the method described in Chapter 4 using data from the references indicated in the table

[(4)] The operating temperature was selected as 32°C, as this is intermediate between the temperatures used in the cited references for each species

It was assumed that only ammonium (NH_4^+), and not ammonia (NH_3), was the nitrogen source able to be used for biomass synthesis. Therefore, the fraction of total ammonia-nitrogen present in the system as ammonium (NH_4^+) versus that present as ammonia (NH_3) was calculated using a simple model for the NH_4^+-NH_3 equilibrium as a function of temperature and pH (Bell et al. 2007). This calculation is detailed in Appendix F. The phosphorus and sulfur sources for biomass synthesis were assumed to be phosphate (PO_4^{3-}) and sulfate (SO_4^{2-}), respectively, and the concentrations available were assumed to be constant. The actual concentrations utilized in the calculations are reported in Appendix F and the values were obtained from the MR26 medium utilized to cultivate *Rhodobacter* species in the Curtis Lab (Appendix A.3). The intra-cellular concentrations of the cellular intermediate Acetyl-CoA, the metabolite Co-A, and the cellular electron carrier NADH were obtained from Thauer et al. 1977, and are also provided in Appendix F.

Even within the base case, where the parameters are held constant to the values in Table 6.1, the predicted yields of cell mass and botryococcene hydrocarbon on any of the main gas-phase substrates (hydrogen, oxygen, and carbon dioxide) are heavily reliant on several overarching assumptions. The first of these critical assumptions is the value selected for the efficiency of the cellular synthesis process (ε). The second of these assumptions is the decision of whether or not the cellular maintenance rate is to be included in the calculations. The third assumption is whether the kinetics of the system are assumed to be limited only by the intrinsic maximum growth rate of the organism, or limited instead by an external factor (such as the rate of mass transfer of a rate-limiting substrate). Each of these factors have been discussed previously in this work (Chapter 4 and Chapter 5), but they are revisited here to be discussed in the context of their interrelationships. Table 6.4 summarizes the permutations of these three assumptions, which have been layered in order to create four different assumption sets that range from the most 'optimistic' to the most 'realistic':

- The Thermodynamic Limit Assumption (TL)
- The Maximum Biological Limit (MBL)
- The Non-Limited Net-Yield Assumption (Y^{NET}-NL)
- The Mass-transfer Limited Net-Yield Assumption (Y^{NET}-MTL)

Each of these four assumption sets are discussed in further detail in the following sections.

Table 6.4: The permutations of assumptions on cellular efficiency, cellular maintenance, and growth rate examined in the Base Case Scenario.

ε_{calc} = cellular efficiency as calculated in Chapter 4; μ^T = true growth rate (growth rate possible if maintenance not accounted for); μ^{NET} = net growth rate, accounting for maintenance rate; b = maintenance rate

	Description	Value of ε	Maint. incl.?	Rate-Limiting Factor?	μ^{NET}	Notes
TL	Thermodynamic Limit; this case predicts yields as bounded only by the 1st Law of Thermodynamics	1.0	no	Intrinsic Max Growth Rate (μ_{max})	n/a	Net cellular growth rate can only be calculated if maintenance is accounted for
MBL	Maximum Biological Limit: This case predicts yields accounting for the 2nd law of thermodynamics and cellular inefficiency but in the absence of cellular maintenance.	ε_{calc} for species	no	Intrinsic Max Growth (μ_{max})	n/a	
Y^{NET}-NL	Net Yield, Non-Limited Scenario: This case predicts yields under non-limited growth conditions	ε_{calc} for species	yes	Intrinsic Max Growth (μ_{max})	$= \mu^{T}_{max} - b$	μ^{T}_{max} is the maximum true growth rate inherent to the organism
Y^{NET}-MTL	Net Yield under Mass-Transfer Limited conditions: This case predicts yields under mass-transfer limitations due to rate-limiting supply of one of the gas phase growth substrates	ε_{calc} for species	yes	Mass-Transfer Rate	$= \mu^{T}_{MTL} - b$	μ^{T}_{MTL} is the max true growth rate allowed by mass-transfer limitations in the system

As will be shown, the assumptions of Table 6.4 have a major impact on the outcome of the analysis. It is emphasized that these four assumption sets were evaluated independently of the variations on the values of the parameters presented in Table 6.1. Furthermore, because only the final assumption set (Y^{NET}-MTL) is considered to be realistic, all four assumption sets are only

evaluated within the Base Case Scenario. The purpose of evaluating all four of these assumption sets, including the ones considered unrealistic is to demonstrate the effect of the assumptions employed during model development have an enormous impact on the resulting analysis, particularly if mass transfer and rate-limitations are neglected.

The Thermodynamic Limit Assumption Set (TL)

As discussed previously in Chapter 4, the efficiency (ε) of the cell is bounded at the upper end by the 1st law of thermodynamics; the maximum amount of energy that can be captured into synthesizing biomass is that which is released by the energy-generating reaction (the oxidation of H_2 to H_2O). Therefore, the yields calculated using the cellular efficiency at the Thermodynamic Limit (TL; $\varepsilon_{TL} = 1.00$) represent the maximum yields allowed by thermodynamics under the assumption of 100% conversion of energy to useful work (growth or fuel synthesis). However, these TL yields are not attainable in practice and instead are significant overestimates of a system's potential because cellular processes are irreversible; for metabolism to proceed at a tangible rate, a Gibbs Free Energy gradient must exist in order to drive metabolism forward. This results in entropy generation and in the conversion of some energy to heat rather than useful work (von Stockar et al. 2006). Furthermore, real biological processes are not 100% efficient at capturing all the energy released from the energy generating reaction. Therefore, the TL assumption represents an absolute upper bound to expected yields that can only be approached and not attained. In theory, if the cellular efficiency could be improved through genetic engineering and synthetic biology approaches, for example by reducing 'leakiness' of the proton motive force, then the TL yield could be incrementally approached. However, because metabolism requires an energy gradient to proceed, the inherent irreversibility of biological processes will prevent an efficiency factor of $\varepsilon = 1.0$ of being attained in practice. If it were

possible to manipulate the efficiency of organisms to approach $\varepsilon = 1.0$, this would come at the cost of a reduced rate of synthesis of cell mass and botryococcene product.

The Maximum Biological Limit (MBL)

This scenario is produced by utilizing a realistic ε for the species, but neglecting cellular maintenance needs. It is noted here that this assumption set is not directly related to the 'maximum biological yield' discussed in the field of Metabolic Engineering. The ε were calculated (ε_{calc}) from growth data in the literature for each *Rs. eutropha* (Bongers 1970) and *Rb. capsulatus* (Madigan and Gest 1979). Utilizing a realistic cellular efficiency for each *Rs. eutropha* and *Rb. capsulatus*, calculated from literature data as described in Chapter 4, to determine growth and BPF synthesis yields resulted in lower yields than those calculated under the thermodynamic limit ($Y^{MAX} < Y^{TL}$). However, the Y^{MAX} yields are still overestimates because cellular maintenance requirements, energy diverted to essential, non-growth cellular processes, are not taken into account. This case represents the yields which could only be approached under non-limited growth conditions; under these conditions the rate of energy required for maintenance processes would be small compared to the rate of energy required for growth. Non-limited growth conditions could only be achieved in the absence of mass-transfer limitations in providing gas-phase substrates for biomass growth, which requires very low density systems with maximal power input for high gas mass-transfer rates. However, it is emphasized that these yields and productivities can only be approached and not actually be attained, because cellular maintenance has a finite value greater than zero, and must be accounted for in realistic yield predictions.

The Non-Limited, Net Yield Assumption (Y^{NET}-NL) and the Mass Transfer Limited, Net Yield Assumption (Y^{NET}-MTL)

The rate of cellular maintenance was incorporated via Equation 5.12 to adjust the maximum yields (f_S) to net yields (f_S^0) for both the Non-Limited (NL) and Mass-transfer Limited (MTL) scenarios, as described in detail in Chapters 4 and 5). This adjustment was made for two different 'true' (i.e. in the absence of maintenance) growth rates:

- $\mu_{\max}^{\mathrm{T}}$ is the maximum possible growth rate intrinsic to each *Rs. eutropha* and *Rb. capsulatus* (see Table 6.3); utilizing this growth rate results in a scenario that represents the net yields under non-limited growth conditions (Y^{NET}-NL) which are (in theory) attainable for low-density, high mass transfer systems in the absence of other limiting factors for growth. Therefore, in this scenario the maintenance would exert a minimum effect because cell growth rate is at a maximum.
- $\mu_{\mathrm{MTL}}^{\mathrm{T}}$ is the 'true' growth rate allowed by the rate of the mass-transfer-limited substrate, representing a scenario for net yields theoretically attainable under more realistic conditions in a scaled-up process, where mass-transfer limitation is highly likely (Y^{NET}-MTL). Under this scenario, maintenance has a larger effect on the yields because the growth rate μ is smaller. Because only the limitation imposed by mass transfer of the gas-phase substrates was considered (H_2, O_2, and CO_2), and other potential sources of limitation (inorganic nutrient limitation; quorum sensing) were not accounted for in this model, the yields and productivities stated under the Y^{NET}-MTL assumption should still be regarded as optimistic.

Effect of System Assumptions (TL, MBL, Y^{NET}-NL, Y^{NET}-MTL) on Results in the Base Case Scenario

Yield Predictions in the Base Case

The effect of the TL, MBL, Y^{NET}-NL, and Y^{NET}-MTL assumptions on the base case scenario for assessed for each *Ralstonia eutropha* and *Rhodobacter capsulatus.* Figure 6.1 presents the botryococcene product yields and cell growth yields on each gas-phase substrate: H_2 (a), O_2 (b), and CO_2 (c). The stoichiometry of the overall growth equations as predicted under the Y^{NET}-MTL assumption are presented in Table 6.5. The determination of the rate-limiting substrate and the yield effects are presented in Table 6.5. Energy yields (kJ BPF/kJ H_2) are presented in Table 6.7. The following characteristics of Figure 6.1 and the three tables are discussed and interpreted:

- Predicted yields decrease as a function of the system assumptions applied (TL > MBL > Y^{NET}-NL > Y^{NET}-MTL)
- Predicted yields by *Rs. eutropha* consistently exceed those for *Rb. capsulatus*
- Yields on CO_2 are independent of the system assumptions applied
- Energy yields (kJ captured into BPF/kJ H_2 oxidized) are low for the base case scenario

Predicted yields descrease as a function of the system assumptions applied (TL > MBL > Y^{NET}-NL > Y^{NET}-MTL)

For both *Rs. eutropha* and *Rb. capsulatus*, Figure 6.1 (a) and (b) show similar trends for yields on hydrogen and oxygen as a function of the assumption set applied: the yields are at a

Figure 6.1: BPF and Cell Yields calculated using Base Case parameters, as affected by the assumptions made on cellular efficiency, maintenance, and mass-transfer limitations

Yields on (a) Hydrogen, (b), Oxygen, (c) Carbon Dioxide. TL = assumption at the thermodynamic limit (cellular efficiency ε = 1.0); YMAX = assumption of calculated species-specific (ε <1), no maintenance demands; YNET-NL = maintenance demands accounted for, growth rates are under non-limited conditions; YNET-MTL = maintenance + mass transfer limited growth rates

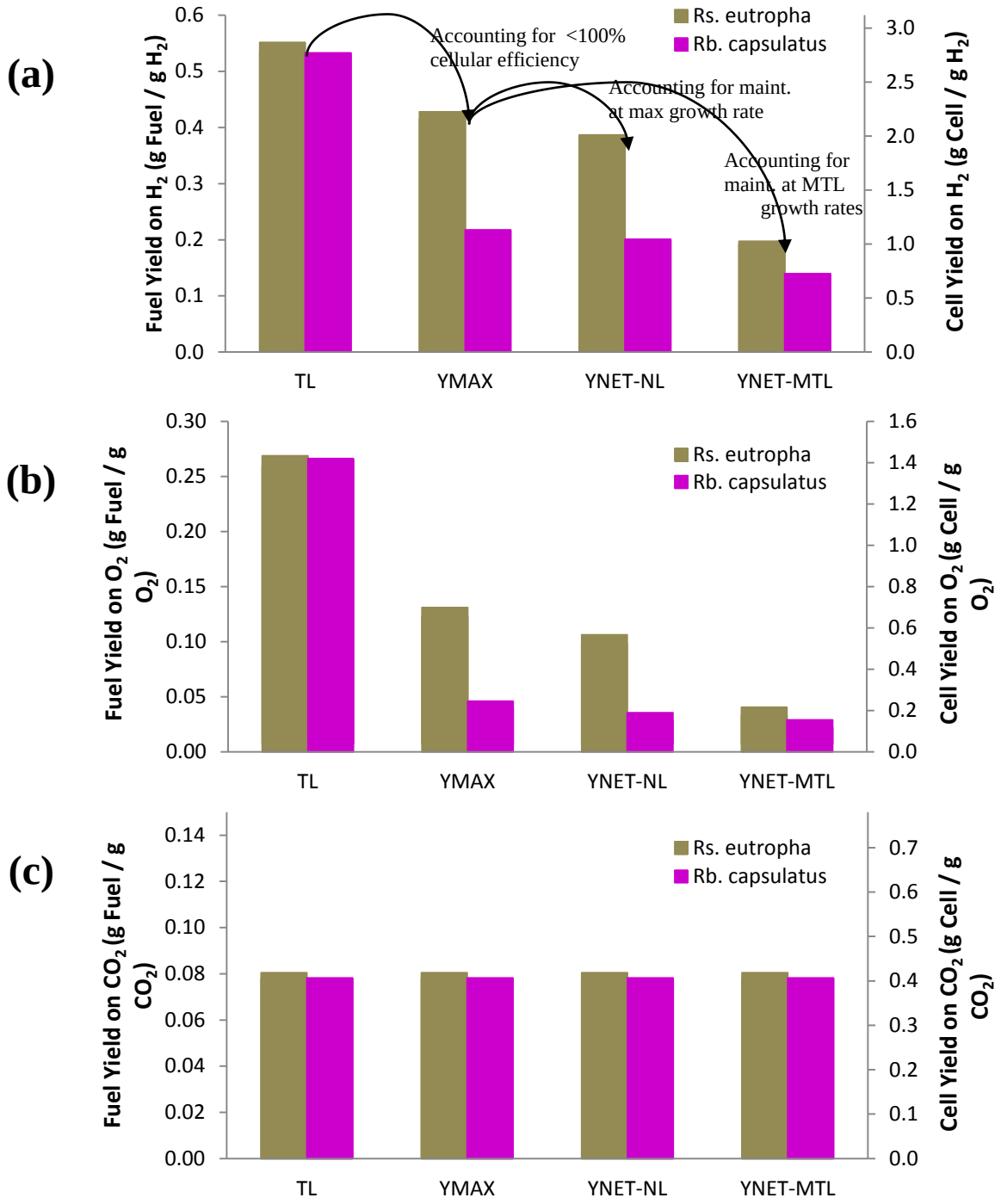

maximum at the thermodynamic limit, and subsequently decrease as more realistic conditions are applied to the calculations.

The drop in yield from the TL assumption to the MBL assumption occurs because it is no longer assumed that all the energy released in the energy generating reaction is available for cellular growth and other processes, and instead is lost as heat.

The rather small drop in yield from the MBL case to the Y^{NET}-NL case is due to the inclusion of cellular maintenance demands in the model assumptions, which siphon available energy away from net cell and fuel synthesis; meeting maintenance demands are a pre-requisite to the utilization of energy for cell and BPF synthesis. Because in the non-limited case, the organism is not limited by any substrate; therefore, the rate of energy available from the energy-generating reaction is sufficient to meet first the maintenance demands, but also to meet any and all demands for fuel and cell synthesis, all the way to the maximum true growth rate inherently possible for the organism ($\mu_{\mathrm{MAX}}^{\mathrm{T}}$). In using Equation 5.12 and Equation 5.16(reiterated here for convenience) to quantify the effect of the maintenance rate on the yield on electron donor, it can be easily seen that when the growth rate is at the organism's maximum ($\mu^{T} = \mu_{\mathrm{MAX}}^{\mathrm{T}}$), the relative contribution of the maintenance rate (b) in diminishing the growth and synthesis yields will be at a minimum.

Relationship of f_S to f_S^0 $$f_s = f_s^0 \left(\frac{\mu^{NET}}{\mu^{NET} + b} \right)$$ **Equation 5.12:**

Relationship between net yield and max/true yield on the ED $$Y_{X/H_2}^{NET} = Y_{X/H_2}^{MAX} \left(\frac{\mu^{NET}}{\mu^{NET} + b} \right)$$ **Equation 5.16:**

In other words, the rate of energy required per time for growth is large compared to the assumed-constant rate of energy required for maintenance; thus, the calculated reduction in yields on account of the maintenance demands under non-limited growth conditions is apparent, but not dramatic (compare the MBL and Y^{NET}-NL assumption sets in Figure 6.1). The drop in yields

Table 6.5: Overall Growth Equations determined using Base Case parameters and the Mass-Transfer Limited Assumption

The substrate species are shown in the top row, and the cell and botryococcene product fuel are in the second row. The chemical formula for cell mass is $C_{4.1}H_{7.1}O_{1.9}N_{0.76}P_{0.05}S_{0.01}$ and the chemical formula for botryococcene product fuel (BPF) is $C_{34}H_{58}$.

Ralstonia eutropha										
0.5000 $\mathbf{H_2}$	+	0.1837 $\mathbf{O_2}$	+	0.0562 $\mathbf{CO_2}$	+	0.0078 $\mathbf{NH_4^+}$	+	0.0010 $\mathbf{PO_4^{3-}}$	+	0.0001 $\mathbf{SO_4^{2-}}$
	$\longrightarrow$	0.0103 $\mathbf{C_{4.1}H_{7.1}O_{1.9}N_{0.76}P_{0.05}S_{0.01}}$	+	0.0004 $\mathbf{C_{34}H_{58}}$	+	0.4624 $\mathbf{H_2O}$	+	0.0047 $\mathbf{H^+}$		
Rhodobacter capsulatus										
0.5000 $\mathbf{H_2}$	+	0.2011 $\mathbf{O_2}$	+	0.0408 $\mathbf{CO_2}$	+	0.0040 $\mathbf{NH_4^+}$	+	0.0007 $\mathbf{PO_4^{3-}}$	+	0.0001 $\mathbf{SO_4^{2-}}$
	$\longrightarrow$	0.0061 $\mathbf{C_5H_{8.4}O_{2.35}N_{0.65}P_{0.05}S_{0.01}}$	+	0.0003 $\mathbf{C_{34}H_{58}}$	+	0.4727 $\mathbf{H_2O}$	+	0.0017 $\mathbf{H^+}$		

from the MBL assumption to the Y^{NET}-NL assumption is more significant for *Rs. eutropha* than for *Rb. capsulatus*, due to the larger maintenance rate of *Rs. eutropha* (see Table 6.6 for further clarification).

However, when the delivery rate of at least one of the substrates constrains the metabolic rate of the cell, the Mass-transfer Limited scenario results (Y_{NET}-MTL). This constraint could be the rate of energy-generation if the rate-limiting substrate is H_2 or O_2. In this case, less energy is available for growth and BPF synthesis after maintenance demands are satisfied, such that the maximum growth rate can no longer be maintained (recalling that the cell concentration for this system is being held constant). Conceptually, the effect is that, per unit time, a larger fraction of the available substrates are spent on the non-growth, non-synthesis cellular maintenance processes rather than growth and synthesis. This reduces the net yields on all substrates, an effect that is quantified by Equation 5.16 (for the electron donor) and Equation 5.12 (for all substrates). The reduced net growth rate results in an increase in the importance of *b*, and the net yields are diminished. If instead the rate constraint was due to a substrate not involved in energy generation (i.e. CO_2), the net growth rate of the organism would is still diminished because CO_2 supply is essential for growth and synthesis, and so a decrease in the net yields on H_2 is predicted by Equation 5.16 even though H_2 is not the substrate imposing the rate-constraint. Equation 5.12

also predicts a decrease in the yield on the electron acceptor O_2: the diminished f_S means a larger f_E, and so a higher proportion of electrons from H_2 will go to oxidizing O_2, increasing the demand for O_2 and decreasing the yield on O_2. Biologically, this can be explained by the following: much of the energy generated under these conditions cannot be used for cellular synthesis because the supply rate of CO_2 cannot 'keep up' with demand. Any excess energy will be dissipated, with the effect that the cell and BPF synthesis yields on the electron donor and electron acceptor still decrease.

Note that following this logic, it is expected that net yields on CO_2 will not decrease under mass-transfer limited conditions – all CO_2 taken up by the organism is used for cell or BPF synthesis, but is not utilized in maintenance demands. This expectation is confirmed by Figure 6.1, where the yields on CO_2 are independent of which assumption (TL, MBL, Y^{NET}-NL, Y^{NET}-MTL) is applied to construct the model.

In the base case scenario, the substrate which imposes the largest rate constraint is oxygen (see Table 6.6); this is established by comparing the available supply rates of each substrate, then using the maximum (true) yield of cell growth on each substrate to predict the possible true growth rate. As O_2 was the substrate that resulted in the slowest possible true growth rate, this is the rate-limiting substrate. In this base case scenario, the μ^T possible is only double the maintenance rate of *Rs. eutropha*, and triple the maintenance rate of *Rb. capsulatus*. Therefore, a very high proportion of the energy available from the oxidation of H_2 must be spent on non-growth, non-synthesis maintenance needs, and the portion of the energy left over for cell and BPF synthesis is small; thus model predicts significantly diminished yields in the base case. It is important to clarify that the absolute energy requirement to synthesize a gram of cell (on a mass basis) has not changed; rather, the diminished rate of energy supply under the MTL scenario means that a larger proportion of the substrates must be used to satisfy non-growth maintenance needs, resulting in the apparent (net) decrease in the yield. Therefore, the net yields predicted

Table 6.6: O_2 is the rate-limiting substrate due to mass transfer limitations in the Base Case scenario

This table shows the resulting true (μ^T) and net (μ^{NET}) growth rates calculated due to mass-transfer limitations for each gas-phase substrate. The mass-transfer rate of oxygen is much slower than either hydrogen or carbon dioxide, a result of low solubility and low partial pressure in the gas-phase, and the rate of O_2 results in the smallest predicted μ^T (highlighted in red). The large yield on oxygen is not sufficient to overcome its slow transfer rate, and it is the rate-limiting substrate for growth in the base case scenario. The resulting net growth rates and net yields due to this limitation are presented.

		Ralstonia eutropha			***Rhodobacter capsulatus***		
	Substrate *i*:	**H_2**	**O_2**	**CO_2**	**H_2**	**O_2**	**CO_2**
Max rate of mass transfer [1]	(mol i/L/hr)	0.249	0.045	0.545	0.249	0.045	0.545
Maximum (true) yield, $Y_{X/i}^{MAX}$	(g cell/g i)	2.128	0.595	0.419	1.090	0.195	0.406
Possible True Growth Rate μ^T [2]	h^{-1}	0.107	**0.087**	1.004	0.055	**0.028**	0.974
Maintenance rate, b	h^{-1}		0.045			0.009	
Net Growth Rate $\mu^{NET} = \mu^T - b$	h^{-1}		0.042			0.019	
Net Yield, $Y_{X/i}^{NET}$ [3]	(g cell/g i)	1.026	0.176	0.140	0.724	0.113	0.135

[1] For O_2 and H_2: Calculated assuming $C_{i,min}$ is 10% of K_i as reported by Siegel and Ollis, 1984. For CO_2: Calculated assuming the same ratio of $C_{i,min}/Ci^*$ for O_2.
[2] Calculated assuming the base case biomass concentration of 10 g cell/L.
[3] $Y_{X/i}^{NET}$ can be calculated for i=H_2 using EQUATION 5.16 and for i=O_2 and CO_2 by first constructing the stoichiometric net growth equation

under an assumption of mass-transfer limitation are lower than those predicted assuming a non-limited scenario, even though both assumptions account for the maintenance demands of the cell.

Due to the larger maintenance demands of *Rs. eutropha*, the magnitude of the difference between the net mass-transfer limited growth rate μ_{MTL}^{NET} and the true growth rate are more dramatic: μ_{MTL}^{NET} for *Rs. eutropha* is only about half of the μ_{MTL}^{T} possible; μ_{MTL}^{NET} for *Rb. capsulatus* is about 2/3 of μ_{MTL}^{T}, as shown above in Table 6.6. In summary, in the base case scenario, the large magnitude of the maintenance rate compared to the constrained growth rate results in a large portion of the energy available to the cell being spent on either maintenance (in the case of ED or EA limitation) or being dissipated because the rate of CO_2 fixation cannot supply carbon fast enough for synthesis (in the case of CO_2 limitation); the end result is that the utilization of H_2 and O_2 for non-growth processes results in diminished yields.

Predicted yields by Rs. eutropha consistently exceed those for Rb. capsulatus

Another characteristic of Figure 6.1 is discussed and described here: for all substrates and under each assumption, the yield of *Rs. eutropha* is higher than the yield of *Rb. capsulatus*. While the difference is slight under the TL assumption, where yields are the maximum allowable by thermodynamics, this difference becomes dramatically different as soon as the cellular inefficiency factor is included. Recalling the discussion on the requirement of Reversed Electron Transport for *Rb. capsulatus* (Chapter 3), this can be rationalized as follows. Simply summing the energy required for each step of cellular synthesis for each *Rs. eutropha* and *Rb. capsulatus* results in very similar values (36.3 kJ/electron equivalent (eeq) and 35.1 kJ/eeq under the base case conditions, respectively). The slightly lower mass yield for *Rb. capsulatus* occurs because this biomass is slightly more reduced than *Rs. eutropha,* therefore requiring in theory a larger number of electrons per mass of cell than does *Rs. eutropha*. Because *Rb. capsulatus* cannot directly transfer electrons from H_2 to NADH, the electrons must first enter the Electron Transport Chain (ETC). This results in a drop of the electron potential to the level of ubiquinone, which is lower than the potential required to reduce NAD^+. Therefore energy must be added in order to drive the reduction of NAD^+ to NADH at the expense of oxidation of ubiquinol. When the energy lost at each step is accounted for by the cellular inefficiency factor ε, the difference in energy requirements for cell synthesis becomes much more dramatic between the two organisms: 53.2 kJ/eeq for *Rs. eutropha* and 124.7 kJ/eeq for *Rb. capsulatus*. This increased energetic demand is a result of the larger magnitude of energy changes with the multi-step process of NADH production in *Rb. capsulatus* paired with this organism's lower calculated value for the cellular efficiency, and the ultimate result is the significantly lower predicted yields compared to *Rs. eutropha*.

Yields on CO_2 are independent of the system assumptions applied

The yields on carbon dioxide (Figure 6.1 c) are the same for all assumptions (TL, MBL, Y^{NET}-NL, Y^{NET}-MTL), and thus are independent of whether cellular efficiency, maintenance, or diminished growth rates is accounted for. The reason for this behavior is because the model assumes that carbon dioxide is only taken up for cellular synthesis, and it is taken up in stoichiometric proportion with the cellular composition. CO_2 is not at all involved in the energy generating reaction nor in the transfer of electrons from H_2 to NADH, and so it is decoupled from the energetics of the microbial metabolism. Therefore, the yields on carbon dioxide are only tied to the elemental composition of the cell mass and the fuel. This calculation thus provides an 'internal control' for this overall mass balance procedure.

Energy yields (kJ captured into BPF/kJ H_2 oxidized) are low for the base case scenario

From the yields of botryococcene product fuel (BPF) on hydrogen, an 'energy yield' can be calculated as the amount of energy captured into the product fuel from the original mass of hydrogen required to produce it (Equation 6.1).

$$\boldsymbol{Energy\ Yield} = \boldsymbol{Y_{fuel/H2}}\left(\frac{\boldsymbol{\Delta_C H_{fuel}^{HHV}}}{\boldsymbol{\Delta_C H_{H2}^{HHV}}}\right) \qquad \textbf{Equation 6.1}$$

High heating values for the enthalpies of combustion for each H_2 ($\Delta_C H_{H2}^{HHV}$ = -141.9 kJ/g H_2) and the product fuel ($\Delta_C H_{fuel}^{HHV}$ = -43.9 kJ/g $C_{34}H_{58}$) were utilized for this calculation. The energy yields are presented for the base case scenario in Table 6.7. Even in the thermodynamic limit, the energy yields for both organisms are less than 20%. A large portion of the electrons in H_2 end up reducing O_2 to H_2O in order to generate the energy for ATP production, which is required for the cell and fuel synthesis. Another large portion therefore of the energy in H_2 is incorporated into

Table 6.7: Energy Yields calculated for the Base Case Scenario as affected by assumptions on cellular efficiency, maintenance, and mass-transfer limitations

In the Base Case Scenario, all energy yields are very low, even using the assumption set of the thermodynamic limit. Under a more-likely mass-transfer limited system, the yields are prohibitively low for economic feasibility, prompting investigation into how the yields could be improved (the subject of later sections of this chapter). See Table 6.4 for a summary of the assumption sets employed. All the parameters for the base case as specified in Table 6.1 remain the same.

Assumption Set		Energy Yield	
		Rs. eutropha	*Rb. capsulatus*
Thermodynamic Limit	kJ fuel / kJ H_2	16.4%	16.3%
$\mathbf{Y^{MAX}}$		12.7%	6.7%
$\mathbf{Y^{NET,\ NL}}$		11.5%	6.2%
$\mathbf{Y^{NET,\ MTL}}$		5.9%	4.3%

cell mass rather than botryococcene product fuel. This provides motivation for investigating methods to increase the degree of incorporation of the hydrogen's energy into fuel rather than cell matter. Under the most realistic assumption of a mass-transfer limited system, the calculated energy yields are extremely low, showing that only 5.9% (*Rs. eutropha*) and 4.3% (*Rb. capsulatus*) of the energy of the hydrogen substrate is being captured into the fuel. In this case, the additional 'lost' energy compared to the thermodynamically limiting case can be accounted for in heat production and the demands of cellular maintenance processes.

Productivity Projections in the Base Case Scenario

With estimated yields and growth rates for the system, volumetric productivities, feedstock costs, and power costs can be determined; these metrics are key assessment parameters for the initial analysis of a process's economic feasibility. The mass balances developed in Chapter 5 for a steady-state, continuous-growth reactor system provided a means to calculate both cell (P_X) and BPF (P_{BPF}) productivities, which are conceptualized as the rates at which cell and

BPF are removed from the system. The expressions for P_X and P_{BPF} developed in Chapter 5 are shown below:

Cell Productivity Calculation

$$P_X = \mu^{NET} X_R \qquad \textbf{Equation 5.42}$$

BPF Productivity Calculation

$$P_f = \mu^{NET} C_{BPF,R} = \mu^{NET} X_R \bar{F} \qquad \textbf{Equation 5.41}$$

In the expressions above, X_R is the cell concentration (in g cell/L), $C_{BPF,R}$ is the BPF concentration in the reactor (g BPF/L), and $\bar{F}$ mass ratio of BPF produced to cell synthesized.

In calculating productivities for the non-rate-limited scenario (Y^{NET}-NL), $\mu^{NET} = \mu_{MAX}^{T} - b$, the net growth when the true growth is equal to the maximum intrinsic growth rate specific to each species. To calculate productivities for the scenario where mass-transfer limitation by substrate supply occurs (Y^{NET}-MTL), $\mu^{NET} = \mu_{MTL}^{T} - b$, where μ_{MTL}^{T} is the true growth rate possible as a function of the mass-transfer limitation; it is calculated by the rearranged substrate mass balance (Equation 5.37). Recall that μ^{NET} (and therefore D, the dilution rate of the system) are not set independently, but are set by the fixed cell density of the system, chosen to be 10 g cell/L. The mass-transfer limited growth rate (μ_{MTL}^{NET}) calculated in the Base Case is provided in Table 6.6 above for each *Rs. eutropha* and *Rb. capsulatus*.

Productivity is highly influenced by the assumed value of μ^{NET}; using the maximum net growth rate possible (μ_{MAX}^{NET}) is making an assumption of unlimited growth, which is only applicable for low-density systems with excellent mass-transfer rates, and is unrealistic for any scaled-up operation. Therefore, under the assumption of mass-transfer limited conditions, the net growth rate calculated to be possible for the rate-limiting substrate (μ_{MTL}^{NET}, per Equation 5.38) should be used for realistic productivity calculations.

To analyze the feasibility of this bioenergy production process, the calculated base case productivities for each cell mass and biofuel under the Mass-transfer Limited assumption, as well as the Non-Limited growth assumption for comparison, are presented Figure 6.2 below.

Figure 6.2: Fuel and Cell mass productivities for both species in the base-case scenario

The fuel (primary axis) and cell mass (secondary axis) productivities calculated from the mass-transfer limited assumption are compared with those predicted assuming a non-limited growth scenario. The difference in magnitude from the Y^{NET}-NL case to the Y^{NET}-MTL case results both from the diminished growth under mass-transfer limitation, as well as the diminished yields that result under restricted growth rates. The productivities associated with *Rs. eutropha* far exceed those predicted for *Rb. capsulatus* in the base case, mainly because of the difference in yields on oxygen between the species under the Base Case scenario conditions. The fuel productivities are much lower than the cell productivities (notice the axis scale) because the Carbon Flux to Fuel in the Base Case Scenario is only 25%.

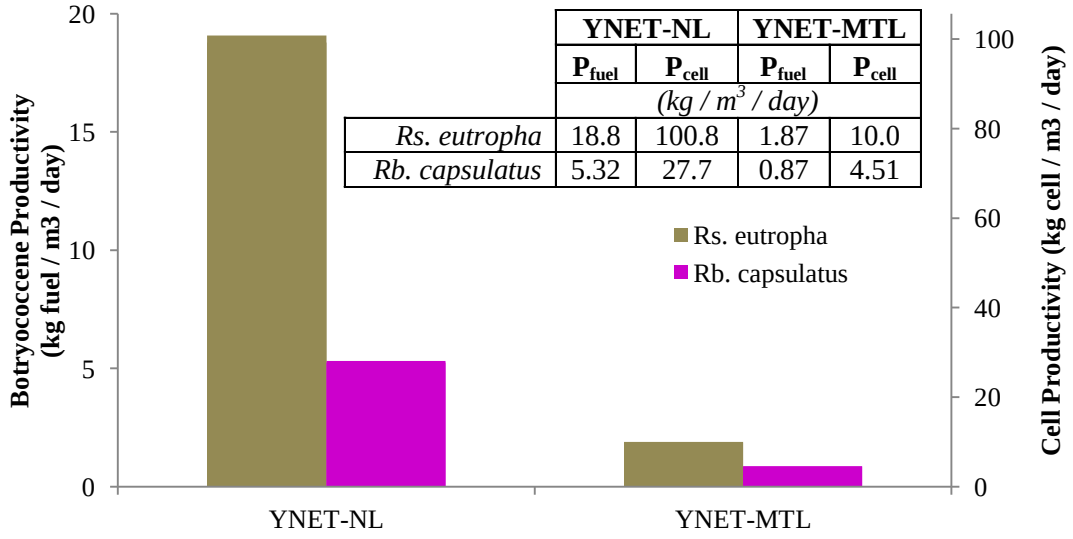

	YNET-NL		YNET-MTL	
	P_{fuel}	P_{cell}	P_{fuel}	P_{cell}
	(kg / m³ / day)			
Rs. eutropha	18.8	100.8	1.87	10.0
Rb. capsulatus	5.32	27.7	0.87	4.51

It is rapidly observed from Figure 6.2 that the volumetric productivities (ie. per liquid process volume) predicted under an assumption of non-limited growth are much higher than those predicted using a mass-transfer limited growth assumption. While it of course possible that the net growth rate of the organism can be increased by increasing mass transfer (and this is explored in later sections of this chapter), this demonstrates that the selection of appropriate assumptions in extrapolating process productivities is critical. It is also observed that the productivities of cell mass greatly exceed those for fuel, by examining the different scales of the y-axes in Figure 6.2 for the botryococcene product (primary) and the cell (secondary). This large difference is due to

the small CF_f (carbon flux to fuel ratio) selected for the base case scenario (CF_{fuel} = 25%); for a greater proportion of the fixed carbon to be driven towards fuel production rather than cell production, this ratio would need to be manipulated via metabolic engineering and/or processing conditions. The next scenario evaluated examines the effect of CF_{fuel} and discusses approaches toward increasing this value, including alternative processing scenarios.

The productivities of *Rs. eutropha* are also higher than those of *Rb. capsulatus*, as can be seen in Figure 6.2*;* this is true for both the assumption of a non-rate-limited system and in a mass-transfer limited system. In the non-limited scenario, the productivity of *Rs. eutropha* for both fuel and cell is 3.5x higher than *Rb. capsulatus*; while this margin decreases in the MTL scenario to only 2.2x, *Rs. eutropha* far out-performs *Rb. capsulatus* in the base case scenario. Note that the margin in *Rs. eutropha's* predicted yields over *Rb. capsulatus* in these scenarios is much lower, which raises the question of what the source of the enhanced difference in productivities is due to. This result is interesting in that the preliminary expectation was that under mass-transfer limited conditions, with identical mass-transfer rates of the limiting substrate, the growth rate of the two organisms should be very similar, resulting in similar cell growth productivities (as was observed in the case of *B. braunii* and *C. vulgaris* (Chapter 2). This hypothesis is based on the implicit presumption that the yields on the rate limiting substrate would also be very similar. As can be seen by Figure 6.1b, the yield of *Rs. eutropha* on oxygen (the rate limiting substrate) is larger than that of *Rb. capsulatus* by 50%. The mass-transfer rate of the rate-limiting substrate will set the maximum specific utilization rate of this substrate for each organism, and the net growth rate is inversely proportional to the yield at a fixed utilization rate. Thus, the reduced yield of *Rb. capsulatus* on O_2 results in a much greater difference in its growth rate.

The higher demand for O_2 of *Rb. capsulatus* in this base case scenario is a result of its less energetically efficient growth, requiring that more electrons from hydrogen be transferred to O_2 in the energy-generating reaction to generate sufficient energy for growth. It follows, then

that in the scenario of a carbon-dioxide limited situation, it would be expected that the growth rates (and therefore the productivities) of each species would converge. At very low rates of CO_2 mass transfer, this is true; the range of gas-phase concentrations where CO_2 is the limiting substrate is very narrow, and the yields in this range are explored further in a later section, under Scenario II.

Fuel Production Costs (Feedstocks and Power Costs) in the Base Case Scenario

The feedstock costs per kg of fuel were determined for the feedstocks of hydrogen, carbon dioxide, and a base to maintain pH by neutralizing the acid co-produced with biomass. Because oxygen is produced as a by-product of hydrogen production by water electrolysis, the cost of oxygen as a substrate was not considered as a separate input cost for the process. Instead its cost was considered to be accounted for in both the cost of hydrogen production and in the cost of the power necessary for mass transfer, which is considered separately and discussed below. For H_2 and CO_2, the cost per kg of fuel produced can be determined by Equation 6.2 below, using the yields determined from the overall balanced growth equation for each substrate:

$$\frac{\boldsymbol{Cost\ i}}{\boldsymbol{kg\ fuel}} = \left(\frac{\boldsymbol{Cost\ i}}{\boldsymbol{mass}}\right)\frac{\mathbf{1}}{\boldsymbol{Y_{fuel/i}^{NET}}} \qquad \textbf{Equation 6.2}$$

The cost of the substrates of CO_2 and H_2 selected for this analysis were discussed in Chapter 1, but are re-summarized here in Table 6.8 for convenience.

Table 6.8: Substrate pricing used to determine fuel production costs

H_2	\$3.82 / kg
CO_2	\$87 / ton
NaOH	\$0.0374 / mol
electricity	\$0.087 / kwh

The acid-neutralizing costs for a L of oil produced were determined by:

$$\frac{Cost\ OH^-}{kg\ fuel} = \left(\frac{\nu_{H+}}{\nu_{fuel}}\right)\left(\frac{1\ mol\ OH^-}{1\ mol\ H^+}\right)\left(\frac{Cost\ OH^-}{mol\ OH^-}\right)\frac{1}{(MW_{fuel})}\left(\frac{1000g}{kg}\right) \quad \textbf{Equation 6.3}$$

where ν_{H+} and ν_{fuel} are from the overall balanced growth equation, and it was assumed that to maintain pH at a steady state every H^+ produced would need to be countered by an OH^-. The base NaOH was selected as the acid-neutralizing agent, and was assumed to have a cost of \$0.405/lb NaOH (\$0.0374/mol OH^-), which was based upon the high-end 2008 pricing for a short-ton of NaOH (Chang 2008). The resulting costs for each feedstock per liter of fuel for the Mass-Transfer Limited scenario are presented in Table 6.9. As would be expected from the lower yields of *Rb. capsulatus* production on each substrate, the cost of each substrate per liter of fuel produced from *Rb. capsulatus* are higher than those for *Rs. eutropha* under the mass-transfer limited assumption. Because feedstock cost is directly related to the yield of fuel on the feedstock, price drops sharply with increased yields. The costs calculated using TL yields provide an absolute (and unattainable) minimum for botryococcene product fuel (BPF) produced in the system represented by the base case scenario, but the cost associated with the Y^{NET}-MTL assumption are more realistic.

In order to estimate the operating cost due to the power required for gas transfer, a relationship between the oxygen mass transfer coefficient (k_La) and power is required. The k_La selected for the base case, 250 hr^{-1}, is a mid-range value for an industrial scale stirred tank fermentor (Ho, Baddour, and Stalker 1987). A relationship between k_La (in s^{-1}) and the power per volume input (Watts/m^3) and superficial gas velocity (v_S, m/s) is provided by Van't Riet 1979:

$$k_La = 2.6 \times 10^{-2}\left(\frac{P}{V}\right)^{0.4} v_s^{0.5}\ (s^{-1}) \quad \textbf{Equation 6.4}$$

As this model was developed for pure water, only for up to volumes of 2.6 m^3, and only for power/per volume inputs ranging from 500-10,000 W/m^3, this model can only be relied on to give a ballpark estimate of the power requirement. Assuming a typical superficial gas flow rate of

Table 6.9: Operating Costs (Feedstock + Power) in the Base Case scenario

The costs for feedstocks (Hydrogen, Carbon Dioxide, and Acid neutralization) and mass-transfer costs are presented for both *Rs. eutropha* and *Rb. capsulatus* in the base case scenario; the costs projected under an assumption of Mass-Transfer Limitation are presented alongside those calculated for the TL assumption. As can be seen, the projected cost for fuel produced by *Rs. eutropha* is lower than *Rb. capsulatus*, but the costs are much greater under the assumption of mass transfer limitation than if the thermodynamic limit could be achieved.

	Y^{NET}-MTL		**Thermodynamic Limit**	
	Ralstonia eutropha	***Rhodobacter capsulatus***	***Ralstonia eutropha***	***Rhodobacter capsulatus***
	$ / kg fuel	$ / kg fuel	$ / kg fuel	$ / kg fuel
H_2	$19.97	$27.47	$7.15	$7.19
CO_2	$1.23	$1.23	$1.23	$1.23
Acid neutralization	$0.91	$0.45	$0.91	$0.45
Total Feedstock Cost	$22.11	$29.15	$9.28	$8.87
Cost of Power for Mass Transfer	$1.74	$3.75	----	----
Total Operating Cost of Fuel:	**$23.85**	**$32.90**	**----**	**----**

0.02 m/s, this model was utilized to predict the required power/volume input in the k_La range of 159-526 hr^{-1} (which correspond to the upper and lower limits of the power per volume input at the limits of the model). The determined value was then utilized in conjunction with the assumed price of electricity and the volumetric fuel productivity P_{BPF} to predict a cost of mass transfer per kg fuel (Equation 6.5).

$$\frac{\boldsymbol{Mass\ Transfer\ Cost}}{\boldsymbol{kg\ fuel}} = \frac{\left(\frac{\boldsymbol{P}}{\boldsymbol{V}}\left[\frac{\boldsymbol{W}}{\boldsymbol{m^3}}\right]\right)\left(\boldsymbol{Electricity\ Price}\left[\frac{\$}{\boldsymbol{kwh}}\right]\right)\left(\frac{\boldsymbol{3600\ s}}{\boldsymbol{hr}}\right)\left(\frac{\boldsymbol{24\ hr}}{\boldsymbol{day}}\right)}{\boldsymbol{P_{fuel}}\left[\frac{\boldsymbol{kg\ fuel}}{\boldsymbol{m^3 day}}\right]} \qquad \textbf{Equation 6.5}$$

The estimated cost of power for mass transfer is shown in Table 6.9 for the Y^{NET}-MTL assumption, and it is seen that the mass transfer costs alone are significant in the context of the public perception of what fuel 'should' cost: the mass transfer costs alone for *Rs. eutropha* and *Rb. capsulatus* would translate to $5.66/gallon and $12.20/gallon, respectively (calculated using the density of squalene as the approximate density of botryococcene oil (Eroglu and Melis 2009). However, it is also seen that these mass transfer costs make up but a small proportion of the

overall operating costs of the fuel, roughly 7% for *Rs. eutropha* and 11% for *Rb. capsulatus*, and that the overall operating costs make the base case scenario immediately economically infeasible. It should be noted that economies of scale will not apply here to reduce the operating costs associated with BPF production in the base case, as making more fuel requires proportionally more feedstock and more mass transfer. Economies of scale could potentially reduce capital-associated costs, but these are out of the scope of the current analysis and are not considered here. Mass transfer costs are not applicable for the assumption of thermodynamic maximum yields, because mass transfer limitations are not considered.

As can be seen from Table 6.9, it is the price of hydrogen which dominates the total operating costs for BPF production by aerobic hydrogen oxidation processes in the Base Case scenario, particularly under the Y^{NET}-MTL assumption, accounting for 84% of the minimal production costs and 90 to 94% of the feedstock costs. Under the thermodynamic limitation assumption, H_2 costs are greatly reduced; however, they still make up the majority of the feedstock costs. This effect is due to the extent of energy from H_2 oxidation going to cell growth and maintenance requirements and rather than botryococcene fuel synthesis. This behavior, coupled with the extremely low Energy Efficiency of the process in the Base Case Scenario motivates the investigation of the effect of a variety of parameters on the yields, productivities, and costs associated with BPF production. The next four sections are dedicated to assessing how the parameters of CF_{fuel}, the gas-phase composition, and oxygen mass transfer coefficient (k_La) could be adjusted to achieve better conversion of the energy of hydrogen oxidation to fuel.

Scenario I: Effect of CF_f (Carbon Flux to Fuel) on Yields, Productivities, and Costs

In scenario I, the ratio of carbon directed to fuel production (carbon flux to fuel, CF_f) versus cell production was varied from 0% to 95% and the effects on the yields, productivities,

and costs were examined. At the low range of this spectrum, the biomass produces only native cell material and no targeted product fuel species; only the cell yields are reported for the 0% case, as no biofuel is produced.

Scenario I Results: Yields of Cell, Botryococcene Product, and Energy as a Function of CF_{fuel}

To investigate the effects of the CF_f across all four basic assumption sets (TL, MBL, Y^{NET}-NL, Y^{NET}-MTL), yields of each cell, fuel, and energy on hydrogen were investigated over the CF_{fuel} range; the results are presented in Figure 6.3 (Cell Yield on H_2), Figure 6.4 (Oxygen Demand), and Figure 6.5 (BPF Fuel Yield on H_2). There are two key characteristics of these graphs that will be addressed in the discussion: first, under-mass transfer limited conditions both the net cell and the BPF yields go to zero at some high value of CF_{fuel}; in summary, the reason for this is an insufficient rate of energy availability to support maintenance needs, growth, and fuel synthesis needs at high rates of fuel production. The other notable characteristic is that a maximum yield of PBF is observed as a function of a CF_{fuel} under the assumption of mass-transfer limitation; increases in the metabolic flux to fuel synthesis only result in increases to fuel yields up to a certain CF_{fuel}.

Under mass-transfer limited conditions, both the net cell and BPF yields go to zero at some high value of CF_{fuel}

In Figure 6.3, the cell yields decrease with increasing CF_{fuel} for both *Rs. eutropha* and *Rb. capsulatus* across all basic assumptions sets, even though the cell concentration in the system is held constant at 10 g DW/L. This result is rather trivial because the carbon directed to cell

Figure 6.3: Effect of CF_f on Cell Yields on Hydrogen for *Rs. eutropha* and *Rb. capsulatus*

Cell yields on H_2 with cell concentration held constant at 10 g DW/ L for (a) *Rs. eutropha*, (b) *Rb. capsulatus*. The cell yields decrease as CF_f increases, as carbon flux is directed towards fuel production rather than cell production. The behavior of the yields with respect to the basic assumption for calculation (TL, Y^{MAX}, Y^{NET}-NL, or Y^{NET}-MTL) follows that observed in the base case. The point where cell yields in under MTL go to zero indicates where the maintenance demands (per cell mass) for the rate-limiting substrate (O_2) exceed the rate of mass transfer. CF_f = carbon flux to fuel; TL = thermodynamic limit; Y^{MAX} = maximum theoretical yields using the calculated cellular efficiency for each species (ε); Y^{NET}-NL = net yields under unlimited growth; Y^{NET}-MTL = net yields under mass transfer limited growth; ε = cellular efficiency factor

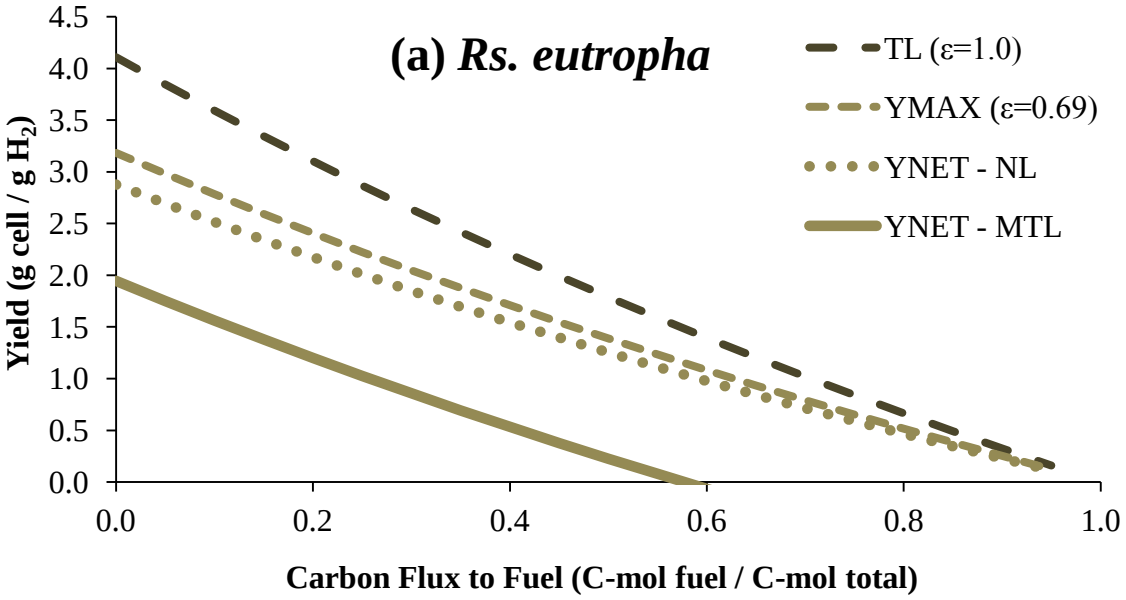

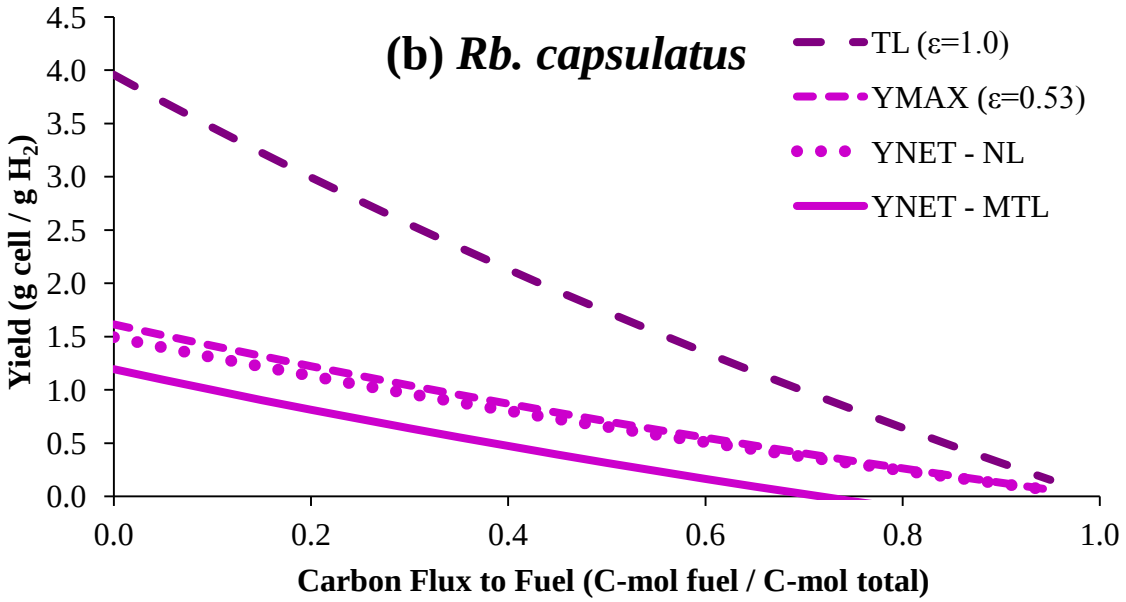

Figure 6.4: Effect of CF_{fuel} on Cellular Oxygen Demand

Under the mass transfer limited (MTL) assumption (solid lines), as CF_{fuel} increases the oxygen demand per gram cell ($1/Y_{X/O2}^{NET}$) increases due to both 1) increased energy demand for synthesis of high-energy content fuels and 2) diminished yields due to decreased growth rate and an increased effect of cellular maintenance. Where the O_2-demand curves for *Rs. eutropha* and *Rb. capsulatus* cross each under (for the Mass-Transfer Limited assumption) corresponds to the point at which *Rb. capsulatus* has a higher yield on O_2 due to its lower maintenance rate at low cell growth rates. By comparison, under an assumption of non-limited (NL) conditions (dashed lines), the rate of growth is assumed to be independent of mass-transfer limitations, and therefore under this assumption cellular maintenance does not become more significant at higher CF_{fuel}.

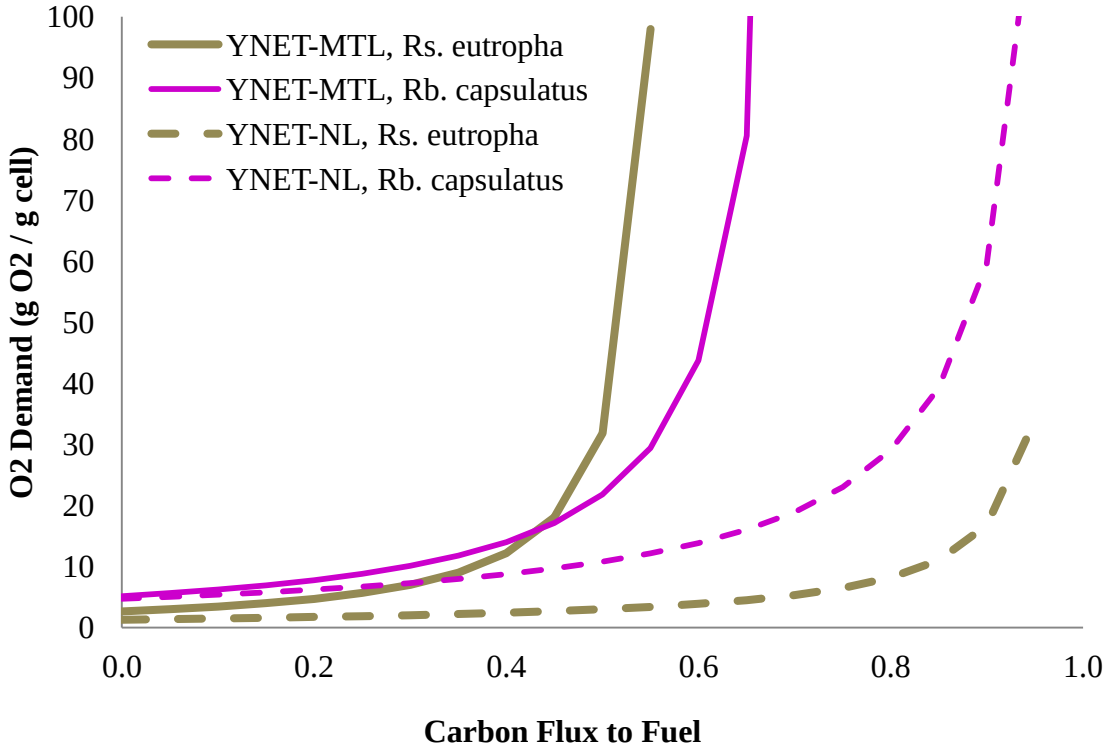

synthesis obviously decreases as the CF_f is increased. Examining the energetic assumptions indicated by separate curves on the graphs, the biomass yields decrease from their maximums under the TL assumption in a pattern similar to that observed in the Base Case analysis. Since the interpretation of the reasons for the decrease in yield from the TL assumption down to each more realistic assumption set is the same as previously discussed under the base case scenario, it will not be elaborated upon further here.

However, there is an immediate, obvious difference in Figure 6.3 between the yields predicted under the mass-transfer limited assumption (Y^{NET}-MTL) in that the cellular yields

become zero at a certain carbon flux to fuel ratio; for *Rs. eutropha*, this occurs at a CF_f of 0.58, and for *Rb. capsulatus* this occurs at a CF_f of 0.72. This should be interpreted as the inability of the chemostat system to reach a non-zero steady state above CF_{fuel} of 0.58 and 0.72 for the two species; this should not be interpreted as an increase in the amount of energy required to synthesize cell mass. This effect is explained as follows.

In this scenario, the assessment is of the effect of CF_{fuel} on the yields, and so all other independent variables (the cell concentration in the system, the rate of mass transfer, and the gas phase-composition are each held constant). Therefore, in this scenario the rate of substrate availability (and therefore energy availability) is also constant. This rate of energy availability must first be used to satisfy the rate of energy requirements; energy available after maintenance requirements are satisfied can be used for cell synthesis and BPF synthesis. As the CF_f increases while holding the active cell concentration constant at 10 g/L, the rate of synthesis of fuel increases. The high energy content of the fuel increases the energy demand of the cells when fuel synthesis increases, and so a higher proportion of the electrons from the electron donor must be sent to oxygen in the energy-generating reaction. This serves to increase the demand of O_2 per mass of cell synthesized, which clearly illustrated by Figure 6.4, which shows the increase in oxygen demand per mass cell as the carbon flux to fuel increases. Under the mass transfer limited assumption (Y^{NET}-MTL), at higher CF_f the oxygen demand increases (yield decreases) more rapidly with each incremental increase in CF_f due to the influence of both higher energetic demands for fuel synthesis as well as increased significance of the maintenance rate. Comparing the Y^{NET}-MTL assumption with the Y^{NET}-NL assumption in Figure 6.4, it is observed that the oxygen demand increases more dramatically at higher CF_f; this is due to the additional influence of decreasing growth rate under the mass transfer limited assumption. This serves to decreases in the yield of apparent cell growth on O_2 and in order for the cell concentration in the system to remain constant, the dilution rate of the system must therefore also decrease.

As this occurs, the maintenance rate of the cells becomes more and more significant with respect to the growth rate, and so the yields decrease even 'faster' than just due to the increased energetic demands (Equation 5.12). At some point, the rate of O_2 available in the system is only enough to supply the energy demands for maintenance, and the fuel synthesis; and at this point, net cell growth ceases, and there is no dilution rate able to maintain a steady-state cell density in the system. This suggests that to obtain high fuel synthesis relative to cell growth, a bioprocess system without a requirement of active cell growth for the continuous process is essential. Because the maintenance rate of *Rb. capsulatus* is smaller than *Rs. eutropha,* a positive value of the *Rb. capsulatus* net cell yields is possible to higher values of CF_{fuel} due to the comparatively smaller energy demands for maintenance.

In the analysis of Scenario I, it is presumed that the Carbon Flux to Fuel ratio is able to be fixed to a particular value by different genetic and metabolic engineering strategies; whether this is possible in practice remains to be demonstrated, and obviously it is not realistic to think of the CF_f being 'increased' in a single reactor run. However, this analysis is useful for conceptually determining a maximum CF_f possible for a given k_La and mass transfer rate before mass transfer becomes limiting.

In a mass-transfer-limited system, a maximum yield of PBF is observed as a function of a CF_{fuel}

The effect of CF_{fuel} on botryococcene product yields on H_2 is presented in Figure 6.5, and it clearly demonstrates the very different behavior observed under the assumption of mass-transfer limitation compared to assumptions of non-limited kinetics. For all assumptions except for mass-transfer limitation (TL, MBL, Y^{NET}-NL), the fuel yield on hydrogen increases

Figure 6.5: Effect of CF_f on Botryococcene Product Fuel Mass and Energy Yields on H_2 for *Rs. eutropha* and *Rb. capsulatus*

Fuel mass (primary axis) and energy (secondary axid) yields on H_2 with cell concentration held constant at 10 g DW/ L for (a) *Rs. eutropha*, (b) *Rb. capsulatus*. Fuel yields reach a maximum and then decline with further increases in CF_{fuel} under the mass-transfer limited assumption. (c) *Rs. eutropha* and *Rb capsulatus* yields under MTL assumption plotted on the same axis to show the CF_{fuel} where *Rb capsulatus* is predicted to have higher yields. TL = thermodynamic limit; Y^{MAX} = maximum theoretical yields using the calculated cellular efficiency for each species (ε); Y^{NET}-NL = net yields under unlimited growth; Y^{NET}-MTL = net yields under mass transfer limited growth; ε = cellular efficiency factor

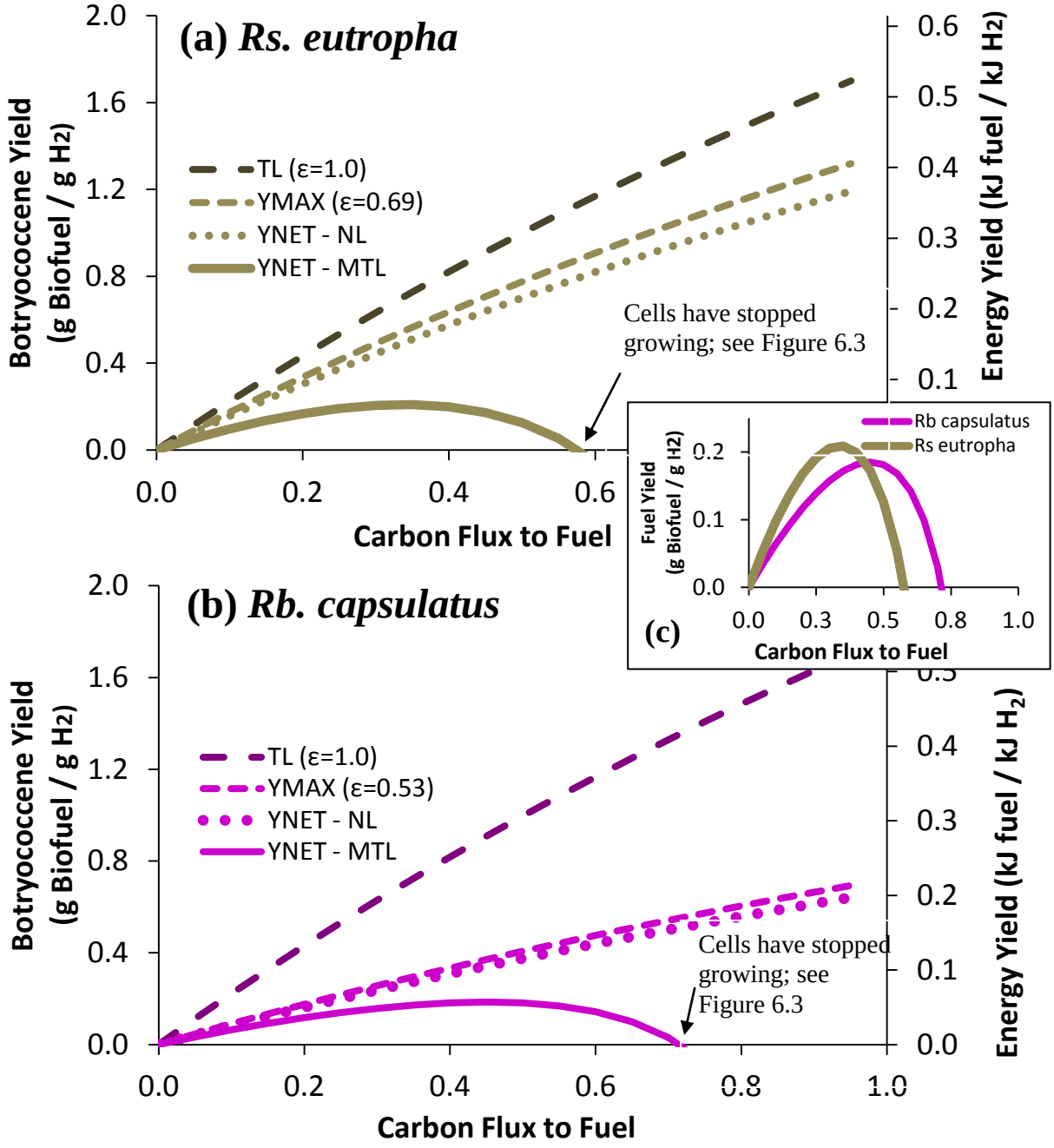

monotonically with increased CF_f; this effect makes sense because it is expected that as the carbon flux is driven towards fuel rather than cell mass, the fuel yields would increase. The situation for the mass transfer limited assumption (Y^{NET}-MTL) is more complicated and also more interesting. At low CF_{fuel} the incremental increase in carbon flux to fuel results in an increase in the net yield of fuel on hydrogen, as would be expected. However, the effect of increasing CF_{fuel} takes an energetic toll on the cells supporting the fuel production, and the cells require larger and larger amounts of substrate (cell mass yield decreases while fuel yield increases) to sustain the increased energetic demands for fuel synthesis simultaneously with growth. At some point, the increased yield on fuel due to increasing the carbon flux to fuel is negatively balanced out by the effect of decreasing yields on H_2 due to 1) the limited rate of oxygen supply and the diminishing growth rate of the cells, and 2) the increased energy demands for fuel synthesis. At an approximate CF_f of 0.35 for *Rs. eutropha* and 0.45 for *Rb. capsulatus*, the yield of botryococcene fuel on H_2 is at a maximum with respect to increasing CF_f. After this point, further increases in CF_{fuel} under the conditions of fixed gas mass transfer rate and fixed cell concentration in the reactor, the only way to force a higher proportion of the cellular metabolism towards fuel production is to decrease the overall growth rate of the cells. As the growth rate decreases, the proportion of energy consumed for cellular maintenance costs increases; therefore, the yields of fuel on hydrogen actually decrease with further increases to CF_f. When there is no energy 'left over' for cell synthesis after satisfying maintenance demands and fuel synthesis, the net growth rate of the cell (and therefore the fuel synthesis rate) are zero.

The results of this section can be summarized as follows:

Recalling Table 6.6, it is readily obvious that the maintenance energy requirements are on par (33-50% of) with the mass-transfer facilitated growth rates. Therefore, the forced shift of resources towards fuel synthesis (by fixing CF_{fuel}) causes the net rate of growth to drop to values lower than the rate of maintenance. The net result of this is that so much of the available energy

from hydrogen oxidation is being used for maintenance, such that what is left over for the production of fuel is only a small fraction of the H_2 and O_2 substrates consumed; therefore the BPF yield on H_2 and O_2 drops towards zero. There is a Catch-22 coupling that is an artifact of this model: oil cannot be synthesized without energy being available to have a net production of cell mass, but making more oil prevents net cell synthesis. This result clearly points to the utility of organisms with totally decoupled growth and botryococcene fuel biosynthesis, as well as a bioreactor operational configuration that allows the organisms to devote the majority of their energy to fuel production rather than cell growth (i.e. recycling of cells to the reactor after fuel separation, such that growth is not required). This alternative bioreactor is discussed in the final section of this chapter.

Under Mass-transfer Limited conditions, at low CF_f where higher cell growth rates are possible for a fixed cell concentration, the biomass and fuel yields on hydrogen and oxygen for *Rs. eutropha* exceed those for *Rb. capsulatus*, because *Rs. eutropha* has more energetically effective pathways and higher cellular efficiency. However, at higher CF_f, when mass-transfer limitations result in the cellular maintenance demands becoming dominant compared to the rate of growth demands, *Rb. capsulatus* actually has greater yields (above a CF_{fuel} of 0.43); this is shown explicitly in the inset (c) in Figure 6.5. It should be reiterated, however, the yields of *Rs. eutropha* still reach a slightly higher maximum than *Rb. capsulatus*. Figure 6.5 very clearly demonstrates that mass-transfer limitations can result in very different yields than those predicted without accounting for this effect.

Unlike the yields on hydrogen and oxygen substrates presented in Figure 6.3, Figure 6.4, and Figure 6.5, the biomass and fuel yields on carbon dioxide are nearly identical for both species, and the yields are identical between each energetic assumption (data not shown). The reason for the inflexibility of the carbon dioxide yields to the carbon flux to fuel is that carbon fixation does not directly participate in the energy generation reactions in the metabolism of *Rs.*

eutropha and *Rb. capsulatus*, and therefore the yield of cell growth and fuel production of CO_2 is linked only to the biomass elemental composition and fuel fraction as discussed previously in this chapter.

Scenario I Results: Productivities and Costs as a function of CF_{fuel}

The productivities and cost of hydrogen per liter of fuel were evaluated for carbon flux to fuel ratios ranging from 0 – 0.7, and are presented in Figure 6.6. Fuel productivity as a function of CF_{fuel} demonstrated similar behavior as the fuel yields, peaking at 2.04 kg fuel/m^3/day at a CF_{fuel} of 0.35 for *Rs. eutropha* and at 1.15 kg fuel/m^3/day at a CF_{fuel} of 0.45 for *Rb. capsulatus*. The costs of H_2 for each species reached their minimum values at the same CF_{fuel} at which the productivity was at a maximum. At high CF_{fuel}, the productivities of *Rb. capsulatus* again exceed those for *Rs. eutropha*; however, this occurs at a higher CF_{fuel} than for the yields (CF_{fuel} = 0.52, compared to 0.45), and the maximum productivities achieved by *Rs. eutropha* exceed the maximum productivity of *Rb. capsulatus* by nearly two-fold. This effect can be explained by the fact that the mass-transfer limited growth rates of *Rs. eutropha* always exceed those of *Rb. capsulatus* (except at very high CF_{fuel}) due to the significantly higher yields of *Rs. eutropha* on oxygen, the rate limiting substrate.

However, close-to-optimal productivities (maximum) and costs (minimum) could be attained at significantly lower CF_{fuel} than at the actual optimums; the CF_{fuel} required for 90% of the maximum productivity and 110% of the minimum cost are presented in Table 6.10. While for Scenario I, the overall productivities remain too low and the H_2 costs too high for economic feasibility, this analysis demonstrates an important point; productivities and costs within 10% of their optimum value can be attained at a much lower metabolic flux to fuel. This

Figure 6.6: Effect of CF_{fuel} on Volumetric Productivity and Hydrogen Costs

Productivity (primary axis) and hydrogen cost (secondary axis) under the Mass transfer limited assumption for each *Rs. eutropha* and *Rb. capsulatus*, for CF_{fuel} ranging from 0 to 0.7. The productivities and hydrogen costs reach a maximum and minimum, respectively, at the same CF_{fuel} for each species. At CF_{fuel} greater that this optimal point, the productivities rapidly decrease and the costs rapidly increase due to further decreases in growth rate from mass-transfer limitation of oxygen.

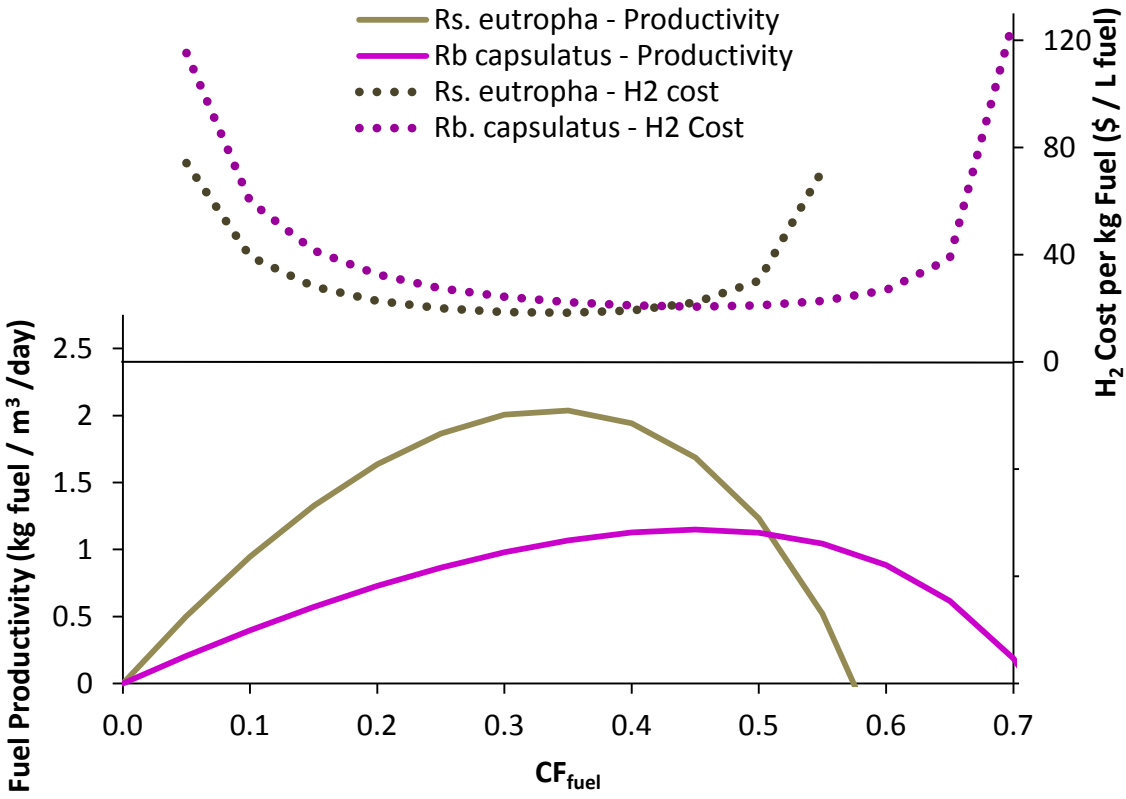

Table 6.10: Sub-optimal "90%" CF_{fuel}

This table presents the optimal carbon flux to fuel rations (CF_{fuel}) for maximum productivity and minimum hydrogen cost for each *Rs. eutropha* and *Rb capsulatus*, and also a lower CF_{fuel} for which 90% of the maximum productivity / 110% of the minimum cost could be attained. This table demonstrates the ability to achieve close to optimal performance at diminished CF_{fuel}, which could be important for technical feasibility.

	Rs. eutropha			***Rb. capsulatus***		
	CF_{fuel}	**Productivity** kg oil / m^3 / day	**Cost H_2 / L fuel** $ / kg fuel	**CF_{fuel}**	**Productivity** kg oil / m^3 / day	**Cost H_2 / L fuel** $ / kg fuel
Scenario I Optimum	0.35	2.04	$18.30	0.45	1.15	$20.65
"90%" Sub-optimum	0.25	1.87	$19.97	0.35	1.07	$22.23
% Reduction/ Increase from Optimum	-28.6%	-8.4%	+9.1%	-22.2%	-7.0%	+7.6%

is important because the ability to induce a host organism to preferentially shuttle carbon to production of BPF rather than cell mass, whether by environmental or by genetic engineering methods, is currently not established for these organism/fuel combinations. The ability to attain productivities and hydrogen costs within 10% of the optimum at a significantly reduced CF_{fuel} could be very beneficial in terms of technical feasibility.

Scenarios II and III: Effect of P_{H2}, P_{O2}, and P_{CO2} on Yields, Productivities, and Costs

As described in detail in Chapter 5, the gas-phase partial pressures of the three main substrates for growth, P_{H2}, P_{O2}, and P_{CO2} determine the equilibrium liquid phase concentrations, C_i^*, according to Henry's Law (Equation 5.31). The mass transfer rate of the substrate into the liquid phase is dependent upon C_i^* (Equation 5.30) and the current concentration of the substrate, C_i, as well as the substrate-specific mass transfer coefficient, $(k_La)_i$. Since production conditions will result in growth rates that are much slower than intrinsic growth rates, the mass-transfer rate of the rate-limiting substrate ultimately determines the rate of growth of the organism, which subsequently determines the net yield of the process. Therefore, the partial pressure of each H_2, O_2, and CO_2 determines which substrate is mass-transfer (rate) limiting, as well as the extent of the limitation. The behavior of mass-transfer limited yields and productivities resulting from varying gas-phase compositions can help inform ideal compositions for maximal productivity and minimal cost.

Furthermore, the liquid phase concentration of each substrate affects the energetics associated with both the energy generating reaction as well as the cell synthesis reactions (refer to Equation 4.7), the effect of which is quantitatively determined by estimating an activity for the substrate and using this to adjust the ΔG associated with the reaction at standard conditions. For the full range of compositions of the gasses, the effect of the activity on the energetics is

negligible except at very low partial pressures of each of the substrates. This effect of varying gas compositions can be studied independently of the mass-transfer effects by examining the yields predicted by the non-limited growth assumption (Y^{NET}-NL) and comparing them with the yields predicted by the mass-transfer limited assumption (Y^{NET}-MTL).

In this model, it was assumed that H_2, O_2, and CO_2 are the sole gasses in the mix. In reality, water vapor will make up some portion of this gas mixture as well, but in this model it is assumed to be small and additive to the pressures of the substrate gasses such that the partial pressures of the substrates is unchanged by water vapor presence. Furthermore, it was assumed that the sum of the gasses always totals 1.0 atmosphere. Increasing the total reactor pressure would increase the partial pressure of each substrate gas, increasing the driving force for the oxidation of H_2 to H_2O and therefore the free energy available from this reaction, and subsequently the process yields. However, running a reactor system containing an explosive gas mix (H_2 and O_2) at elevated pressures is a considerable safety risk, and therefore for this model it was assumed that the reactor system would remain at atmospheric conditions.

Scenario II Results: Yields as a function of P_{H2} and P_{CO2} while holding P_{O2} Constant

For scenario II, P_{O2} was held constant at 0.16atm, and the pressure of P_{H2} was varied from 10^{-7} atm. to 0.8363 atm (*Rs. eutropha*) or 0.8392 (*Rb. capsulatus*). P_{CO2} was allowed to 'float' such that the total pressure of H_2, O_2, and CO_2 remained at 1.000 atm. These values were chosen in order to create both very low H_2 compositions as well as very low (<0.005 atm) CO_2 compositions; this enabled an examination of the effect of very low gas concentrations on the yields. In the mass transfer limited assumption, CO_2 only becomes the rate-limiting substrate at very low partial pressures ($\ll$ 1 atm), and therefore the most dramatic changes in yield with respect to the change in P_{H2} occurs at a P_{H2} above 0.83. The net yields calculated each under the

Figure 6.7: Effect of Hydrogen/Carbon Dioxide Partial Pressure on Yields of BPF and Cell on Hydrogen

Botryococcene product yields (primary axis) and Cell yields (secondary axis) are shown for (a) *Rs. eutropha* and (b) *Rb. capsulatus*. The yields predicted under the assumption of Mass Transfer Limited conditions (Y^{NET}-MTL) are much more sensitive to the H_2 / CO_2 partial pressures than those predicted under a non-limited growth assumption (Y^{NET}-NL). The transitions of the rate-rate-limiting substrate from H_2 to O_2 to CO_2 are marked.

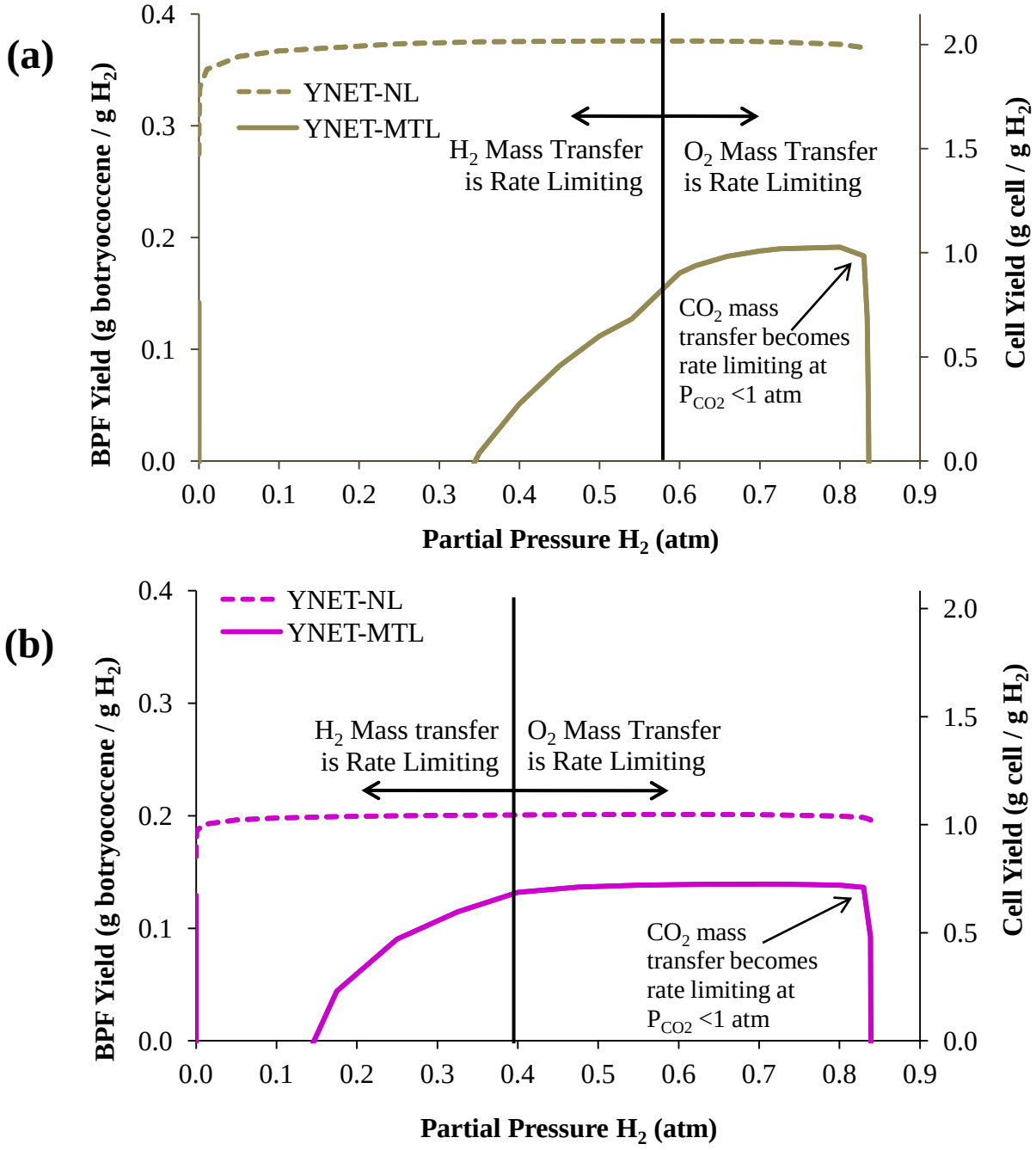

mass-transfer limited assumption (Y^{NET}-MTL) and the non-limited assumption (Y^{NET}-NL) are presented as a function of the P_{H2} in Figure 6.7 (a) for *Rs. eutropha* and in Figure 6.7 (b) for *Rb. capsulatus*.

Accounting for mass transfer results in significantly lower yields than would otherwise be expected since the rate of substrate availability via mass transfer is substantially limiting for the base case ($k_La = 250\ hr^{-1}$). This results in an increase in the proportion of metabolic energy spent on maintenance (Figure 6.7 (a) and (b)), leading to decreased yields on H_2 for the full range of gas-phase compositions. Furthermore, when the P_{H2} is below 0.35 atm (for *Rs. eutropha*) and below 0.15 atm (for *Rb. capsulatus*), the rate of energy generation possible due to the rate of H_2 supply is insufficient to even satisfy the demands of cellular maintenance, and there is no net cell or fuel synthesis possible. Under an assumption of <u>non</u>-limited growth (Y^{NET}-NL), the predicted yields are significantly higher than for Y^{NET}-MTL assumption because the proportion of metabolic energy spent on non-growth maintenance is smaller and relatively constant. Furthermore, under an assumption of non-limited growth, the yields appear largely independent of the P_{H2} except at very low concentrations of both H_2 and CO_2; this behavior is occurs because the metabolic reactions (hydrogen oxidation and carbon fixation) become less thermodynamically favorable when the substrate activity is very low (Equation 4.7).

Thus, the introduction of mass transfer limitations results in the prediction of gas phase composition where growth and oil production are not possible. Noting that the base case has a fixed cell density of 10 gDW/L, if the rate of supply of H_2 or CO_2 are too low to support growth and maintenance, then the yield becomes zero since the mass and energy balances cannot be satisfied. As is to be expected, the yields of *Rs. eutropha* on H_2 under the assumption of non-limitation are higher than *Rb. capsulatus* for the entire range of P_{H2} examined due to more efficient capture of energy by *R.s. eutropha*. Under the mass-transfer limited assumption, the yields are very sensitive to P_{H2} when H_2 is limiting; increasing the P_{H2} in this regime results in

large increases to the rate of H_2 able to be provided to the organism above the maintenance requirements.

It should be noted that under the mass transfer limited assumption, the yield of *Rb. capsulatus* exceeds *Rs. eutropha* in the range of P_{H2} from 0.15atm up to approximately 0.60 atm. This is because at low P_{H2} (less than 0.34 atm) the rate of hydrogen supply would not be sufficient to overcome the rate of energy demand for cellular maintenance, and allow growth of *Rs. eutropha*. Comparatively, a P_{H2} greater than 0.15 atm is sufficient to provide energy at a rate sufficient to satisfy maintenance needs and allow growth of *Rb. capsulatus*. This is because the e maintenance rate of *Rb. capsulatus* is smaller than *Rs. eutropha* (Table 6.3), allowing *Rb. capsulatus* to grow at lower rates of hydrogen supply (i.e. lower P_{H2}), even though the cell synthesis pathways are more significantly energy demanding.

At high P_{H2}, it can be seen that the mass-transfer-limited yields for each *Rs. eutropha* and *Rb. capsulatus* drop off sharply at P_{H2} of greater than approximately 0.83 atm. This H_2 partial pressure corresponds to a CO_2 partial pressure of 0.01 atm (recalling that P_{O2} is held constant at 0.16atm in this case). Therefore, at $P_{CO2} < 0.01$atm, CO_2 becomes the rate-limiting substrate to growth, as its supply is not sufficient to supply carbon to cell synthesis pathways at a rate commensurate with the rate of energy supply. Under these reduced growth rates, maintenance demands become large proportional to the rate of energy demand for growth and synthesis. Therefore, there is no net cell or fuel synthesis possible as P_{CO2} approaches 0 atm. CO_2 is only limiting for a very narrow range of P_{CO2} because CO_2 is not involved in the energy generating reactions of the metabolism of these species and also because of its elevated solubility in water (relative to H_2 and O_2).

Between the extremes of very low P_{H2}, where H_2 is limiting, and very high P_{H2}, where CO_2 is limiting (at a constant P_{O2}), for each species there is a transition from hydrogen mass transfer limitation over to oxygen mass transfer limitation. For P_{H2} less than this transition point,

the yields on H_2 are sensitive to the P_{H2}, but once this transition point is reached, yields are fairly insensitive to increases in P_{H2}. When oxygen mass transfer is limiting, energy generating reactions are limited by O_2 rather than H_2 and so overall growth rate remains limited, with the maintenance still siphoning a significant proportion of the energy supplied to the organism.

Scenario III: Effect on Net Yields, Varying P_{O2} and P_{H2} while holding P_{CO2} Constant

For scenario III, P_{CO2} was held constant at 0.09atm, and the pressure of P_{O2} was varied from 0.05 atm. to 0.3 atm; P_{H2} was allowed to 'float' such that the total pressure of H_2, O_2, and CO_2 remained at 1.000 atm. The Net yields calculated each under the mass-transfer limited assumption (Y^{NET}-MTL) and the non-limited assumption (Y^{NET}-NL) are presented as a function of the PO_2 in Figure 6.8 (a) for *Rs. eutropha* and in Figure 6.8 (b) for *Rb. capsulatus*.

Below a P_{O2} of 0.08 atm. for *Rs. eutropha* and of 0.055 atm for *Rb. capsulatus*, the rate of energy generation was not sufficient to overcome the maintenance rates of the organisms. P_{O2} above 0.30 atm were not examined because high oxygen concentrations can be inhibiting to both *Rs. eutropha* and *Rb. capsulatus*, and so examining cases of higher oxygen partial pressure is not relevant to a realistic growth scenario. Literature reports of oxygen inhibition to *Rs. eutropha* state that the threshold for oxygen inhibition is strain dependent, ranging from 4-20% O_2 in the gas-phase atmosphere (Siegel and Ollis 1984; Bowien and Schlegel 1981). However, organisms experience the liquid-phase O_2 concentration as the factor ultimately inducing inhibition, not the gas phase composition. Therefore, the exact onset of oxygen inhibition for the two species is challenging to interpret from the data; because oxygen is fed from the gas phase along with H_2, the working concentration of oxygen in the liquid phase will be entirely dependent upon both the overall rate of mass transfer, as well as the rate of hydrogen transfer; the former affects the

Figure 6.8: Effect of Oxygen/Hydrogen Partial Pressure on Yields of BPF and Cell on Hydrogen

Botryococcene product fuel yields (primary axis) and Cell yields (secondary axis) are shown for (a) *Rs. eutropha* and (b) *Rb. capsulatus*. The yields predicted under the assumption of Mass Transfer Limited conditions (Y^{NET}-MTL) are much more sensitive to the O_2 / H_2 partial pressures than those predicted under a non-limited growth assumption (Y^{NET}-NL). The transition from oxygen limitation to hydrogen limitation by mass transfer is marked.

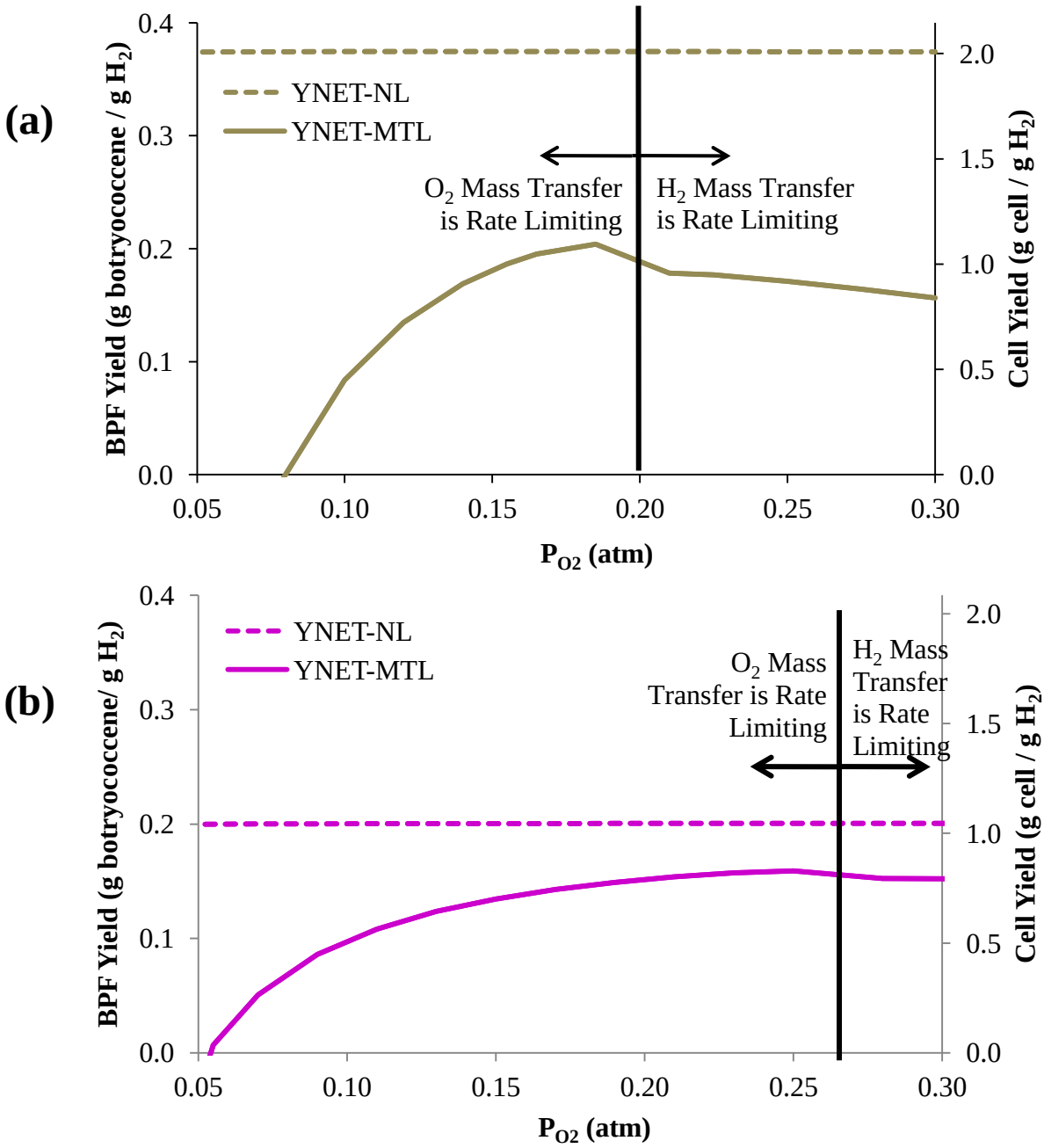

replenishment of O_2 in the liquid phase as it is consumed, the latter affects the rate at which the organism is able to utilize the O_2. A number of experiments, where the partial pressures of each hydrogen, oxygen, and CO_2 in the gas phase are carefully controlled and their liquid phase concentrations monitored, would be required in order to conclusively deduce the limits of oxygen limitation. Contrary to the scenario where P_{H2} is the dependent variable, the minimum predicted P_{O2} necessary to allow growth is very similar between the two species, at approximately 0.08 atm for *Rs. eutropha* and0.055 atm for *Rb. capsulatus*. The reason for this difference in behavior, considering that *Rs. eutropha* is still subject to a higher maintenance rate than *Rb. capsulatus* and should therefore require a higher rate of energy supply in order to commence growth, is not immediately clear.

Analogous to the effect of P_{H2}, the assumption of non-limited growth (Y^{NET}-NL), the predicted yields that are significantly higher than for Y^{NET}-MTL due to the diminished growth rate under the mass-transfer limited scenario Figure 6.8(a) and (b),. Furthermore, the the non-mass transfer limited yields appear largely independent of the P_{O2}; this behavior is solely caused by the effect of low concentration on the energetics of H_2 oxidation. As is to be expected, the yields of *Rs. eutropha* on H_2 under the assumption of non-limitation are higher than *Rb. capsulatus* for the entire range of P_{O2} examined.

According to the model, the oxygen ceases to be the rate-limiting substrate for growth at oxygen partial pressures greater than 0.19 atm (*Rs. eutropha*) and 0.27 atm (*Rb. capsulatus*), and at higher O_2 partial pressures the hydrogen becomes the rate-limiting growth substrate. Because this model did not account for the effect of oxygen inhibition on the growth of the organisms, this transition point is likely not entirely realistic, and the inhibition effects would need to be elucidated and incorporated into the model to better determine the point of oxygen inhibition. Regardless of accounting for inhibition, the results suggest that *Rb. capsulatus* is more likely to

experience oxygen inhibition in the base case scenario; its higher yield on O_2 means that less O_2 will be required for consumption, resulting in a lower threshold P_{O2} would become inhibitory.

Effect of simultaneously varying P_{H2}, P_{O2}, and P_{CO2} on Net Mass-Transfer Limited Productivities and Costs

Because the goal of this analysis was to determine the processing characteristics required to create an economically feasible biofuels process, the effect of varying gas phase composition on the productivities and costs associated with the process is of interest. Varying only two of the three gas phase compositions at once allows only a limited view of where an optimal gas-phase composition for maximum productivities would occur. Therefore and additional analysis was undertaken where all three gas phase compositions were allowed to vary. P_{H2} and P_{CO2} were varied as the independent variables and P_{O2} was allowed to 'float' to ensure that the sum of the three partial pressures always totaled one atmosphere. The results of this analysis for each *Rs. eutropha* and *Rb. capsulatus* are shown in Figure 6.9 (a) and (b) respectively.

The optimal gas phase compositions (P_{H2}:P_{O2}:P_{CO2}) resulting in calculated maximums for botryococcene product fuel productivity (under the assumption of mass-transfer limited conditions and a k_La of 250 hr^{-1}) were found to be 0.77 : 0.215 : 0.015 atm for *Rs. eutropha*, and 0.69 : 0.285 : 0.025 atm for *Rb. capsulatus*. The behavior of productivity as a function of gas phase compositions is qualitatively similar for both species: the point of maximum productivity occurs at very low carbon dioxide partial pressures and at the transition between surfaces defining growth-limitation by H_2 and O_2. Below the optimum, productivity drops off extremely rapidly with decreasing P_{CO2}. For each species, the range of compositions where H_2 is limiting is the largest, and the productivity is least sensitive to H_2 composition moving away from the optimum. For *Rs. eutropha*, the range of compositions where O_2 is limiting is much smaller than those for

Figure 6.9: Botryococcene fuel productivity under mass-transfer limited conditions as a function of varying P_{H2}, P_{O2}, and P_{CO2}.

For each **(a)** *Rs. eutropha* **(b)** *Rb. capsulatus*, the fuel productivity is graphed on the z-axis versus varying P_{H2} and P_{CO2}, with P_{O2} allowed to float so that total pressure of the gasses sums to 1 atm. The faces of the surface function corresponding growth limitation by each H_2, O_2, and CO_2 are indicated. Other conditions are as specified for the Base Case Scenario.
P_{H2} = partial pressure of H_2 in atm; P_{O2} = partial pressure of O_2 in atm; P_{CO2} = partial pressure of CO_2 in atm.

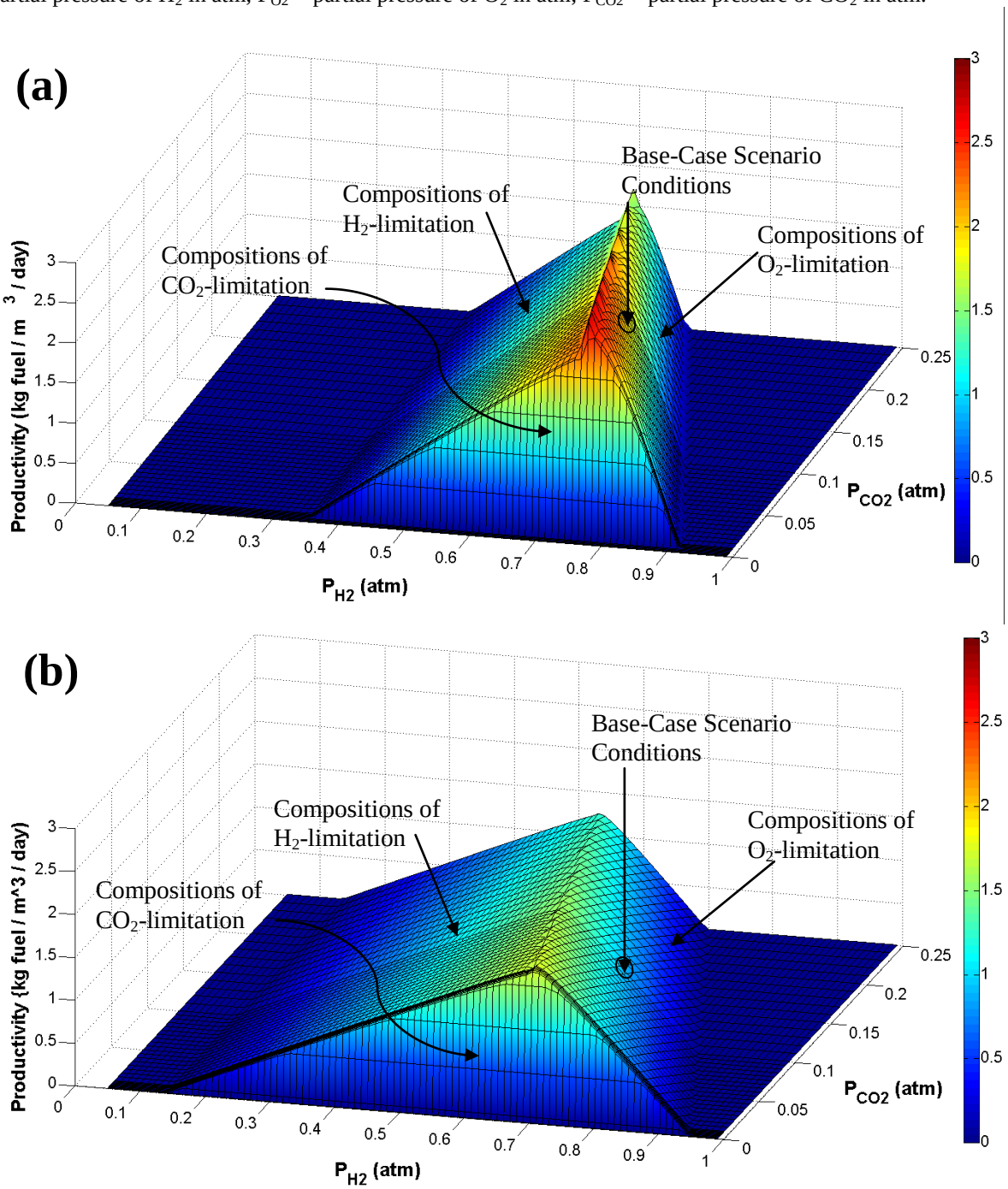

Rb. capsulatus, and the sensitivity to oxygen concentration moving away from the optimum is much greater as well. It should be noted that the Base Case gas phase composition (H_2:O_2:CO_2 = 75:16:9) is definitely offset from the apparent optimum compositions, as indicated in Figure 6.9.

The precise value of the maximum productivity is uncertain due to lack of convergence of the model at the transition between H_2 and O_2 limitation; the maximum occurred at the intersection of each the surfaces corresponding to H_2, O_2, and CO_2 limitation. Additionally, because this model does not incorporate inhibition by high concentrations of oxygen, it is possible that the exact location of the optimum is off-set from the true maximum; an improved model that incorporates oxygen inhibition is required to determine a more realistic value. It is interesting to speculate however that so long as oxygen is kept as the rate-limiting growth substrate, the concentration of oxygen in the system will not accumulate to a level toxic to the organisms; this would explain the variable information available on the range of oxygen inhibition, as the exact partial pressure of oxygen corresponding to inhibition will be dependent on a multitude of factors, including the overall mass transfer rate, the hydrogen and carbon dioxide partial pressures (which affect the overall growth rate), the cell density, the temperature, the pH, etc. Combined with the fact that the most rapid drop off in productivity occurs in the CO_2-limited regime, operating exactly at the optimal point will result in instability particularly with respect to CO_2 limitation. Therefore, in the conditions of the base case, a more appropriate operational strategy would be to control P_{H2} towards the optimum level, control P_{CO2} in excess of the optimum (~ 5% CO_2), and allow oxygen to make up the difference such that it is always the rate-limiting substrate.

Scenario IV: Effect of Mass Transfer on Yields, Productivities, and Operating Costs

It is intuitively obvious that under mass-transfer limited conditions, the growth rate of an organism will be limited by the rate at which the substrate is able to be delivered to the cells. At the base case $(k_La)_{O2}$ of 250 hr^{-1}, mass transfer rates of gas-phase growth substrates limit the growth rates (and therefore the fuel synthesis rates) of each *Rs. eutropha* and *Rb. capsulatus* ; these mass-transfer limited net growth rates (μ_{MTL}^{NET}) are severely diminished from the maximum net growth rate (μ_{max}^{NET}) of which each species is intrinsically capable. The top half of Table 6.11 shows the extent of reduction from the maximum net growth rate, μ_{max}^{NET}, due to mass transfer limitations in the Base Case Scenario.

Table 6.11: Effect of Mass-transfer Limitations on Net Growth Rates and Yields in the Base-Case Scenario

The top half of this table presents the ratio of the actually possible net growth rates in the base-case scenario to the maximum possible net growth rate (the intrinsic maximum for the species, limited only by cellular kinetics). As can be seen, the net growth rates in the base case scenario are highly diminished. The bottom half of this table, which has applied the relationship in Equation 5.16, presents the ratio of the net yield in the base case scenario to the maximum yield, where it can be observed that the yield *Rs. eutropha* is more diminished, due to its larger maintenance rate. Finally, the last row shows that if mass-transfer limitations could be minimized by better gas-liquid mass-transfer rates, the reduction from the maximum yield would be much lower.

				Rs. eutropha	***Rb. capsulatus***
Effect of Mass-transfer Limitations on <u>Net Growth Rate</u>	Net <u>mass-transfer-limited</u> growth rate:		μ_{MTL}^{NET} h^{-1}	0.042	0.019
	Net <u>unlimited</u> growth rate:		μ_{max}^{NET} h^{-1}	0.420	0.116
	Ratio of net growth rate in the base case to maximum intrinsic growth rate		$\frac{\mu_{MTL}^{NET}}{\mu_{max}^{NET}}$ %	9.9%	16%
Effect of Mass-transfer Limitations on H_2 <u>Yield</u> (due to Maintenance)	Ratio of net to maximum yields on H_2 in the Base Case:	$\frac{\mu_{MTL}^{NET}}{(\mu_{MTL}^{NET}+b)}$	h^{-1}	48%	66%
	Maximum possible ratio of net to maximum yields on H_2	$\frac{\mu_{max}^{NET}}{(\mu_{max}^{NET}+b)}$	h^{-1}	90%	92%

Because the fuel productivity is directly related to the net possible growth rate under mass transfer limited conditions, μ_{MTL}^{NET}, by Equation 5.38, improvements in growth rates that result from increases in mass transfer result in increased productivities. However, increased growth rates have a secondary benefit of increasing the growth yield of the organism on its various growth substrates as well, by reducing the negative impact of maintenance. This is because the net yield on the electron donor hydrogen depends directly on the ratio of the net growth rate (μ^{NET}) to the true growth rate (μ^{T}), as shown by Equation 5.16 (re-stated here for clarity, and changing from the terminology 'true yield' used in Chapter 5 to 'maximum yield' used in this Chapter to refer to yields not accounting for maintenance demands).

$$Y_{X/H2}^{NET} = Y_{X/H2}^{MAX}\left(\frac{\mu^{NET}}{\mu^{T}}\right) \qquad \textbf{Equation 5.16}$$

Under mass-transfer limited conditions and assuming that the rate of maintenance is a constant, the ratio of the net growth rate to the true growth rate,

$$\frac{\mu^{NET}}{\mu^{T}} = \frac{\mu_{MTL}^{NET}}{\mu_{MTL}^{T}} = \frac{\mu_{MTL}^{NET}}{\mu_{MTL}^{NET} + b} \qquad \textbf{Equation 6.6}$$

approaches unity as μ_{MTL}^{NET} increases and becomes larger relative to the maintenance rate. This ratio reaches a maximum when the true growth rate μ^{T} is equal to the maximum inherent growth rate of the organism, μ_{max}^{T}:

$$\frac{\mu^{NET}}{\mu^{T}} = \frac{\mu_{max}^{NET}}{\mu_{max}^{T}} = \frac{\mu_{max}^{T} - b}{\mu_{max}^{T}} \qquad \textbf{Equation 6.7}$$

Therefore, although there is always an offset between the true yield (Y^{MAX}) and the net yield due to the contribution of the maintenance rate, this is minimized as growth rates increase. The minimum offset between the true yield and the net yield occurs when the ratio in Equation 6.7 is at a maximum, and this maximum for each *Rs. eutropha* and *Rb. capsulatus* is presented in the second half of Table 6.11 along with the ratio at the Base Case Conditions.

Effect of Mass Transfer on Fuel Yields

The effect of increasing the oxygen mass transfer coefficient $(k_La)_{O2}$ from 250 hr^{-1} to 1000 hr^{-1} (while holding all other parameters constant to the base case values) on the net product fuel yields on hydrogen are shown in Figure 6.10 (a) *Rs. eutropha* and (b) *Rb. capsulatus*. Increasing $(k_La)_{O2}$ results in increases to the mass-transfer coefficients for H_2 and CO_2, according to Equation 5.33. Net yields are plotted versus the CF_{fuel} of the biomass at both k_La values, along with the yields under the biological limit assumption (MBL) and the net yields under non-limited growth conditions (Y^{NET}-NL) for comparison. Y^{NET}-NL represents the maximum achievable net yield for the conditions because this is the case when the net growth rate is at its maximum value in the absence of a limiting factor. As can be seen in Figure 6.10, increasing the k_La significantly improves the mass transfer limited net yields across the full range of CF_{fuel} for both species, shifting the mass-transfer limited curves closer to the non-limited growth curves. At the higher $(k_La)_{O2}$ value, the yields predicted under the mass-transfer limited assumption trend closer to the non limited conditions for higher values of CF_{fuel}, because the increased rate of mass transfer provides a higher rate of substrate in supporting growth and fuel production. Particularly at high CF_{fuel}, the magnitude of improvement due to increased mass transfer for *Rs. eutropha* is more pronounced. This is because at high carbon flux to fuel ratios the energy demand per mass of biomass synthesized is greater. Under more severely mass transfer limited conditions ($(k_La)_{O2}$ = 250 hr^{-1}), this increased energy demand at high CF_{oil} results in a more severely diminished true growth rate; subsequently, the maintenance rate becomes proportionally more significant, the ratio between the net growth rate and true growth rate gets smaller, and the net yield becomes even more significantly diminished. Thus, at high $CF_{oil,}$ the yield has a higher 'potential for improvement' than at low CF_{oil}. This effect is less pronounced for *Rb. capsulatus* because its mainteance rate is lower, and therefore the 'potential for improvement' in the yields at high CF_{oil}

Figure 6.10: Net, mass transfer limited fuel yields on hydrogen at k_La = 1000 hr^{-1} and k_La = 250 hr^{-1} versus CF_{fuel} for each (a) *Rs. eutropha.* (b) *Rb. capsulatus*.

The maximum yield for the conditions (Y^{MAX}) and the net yield in non-limited growth condtions (Y^{NET}) are included for comparison. Net, mass transfer limited yields at the higher k_La are shifted closer to the non-limited net yields, although they still drop off at high CF_{fuel}.

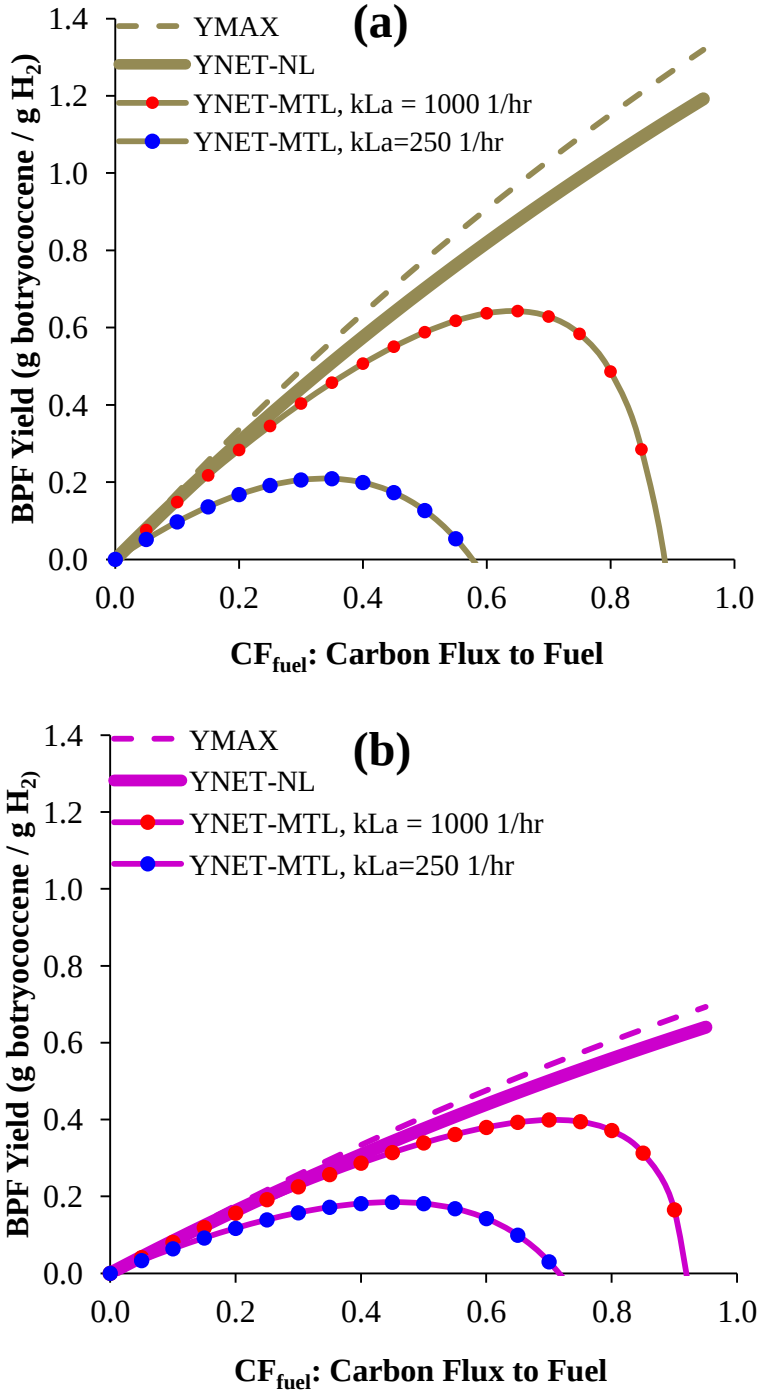

is less than *Rs. eutropha*. Furthermore, the true yields of *Rs. eutropha* on the mass-transfer limiting substrate oxygen are consistently higher than those for *Rb. capsulatus*, contributing to the larger positive impact of the higher k_La.

At a $(k_La)_{O2}$ of 1000 hr^{-1}, the CF_{fuel} at which the yields of *Rb. capsulatus* on hydrogen exceed those of *Rs. eutropha* is shifted out to above 0.8 (compared to above 0.45 for a $(k_La)_{O2}$ of 250 hr^{-1}).

At these high values for CF_{fuel}, the higher demand to support botryococcene product fuel production results in a diminished true yield, and therefore the net growth rate decreases as the CF_{fuel} increases for *Rs. eutropha*. Because the lower maintenance rate of *Rb. capsulatus* mitigates this effect, shifting the CF_{fuel} at which it reaches a maximum to a higher value compared to *Rs. eutropha*, a question of whether the yields or productivities of *Rs. eutropha* and *Rb. capsulatus* will converge when the growth rate is limited enough arises.

To investigate this, the mass-transfer limited, net yields and productivities at very low $(k_La)_{O2}$ values (125, 170, and 200 hr^{-1}) were plotted versus the carbon flux to fuel ratio; the results are presented in Figure 6.11 (a) yields and (b) productivities. At low $(k_La)_{O2}$, it is evident that the net yield of *Rb. capsulatus* exceeds the net yields of *Rs. eutropha* at CF_{fuel} greater than 0.3 and 0.2 for $(k_La)_{O2}$ of 200 and 100 hr^{-1}, respectively, and at all CF_{fuel} for a $(k_La)_{O2}$ of 125 hr^{-1}. At all $(k_La)_{O2}$ values, the yields of *Rs. eutropha* fall below zero at a lower CF_{fuel} than *Rb. capsulatus*. However, the combination of k_La and carbon flux to fuel ratio at which the *Rb. capsulatus* productivities (Figure 6.11 (b)) exceed the *Rs. eutropha* productivities does not correspond with the combination of k_La and CF_{fuel} where the *Rb capsulatus* yields surpass *Rs. eutropha* yields. At each $(k_La)_{O2}$, productivities for *Rb. capsulatus* do not exceed those for *Rs. eutropha* until a higher CF_{fuel}: 0.4, 0.33, and 0.125 for k_La of 200, 170, and 125 hr^{-1}, respectively. Because we assume that the cell concentration (X) in the system is constant at 10 g DW/L, it follows from Equation 5.41 (repeated here for convenience) that the mass transfer limited growth rate of *Rs. eutropha*

Figure 6.11: Fuel yield on H_2 (a) and Productivity (b) at low mass transfer rates as a function of the CF_{fuel}.

As k_La decreases, and mass-transfer severely limits the net growth rates of the organisms, the yield and productivity of *Rb. capsulatus* is observed to actually exceed that for *Rs. eutropha* at high carbon flux to fuel ratios (CF_{fuel}). Conditions other than k_La and CF_{fuel} are as per the Base Case Scenario.

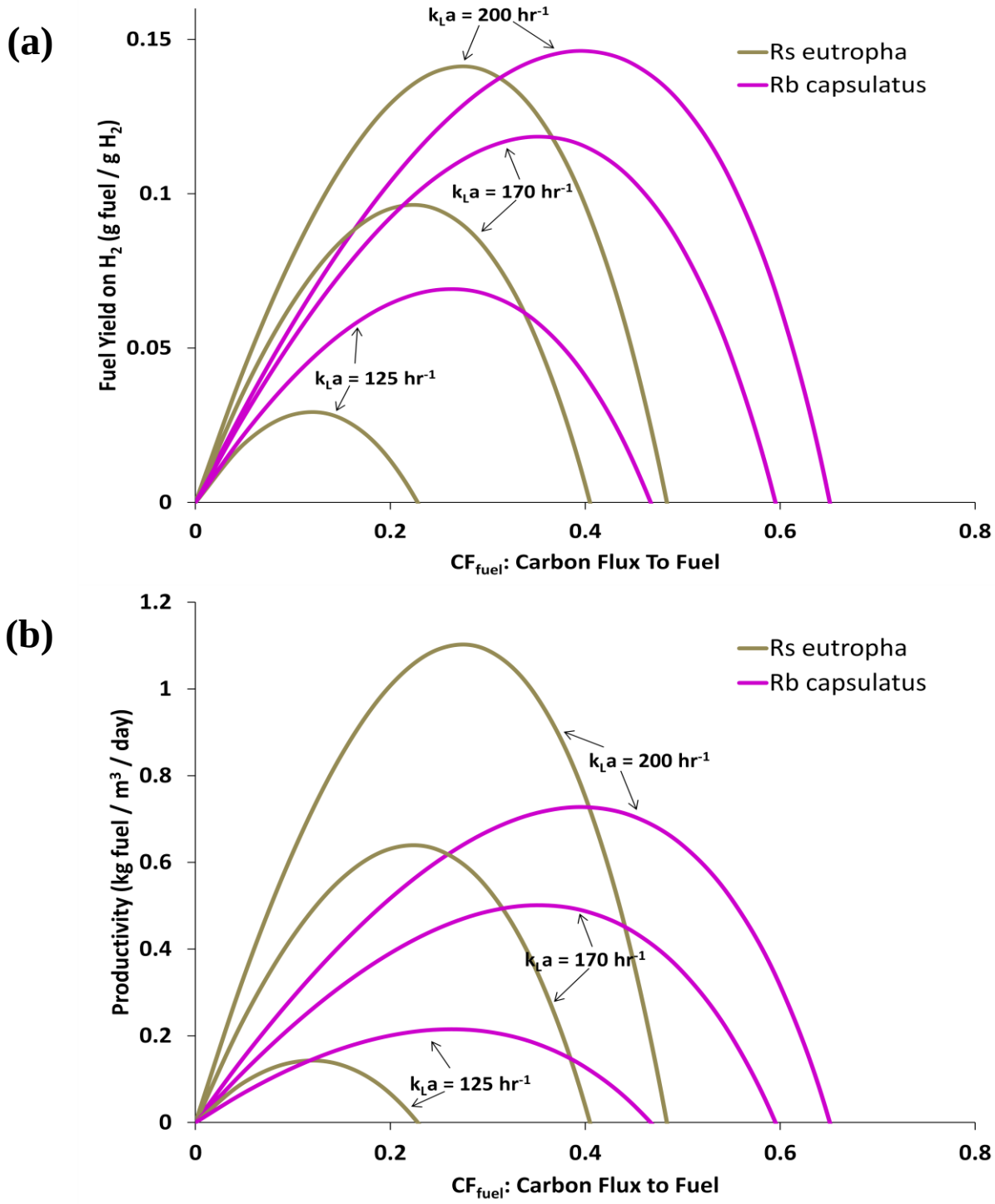

must be greater than *Rb. capsulatus* for the fuel productivity to be higher ($\bar{F}$ is set by the value CF_{fuel} and therefore is the same between the two species.

$$P_{fuel} = \bar{F}\,\mu_{MTL}^{NET}\,X \qquad \textbf{Equation 5.41}$$

Because μ_{MTL}^{NET} is determined by Equation 5.38 (repeated here for convenience) this means that even when the net yield of *Rb. capsulatus* exceeds *Rs. eutropha*, the true yield can still be greater.

$$\mu^{NET} = \mu^{T} - b = \frac{Y_i^T\,(k_L a)_i\,(C_i^* - C_i) - bX}{X - \left(C_{i,in} - C_i\right)Y_i^T} \qquad \textbf{Equation 5.38}$$

Again, because the maintenance rate of *Rs. eutropha* is greater than that of *Rb. capsulatus*, when the net growth rate is small enough, the true yield can be higher resulting in higher mass-transfer limited growth rates even when the net yield is lower.

Effect of Mass Transfer on Productivities

As was observed in Figure 6.10, increasing the k_La increased net yields, approaching the net yields predicted under non-limited growth scenarios. As k_La increases, this reduces the limitation of mass-transfer, and therefore there should be a point at which the k_La becomes sufficient to completely eliminate mass transfer limitations, providing substrates at rates high enough the new limiting factor is the intrinsic cellular kinetics of the organism (growth occurs at the maximum intrinsic growth rate). To determine this point for the base case conditions, the productivity was plotted versus k_La for each *Rs. eutropha* and *Rb. capsulatus*. The results are presented in Figure 6.12. The data show a nearly linear relationship of productivity with k_La until the curves merge together at the productivity predicted by the non-limited growth rate asumption. While the maximum possible productivity for *Rb. capsulatus* is nearly four-times less than that for.

Figure 6.12: Volumetric fuel productivity versus oxygen mass transfer coefficient (k_La) for *Rs. eutropha* and *Rb. capsulatus*.

The productivity predicted by the mass-transfer limited assumption (MTL) approaches the productivity predicted by the assumption of non-limited (NL) growth at high mass transfer coefficient $(k_La)_{O2}$.

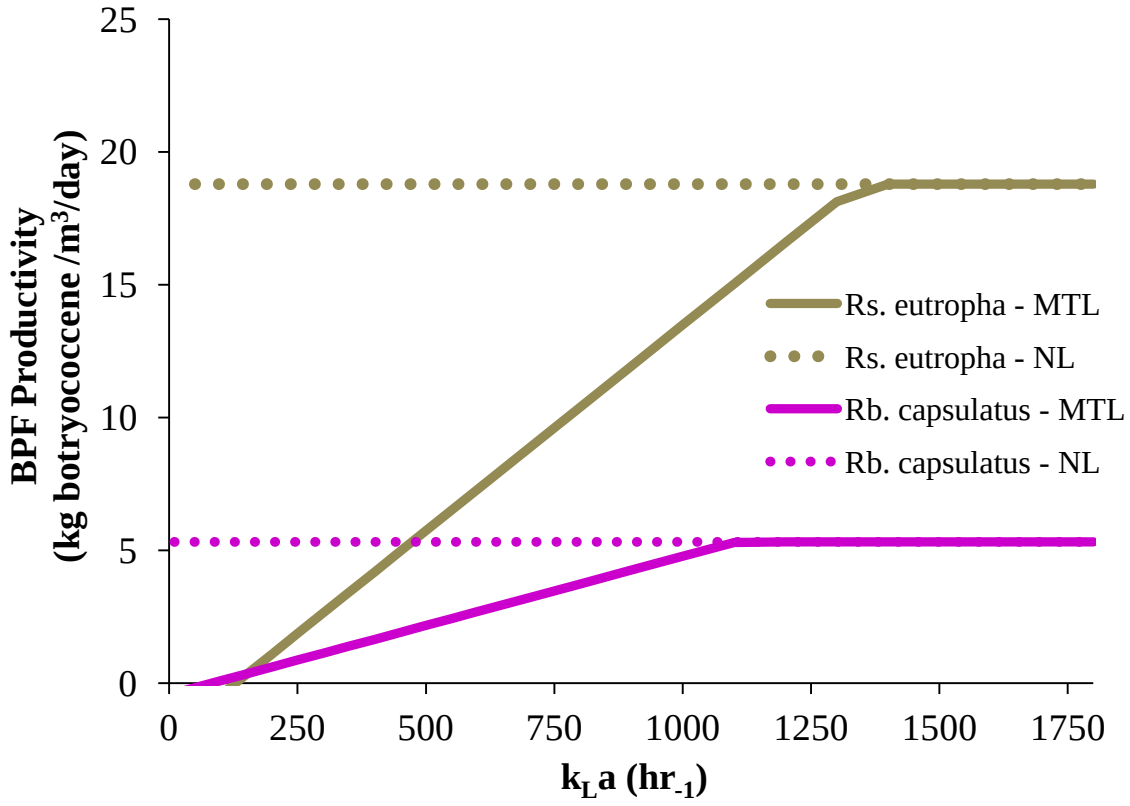

Rs. eutropha, the k_La at which the maximum is achieved is slightly lower: 1100 hr^{-1} versus 1350 hr^{-1}. This data shows that there is no further benefit to increasing k_La beyond the extent required to produce non-limited growth rates in the system, because further increases in mass transfer do not increase productivity

Relationship between Mass Transfer, Productivity, and Fuel Production Costs

Because mass transfer requires a significant driving force in the form of a power input to the system, this suggests there should be a point at which further increases in mass transfer rate

are more expensive due to energy costs than the gains in productivity obtained. A number of reactor configurations have been developed over the years to achieve mass transfer through a variety of different mechanisms. In a stirred tank design, the mechanism of mass transfer is by the entrainment of small gas bubbles in the liquid phase, creating a large surface area for mass transfer. This design typically requires high energy input; energy is required to turn an impeller (for stirring and shearing of the gas bubbles) as well as for compression of the gas to pressures high enough to sparge the gas through the reactor. Because the pressure drop of the gas as it moves through the liquid phase is high, very large compression costs are realized. In bubble column and airlift designs, where gas is bubbled up through a liquid column, gas compression is typically the sole energy input required. These types of designs are often associated with lower shear and lower power per unit volume than the stirred tank style reactors, beneficial for systems with more fragile cells, but also lower mass transfer rates. In a trickle bed, liquid flowing over a substrate creates a turbulent, thin film through which mass transfer occurs; forced gas flow countercurrent with the liquid flow enhances the mass transfer, and energetic requirements for this system are present in the form of liquid pumping against gravity and gas compression.

As already demonstrated, higher mass transfer results in higher productivities by eliminating mass transfer limitations on the growth rate of the organisms; however this mass-transfer comes in the form of an energetic cost. In order to estimate this cost for a specified mass transfer coefficient (k_La), the rate of energy needed to be supplied to attain the k_La needs to be known; this is the power per unit volume (P/V) associated with the mass transfer. The P/V can be translated into a cost per volume per time using the assumed price of electricity ($0.0872/kwh, Chapter 1), and then this is used to calculate a mass-transfer cost per kg oil produced using the productivity (Equation 6.8).

$$Energy\ Costs = \frac{\left({}^{P}/_{V}\right)(electricity\ cost)}{P_{fuel}} \qquad \textbf{Equation 6.8}$$

Three separate reactor mass-transfer configurations were examined in this analysis. These are listed below in Table 6.12, along with relevant operating ranges and references for the correlations relating P/V to $(k_La)_{O2}$.

Table 6.12: Reactor configurations utilized for power cost analysis

Configuration	Relevant k_La Range	Other information / restrictions	Reference
Stirred Tank	159-527 hr^{-1}	superficial gas velocity = 0.02 m/s	(Van't Riet 1979)
Bubble Column	100-433 hr^{-1}	superficial gas velocity = 0.0137-0.086 m/s; compressor efficiency of 50%; diameter = 0.152 m; height = 1.8 m	(M Y Chisti 1989)
Trickle Bed	725-1475 hr^{-1}	liquid velocity=0.014 m/s; gas velocity = 0.023 m/s; bed length = 2m; bed diameter = 2 m; particle diameter = 0.12 cm.	(Larachi et al., 1991)

To illustrate the 'cost' of increased productivities due to improvements in mass transfer, power costs were calculated for each of the reactor configurations; these are plotted versus productivity for each *Rs. eutropha* and *Rb. capsulatus* in Figure 6.13. Several important trends emerge; first, $(k_La)_{O2}$ from stirred tank power is more energetically expensive than $(k_La)_{O2}$ from bubble column power. However, the mass transfer from a trickle bed system is much cheaper than either of these technologies. When the k_La has increased such that further mass-transfer increases do not result in further productivity improvements, this appears as a vertical asymptote in Figure 6.13 (marked). Only the trickle bed k_La correlation was for a range sufficient to bring the $(k_La)_{O2}$ high enough to completely eliminate mass transfer limitations.

In order to compare the operating costs due to mass-transfer associated power as a proportion of the total operating costs, the total costs per kg of botryococcene product fuel for a range of mass-transfer coefficient $(k_La)_{O2}$ values were determined. This data is presented in Figure 6.14, broken down into power costs and feedstock costs, which include hydrogen, carbon dioxide, and neutralization costs. For both *Rs. eutropha* and *Rb. capsulatus*, the feedstock costs dominate the total operating costs; the power costs for *Rs. eutropha* are shown to be very low

across all k_La. Power costs are more significant for *Rb. capsulatus*, particularly when the reactor configuration used is a stirred tank design. However, the power costs still are, at a maximum, 37% of the considered operating costs.

Figure 6.13: Power Cost versus Productivity for various mass transfer technologies.

The cost of the power is plotted versus productivity to provide an indication of the 'cost' of attaining increased productivities due to mass transfer improvements. Various reactor configurations are compared; stirred tank and bubble column configurations have significantly higher costs than the trickle bed technology to provide a comparable $(k_La)_{O2}$.

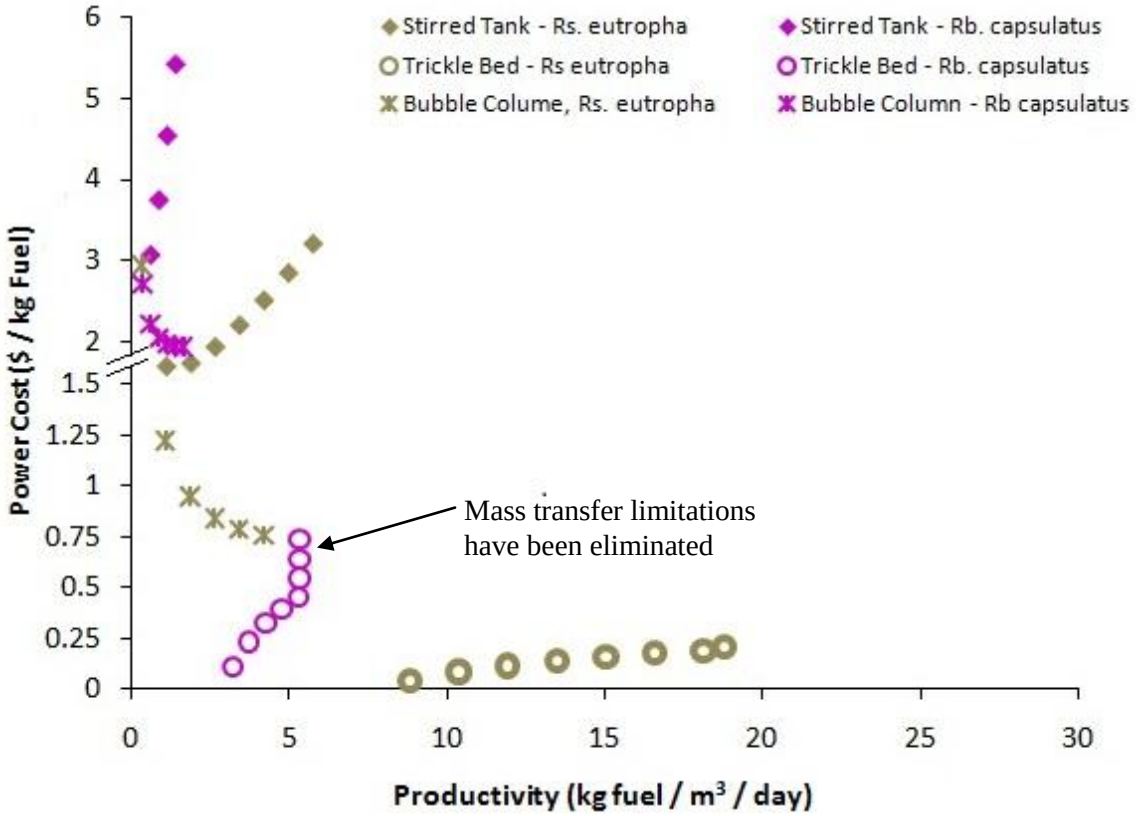

At low mass transfer rates, increasing the k_La initially results in large reductions in operating costs; this is a result of the increase in the net growth rates, improving the yield on hydrogen and other feedstocks, and therefore reducing the feedstock costs. However, above a $(k_La)_{O2}$ of 750 hr^{-1}, further increases in k_La do little to further decrease the operating costs for either *Rs. eutropha* or for *Rb. capsulatus*, particularly in terms of the feedstock costs.

Figure 6.14: Total operating costs per liter of fuel plotted as a function of mass transfer coefficient (k_La) for each (a) *Rs eutropha* and (b) *Rb capsulatus*

The operating costs calculated per liter of fuel include feedstock costs (hydrogen, CO_2, and acid neutralization) and power costs for mass transfer. The power costs are shown for each a Bubble Column, Trickle Bed, and a Stirred Tank in the k_La ranges for which they are applicable. Increases in mass transfer at low k_La have a large impact in reducing costs, but the improvements become negligible at higher mass transfer costs.

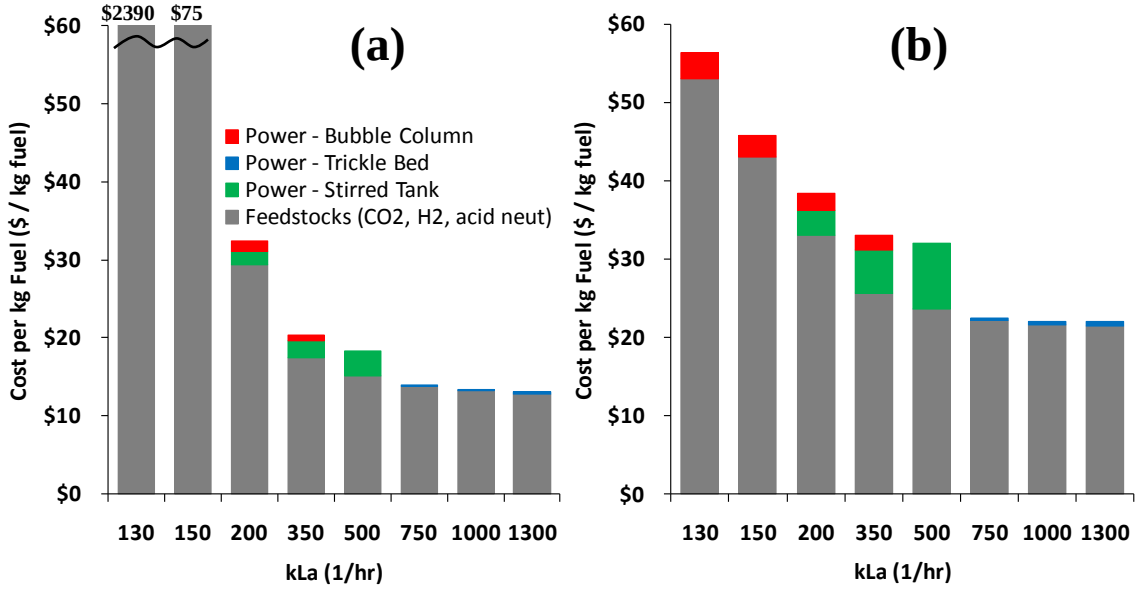

'Optimum' Predicted Conditions for Maximal Productivity and Minimal Operational Costs

To further elucidate the driving forces in both cost reductions and productivity improvements, as well as to obtain estimates for the maximum productivity / minimum costs possible from this Electrofuels Process, total operating cost per kilogram fuel was plotted versus productivity; CF_{fuel} and mass transfer coefficient values were varied (Figure 6.15). For this exercise, near-optimum gas-phase compositions were utilized rather than the base case gas-phase compositions (see Table 6.13). Only the data for *Rs. eutropha* is presented here. The $(k_La)_{O2}$ curves are grouped into two clusters – Stirred tank for low $(k_La)_{O2}$ values (green lines) and trickle bed for high $(k_La)_{O2}$ (orange lines). Both sets of data were included in the plot to cover a wider range of $(k_La)_{O2}$ values. Along each $(k_La)_{O2}$ curve the CF_{fuel} was varied to obtain the effect on

Figure 6.15: Botryococcene fuel produced by *Rs. eutropha*: Fuel cost versus productivity for varying k_La (separate curves) and varying Carbon Fuel Flux (CF_{fuel} – points within a single curve).

This plot demonstrates that both high CF_{fuel} fraction and cost-effective improvements in k_La are required for economic feasibility of this electrofuels process. The point corresponding to the base-case scenario is indicated with the yellow star. Blue points along the curves indicate CF_{fuel} = 0.25. Increasing k_La increases productivity across the entire spectrum of CF_{fuel}, but only result in improvements in cost at very low k_La values. Increasing CF_{fuel} results in decreases in production costs over the whole range of k_La values, but only result in substantial productivity increases at both high k_La and CF_{fuel}. For each k_La curve, there is a point at which additional increases in CF_{fuel} result in diminished productivities and increased costs, as observed by the 'turn-around' of the curve. The CF_{fuel} corresponding to max productivities/minimum costs are indicated in the chart. Gas phase composition is at the optimum determined in Scenario II/II.

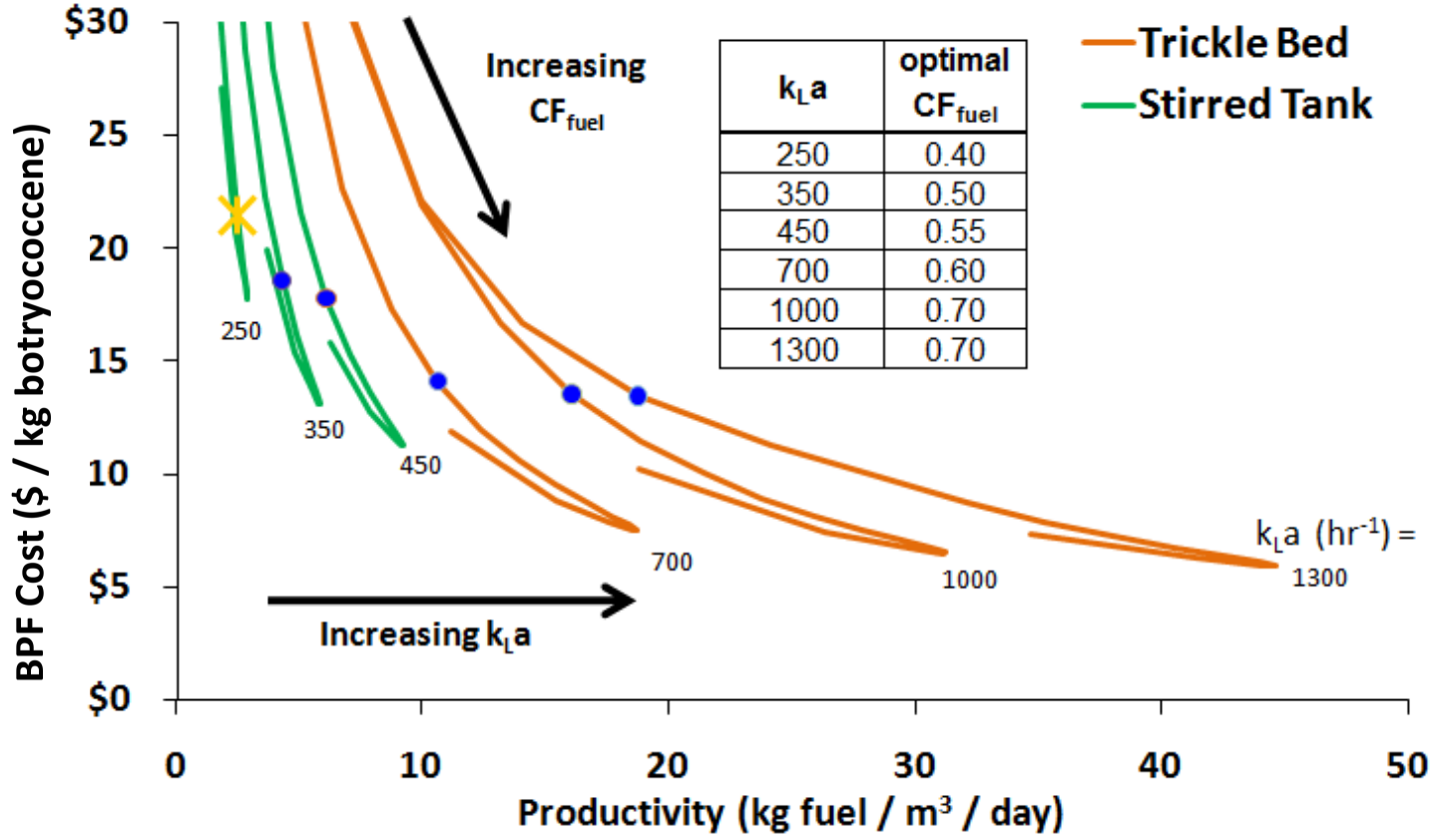

both cost per kilogram fuel and the volumetric fuel productivity. The point corresponding to the Base Case Scenario conditions is indicated with an yellow star; it is very apparent that the base case is much lower than the fuel cost and productivity theoretically possible under improved mass transfer and carbon flux to fuel conditions. It is also apparent that above a certain CF_{fuel} for a given $(k_La)_{O2}$ curve, further increases in CF_{fuel} actually lead to diminished productivities and increased costs; this can be observed by the fact that each curve 'turns around' after some value of CF_{fuel}. The reason for this effect is that above the optimal CF_{fuel} value, yields and productivities decrease with further increases to $(k_La)_{O2}$ because energy cannot be supplied fast enough to support growth, maintenance, and botryococcene synthesis. The table inset in Figure 6.15 provides the 'optimal' CF_{fuel} associated with each k_La curve.

For a constant Carbon Flux to Fuel ratio (CF_{fuel}), (blue marked points along the curves indicate a CF_{fuel} of 0.25) at low $(k_La)_{O2}$ (250-450 hr^{-1}), increases in $(k_La)_{O2}$ result in a decreased fuel cost; however, above a $(k_La)_{O2}$ of 700 hr^{-1}, further increases in $(k_La)_{O2}$ (within a single technology and for constant CF_{fuel}) do little to further decrease fuel costs, but do increase productivity. The enhancement in productivity associated with increases in mass transfer are more pronounced at higher fuel mass fractions (that are less than the 'optimal' CF_{fuel} for a given $(k_La)_{O2}$. There is a step-change decrease in fuel price observed in the transition from the stirred tank technology to the trickle bed technology, which is to be expected based on the previously discussed relative operational power requirements of these two technologies.

For a constant $(k_La)_{O2}$ (along a single curve), increases in Carbon Fuel Flux serve to decrease operational costs whenever the $(k_La)_{O2}$ is low (<250 hr^{-1}) without substantially increasing productivity. For higher $(k_La)_{O2}$ curves, increases in CF_{fuel} serve to both decrease fuel costs as well as to increase productivity, although the increases in productivity are much more dramatic at $(k_La)_{O2}$ above 700 hr^{-1}.

This figure serves to show the enhancing effect of increasing both k_La and Carbon Fuel Flux; if either $(k_La)_{O2}$ or fuel mass fraction are poor, economic feasibility will be poor in terms of both cost and productivity. For example, at low $(k_La)_{O2}$, high CF_{fuel} (above 0.4-0.55) actually deceases productivities and increases operational costs (consider the curves for $(k_La)_{O2}$ 250, 350, 450 hr^{-1}). It should be noted that the increases in productivity and decreases in cost in this region are proportionally very large for each improvement made, but the overall productivities remain small and costs remain high. Similarly, for low fuel mass fractions (<0.25), increases in $(k_La)_{O2}$ do increase productivity, but the range of productivities achievable is much smaller, and costs remain high. Only with both high $(k_La)_{O2}$ and high fuel mass fraction will this permutation of the Electrofuels production strategy approach an economically feasible technology.

Because the base case scenario was offset from the optimum for each condition selected, as evidenced from Figure 6.15, a new set of optimal conditions was predicted for *Rs. eutropha* making botryococcene hydrocarbons. Table 6.13 below compares the selected optimal conditions for each species with the Base Case Scenario, along with the predicted productivity and the predicted operational costs per MJ of energy in fuel. The metric of cost per energy content of the fuel was selected in order enable direct assessment economic feasibility under the most optimistic-realistic conditions that could be compared to technologies producing fuels of other types, which would inherently have a different energy content per volume. Because the parameter of fuel mass fraction is one of the largest unknowns, and because it cannot be directly controlled (like a gas-composition could be by operational strategy), results are presented for the optimal CF_{fuel} for the reasonably high $(k_La)_{O2}$ value of 1000 hr^{-1}: CF_{fuel} = 0.67 for *Rs. eutropha* and CF_{fuel} = 0.77 for *Rb. capsulatus*. For this analysis, it was assumed that the ideal gas-phase compositions would not change with changed CF_{fuel}. Furthermore, the gas-phase composition was selected slightly offset from the actual optimal (because currently the model won't completely converge at the optimum point. The optimal k_La was set to 1000 hr^{-1}, which is a

Table 6.13: Continuous-growth process botryococcene product fuel (BPF) costs, productivities, and energy yields under near-optimal process conditions for each *Rs. eutropha* and *Rb. capsulatus*, compared to the theoretical non-biological maximum

Gas phase-compositions were selected close to the optimums determined for each species, off-set slightly to the oxygen mass transfer limited side. $(k_La)_{O2}$ was selected to be 1000 hr^{-1}, as a reasonable value using trickle-bed technology. Values are reported for a low and a high CF_{fuel} value, and are for a continuous, steady state system operated at 10 g cell mass / L. The right-most column provides the absolute upper maximum for BPF fuel production by H_2 oxidation, in the limit of a completely reversible process (the thermodynamic limit (TL), ε=1.0) and in the limit of 100% of the carbon flux being directed towards fuel. This case is a theoretical reference since this thermodynamic limit could not be obtained due to biological inefficiencies.

	Theoretically feasible optimum		**Absolute upper bound** ε=1.0 CF_{fuel}=1.0
	Rs. eutropha	***Rb. capsulatus***	
Gas-phase Composition (atm)			
H_2:O_2:CO_2	77 : 20.5 : 2.5	69 : 28.5 : 2.5	75 : 16 : 9
pH	7.0	7.0	7.0
$(k_La)_{O2}$ (hr^{-1})	1000	1000	n/a
High-end CF_{fuel} =	**0.67**	**0.77**	**1.00**
Power cost ($ / MJ BPF)	$0.00	$0.00	---
Feedstock cost ($ / MJ BPF)	$0.14	$0.20	$0.06
Total cost ($ / MJ BPF)	**$0.14**	**$0.21**	**$0.06**
Total cost ($ / kg BPF)	$6.48	$9.28	$2.47
Productivity (MJ BPF / m^3 / day)	**1403**	**823**	**---**
Productivity (kg BPF / m^3 / day)	31	18	**---**
Hydrogen Energy Yield (MJ BPF / MJ H_2)	**20.6%**	**13.7%**	**55.4%**
Base Case Scenario; CF_{fuel} =	**0.25**	**0.25**	
Power cost ($ / MJ BPF)	$0.00	$0.01	
Feedstock cost ($ / MJ BPF)	$0.30	$0.47	
Total cost ($ / MJ BPF)	**$0.30**	**$0.48**	
Total cost ($ / kg BPF)	$13.56	$21.56	
Productivity (MJ BPF / m^3 / day)	**721**	**238**	
Productivity (kg BPF / m^3 / day)	16	5	
Hydrogen Energy Yield (MJ BPF / MJ H_2)	**10.6%**	**6.1%**	

reasonable, attainable $(k_La)_{O2}$ using a trickle bed technology; the power costing provided in the table was based on the trickle bed reactor configuration.

The high end CF_{fuel} scenario presented in Table 6.13 below is possibly very optimistic in terms of the ability to manipulate an organism to achieve that magnitude of carbon flux to fuel synthesis. Furthermore, it is re-emphasized here that no capital costs have been incorporated into

this analysis, nor any assumed rate of downtime of the production facility. Furthermore, it should be emphasized that the per volume data indicated in the table is per volume of process liquid, not per operational volume (which would include gas space).

The far right column of Table 6.13 reports the costs, productivities, and energy yields associated with the absolute upper bound of BPF production by hydrogen oxidation. This upper bound is that associated with the thermodynamic limit of a completely reversible process (ε=1.0), where all energy from the oxidation of hydrogen is transformed into useful work (i.e. botryococcene synthesis). It is also associated with the case where 100% of available energy and carbon is directed towards fuel synthesis. There is no growth rate that could possibly be associated with this process because positive growth rates require an energy gradient to occur, which goes against the assumption of reversibility necessary to assume a completely efficient organism. Extrapolations to the non-growth perfusion culture condition are discussed under future work. Therefore, this case represents a non-biological process that could only ever be approached; these values cannot be realized in practice.

This table points out two very important trends:

1. The cost of fuel production is completely dominated by the feedstock cost. Furthermore, this feedstock cost is totally dominated by the cost of H_2 and not CO_2.
2. The maximum extent of the energy contained in H_2 that can be converted into fuel synthesis, even at the absolute upper limit, is 55.4%. In the case of the theoretically feasible biological processes, these values are much lower.

With regards to the first point, this is important because production costs dominated by the feedstock costs cannot take advantage of economies of scale – producing fuel at a larger scale will limit scaled cost reductions to capital, facilities and personnel (not considered in the current analysis). The only possible ways for fuel cost to be decreased is to maximize the yield on H_2, and seek increasingly low-cost H_2 production technologies.

With regards to the second point, the logical question that arises is: if the energy from hydrogen is not going to BPF production, where is it going? The answer is that the electrons from hydrogen must go to reduce oxygen, which produces water, in the generation of energy for fuel synthesis. Furthermore, water is also produced in the reduction of CO_2 by H_2 to $C_{34}H_{58}$, according to its balanced half reaction. The half reactions relevant to this process are reiterated below in Figure 6.14. Then, for the energetics of this process to work out, the energy produced by hydrogen oxidation must balance that required for reduction of CO_2 to the botryococcene fuel. When it is considered that <u>all</u> the energy available from hydrogen oxidation is converted to product fuel production ($C_{34}H_{58}$), the balanced stoichiometry presented in Table 6.14 results. Calculating out mass yields from this molar stoichiometry, we learn that the BPF and water yields in the absolute upper bound are 1.77 g $C_{34}H_{58}$/g H_2 and 6.96 g H_2O/g H_2. Therefore, much more of the <u>mass</u> of the H_2 substrate is being directed towards water, although 55% of the <u>energy</u> contained in H_2 is directed towards $C_{34}H_{58}$. In the limits of the theoretical optimum for each species (Table 6.13), the proportion of water produced is much greater. These results are presented in Table 6.15 below.

Table 6.14: Half reactions and overall reaction for fuel synthesis production by hydrogen oxidation in the absolute maximum limit

$$H_2 = 2\,H^+ + 2\,e^-$$
$$O_2 = 2\,H_2O - 4\,H^+ - 4\,e^-$$
$$34\,CO_2 + 97\,H_2 = C_{34}H_{58} + 68\,H_2O - 194\,H^+ + 194\,e^-$$

↓ *Balancing of half reactions and energetics* ↓

$$\mathbf{0.13\,CO_2 + 0.065\,O_2 + 0.5\,H_2 \rightarrow 0.0038\,C_{34}H_{58} + 0.39\,H_2O}$$

Table 6.15: Comparison of BPF ($C_{34}H_{58}$) and water yields on H_2 for the theoretical optimums at a k_La of 1000 hr^{-1} (CF_{fuel} = 0.77 for *Rs. eutropha* and 0.70 for *Rb. capsulatus*) and the absolute upper bound.

Yields reported as g $C_{34}H_{58}$/g H_2 and g H_2O/g H_2

	Rs eutropha		***Rb capsulatus***		**Absolute upper bound (ε = 1.0; CF_{fuel} = 1.0)**	
	$C_{34}H_{58}$	**water**	**$C_{34}H_{58}$**	**water**	**$C_{34}H_{58}$**	**water**
high CF_{fuel}	0.66	7.97	0.44	8.34	1.77	6.96
low CF_{fuel}=0.25	0.34	7.82	0.20	8.25		

Discussion: Relationship of the Carbon Flux to Fuel Parameter with the Process Operational Mode

The initial scenario chosen for analysis in this work assumed a continuous chemostat-like bioreactor process configuration, where cell and botryococcene product is removed from the system at a rate that matches the growth/production rate, resulting in a steady cell concentration and environmental conditions within the reactor system. The logic in this choice of continuous production is that continuous systems have much higher volumetric productivity as compared to their batch counterparts. Besides the observation that growth-associated kinetics of botryococcene synthesis are observed in their native host, *Botryococcus braunii* (Anirban Banerjee et al. 2002), some degree of cell growth is invariably necessary to retain cell viability and productivity, and the ideal case of all energy and carbon being processed into a fuel product is not currently within reach of genetic engineering strategies. The overall objective of this analysis is to allow for quantitative assessment of yields and productivities under 'reasonable' operating conditions. Major factors that determine the productivity of the system are the dilution rate and the cell density. A 'reasonable' cell density of 10g DW/L was chosen in part because it quickly became clear that the high cell maintenance costs of autotrophic organisms relative to reasonable mass transfer rates would constrain operation to very high cell concentrations. At this cell density, nearly half of the base case kLa of 250 hr^{-1} is supporting maintenance energy costs. The dilution rate (D) is fixed by the net possible growth rate of the cells in a continuous system

(μ^{NET}), which in turn is fixed by the rate at which the electron donor and electron acceptor are supplied to the system (the gas mass transfer rate) and the efficiency of the metabolism in supporting cell growth while simultaneously making fuel. As the CF_{fuel} increases, the available rate at which the rate-limiting substrate is supplied is diverted towards fuel production, at the expense of growth. For a fixed cell concentration (X), the substrate requirements for cell maintenances, growth, and fuel synthesis will exceed the rate possible by mass transfer at a certain CF_{fuel}. At the point where the rate of energy able to be supplied by the mass transfer is only sufficient to meet the demands of cell maintenance, the cells no longer are able to grow or produce fuel.

Because the model developed and utilized in this work coupled product formation to growth through a carbon flux ratio to fuel (CF), the rate of fuel synthesis ceased when growth ceased. This significant limitation for this fuel production process is revealed by this modeling effort; the extent to which the energy contained in hydrogen can be converted into fuel synthesis is constrained by the extent to which the metabolic flux can be shifted towards fuel synthesis (CF_{fuel}). However, higher CF_{fuel} values diminish the energy available for growth with a net effect of preventing fuel synthesis in this system. The maintenance requirements of the chosen cell concentration of 10g DW/L are simply too high to allow for significant production of fuel at moderate mass transfer rates that would be typical of large scale bioreactor operation. Reducing operational cell density could allow for CF_{fuel} on the order off 80-90%, but productivity would be diminished due to the reduced cell concentrations. Approaches to achieving higher yields and productivities, are discussed below.

First, to achieve extremely high CF ratios, fuel biosynthesis would need to be metabolically decoupled from growth so that the metabolism can be directed more fully to fuel synthesis, even in the absence of net cell growth. This strategy would need to be implemented in the genetic engineering strategies when constructing the botryococcene synthesis pathways into

either *Rs. eutropha* or *Rb. capsulatus*. In addition to the mere presence of the required pathways, metabolic engineering strategies will need to be implemented in order to overexpress the botryococcene synthesis pathways while minimizing flux through non-fuel-synthesis pathways. One aspect that will need to be considered when engineering the botryococcene pathways into *Rs. eutropha* or *Rb. capsulatus* will be ensuring a sufficient supply of cellular reducing power (in the form of co-factors such as NADPH and FdH_2) to support continued botryococcene biosynthesis. For each C_{34} botryococcene molecule produced from the intermediate Acetyl-CoA, 13 molecules of NADPH are required, as described in Chapter 3. Therefore simultaneous overexpression of pathways producing NADPH will also be required to support botryococcene synthesis, as well as for CO_2 fixation. This approach would enable a capture of a maximal amount of the substrate (H_2) energy into the targeted product fuel, resulting in improved energy yields compared to those reported in Figure 6.5. Currently the ability to manipulate these prokaryotic species to exclusively and continuously produce $C_{34}H_{58}$ fuel (or any other biofuel) is a tremendous challenge beyond current efforts to simply produce g/L titers in batch induced systems.

Secondly, an alternative bioprocessing configuration that does not require continuous growth of the cells to maintain the cell density in the bioreactor would leave more cellular energy available for botryococcene biosynthesis. This could be achieved through the implementation of a perfusion bioreactor configuration, where the cells are either immobilized or recycled to the reactor for continued fuel synthesis after a separation step to remove the fuel product. This type of operation allows for setting the operational cell concentration independent of the dilution rate which now primarily plays the role of inorganic nutrient addition and waste removal.

This hypothetical, ideal process requires an organism engineered with botryococcene synthesis pathways that are both decoupled from growth and sufficiently overexpressed to eliminate the need for continuous growth of the cells, but preserve the ability for continuous botryococcene fuel synthesis. This would also allow for an increased cell concentration in the

reactor, where it should be considered that an organism with a lower maintenance energy would be able to capture a larger amount of the energy of H_2 into botryococcene biosynthesis, assuming similar yields.

The reality for current efforts to generate an autotrophic organism that can produce botryococcenes will invariably fall somewhere between a purely growth associated production and growth dissociated production. In the native algal host, *Botryococcus braunii*, botryococcene hydrocarbon product makes up 15-40% of the biomass dry weight, where the product formation kinetics are growth-associated (Metzger et al. 1985; Okada, Murakami, and Yamaguchi 1995; Grady 2010). Even this impressive range of productivity represents a reduced flux of carbon to fuel for this organism/product pair, compared to the >80-90% suggested for economic feasibility of this proposed genetically engineered system. Although the 'wasted' carbon flux of the growth-associated system will necessarily lead to diminished yields on H_2 compared to a fully decoupled metabolism, the system that would provide higher productivities would be a function of the botryococcene production kinetics of each system. The volumetric productivities for a growth-associated continuous system and a metabolically-decoupled perfusion mode system would be determined by both the density of the biomass as well as the specific rate of product formation associated with each mode. A comparison of these models by the extension of the theoretical framework in this work to include decoupled metabolism and alternative bioprocessing strategies is a key trajectory in future work for this project.

Another alternative process operational scheme worth mentioning is a batch production mode. Batch production would be the logical choice in the event that product formation is growth dis-associated, which means that the product is formed when growth of the biomass has ceased or a production phase is induced after a batch growth period. This is similar to the kinetics of lipid production exhibited by many algae species, which accumulate lipids only when deprived of an essential inorganic nutrient for growth, typically nitrogen or phosphorus

(Moellering and Benning 2010; Zi Teng Wang et al. 2009). Because lipids are a native algae co-product, the physiological triggers for lipid accumulation have been studied (Shifrin and Chisholm 1981; Zhi-Yuan Liu, Guang-Ce Wang, and Zhou 2008; Yanqun Li et al. 2008; Rodolfi et al. 2009; Pruvost et al. 2009). In contrast, because the botryococcene product fuels proposed for production by *Rs. eutropha* or *Rb. capsulatus* in this work will be invariably genetically engineered into the host organisms, the physiological triggers for a growth dissociated product formation could be engineered into the organism as well. In fact, the most common approach to demonstrating proof of concept for genetic engineering strategies is induction using operons such as the IPTG-inducible lac operon. Despite the prevalence of inducible gene expression systems, it should be recognized that a batch growth and product production scenario results in volumetric productivities that are generally lower than both perfusion and a continuous system due to increased downtime of the equipment and the fact that product synthesis and accumulation occurs only during a fraction of the overall growth phase.

Chapter 7

Conclusions and Future Work

In this work, the Electron Balance method of McCarty for making biological growth yield predictions was enhanced to accommodate a chemolithoautotrophic growth process involving hydrogen oxidation for a botryococcene hydrocarbon fuel product. Specifically, the determination of the $\Delta\hat{G}_{SYNTH}$ was modified to account for autotrophic metabolic processes, including reversed electron transport for NADH production, and to allow a variable cell composition and the production of a highly reduced hydrocarbon. While the scope of the biological system under investigation necessitated these changes, it is expected that similar modifications could be applied in other microbial metabolic scenarios. Another benefit of the utilization of the EB method as a foundation for this model was the ability to make product fuel yield predictions prior to the engineering of the botryococcene pathway into the organism. Rather than requiring the development of a genome scale model, which first would have required knowledge of the genome sequence of *Rs. eutropha* and *Rb. capsulatus*, this method enabled yield predictions with a much more limited data set. In addition, a model with any additional levels of detail would only be fit to data to provide a qualitative assessment of the microbial energetics that are captured in this model with cellular efficiencies. This eliminated the need to obtain knowledge on all cellular pathways; instead lumped pathways for energy generations and cellular synthesis were sufficient for this analysis, beyond the necessary knowledge of reversed electron transport in *Rb. capsulatus.* Furthermore, the EB method only required fitting of a single adjustable parameter using growth and yield data, the cellular efficiency factor, ε. Therefore, yield and productivity predictions using this model were possible using only a small data set. The approach presented here is a compromise between dealing with biological complexity and process engineering complexity. The microbial energetics analytical approach allowed for incorporation

of metabolic details of energy assimilation, while simultaneously allowing for an evaluation of the effects of process conditions. It would be interesting to challenge this model for validation against larger data sets of *Rb. capsulatus* and *Rs. eutropha* growth data under a number of different conditions; however, it should be recognized that the power and the value of this approach was to gain insights into the general feasibility and opportunities for improvement for this hypothetical process. Varying cell growth rates, gas mass transfer rates, and gas phase compositions would provide the most significant perturbations to processing conditions resulting in changes to the observed microbial yields and ultimately economic feasibility. This work provides a tool that can be refined and updated as the research progresses, while keeping track of overall process economics.

Recently, Imam et al. (2011) reported the development of a genome-scale reconstruction of the *Rhodobacter sphaeroides* metabolism. *Rb. sphaeroides* and *Rb. capsulatus* share common metabolic pathways, although a critical pathway not present in *Rb. sphaeoides* is chemolithotrophic growth by H_2 oxidation. The overall analytical framework for analyzing this process can certainly accommodate an increase in the detail of biological complexity if it can capture more details on energy generation or biosynthesis. It would be an interesting collaboration if the authors were interested in leveraging the work with the *Rb. sphaeroides* genome scale model to develop a related one for *Rb. capsulatus*, which could be compared the results of the model presented in this work.

A more important focus of future work will be to improve the accuracy of the parameters that currently are only poorly characterized, yet have a large impact on overall process economics. There is additional data collection required to further refine the EB model developed in this thesis. Specifically, while the maintenance rate of each organism is not a true adjustable parameter of the model, and is calculated through models other than the one developed in this work, an accurate maintenance rate of the organisms will be critical to making accurate net yield

predictions. This is particularly true in a perfusion mode scenario (this is discussed further below). While several determinations of the maintenance coefficient of *Rs. eutropha* under chemolithotrophic growth have been reported in the literature (Bongers 1970; Siegel and Ollis 1984; Miura et al. 1981; Y et al. 1978), from which the maintenance rate was calculated, corresponding data for *Rb. capsulatus* has not been collected. The maintenance rate utilized in this work was calculated based on photoheterotrophic growth using data from Hoekema et al. (2006), under the assumption that the maintenance rate of the organism would be relatively independent of the growth mode. Experiments to directly measure the maintenance rate of each *Rs. eutropha* and *Rb. capsulatus* are already planned in the Curtis lab.

One of the reasons that a fully characterized maintenance rate for the organisms is desired is its large effect on cellular energy demands under conditions of low growth. The (unachievable) upper limit of botryococcene product fuel yield on H_2 would occur when all energy derived from the oxidation of H_2 was captured into product fuel (Table 6.13). Minimizing maintenance energy demands of the organism (or selecting an organism with low maintenance energy demands) would minimize this competing demand for cellular energy. Based on the currently available information for maintenance rates of the organisms, it appears that *Rb. capsulatus* out-performs *Rs. eutropha* in this respect: *Rs. eutropha* has a maintenance rate estimated to be 0.045 hr^{-1} compared to the 0.0095 estimated for *Rb. capsulatus.*

The benefit of a low maintenance rate is particularly obvious in a processing scenario of minimal cellular growth, where the maximum amount of energy available from hydrogen oxidation by the organism could be shuttled to fuel synthesis. In this case, it is obvious that any energy utilized for maintenance demands directly diminishes that available for fuel synthesis. Selection of an organism with a low maintenance rate would minimize the energy spent for cell needs outside of botryococcene fuel synthesis.

A low-growth process configuration would also maximize the energy available for fuel synthesis, provided that the energy could be effectively redirected. To implement a minimal-growth, continuous process for botryococcene production, two coupled approaches would be required (assuming the stable integration botryococcene synthesis pathways into the organisms has been achieved). First, hydrocarbon synthesis pathways would need to be engineered such that they are totally decoupled from growth processes, proceeding independently of and with a much greater flux than growth. Attempts to eliminate or minimize pathways not contributing to either essential cell processes or fuel synthesis could be approached through metabolic engineering strategies. Secondly, a perfusion-type process would need to be defined, where the synthesized fuel was continuously removed, the substrates required for fuel synthesis (H_2, O_2, and CO_2) would be continuously provided, and biomass would be recycled back to the reactor so that energy for the regeneration of cells would only be required to a minimal extent. An obvious next step would be the modification of the EB model for yield and productivity predictions in a perfusion type scenario; the current design of the model is for a growth-associated fuel product where portioning between cell growth and fuel synthesis can be characterized by the CF_{fuel} (Carbon flux to fuel parameter). For the model to correctly simulate the yields of a product not coupled to growth, the metabolic basis would need to be shifted to that of the electron donor. On this basis, the metabolism would need to be conceptually partitioned into electrons for fuel synthesis, growth, maintenance, and energy generation. The maximum ratio of electrons to fuel / total electrons in donor would have an upper limit less than one, which would be a function of the maintenance rate, the rate of H_2 availability, and other factors. Furthermore, the ratio of electron partitioning between only fuel and cell synthesis would not be the appropriate 'user variable' to be adjusted: because the fuel product would be assumed as decoupled from growth, a more appropriate ratio as a user input to the model would be the proportion of total available electrons from the donor (after maintenance and efficiency losses accounted for) that were directed to fuel

synthesis. Thus, the reformulation of the model to predict yields in a perfusion scenario will require more than a trivial adjustment, although in theory it is possible.

There is another aspect of the organisms' metabolism that will need to be considered (and potentially addressed) in the context of metabolic engineering strategies; the assurance of a sufficient rate of regeneration of reduced electron carriers (NADH, NADPH, FDH_2, etc.) to support over-expressed fuel synthesis pathways. It has been demonstrated on multiple occasions that for successful metabolic engineering of enhanced product synthesis (sorbitol, mannitol, succinate, thymidine, and most notably 1,3-propanediol) manipulation of the redox energy pool in an additional layer of engineering has been required to eliminate cofactor regeneration as a metabolic bottleneck (Sánchez, Bennett, and San 2005; Monedero, Pérez-Martínez, and Yebra 2010; Hyeon Cheol Lee et al. 2010; Zhen Chen, Hongjuan Liu, and Dehua Liu 2009; Hao et al. 2008). This also raises the question of whether *Rs. eutropha* might be a more appropriate host in this respect because of its ability to directly transfer electrons from hydrogen to NADH without the need for the rate-limiting and energy-demanding reversed electron transport (RET) process. For *Rb. capsulatus*, it is likely that the need to perform RET in the generation of reduced electron carriers would be a significant bottleneck in hydrocarbon fuel production.

The implementation of the EB stoichiometric model for the prediction of growth and fuel botryococcene synthesis yields in this work provided key observations and insights critical to future development ofhydrogen oxidation by chemolithotrophic organisms (*Rs. eutropha, Rb. capculatus*) as a means of renewable fuel production. First of all, a critical parameter in this model is the cellular efficiency factor, ε. Yields predicted in the thermodynamic limit (ε=1.0) greatly exceed those predicted utilizing biologically realistic values of this parameter (ε=0.69 for *Rs. eutropha* and ε=0.53 for *Rb. capsulatus*). Because all growth processes must maintain a negative Gibbs free energy gradient between substrates and products in order to have a driving force for growth at finite rates, the price to pay is incomplete capture of the energy of hydrogen

into useful work by the cell; thermodynamics dictate that entropy generation must occur in irreversible processes, and therefore some energy must be dissipated as heat. Failing to account for this in yield predictions would lead to gross overestimations of the yields possible.

Another aspect of this process that could be easily overlooked, and that this model emphasized, was the need to take into account external rate-limitations in predicting both yields and process productivities. It was reasoned that the rate-limiting step in the chemolithoautotrophic growth of *Rs. eutropha* and *Rb. capsulatus* would be the rate of gaseous substrate supply (H_2, O_2, and CO_2). The transfer of a gas-phase substrate to the liquid phase has been a challenge to bioprocess design; the dissolution of a gas into a liquid is proportional to a thermodynamic driving force, namely the difference between the equilibrium concentration of the gas and the actual concentration of the gas in the liquid phase. However, the kinetics of this dissolution are restricted by the rate at which mass transfer can occur and the surface area for which that transfer to occur; in the absence of mass-transfer, the kinetics of dissolution, even in the presence of a large driving force will be very slow. Historically, the strategy to increase the rate of mass-transfer from the gas to the liquid phase has been to provide a velocity gradient between the phases and increase the surface area between thephases. Mass transfer strategies range from bubble columns, where the dissolution is driven by the movement of gas bubbles through a liquid phase, to the aerated, stirred tank, where sparged gas is broken into smaller bubbles by the action of a high-speed impeller, to a trickle-bed system, where turbulent flow of the liquid over a substrate induces the mass transfer between the two phases. In mammalian cell culture processes, oxygen mass transfer is particularly problematic; the fragility of the cell structure prevents obtaining mass-transfer through high-shear means, and the large size of mammalian cells provides an additional barrier to mass transfer from the culture broth to the interior of the cell (reduced surface area to cell volume ratio). In the microbial processes discussed in this work, shear and cell surface area-to-volume ratio is expected to be less of an

issue; however, each the electron donor (H_2), electron acceptor (O_2), and carbon source (CO_2) will be delivered through gas-liquid mass transfer. Thus, the performance of the process will be directly related to the efficiency of mass-transfer.

In the absence of a sufficient rate of substrate provision, the model predicted severe limitation in the growth rate; subsequently, due to the increased proportion of cellular energy that must now be spent on maintenance needs, diminished yields were predicted. The effect of both diminished growth rates and the diminished yields on the model was the prediction of stunted process productivities. Comparing the yields and productivities predicted under an assumption of external rate-limitation by substrate mass-transfer to those predicted assuming that the kinetic constraint was the intrinsic maximum growth rate of the organism show markedly divergent predictions (Figure 6.10), particularly at low mass-transfer rates and a high CF_{fuel}. This emphasizes the importance of bioprocess production development for effective gas-liquid mass transfer in conjunction with biological development of the targeted organism.

Based on the results in this work for a continuously-growing bioprocess, both high mass transfer and high metabolic flux toward fuel synthesis were required to drive process yields and productivities towards economic feasibility (Figure 6.15). In the absence of either component, yields and productivities remained low.

An interesting trend which emerged when modeling the process, is that at fixed cell concentration and mass transfer rate, increasing the CF_{fuel} only increased yields and productivities to a point. At values of CF_{fuel} higher than this point (which was a function of the overall mass transfer rate), yields and productivities actually declined. This effect is an artifact of the choice of a continuous-growth bioprocess system at steady-state as the initial model scenario. In this model, cell mass and fuel are continuously removed, and so to maintain a fixed cell concentration (as constrained by the model), growth of biomass would have to occur. This requirement for continued growth, in addition to fuel synthesis, manifested as a large metabolic load on the cell.

Because the growth rate of the cells is the dependent parameter in the model, the higher energy demands for fuel synthesis at high CF_{fuel} came at the expense of a reduced growth rate (and therefore a reduced dilution rate of the system). At high CF_{fuel}, the energy available from hydrogen oxidation (which was limited by the rate of mass transfer) has to be split between maintenance demands (fixed), fuel synthesis demands (fixed with respect to cell synthesis), and cell growth. Therefore, at high enough CF_{fuel}, incremental increases to the CF_{fuel} no longer led to an increase in the yield or productivity, but a decrease because the decrease in cell growth rate outweighed the increase due to higher metabolic flux to fuel. At some higher CF_{fuel}, the rate of energy required for fuel and maintenance would 'force' a negative growth rate, therefore predicting yields and productivities that drop to zero.

While, in a real process, fixing the cell concentration at the expense of a variable growth rate is not realistic, model outcome still emphasizes that a bioprocess requiring cell growth is wasting energy from H_2 that could otherwise be partitioned towards fuel biosynthesis. This raises the case for redevelopment of the model to predict a non-growth bioprocess, that of a perfusion bioreactor. This also suggests that decoupling of fuel synthesis pathways from growth pathways in the genetic and metabolic engineering of *Rs. eutropha* or *Rb. capsulatus* for botryococcene fuel production will be critical for a feasible process. This is discussed in further detail below.

Another challenge to the gas-delivery of this process which requires additional investigation and incorporation into the model is that of O_2 inhibition to the metabolism of both *Rs. eutropha* and *Rb. capsulatus*. This effect has been reported by several investigators (Bowien and Schlegel 1981; Siegel and Ollis 1984); however, there is a lack of consensus on the gas phase 'composition' of O_2 at which inhibition occurs. The determination of an O_2 inhibition threshold is actually much more complex, and the lack of agreement in the literature about where O_2 inhibition occurs is likely because it is not the gas phase concentration of O_2 that matters, but rather the liquid phase O_2 concentration that the organism 'sees'. Furthermore, the liquid-phase

concentration is a function of the mass transfer rate of O_2 (which is, of course, dependent on the gas phase composition) and the rate of O_2 utilization. To avoid O_2 accumulation in the liquid phase, O_2 must be used at a rate just equal to its supply; under these conditions O_2 is the rate-limiting substrate. None of the literature accounts of the O_2 inhibition document the liquid phase concentration of O_2 at the point of inhibition, or provides a gas-liquid mass transfer rate that characterizes the process. Therefore, to address this carefully planned and executed experiments will be required to measure the liquid phase concentration of O_2, the gas-phase composition, and the overall O_2 mass-transfer rate to deduce the O_2 uptake rate. Obtaining these measurements in a scenario of fixed mass-transfer rate while slowly increasing O_2 concentration in the gas-phase, and monitoring both liquid phase composition and the point of O_2 inhibition would provide very valuable insight into this process. With knowledge of the liquid phase composition at which O_2 inhibition occurs, engineering of a bioprocess control scheme could be undertaken to ensure that feeding of H_2, O_2, and CO_2 resulted in O_2-limited growth, and did not lead to O_2 accumulation in the liquid phase.

The ultimate and most important outcome of this analysis was the prediction of production costs (substrate and mass-transfer energy requirements) per kg and per MJ of botryococcene product fuel produced for both a low and a high CF_{fuel}; these results are presented in Table 6.13. As was shown and discussed, the majority of the processing costs are due to the cost of hydrogen itself, and not any other substrate or the cost of energy for mass-transfer. This means that this process would not benefit from economies of scale; increasing the size of the process will not reduce the cost per unit of fuel produced, because the feedstocks scale with the fuel production scale. Therefore the only possible ways for fuel cost to be decreased is to maximize the yield on H_2, and seek increasingly low-cost H_2 production technologies. An additional result highlighted by Table 6.13, was that the extent of the energy derived from hydrogen oxidation able to be directed toward BPF synthesis is very limited, even in the absolute

upper limit. Because of the need to stoichiometrically balance the oxygen from O_2 and from CO_2 in fuel production, and because these are both oxidized compounds, much of the hydrogen goes to the production of water, the only sink for oxygen production in the limit of no biomass production. The large amount of water produced will need to be separated from the product fuel, and the costs of separation and treatment of this waste water could be very high; this is an additional cost not currently factored into the analysis that will need to be considered. It could be possible to re-use the water produced in the process to be fed back into the water-splitting operation from where the H_2 and O_2 were originally produced.

Appendix A

Algal and Microbial Culture Media Formulations

A.1 Wayne's Freshwater Algae Medium (1X WFAM)*

	MW	[final]	[stock]	prep / L	/ 250 mL
KNO_3	101.11	--	**-na-**	**0.60**	0.15
NH_4NO_3	80.04	--	**-na-**	**0.61**	0.153
MR26 Phosphates (50x, 1M) (pH 6.8) 1M				**1 mL**	0.25 mL
K_2HPO_4 (dibasic)	174.18	0.115 g/L	115 g/L		
KH_2PO_4 (monobasic)	136.09	0.045 g/L	44.9 g/L		
pH to 6.8 with KOH or H_3PO_4					
WFAM MICROnutrients (1000x)			g/L stock	**1 mL**	0.25 mL
H_3BO_3 (boric acid)	61.83	1/1000th or mg/L	1.86		
$MnCl_2 \bullet 4H_20$	197.41		0.54		
$ZnSO_4 \bullet 7H_20$	287.56		0.066		
$ZnSO_4 \bullet H_20$	179		0.0411		
$ZnSO_4$ (anhydrous)	161.47		0.0371		
Na_2MoO_4-$2H_2O$	241.95		0.031		
$(NH_4)_6Mo_7O_{24} \bullet 4H_20$	1235.86		0.0229		
$CoCl_2 \bullet 6H_20$	237.93		0.030		
$CuSO_4 \bullet 5H_20$	249.7		0.0075		
Fe-EDTA$\bullet 2H_20$ (F) (anhydrous)	403.1	0.024 g/L	4.0 g/L (4 mg/mL)	**6 mL**	1.5 mL
After autoclaving **add Mg and Ca aseptically****					
Magnesium Solution (1M, filter sterilized)			g / 50mL stock	**1 mL**	0.25 mL
$MgSO_4 \bullet 7H_20$	246.5	0.121 g/L	6.03		
$MgSO_4$ (anhydrous)	120.0	0.0588	2.94		
$MgCl_2$	95.21	0.0486 g/L	2.43		
1X Calcium Solution (1M, filter sterilized)			g / 50mL stock	**0.88 mL**	0.22 mL
$CaCl_2 \bullet 2H_20$	147	0.132 g/L	7.5		
$CaCl_2$ (anhydrous)	111	0.100	5.66		

* To make a concentrated form of WFAM (i.e. 4X WFAM), multiply the prep/L of solution by the concentration factor (use same stock solutions).
** Precipitation in WFAM can be minimized by adding the Mg and Ca solutions aseptically to small batches of media from the original media.

A.2 Preparation Matrix for WFAM with varying NH4+ / NO3- Ratios

Preparation Matrix for WFAM Formulations based on 0.297 g N/L @ 1X 1/18/2011 ALT

This matrix gives the amounts of KNO3 and NH4NO3 to weigh out for a 1L prep of varying permutations of WFAM, where the basis is that a 1X overall concentration contains a total of 0.297 gN/L. ***Permutations that result in overall POTASSIUM concentrations close to the 0.271 g K/L of WFAM are highlighted in red.***

NOTE: *the original WFAMc formulation does NOT fall in this category, as it was designed to have 0.32 gN/L.*

NOTE: *using Mg for Chlorella will modify the total N concentration and the NH4 ratio as this solution contains MgNO3. This table is based on using the original Mg for Botry solution.*

HOW TO USE THE TABLES: Knowing the overall desired strength (vertical axis) and desired NH4 strength (relative to the ORIGINAL WFAM - horizontal axis) the appropriate amounts of each N source can be determined by the intersection of the row and column. For example, to make 20X strength 1.1x NH4, you need 13.420 g NH4NO3 and 8.918 g KNO3 (shown in grey).

NH4NO3 GRAMS PER LITER PREP:

NH4 Strength:	0 NH4	1/8 NH4	1/4 NH4	1/2 NH4	WFAM	1.1 NH4	1.2 NH4	1.3 NH4	1.35 NH4	NH4NO3
Overall Strength:	**0**	**0.125**	**0.25**	**0.5**	**1**	**1.1**	**1.2**	**1.31**	**1.35**	**1.389355**
0.25 X	0.000	0.019	0.038	0.076	0.153	0.168	0.183	0.200	0.206	0.212
0.325 X	0.000	0.025	0.050	0.099	0.198	0.218	0.238	0.260	0.268	0.275
0.5 X	0.000	0.038	0.076	0.153	0.305	0.336	0.366	0.400	0.412	0.424
1 X	0.000	0.076	0.153	0.305	0.610	0.671	0.732	0.799	0.824	0.848
1.5 X	0.000	0.114	0.229	0.458	0.915	1.007	1.098	1.199	1.235	1.271
2 X	0.000	0.153	0.305	0.610	1.220	1.342	1.464	1.598	1.647	1.695
5 X	0.000	0.381	0.763	1.525	3.050	3.355	3.660	3.996	4.118	4.238
10 X	0.000	0.763	1.525	3.050	6.100	6.710	7.320	7.991	8.235	8.475
15 X	0.000	1.144	2.288	4.575	9.150	10.065	10.980	11.987	12.353	12.713
20 X	0.000	1.525	3.050	6.100	12.200	13.420	14.640	15.982	16.470	16.950

KNO3 GRAMS PER LITER PREP:

NH4 Strength:	0 NH4	1/8 NH4	1/4 NH4	1/2 NH4	WFAM	1.1 NH4	1.2 NH4	1.3 NH4	1.35 NH4	NH4NO3
Overall Strength:	**0**	**0.125**	**0.25**	**0.5**	**1**	**1.1**	**1.2**	**1.31**	**1.35**	**1.389355**
0.25 X	0.535	0.487	0.439	0.343	0.150	0.111	0.073	0.031	0.015	0.000
0.325 X	0.696	0.633	0.571	0.445	0.195	0.145	0.095	0.040	0.020	0.000
0.5 X	1.070	0.974	0.878	0.685	0.300	0.223	0.146	0.061	0.030	0.000
1 X	2.141	1.948	1.756	1.370	0.600	0.446	0.292	0.122	0.061	0.000
1.5 X	3.211	2.922	2.634	2.056	0.900	0.669	0.438	0.183	0.091	0.000
2 X	4.282	3.897	3.511	2.741	1.200	0.892	0.584	0.245	0.121	0.000
5 X	10.705	9.742	8.778	6.852	3.000	2.230	1.459	0.612	0.303	0.000
10 X	21.409	19.483	17.557	13.705	6.000	4.459	2.918	1.223	0.607	0.000
15 X	32.114	29.225	26.335	20.557	9.000	6.689	4.377	1.835	0.910	0.000
20 X	42.819	38.966	35.114	27.409	12.000	8.918	5.836	2.446	1.214	0.001

A.3 Rhodobacter capsulatus Medium (MR26+) – Defined Media

	MW	[final]	[stock]	prep / L	/ 250 mL
Ammonium Succinate Solution				**20 mL**	5 mL
Succinic acid (free)	118.09	1.83	**91.5 g/L**		
Ammonium Hydroxide (NH_4OH) (in liquid form)	35.05		**104.5 mL/L** (~14.9 N)		
pH to 6.8 (in ~500mL) with NH_4OH					
Ammonium Succinate	152.15	2.36 g/L	**-na-**	2.36 g	0.59 g
The following generates additional NaCl					
Na_2-succinate ($Na_2C_4H_4O_4$-$6H_2O$)	270.1	4.19	**-na-**	4.19	1.05
NH_4Cl	53.49	1.66	**-na-**	1.66	0.415
MR26 Phosphates (50x, 1M) (pH 6.8) 1M				**20 mL**	5 mL
K_2HPO_4 (dibasic)	174.18	2.3 g/L	115 g/L		
KH_2PO_4 (monobasic)	136.09	0.898 g/L	44.9 g/L		
pH to 6.8 with KOH or H_3PO_4					
MR26 MICROnutrients (1000x)			g/L stock	**1 mL**	0.25 mL
$ZnSO_4 \bullet 7H_20$	287.56	0.0109	10.9		
$ZnSO_4 \bullet H_20$	179	0.00679	6.79		
$ZnSO_4$ (anhydrous)	161.47	0.00612	6.12		
$MnCl_2 \bullet 4H_20$	197.41	0.0013	1.3		
$CuSO_4 \bullet 5H_20$	249.7	0.000392	0.392		
$CoCl_2 \bullet 6H_20$	237.93	0.0002	0.200		
$(NH_4)_6Mo_7O_{24} \bullet 4H_20$	1235.86	0.000186	0.186		
H_3BO_3 (boric acid)	61.83	0.000114	0.114		
Fe-EDTA$\bullet 2H_20$ (F)	403.1	0.0101	4.0 g/L (4 mg/mL)	**2.5 mL**	0.625 mL
NaCl	58.44	0.234 g/L	**-na-**	**0.234 g**	0.059 g
After autoclaving add Mg, Ca, and vitamins aseptically					
Magnesium Solution (2M, filter sterilized)			g /50mL stock	**1.205 mL**	0.301 mL
$MgSO_4 \bullet 7H_20$	246.5	0.596	24.65		
$MgSO_4$ (anhydrous)	120.0	0.29	12.0		
Calcium Solution (1M, filter sterilized)			g /50mL stock	**0.45 mL**	0.1125 mL
$CaCl_2 \bullet 2H_20$	147	0.0662	7.5		
$CaCl_2$ (anhydrous)	111	0.050	5.66		

	MW	[final]	[stock]	prep / L	/ 250 mL
Vitamin Stock (1000x) Filter sterilized, 4°C			g/ 100mL stock	**1 mL**	0.25 mL
Nicotinic acid		3.0 mg/L	0.3		
Nicotinamide ^^		3.0 mg/L	0.3		
Thiamine-HCl		6.0 mg/L	0.6		
Biotin		0.12	0.012		

NOTES: ^^ Nicotimamide not in SIS media; Adaptation of MR26 to reflect Macro/Micro media formulations and use the Fe-EDTA typical of other media of the lab as well as the filter sterilized Ca and Mg solutions of M9 bacterial media.

(F) (Ferrous EDTA: $FeNaC_{10}H_{12}N_2O_8$; anhydrous MW=367.1) The original Iron-chelator solution was created by adding 27.3 mg/L $FeSO_4 \bullet 7H_2O$ (FW=278) plus 37.3 mg/L Na_2-EDTA [although the degree of hydration of di-sodium EDTA is not specified on several venders (Sigma, Gibco) the dihydrate (FW=372.2) is the only available form, and this would give the same molarity (0.100 mM) for both Fe and EDTA. The iron-sodium-EDTA is now available, but apparently it has a variable degree of hydration (3 batches - all were different). Equivalent Fe and EDTA molarity can be calculated: Fe-EDTA$\bullet$[$2H_2O$] (FW=403.1), 4.03 g/L; [$\bullet 2.5H_20$] (FW=412.1), 4.12 g/L; [$\bullet 3H_20$] (FW=421.1), 4.21 g/L

Appendix B

Summary of Theoretical and Experimental Heat of Combustions for Algal Hydrocarbons, Lipids, Biomass, and Total Culture

Table B.1: Summary of Theoretical and Experimental Heat of Combustions for Algal Hydrocarbons, Lipids, Biomass and Total Culture

	Theoretical	Experimental
B. braunii triterpene hydrocarbons (botryococcenes)	-43.9 kJ/g oil (HHV) Notes: assuming the structure shown in Figure B.1 below	-44.8±1.3 kJ/g oil (HHV) Source: *B. braunii*, Race B (var: Showa) algal oil extracts. See method in Ch. 2.
C. vulgaris lipids	-37.3 kJ/g oil Notes: Based on 10 different lipid species found in *C. vulgaris* by DTE and FID. A weighted average according to Table B.1 was calculated.	n/a
B. braunii, Total Culture	n/a	35.5±0.7 kJ/g AFDW total culture Source: Freeze-dried *B. braunii* total culture collected during steady-state of HD, LL, TS Reactor Run
B. braunii, Biomass cell pellet	n/a	37.8±0.8 kJ/g AFDW cell Source: Freeze-dried *B. braunii* cell collected during steady-state of HD, LL, TS Reactor Run
C. vulgaris, Total Culture	n/a	19.5±1.1 kJ/g AFDW total culture Source: Freeze-dried *C. vulgaris* total culture collected during steady-state of HD, LL, TS Reactor Run
C. vulgaris, Biomass cell pellet	n/a	22.6±1.2 kJ/g AFDW cell Source: Freeze-dried *C. vulgaris* cell collected during steady-state of HD, LL, TS Reactor Run
Method:	Bond-energy method (Hill and Holman 2000), assuming complete combustion to CO_2 and H_2O	Adiabatic Bomb Calorimetry with Benzene Standard. See Ch.2 for complete method.

Figure B.1: Structure of $C_{34}H_{58}$ Botryococcene used in theoretical Enthalpy of Combustion Calculation

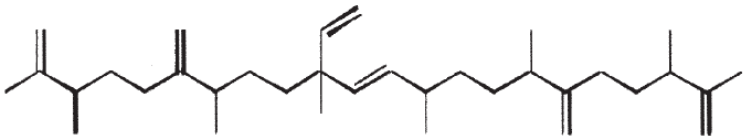

Reference: Anirban Banerjee et al. 2002 (Table 2b, Structure 9)

Table B.2: Lipid species of *C. vulgaris* and proportion of total lipids for weighting of theoretical $\Delta H_{combustion}$ calculation

Conventional abbreviation	IUPAC name	Theoretical ΔH_{comb} (HHV) (kJ/g)	Average % of total lipid:
C16:2($\Delta^{7,10}$)	7,10-hexadecadienoic acid	-36.88	10.55
C16:3($\Delta^{7,10,13}$)	7,10,13-hexadecatrienoic acid	-36.71	8.64
C16:1(Δ^{7})	7 -hexadecenoic acid	-37.04	3.68
C16:1(Δ^{9})	9 -hexadecenoic acid	-37.04	2.09
C16:0	hexadecanoic acid	-37.17	23.72
14Me-C16:0	14-methyl-hexadecanoic acid	-37.57	1.94
C18:2($\Delta^{9,12}$)	9,12-octadecadienoic acid	-37.57	26.40
C18:3($\Delta^{9,12,15}$)	9,12,15-octadecatrienoic acid	-37.44	13.03
C18:1(Δ^{9})	9-octadecenoic acid	-37.72	5.03
C18:1(Δ^{7})	7-octadecenoic acid	-37.72	3.21
C18:0	octadecanoic acid	-37.86	1.69
	Weighted Average:	**-37.3**	

Appendix C

Example Chromatogram for GC Analysis of Triterpene (Botryococcene) Hydrocarbons

Chromatograms of three separate oil samples

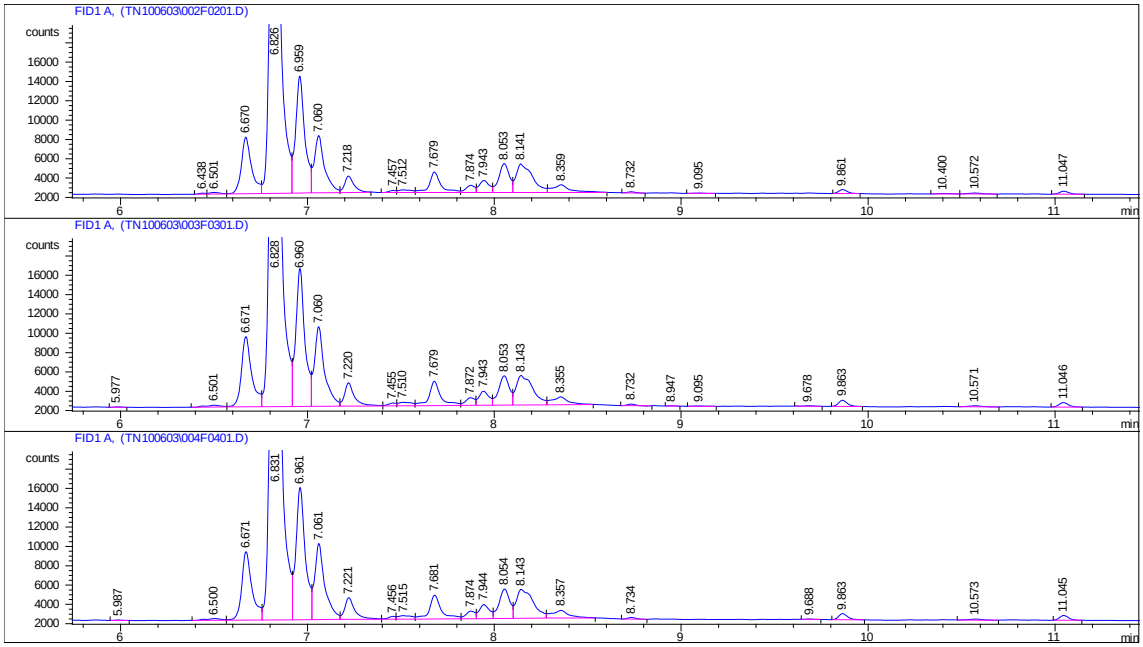

Chromatograms of Squalene Standards of 5 ng/µL, 25 ng/µL, and 100 ng/µL, respectively

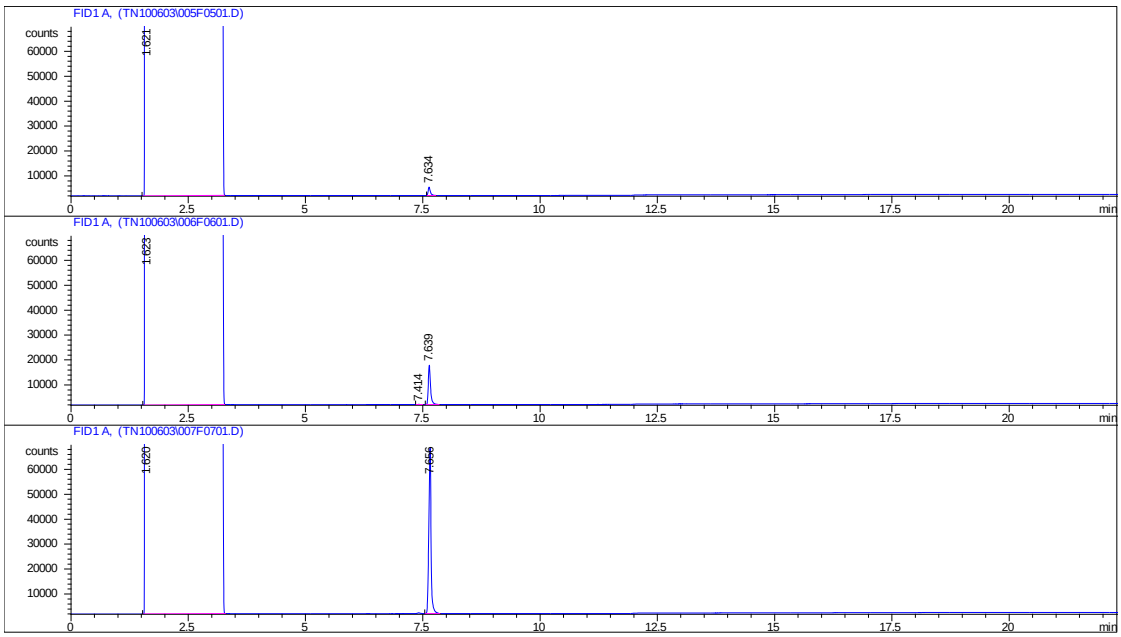

Appendix D

Half Reactions Utilized in the Microbial Energetics Assessment and their $\Delta G^{0'}$

Half Reactions				$\Delta G^{0'}$ (kJ/eeq)
Hydrogen	$H^+ + e^-$	=	$0.5\ H_2$	39.9 [(1)]
Oxygen	$0.25\ O_2 + H^+ + e^-$	=	$0.54\ H_2O$	-78.7 [(1)]
Ubiqinone	$0.5\ UQ + H^+ + e^-$	=	$0.5\ UQH_2$	-10.9 [(2)]
NADH	$0.5\ NAD^+ + 0.5\ H^+ + e^-$	=	0.5 NADH	30.9 [(3)]
Acetyl-CoA	$0.25\ CO_2 + 0.125$ CoA-H$+H^+ + e^-$	=	0.125 AcCoA$+0.375\ H_2O$	33.3 [(4)]

(1) Rittman and McCarty 2001

(2) Value obtained from E= +113 mV potential for reduced ubiquinone (Thauer, Jungermann, and Decker 1977) and Nernst Equation: $\Delta G = -n\ F\ E = -10.9$ kJ/ee

(3) McCarty 2007

(4) Value derived using the value of the redox reaction of pyruvate to AcCoA (www.biochem.arizona.edu/classes/bioc460/spring/460web/lectures/Bioc460Miesfeld-2008/Lec27-Spr2008/27-RedoxRxns.ppt), then subtracting out the reactions for pyruvate and NADH.

Appendix E

Procedure for Constructing Balanced Half-Reactions for Microbial Synthesis

To construct balanced half reactions for biomass synthesis, the following items must be known:

- An empirical formula which represents the cell composition: $C_aH_bO_cN_dP_eS_f$. When a product fuel is synthesized, the overall composition needs to be weighted according to the molar distribution between fuel and cell mass synthesis, using α (mol fuel /mol cell synthesized):
    - If the <u>cell</u> composition is $C_AH_BO_CN_DP_ES_F$ and the fuel formula is $C_XH_YO_Z$, then the elemental subscripts in the <u>biomass</u> formula will be:
        - Carbon: $a = (1-\alpha)A + \alpha\, X$
        - Carbon: $b = (1-\alpha)B + \alpha\, Y$
        - Carbon: $c = (1-\alpha)C + \alpha\, Z$
        - Carbon: $d = (1-\alpha)D$
        - Carbon: $e = (1-\alpha)E$
        - Carbon: $f = (1-\alpha)F$
- The chemical species that are the sources of nitrogen, phosphorus, and sulfur
- The oxidized carbon source is always CO_2

Construction of the balanced half-reaction proceeds by the following steps. The example shownt utilizes NH_4^+, PO_4^{3-}, and SO_4^{2} as the nitrogen, phosphorus, and sulfur sources:

1. Balance the carbon for the creation of 1 mol of biomass:

$$a\ CO_2 = C_aH_bO_cN_dP_eS_f$$

2. Balance the Nitrogen, Phosphorus, and Sulfur:

$$a\ CO_2 + d\ NH_4^+ + e\ PO_4^{3-} + f\ SO_4^{2-} = C_aH_bO_cN_dP_eS_f$$

3. Balance the oxygen by adding water, where in this case $g = (2\cdot a + 4\cdot e + 4\cdot f - c)$:

$$a\ CO_2 + d\ NH_4^+ + e\ PO_4^{3-} + f\ SO_4^{2-} = C_aH_bO_cN_dP_eS_f + g\ H_2O$$

4. Balance the hydrogen by adding H^+, where in this case $h = (b + 2\cdot g - 4\cdot d)$:

$$a\ CO_2 + h\ H^+ + d\ NH_4^+ + e\ PO_4^{3-} + f\ SO_4^{2-} = C_aH_bO_cN_dP_eS_f + g\ H_2O$$

5. Balance the charge by adding electrons (e^-), where in this case $Q = (d + h - 3\cdot e - 2\cdot f)$:

$$a\ CO_2 + h\ H^+ + Q\ e^- + d\ NH_4^+ + e\ PO_4^{3-} + f\ SO_4^{2-} = C_aH_bO_cN_dP_eS_f + g\ H_2O$$

6. Normalize the half-reaction for a single mol of electrons by dividing through by j.

$$\tfrac{a}{Q}\ CO_2 + \tfrac{h}{Q}\ H^+ + 1\ e^- + \tfrac{d}{Q}\ NH_4^+ + \tfrac{e}{Q}\ PO_4^{3-} + \tfrac{f}{Q}\ SO_4^{2-} = \tfrac{1}{Q}\ C_aH_bO_cN_dP_eS_f + \tfrac{g}{Q}\ H_2O$$

Appendix F

Parameters used in EB Calculations for True Yields

Parameter	Value	Units	Reference / Rationale
[CoA-H]	2.42E-04	mol/L	Thauer, Jungermann, and Decker 1977. The values in this reference were for anaerobic bacteria; it was assumed that the same order of magnitude of concentration would apply here.
[AcCoA]	9.20E-04	mol/L	
[NAD^+]	1.25E-02	mol/L	
[NADH]	3.36E-03	mol/L	
[UQ]	1.19E-02	mol/L	in the absence of other information, conc. of (UQ +UQH_2) assumed to be ~ (NAD^++NADH); dist. between UQ and UQH_2 was determined on the basis of the degree of reduction of the pool, assumed to be 25%
[UQH_2]	3.97E-03	mol/L	
[NH_4Cl] [NH_4^+]	0.01869 0.01853	mol / L mol /L @ pH=7.0	Based on concentrations in MR26 Medium (See Appendix A.1)
[PO_4^{3-}]	0.01912	mol/L	
[SO_4^{2-}]	0.00845	mol/L	
$k_{O_2}(298K)$	769.2	L/atm/mol	http://en.wikipedia.org/wiki/Henry's_law
$k_{H_2}(298K)$	1282.1	L/atm/mol	
$k_{CO_2}(298K)$	29.41	L/atm/mol	
φ_{O_2}	1700	K^{-1}	
φ_{H_2}	500	K^{-1}	
φ_{CO_2}	2400	K^{-1}	
D_{O2}	2.5E-09	m^2/s	(Perry and Green 1997)
D_{H2}	5.9E-09	m^2/s	
D_{CO2}	2.0E-09	m^2/s	
$\Delta G^{0'}_{ATP,hydrolysis}$	52.3	kJ/mol ATP	(McCarty 1971)

Parameters for NH_4^+/NH_3 Equilibrium

pKa	$= -0.467 + 2.887.9/T$	(Bell et al. 2007)

Method of Ammonium/Ammonia Equilibrium Calculation:

1. Assuming the equilibrium: $NH_4^+ \leftrightarrow NH_3 + H^+$, with $K_a = \frac{[H^+][NH_3]}{[NH_4^+]}$
2. Use formula $pK_a = -0.467 + 2.887.9/T$ to calculate pK_a
3. $pK_a = pH + \log\left(\frac{[NH_4^+]}{[NH_3]}\right)$, use pH and pK_a to obtain ratio $\frac{[NH_4^+]}{[NH_3]}$
4. Total $[NH_4Cl] = [NH_4^+] + [NH_3]$, on a molar basis

Solve for $[NH_4^+]$ and $[NH_3]$

Appendix G

The Gibbs Energy Dissipation Theory

This theory is discussed extensively elsewhere and the reader is referred to several sources for detailed descriptions and discussion: (Heijnen and van Dijken 1992; Heijnen, van Loosdrecht, and Tijhuis 1992; Tijhuis, van Loosdrecht, and Heijnen 1993; von Stockar et al. 2006; Jingsong Liu et al. 2007). In summary, the main idea of this theory can be stated simply as "Biomass yields are intimately connected to the driving force for microbial growth." Microbial growth occurs spontaneously, and is highly irreversible, so the growth must be coupled to the production of entropy. This seems contradictory to the concept of growth, because growth produces matter in a highly organized form from small simple materials. However, when examining the open-system entropy balance of a cell (von Stockar et al. 2006):

$$\frac{dS}{dt} = \frac{\dot{Q}}{T} + \sum(\bar{s}_i \cdot \dot{n}_i) - \bar{s}_x \cdot \dot{n}_x + \dot{S}_{prod} \qquad \textbf{Equation 7.1}$$

it is observed that entropy variation occurs through several different modes. Entropy is exchanged with the environment due to heat transfer to or from the cell. Entropy is also imported and exported in the cell in by the intake of substrates and the excretion of products, where $\bar{s}_i$ is the partial molar entropy of the *i*th metabolite, and $\dot{n}_i$ is its molar rate of exchange. Newly formed biomass is modeled as a product of the cell leaving at a molar rate of $\dot{n}_x$, and its partial molar entropy $\bar{s}_x$ will necessarily be low. The rate of entropy production, $\dot{S}_{prod}$ is the driving force for the process, and must be positive as dictated by the Second Law of Thermodynamics.

In the assumption of a constant entropy in the cell (dS/dt = 0), to avoid the accumulation of entropy in the cell, excess entropy must be exported. Therefore the sum of the first three terms

on the right hand side of Equation 100 must be be negative and balance out the entropy production term $Sdot_{prod}$. Cells export excess entropy by either:

- creating a large flux of small waste molecules from the substrate (export in the form of chemical entropy)
- releasing considerable amounts of heat.

By multiplying the entropy balance (Equation 7.1) by T, and subtracting from the enthalpy balance (Equation 7.2), the Gibbs free energy balance is obtained (Equation 7.3):

$$\frac{dH}{dt} = \dot{Q} + \dot{W} + \sum_i \left(\bar{h}_i \cdot \dot{n}_i\right) - \bar{h}_x \cdot \dot{n}_x \qquad \textbf{Equation 7.2}$$

$$\frac{dG}{dt} = \dot{W} + \sum_i (\bar{\mu}_i \cdot \dot{n}_i) - \bar{\mu}_x \cdot \dot{n}_x - T\dot{S}_{prod} \qquad \textbf{Equation 7.3}$$

where $\dot{W}$ stands for the power or work done on the cells. dG/dt must be kept at zero despite the loss of Gibbs energy through the newly formed biomass, as the chemical potential of the biomass is necessarily high due to its low entropy, and despite the loss of Gibbs energy through dissipation in the $-T\dot{S}_{prod}$ term, which must be negative. For chemotrophs, where generally no work is done on the cell and therefore $\dot{W}$ is 0, the Gibbs energy must be replenished by the consumption of high energy growth substrates.

Finally, by constructing a molar balance on the cells (Equation 7.4), and assuming steady state (dG/dt and $dn_i/dt = 0$), yields Equation 7.5.

$$\frac{dn_i}{dt} = n_i + \nu_i \cdot \dot{\xi} \qquad \textbf{Equation 7.4}$$

$$\Delta_r G_x = -\frac{T\dot{S}_{prod}}{\dot{\xi}} \qquad \textbf{Equation 7.5}$$

where $\Delta_r G_x$ is the molar Gibbs reaction energy of the overall growth reaction and $\dot{\xi}$ is the rate of the growth reaction in C-mole/s (von Stockar et al. 2006). Because $\dot{S}_{prod}$ can only be positive according to the Second Law of Thermodynamics, $\Delta_r G_x$ must be negative for growth to occur,

and therefore, overall, growth is exergonic. Because of the direct relationship between entropy generation, $\Delta_r G_x$ is considered the driving force for cellular growth.

To better understand the relationship between this driving force $\Delta_r G_x$ and the biomass yield, a formulation for the overall growth equation is created (Equation 7.6). The equation is expressed in terms of the yield of the i^{th} metabolite with respect to biomass ($Y_{i/X}$) and the yield of biomass on the electron donor ($Y_{X/ED}$); ED = electron donor, EA = electron acceptor, NS = nitrogen source, CS = carbon source, X = biomass, P = the reduced electron acceptor, and DOX = the oxidized electron donor.

Equation 7.6

$$\frac{1}{Y_{X/ED}} ED + Y_{EA/X} EA + Y_{CS/X} CS + Y_{NS/X} NS \rightarrow X + Y_{P/X} P + Y_{CS/X} CS + Y_{DOX/X} DOX$$

This overall growth equation is then conceptually split into a catabolic and anabolic part. The anabolic reaction is endergonic, and relies upon the highly exergonic catabolic reaction to provide the energy required for anabolic reactions. The net $\Delta_r G_x$ remaining for the whole process is thus dependent on the extent of the load anabolism places upon catabolism. At one extreme, $\Delta_r G_x$ could approach a maximum of 0 when all the catabolic energy available is re-invested into anabolic reactions, leading to a maximal cell yield, but leaving only a small overall ΔG for the whole process. As the Second Law of Thermodynamics stipulates that the overall ΔG is negative, this situation is therefore the upper bound on yield created by the second law. It represents growth at thermodynamic equilibrium, where growth would proceed infinitely slowly. Note that, as mentioned above, this situation is equivalent in the **EB** theory when the cellular efficiency is set to a value of $\varepsilon = 1$: all the available energy is captured with 100% efficiency. At the other end of the spectrum, however, $\Delta_r G_x$ would approach a maximum when little of the catabolic energy is re-invested into cell mass, leading to very low yields but a large driving force in the ΔG for the process, and thus metabolism would proceed vigorously. Conversely, this situation corresponds

to a $\varepsilon \approx 0$ in the **EB** theory. It is generally believed that organisms have evolved to strike a balance between these two extremes, such that a reasonable yield of biomass is produced with sufficient Gibbs energy dissipation to drive metabolism forward (von Stockar et al. 2006; Jingsong Liu et al. 2007).

The quantitative relationship between $\Delta_r G_X$ and the biomass yield on the electron donor ($Y_{X/ED}$) can be derived by using the formulations for the catabolic and anabolic reactions in Equation 7.7 and Equation 7.8 below, and then observing that the overall growth equation (Equation 7.6) can be re-obtained by dividing Equation 7.7 by $Y_{X/ED}$ and adding this to Equation 7.8, and therefore Equation 7.9 can be deduced.

$$ED + Y_{EA}^{cat} EA \rightarrow Y_P^{cat} P + Y_{DOX}^{cat} ED_{OX} \qquad (\Delta G_{cat}^o) \qquad \textbf{Equation 7.7}$$

$$Y_P^{an} P + Y_{DOX}^{an} ED_{OX} + Y_{NS}^{an} NS \rightarrow X + Y_{EA}^{an} EA \qquad (\Delta G_{an}^o) \qquad \textbf{Equation 7.8}$$

$$-\Delta_r G_X^o = \frac{1}{Y_{X/ED}} \Delta G_{cat}^o + \Delta G_{an}^o \qquad \textbf{Equation 7.9}$$

ΔG_{cat}^o and ΔG_{an}^o are calculated from Equation 7.8 and Equation 7.9, using the Gibbs energy of combustion for each species, calculated on a carbon-mol basis; the authors defined a convenient reference state such that the completely oxidized state of matter (e.g. CO_2, H_2O, O_2) has a Gibbs energy of combustion of zero (Heijnen and van Dijken 1992). When other elements come into play, the reference state also includes them in the most oxidized state in which they occur in the growth equation; thus the nitrogen source is included as at the reference state. Invariably, this stipulates that ED_{OX} will be at the reference state as well. Finally, whenever the electron donor and the carbon source are not the same species, the carbon source is nearly always CO_2, so that Equation 7.8 and Equation 7.9 become significantly simplified. A table with values for a variety of species using this 'combustion reference' can be found in Heijnen and Van Dijken 1992; the value for $\Delta_c G_{H2}^o$ was taken from the value reported in (Jingsong Liu et al. 2007).

It is in this conceptual split between the catabolic and anabolic reactions where the **EB** theory and the Gibbs energy dissipation theory primarily deviate: in the Gibbs Energy dissipation theory, whereas the catabolic reaction has as its substrates the electron donor and the electron acceptor, the anabolic reaction uses as its substrates the *oxidized* electron donor and the reduced electron acceptor. This makes the implicit assumption that the available electron donor is first completely catabolized and then the biomass is formed from the products of the catabolism, which the authors of the Gibbs energy dissipation theory repeatedly recognize as an unrealistic representation of growth (Heijnen and van Dijken 1992; von Stockar et al. 2006; Jingsong Liu et al. 2007). (Jingsong Liu et al. 2007), in fact compared several methods of re-formulating the anabolic reaction for more realistic assumptions for growth, and found that Equation 108 must be re-derived in these cases. However, considering that another way of quantifying $\Delta_r G_x$ is from the overall growth equation (Equation 7.6), Equation 7.10 results after realizing that within the combustion reference frame, $\Delta_c G_A^o$, $\Delta_c G_{DOX}^o$, and $\Delta_c G_{NS}^o$ are all equal to 0. γ_{ED}, γ_P, γ_x, are the degrees of reduction for the Electron Donor, the reduced electron acceptor, and the biomass respectively. This can then be rearranged to Equation 7.11 to solve for the biomass yield on the electron donor; this result is the same no matter what anabolic reaction formulation is chosen (Jingsong Liu et al. 2007) and is also independent of the reference state chosen (Heijnen and van Dijken 1992; von Stockar et al. 2006). In these equations, the Gibbs energy of combustion of biomass at the reference state is taken to be $\Delta_c G_x^* = 474$ kJ/C-mol biomass (Heijnen and van Dijken 1992).

$$-\Delta_r G_x^o = \frac{1}{Y_{X/ED}}\left(\Delta_c G_{ED}^o - \frac{\gamma_D}{\gamma_P}\Delta_c G_P^o\right) + \frac{\gamma_X}{\gamma_P}\Delta_c G_P^o - \Delta_c G_X^* \qquad \textbf{Equation 7.10}$$

$$Y_{X/ED} = \frac{\Delta_c G_{ED}^o - \left(\gamma_{ED}/\gamma_P\right)\Delta_c G_P^o}{\Delta_c G_X^o - \Delta_r G_X^* - \left(\gamma_X/\gamma_P\right)\Delta_c G_P^o} \qquad \textbf{Equation 7.11}$$

Because in aerobic autotrophic growth, P is H_2O, which has a $\Delta_c G_P^o$ of 0, Equation 7.10 simplifies to Equation 7.12 and Equation 7.11simplifies to Equation 7.13(Jingsong Liu et al. 2007).

$$-\Delta_r G_X^o = \frac{1}{Y_{X/ED}} \Delta_c G_{ED}^o - \Delta_c G_X^* \quad \textbf{Equation 7.12}$$

$$Y_{X/ED} = \frac{\Delta_c G_{ED}^o}{\Delta_c G_X^o - \Delta_r G_X^*} \quad \textbf{Equation 7.13}$$

Thus, the hypothesis is that metabolism under optimal conditions for growth will trend towards a predictable value Gibbs energy dissipation (kJ/C-mol biomass produced). Then, armed with the overall growth equation (Equation 7.6) and thermodynamic values associated with the energetics of the catabolic and anabolic reactions, the Gibbs energy dissipation is the factor which will correlate with biomass yield on the electron donor.

Correlation of $\Delta_r G_x^o$ with Yield Data

Heijnen and van Dijken (1992) calculated the Gibbs energy dissipated per biomass grown for a wide range of microorganisms growing on a wide range of carbon sources for which yield data was available; the database for this information is included in their manuscript, and J Liu et al. (2007) supplemented this database with additional data. Heijnen and van Dijken (1992) observed that the Gibbs energy dissipated per C-mol of biomass grown appeared to correlate with both the number of carbon atoms in the carbon source as well as the degree of reduction of the electron donor, but that is independent of the electron acceptor. 'Ideal' electron donor and carbon source substrates, which have a degree of reduction (γ_D) of 3.8 and 6 carbon atoms, generate a minimum value of -200 kJ/C-mol Gibbs free energy, and a correlation accounts for deviations from these ideal properties for the carbon source with a standard error of ±11%

(Equation 7.14). The value of Gibbs energy dissipation for chemotrophic growth with reverse electron transport is simply taken as $-\Delta_r G_x^o$ = 3500 kJ/C-mol (Heijnen and van Dijken 1992).

$$-\Delta_r G_x^o = 200 + 18(6 - n_c)^{1.8} + exp\{[(3.8 - \gamma_s)^2]^{0.16} \times (3.6 + 0.4n_c)\} \quad \textbf{Equation 7.14}$$

J Liu et al. (2007) greatly simplified this correlation, to Equation 7.15 and Equation 7.16, although this correlation applies to aerobic growth only; and also took the value of 3500 kJ/C-mol for reversed electron growth.

$$\Delta_r G_X^o = \frac{-666.2}{\gamma_D} - 243.1 \qquad (\gamma_D \leq 4.67) \quad \textbf{Equation 7.15}$$

$$\Delta_r G_X^o = -157\gamma_D - 339 \qquad (\gamma_D \geq 4.67) \quad \textbf{Equation 7.16}$$

However, the vast majority of the data utilized to develop these correlations is based upon heterotrophic growth on reduced carbon source; only a small fraction of the data is from autotrophic growth. Furthermore, for the very specific metabolism under investigation in this paper, hydrogen oxidation under aerobic conditions, there is only a single entry in the database. The majority of the autotrophic metabolism included in the correlation was anaerobic oxidation of CO_2 to methane or aerobic oxidation of inorganic ions (ammonia, nitrite, iron, hydrogen sulfide, and thiosulfate), the energetics of which are extremely different than aerobic hydrogen oxidation. Plotting the Gibbs free energy predicted by the correlations versus the Gibbs free energy calculated from the yield for all autotrophic growth data, using the database provided in J Liu et al. (2007) results in Figure 7.1-(A). Anaerobic data was not included in the J Liu et al. (2007) correlation points. As can be seen, the correlation based only upon degree of reduction of the electron donor and the number of carbon atoms in the carbon source does not predict Gibbs free energy dissipated for autotrophic growth well. This is further demonstrated in Figure 7.1-(B), which shows the predicted Gibbs Free energy dissipated as a function of γ_D of the electron donor. Therefore, it would appear that the correlations developed by Heijnen and van Dijken (1992) and J Liu et al. (2007) do not describe the Gibbs energy dissipated during growth of

autotrophic organisms, and that the degree of reduction and number of carbon atoms of the electron donor and carbon source are not good predictors of this data set.

Figure 7.1: (A) – Gibbs energy dissipated as calculated from literature data, versus the GED Predicted by Correlations. (B) – GED Caculated from literature date versus electron donor degree of reduction

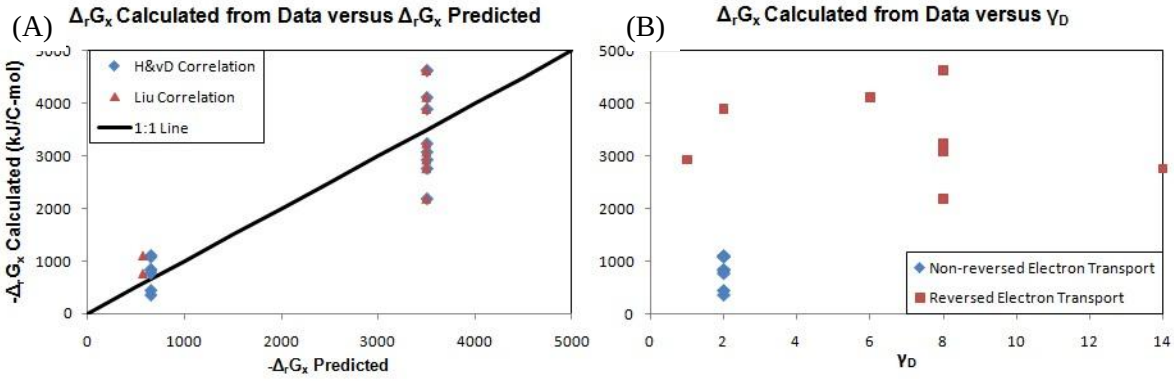

Because the data used to generate the data set came many different sources, there is no standardization in the conditions of growth for the variety of organisms and growth modes. Therefore, there is considerable uncertainty in the yield data used to develop the correlations (Jingsong Liu et al. 2007). Furthermore, although the intent of the Gibbs Energy dissipation correlation is to enable prediction of a *minimal* $\Delta_r G_x$, and therefore a maximum yield (Tijhuis, van Loosdrecht, and Heijnen 1993), it is not immediately clear whether the yield data utilized in the database was based upon measured apparent yields (Y^{AP}) or maximum yields (Y^{M}) estimated from the Pirt equation or another method.

Despite the fact that the correlations developed by Heijnen and van Dijken and J. Liu et al. do not seem to be particularly useful for the prediction of growth by the aerobic oxidation of hydrogen, the concept of a 'typical' minimum Gibbs energy of dissipation is a reasonable theory on how microbial life would have adapted to a competitive compromise between maximal

biomass yields and maximum metabolic rate. This should particularly be true within a single species growing under optimal conditions in a specific metabolic mode.

Relationship and Equivalency between the EB Theory and the GED Theory

The goal of each the EB method and the GED method is the development of a stoichiometrically balanced growth equation, from which yields for biomass production on any of the substrates could then be calculated. Making the assumption that both theories are valid, but different, methods of predicting this stoichiometrically balanced growth equation, then the resulting equations from each theory should be equivalent and furthermore, the Gibbs energy change for the equation (ie. the Gibbs Energy dissipated) should also be the same. However, problems arise because of the single reported value for cell mass, $\Delta_c G_x^*$ in the combustion reference for the GED theory. This value cannot be adjusted for varying cell composition without further information as to how it was originally obtained. Also, in attempting to convert between this value in the combustion reference and the redox reference states, the values do not appear equivalent.

REFERENCES

An, Jin-Young, Sang-Jun Sim, Jin Suk Lee, and Byung Woo Kim. 2003. "Hydrocarbon production from secondarily treated piggery wastewater by the green alga Botryococcus braunii." *Journal of Applied Phycology* 15 (2/3) (March): 185-191. doi:10.1023/A:1023855710410.

Banerjee, Anirban, Rohit Sharma, Yusuf Chisti, and U C Banerjee. 2002. "Botryococcus braunii: a renewable source of hydrocarbons and other chemicals." *Critical reviews in biotechnology* 22 (3) (January): 245-79. doi:10.1080/07388550290789513.

Battley, Edwin H. 1987. *Energetics of Microbial Growth*. *Handbook of Thermal Analysis and Calorimetry. Vol. 4: From Macromolecules to Man.* New York: John Wiley & Sons.

———. 1999. The Thermodynamics of Microbial Growth. In *Handbook of Thermal Analysis and Calorimetry. Vol. 4: From Macromolecules to Man*, ed. Patrick Kent Gallagher, Michael E Brown, and Richard B Kemp, 245. 1st ed. Amsterdam: Elsevier Science B.V.

Bauchop, T, and S R Elsden. 1960. "The growth of micro-organisms in relation to their energy supply." *Journal of general microbiology* 23 (December): 457-69.

Bell, Thomas G., Martin T. Johnson, Timothy D. Jickells, and Peter S. Liss. 2007. "Ammonia/ammonium dissociation coefficient in seawater: A significant numerical correction." *Environmental Chemistry* 4 (3): 183. doi:10.1071/EN07032.

Benemann, John R, and William J Oswald. 1996. *Systems and Economic Analysis of Microalgae Ponds for Conversion of CO2 to Biomass*.

Berberoglu, Halil, Pedro S. Gomez, and Laurent Pilon. 2009. "Radiation characteristics of Botryococcus braunii, Chlorococcum littorale, and Chlorella sp. used for CO2CO2 fixation and biofuel production." *Journal of Quantitative Spectroscopy and Radiative Transfer* 110 (17) (November): 1879-1893. doi:10.1016/j.jqsrt.2009.04.005.

Biggs, William W. *Principles of Radiation Measurement*.

Black, James, and National Energy Technology Laboratory. 2010. *Cost and Performance Baseline for Fossil Energy Plants. Volume 1: Bituminous Coal and Natural Gas to Electricity Final Report*. *National Energy Technology Laboratory*. Vol. 1.

Bongers, L. 1970. "Energy generation and utilization in hydrogen bacteria." *Journal of bacteriology* 104 (1) (October): 145-51.

Bowien, Botho, and Bernhard Kusian. 2002. “Genetics and control of CO2 assimilation in the chemoautotroph Ralstonia eutropha.” *Archives of microbiology* 178 (2) (August): 85-93. doi:10.1007/s00203-002-0441-3.

Bowien, Botho, and Hans G Schlegel. 1981. “Physiology and Biochemistry of Aerobic Hydrogen-Oxidizing Bacteria.” *Annual Reviews in Microbiology* 35 (December): 405-52. doi:10.1016/0167-7799(86)90184-8.

Call, Douglas F, and Bruce E Logan. 2008. “Hydrogen production in a single chamber microbial electrolysis cell lacking a membrane.” *Environmental science & technology* 42 (9) (May 1): 3401-6.

Casadevall, E, D Dif, C Largeau, C Gudin, D Chaumont, and O Desanti. 1985. “Studies on batch and continuous cultures of Botryococcus braunii: hydrocarbon production in relation to physiological state, cell ultrastructure, and phosphate nutrition.” *Biotechnology and bioengineering* 27 (3) (March): 286-95. doi:10.1002/bit.260270312.

Chang, Joseph. 2008. Indicative Chemical Prices A-Z. http://www.icis.com/StaticPages/a-e.htm#C.

Chen, Zhen, Hongjuan Liu, and Dehua Liu. 2009. “Regulation of 3-hydroxypropionaldehyde accumulation in Klebsiella pneumoniae by overexpression of dhaT and dhaD genes.” *Enzyme and Microbial Technology* 45 (4) (October 7): 305-309. doi:10.1016/j.enzmictec.2009.04.005.

Cheng, Shaoan, and Bruce E Logan. 2011. “High hydrogen production rate of microbial electrolysis cell (MEC) with reduced electrode spacing.” *Bioresource technology* 102 (3) (February): 3571-4. doi:10.1016/j.biortech.2010.10.025.

Chisti, M Y. 1989. *Airlift Bioreactors*. New York: Elsevier Applied Science.

Chiu, Sheng-Yi, Chien-Ya Kao, Chiun-Hsun Chen, Tang-Ching Kuan, Seow-Chin Ong, and Chih-Sheng Lin. 2008. “Reduction of CO2 by a high-density culture of Chlorella sp. in a semicontinuous photobioreactor.” *Bioresource technology* 99 (9) (June): 3389-96. doi:10.1016/j.biortech.2007.08.013.

Chu, SP. 1942. “The Influence of the Mineral Composition of the Medium on the Growth of Planktonic Algae: Part I. Methods and Culture Media.” *Journal of Ecology* 30 (2): 284–325.

Collyer, Dorothy M, and G E Fogg. 1955. “Studies on Fat Accumulation by Algae.” *Journal of Experimental Botany* 6 (2): 256-275. doi:10.1093/jxb/6.2.256.

Converti, Attilio, Alessandro a. Casazza, Erika Y. Ortiz, Patrizia Perego, and Marco Del Borghi. 2009. “Effect of temperature and nitrogen concentration on the growth and lipid content of Nannochloropsis oculata and Chlorella vulgaris for biodiesel production.” *Chemical Engineering and Processing: Process Intensification* 48 (6) (June): 1146-1151. doi:10.1016/j.cep.2009.03.006.

Cramm, Rainer. 2009. “Genomic view of energy metabolism in Ralstonia eutropha H16.” *Journal of molecular microbiology and biotechnology* 16 (1-2) (January): 38-52. doi:10.1159/000142893.

Curtis, Wayne R. 1988. Kinetics of Phosphate Limited Growth of Poppy Plant Suspension Cultures. Purdue University.

Cusick, Roland D, Bill Bryan, Denny S Parker, Matthew D Merrill, Maha Mehanna, Patrick D Kiely, Guangli Liu, and Bruce E Logan. 2011. “Performance of a pilot-scale continuous flow microbial electrolysis cell fed winery wastewater.” *Applied microbiology and biotechnology* 89 (6) (March): 2053-63. doi:10.1007/s00253-011-3130-9.

Cusick, Roland D, Patrick D Kiely, and Bruce E Logan. 2010. “A monetary comparison of energy recovered from microbial fuel cells and microbial electrolysis cells fed winery or domestic wastewaters.” *International Journal of Hydrogen Energy* 35 (17) (September): 8855-8861. doi:10.1016/j.ijhydene.2010.06.077.

Degen, Jorg, Andrea Uebele, Ulrike Schmid-Staiger, and Walter Trosch. 2001. “A novel airlift photobioreactor with baffles for improved light utilization through the flashing light effect.” *Journal of Biotechnology* 92 (2): 89-94.

Ditzig, Jenna, Hong Liu, and Bruce E Logan. 2007. “Production of hydrogen from domestic wastewater using a bioelectrochemically assisted microbial reactor (BEAMR).” *International Journal of Hydrogen Energy* 32 (13) (September): 2296-2304. doi:10.1016/j.ijhydene.2007.02.035.

Doty, F David. 2004. *A Realistic Look at Hydrogen Price Projections*. *Carbon*. Vol. 2004. Columbia, SC.

Dubbs, James M, and F Robert Tabita. 2004. “Regulators of nonsulfur purple phototrophic bacteria and the interactive control of CO2 assimilation, nitrogen fixation, hydrogen metabolism and energy generation.” *FEMS Microbiology Reviews* 28 (3) (June): 353-376. doi:10.1016/j.femsre.2004.01.002.

Dupuis, A., A. Peinnequin, E. Darrouzet, and J. Lunardi. 1997. “Genetic disruption of the respiratory NADH-ubiquinone reductase of Rhodobacter capsulatus leads to an unexpected photosynthesis-negative phenotype.” *FEMS microbiology letters* 148 (1): 107–114.

Energy Information Administration. 2008. *The Impact of Increased Use of Hydrogen on Petroleum Consumption and Carbon Dioxide Emissions*. *Carbon*. Washington, DC.

Eroglu, Ela, and Anastasios Melis. 2009. "'Density equilibrium' method for the quantitative and rapid in situ determination of lipid, hydrocarbon, or biopolymer content in microorganisms." *Biotechnology and bioengineering* 102 (5) (April 1): 1406-15. doi:10.1002/bit.22182.

Forrest, W W, and D J Walker. 1971. "The generation and utilization of energy during growth." *Advances in microbial physiology* 5: 213-274.

Friedrich, Bärbel, and Edward Schwartz. 1993. "Molecular biology of hydrogen utilization in aerobic chemolithotrophs." *Annual Reviews in Microbiology* 47 (1): 351–383.

Gamborg, OL, R.A. Miller, and K. Ojima. 1968. "Nutrient requirements of suspension cultures of soybean root cells." *Experimental cell research* 50 (1): 151–158.

Geelhoed, Jeanine S, and Alfons J M Stams. 2011. "Electricity-assisted biological hydrogen production from acetate by Geobacter sulfurreducens." *Environmental science & technology* 45 (2) (January 15): 815-20. doi:10.1021/es102842p.

Geider, Richard J, and Bruce A Osborne. 1992. *Algal Photosynthesis: The Measurement of Algal Gas Exchange*. New York City: Routledge, Chapman & Hall, Inc.

Grady, Lisa K. 2010. A Bioprocessing Comparision of High Density Botryococcus braunii and Chlorella vulgaris verifying light-limited growth. Penn State University, December.

Gray, Kevin A, and Fevzi Daldal. 1995. Mutational studies of the cytochrome bc 1 complexes. In *Anoxygenic Photosynthetic Bacteria*, ed. R E Blankenship, M T Madigan, and C E Bauer, 747–774. Elsevier Academic Publishers.

Grobbelaar, Johan U. 2010. "Microalgal biomass production: challenges and realities." *Photosynthesis research* 106 (1-2) (November): 135-44. doi:10.1007/s11120-010-9573-5.

Hao, Jian, Wei Wang, Jiesheng Tian, Jilun Li, and Dehua Liu. 2008. "Decrease of 3-hydroxypropionaldehyde accumulation in 1,3-propanediol production by over-expressing dhaT gene in Klebsiella pneumoniae TUAC01." *Journal of industrial microbiology & biotechnology* 35 (7) (July): 735-41. doi:10.1007/s10295-008-0340-y.

Harder, W, and J P van Dijken. 1976. Theoretical considerations on the relation between energy production and growth of methaneutilizing bacteria. In *Microbial production*

and utilization of gases (H. G. Schlegel, N. Pfennig, G. Gottschalk, eds.), 403-418. Göttingen: Goltze Verlag.

Heijnen, J J, Mark C M van Loosdrecht, and L Tijhuis. 1992. "A black box mathematical model to calculate auto- and heterotrophic biomass yields based on Gibbs energy dissipation." *Biotechnology and bioengineering* 40 (10) (December 5): 1139-54. doi:10.1002/bit.260401003.

Heijnen, J J, and J P van Dijken. 1992. "In search of a thermodynamic description of biomass yields for the chemotrophic growth of microorganisms." *Biotechnology and bioengineering* 39 (8) (April 5): 833-58. doi:10.1002/bit.260390806.

Hill, Graham, and John Holman. 2000. *Chemistry in Context*. 5th ed. Cheltenham: Thomas Nelson & Sons Ltd.

Hillen, L W, G Pollard, L V Wake, and N White. 1982. "Hydrocracking of the oils of Botryococcus braunii to transport fuels." *Biotechnology and bioengineering* 24 (1) (January): 193-205. doi:10.1002/bit.260240116.

Ho, Chester S, Raymound F Baddour, and Michael J Stalker. 1987. The Oxygen Transfer Coefficient in Aerated Sitrred Reactors and Its Correlation with Oxygen Diffusion Coefficients. In *Biotechnology Processes, Scale-up and Mixing*, ed. Chester S Ho and James Y Oldshue, 85-95. New York: American Institute of Chemical Engineers.

Hoekema, Sebastiaan, Rutger D Douma, Marcel Janssen, Johannes Tramper, and Rene H Wijffels. 2006. "Controlling Light-Use by Rhodobacter capsulatus Continuous Cultures in a Flat-Panel Photobioreactor." *Biotechnology and bioengineering* 95 (4): 614-626. doi:10.1002/bit.

Hogrefe, C, D Römermann, and Bärbel Friedrich. 1984. "Alcaligenes eutrophus hydrogenase genes (Hox)." *Journal of bacteriology* 158 (1) (April): 43-8.

Illman, Am, Ah Scragg, and Sw Shales. 2000. "Increase in Chlorella strains calorific values when grown in low nitrogen medium." *Enzyme and microbial technology* 27 (8) (November 1): 631-635.

Imam, Saheed, Safak Yilmaz, Ugur Sohmen, Alexander S Gorzalski, Jennifer L Reed, Daniel R Noguera, and Timothy J Donohue. 2011. "iRsp1095: A Genome-scale Reconstruction of the Rhodobacter sphaeroides Metabolic Network." *BMC Systems Biology* 5 (1): 116. doi:10.1186/1752-0509-5-116.

Ishizaki, Ayaaki, and K Tanaka. 1990. "Batch culture of Alcaligenes eutrophus ATCC 17697T using recycled gas closed circuit culture system." *Journal of fermentation and bioengineering* 69 (3): 170–174.

Kelly, Don P. 1990. Energetics of Chemolithotrophs. In *THE BACTERIA: A TREATISE ON STRUCTURE AND FUNCTION. Volume XII*, ed. T. A. Krulwich, 479-503. London: Academic Press, LTD.

Kirk, John T O. 1994. *Light and photosynthesis in aquatic ecosystems*. 2nd ed. Cambridge: Cambridge University Press.

Kleihues, Laura, Oliver Lenz, Michael Bernhard, Thorsten Buhrke, and Bärbel Friedrich. 2000. "The H(2) sensor of Ralstonia eutropha is a member of the subclass of regulatory [NiFe] hydrogenases." *Journal of bacteriology* 182 (10) (May): 2716-24.

Kojima, E, and K Zhang. 1999. "Growth and hydrocarbon production of microalga Botryococcus braunii in bubble column photobioreactors." *Journal of bioscience and bioengineering* 87 (6) (January): 811-5.

Kok, B. 1953. Experiments on photosynthesis by Chlorella in flashing light. In *Algal Culture: from laboratory to pilot plant*, ed. JS Burlew, 63-75. Washington: Carnegie Institution of Washington Publication.

Kong, Qing-xue, Ling Li, Blanca Martinez, Paul Chen, and Roger Ruan. 2010. "Culture of microalgae Chlamydomonas reinhardtii in wastewater for biomass feedstock production." *Applied biochemistry and biotechnology* 160 (1) (January): 9-18. doi:10.1007/s12010-009-8670-4.

Kömen, Ralf, Karin Schmidt, and Bärbel Friedrich. 1992. "Hydrogenase mutants of Alcaligenes eutrophus H16 show alterations in the electron transport system." *FEMS microbiology letters* 75 (2-3) (September 15): 173-8.

Kömen, Ralf, Davide Zannoni, W John Ingledew, and Karin Sehmidt. 1991. "The electron transport system of Alcaligenes eutrophas H16 I. Spectroscopic and thermodynamic properties." *Archives of Microbiology* 155: 382 - 390.

Kömen, Ralf, Davide Zannoni, and Karin Schmidt. 1991. "The electron transport system of Alcaligenes eutrophus H16 II. Respiratory activities and effect of specific inhibitors." *Archives of microbiology* 155: 436- 443.

Larachi, Faïcal, André Laurent, Noël Midoux, Gabriel Wild, and Ö É. 1991. "Liquid saturation data in trickle beds operating under elevated pressure." *AIChE journal* 37 (7): 1109–1112.

Laws, E a, K L Terry, J Wickman, and M S Chalup. 1983. "A simple algal production system designed to utilize the flashing light effect." *Biotechnology and bioengineering* 25 (10) (October): 2319-35. doi:10.1002/bit.260251004.

Lee, Hyeon Cheol, Jin Sook Kim, Wonhee Jang, and Sang Yong Kim. 2010. “High NADPH/NADP+ ratio improves thymidine production by a metabolically engineered Escherichia coli strain.” *Journal of biotechnology* 149 (1-2) (August 20): 24-32. doi:10.1016/j.jbiotec.2010.06.011.

Lengeler, Joseph W, Gerhart Drews, and Hans G Schlegel. 1999. *Biology of the Prokaryotes*. Stuttgart, Germany: Georg Thieme Verlag.

Li, Yanqun, Mark Horsman, Bei Wang, Nan Wu, and C.Q. Lan. 2008. “Effects of nitrogen sources on cell growth and lipid accumulation of green alga Neochloris oleoabundans.” *Applied microbiology and biotechnology* 81 (4): 629–636. doi:10.1007/s00253-008-1681-1.

Liu, Hong, Stephen Grot, and Bruce E Logan. 2005. “Electrochemically assisted microbial production of hydrogen from acetate.” *Environmental science & technology* 39 (11) (June 1): 4317-20.

Liu, Jingsong, V. Vojinović, Rodrigo Patiño, Thomas Maskow, and Urs von Stockar. 2007. “A comparison of various Gibbs energy dissipation correlations for predicting microbial growth yields.” *Thermochimica Acta* 458 (1-2) (June 25): 38-46. doi:10.1016/j.tca.2007.01.016.

Liu, Zhi-Yuan, Guang-Ce Wang, and Bai-Cheng Zhou. 2008. “Effect of iron on growth and lipid accumulation in Chlorella vulgaris.” *Bioresource technology* 99 (11) (July): 4717-22. doi:10.1016/j.biortech.2007.09.073.

Logan, Bruce E. 2008. *Microbial Fuel Cells*. Hoboken, NJ: John Wiley & Sons, Inc.

Logan, Bruce E, Douglas F Call, Shaoan Cheng, Hubertus V M Hamelers, Tom H J A Sleutels, Adriaan W Jeremiasse, and René A Rozendal. 2008. “Microbial Electrolysis Cells for High Yield Hydrogen Gas Production from Organic Matter.” *Environmental Science & Technology* 42 (23) (December): 8630-8640. doi:10.1021/es801553z.

Lundquist, T J, I C Woertz, N W T Quinn, and John R Benemann. 2010. *A Realistic Technology and Engineering Assessment of Algae Biofuel Production*. Berkeley.

Lv, Jian-Ming, Li-Hua Cheng, Xin-Hua Xu, Lin Zhang, and Huan-Lin Chen. 2010. “Enhanced lipid production of Chlorella vulgaris by adjustment of cultivation conditions.” *Bioresource technology* 101 (17) (September): 6797-804. doi:10.1016/j.biortech.2010.03.120.

Madigan, M T, and H Gest. 1979. “Growth of the photosynthetic bacterium Rhodopseudomonas capsulata chemoautotrophically in darkness with H2 as the energy source.” *Journal of bacteriology* 137 (1) (January): 524-30.

Mandalam, R K, and B O Palsson. 1998. “Elemental balancing of biomass and medium composition enhances growth capacity in high-density Chlorella vulgaris cultures.” *Biotechnology and bioengineering* 59 (5) (September 5): 605-11.

Mavrovouniotis, M L. 1990. “Group contributions for estimating standard gibbs energies of formation of biochemical compounds in aqueous solution.” *Biotechnology and bioengineering* 36 (10) (December 5): 1070-82. doi:10.1002/bit.260361013.

McCarty, Perry L. 1971. Energetics and Bacterial Growth. In *Organic Compounds in Aquatic Environments*, ed. Samuel J Faust and Joseph V Hunter, 495-531. New York: Marcel Dekker, Inc.

———. 2007. “Thermodynamic electron equivalents model for bacterial yield prediction: Modifications and comparative evaluations.” *Biotechnology and bioengineering* 97 (2): 377–388. doi:10.1002/bit.

McLaughlin, S, J Bouton, D Bransby, B Conger, W Ocumpaugh, D Parrish, C Taliaferro, K Vogel, and S Wullschleger. 1999. Developing switchgrass as a bioenergy crop. In *Persepctives on new crops and new uses*, ed. J Janick. Alexandria, VA: ASHS Press.

Metzger, Pierre, C. Berkaloff, E. Casadevall, and A. Coute. 1985. “Alkadiene- and botryococcene-producing races of wild strains of Botryococcus braunii.” *Phytochemistry* 24 (10): 2305-2312. doi:10.1016/S0031-9422(00)83032-0.

Miura, Y, M Okazaki, K Ohi, and T Nishimura. 1981. “Growth kinetics of hydrogen bacterium Alcaligenes hydrogenophilus.” *Agricultural and biological chemistry* 45: 1181-1186.

Moellering, Eric R, and Christoph Benning. 2010. “RNA interference silencing of a major lipid droplet protein affects lipid droplet size in Chlamydomonas reinhardtii.” *Eukaryotic cell* 9 (1) (January): 97-106. doi:10.1128/EC.00203-09.

Monedero, Vicente, Gaspar Pérez-Martínez, and María J Yebra. 2010. “Perspectives of engineering lactic acid bacteria for biotechnological polyol production.” *Applied microbiology and biotechnology* 86 (4) (April): 1003-15. doi:10.1007/s00253-010-2494-6.

Murashige, Toshio, and Folke Skoog. 1962. “A Revised Medium for Rapid Growth and Bio Assays with Tobacco Tissue Cultures.” *Physiologia Plantarum* 15 (3) (July): 473-497. doi:10.1111/j.1399-3054.1962.tb08052.x.

Niehaus, Tom D, Shigeru Okada, Timothy P Devarenne, David S Watt, Vitaliy Sviripa, and Joseph Chappell. 2011. “Identification of unique mechanisms for triterpene biosynthesis in Botryococcus braunii.” *Proceedings of the National Academy of Sciences* 108 (30) (July 11). doi:10.1073/pnas.1106222108.

Nonomura, Arthur M. 1988. “Botryococcus braunii var. showa (Chlorophyceae) from Berkeley, California, United States of America.” *Jpn J Phycol* 36: 285–291.

Northcote, D H, K J Goulding, and R W Horne. 1958. “The chemical composition and structure of the cell wall of Chlorella pyrenoidosa.” *The Biochemical journal* 70 (3) (November): 391-7.

Okada, Shigeru. 2004. “Characterization of botryococcene synthase enzyme activity, a squalene synthase-like activity from the green microalga Botryococcus braunii, Race B.” *Archives of Biochemistry and Biophysics* 422 (1) (February 1): 110-118. doi:10.1016/j.abb.2003.12.004.

Okada, Shigeru, T P Devarenne, and Joseph Chappell. 2000. “Molecular characterization of squalene synthase from the green microalga Botryococcus braunii, race B.” *Archives of biochemistry and biophysics* 373 (2) (January 15): 307-17. doi:10.1006/abbi.1999.1568.

Okada, Shigeru, Masahiro Murakami, and Katsumi Yamaguchi. 1995. “Hydrocarbon composition of newly isolated strains of the green microalga Botryococcus braunii.” *Journal of Applied Phycology* 7 (6) (December): 555-559. doi:10.1007/BF00003942.

Paoli, George C, and F Robert Tabita. 1998. “Aerobic chemolithoautotrophic growth and RubisCO function in Rhodobacter capsulatus and a spontaneous gain of function mutant of Rhodobacter sphaeroides.” *Archives of microbiology* 170 (1) (July): 8-17.

Perry, R H, and D W Green, eds. 1997. *Perry’s Chemical Engineers' Handbook*. 7th ed. McGraw-Hill.

Piorreck, Margret, Klaus-Hinnerk Baasch, and Peter Pohl. 1984. “Biomass production, total protein, chlorophylls, lipids and fatty acids of freshwater green and blue-green algae under different nitrogen regimes.” *Phytochemistry* 23 (2) (January): 207-216. doi:10.1016/S0031-9422(00)80304-0.

Pipes, W O, and S P Koutsoyannis. 1962. “Light-limited growth of Chlorella in continuous cultures.” *Applied microbiology* 10 (1953) (January): 1-5.

Pirt, S J. 1965. “The maintenance energy of bacteria in growing cultures.” *Proceedings of the Royal Society of London. Series B, Biological Sciences* 163 (991): 224–231.

Pirt, S J, Yuan-Kun Lee, Amos Richmond, and Margaret Watts Pirt. 1980. “The photosynthetic efficiency of Chlorella biomass growth with reference to solar energy utilization.” *Journal of Chemical Technology and Biotechnology* 30 (1): 25-34.

Pruvost, J, G Van Vooren, G Cogne, and J Legrand. 2009. “Investigation of biomass and lipids production with Neochloris oleoabundans in photobioreactor.” *Bioresource technology* 100 (23) (December): 5988-95. doi:10.1016/j.biortech.2009.06.004.

Pulz, O, and K Scheibenbogen. 1998. Photobioreactors: Design and performance with respect to light energy output. In *Advances in biochemical engineering/biotechnology*, ed. T Scheper. Heidelberg: Springer-Verlag.

Ramsden, T, D Steward, and J Zuboy. 2009. *Analyzing the Levelized Cost of Centralized and Distributed Hydrogen Production Using the H2A Production Model , Version 2*. *Contract*.

Repaske, R, and R Mayer. 1976. “Dense autotrophic cultures of Alcaligenes eutrophus.” *Applied and environmental microbiology* 32 (4) (October): 592-7.

Rittman, Bruce E, and Perry L McCarty. 2001. *Environmental Biotechnology: Principles and Applications*. Boston: McGraw-Hill.

Rodolfi, Liliana, Graziella Chini Zittelli, Niccolò Bassi, Giulia Padovani, Natascia Biondi, Gimena Bonini, and Mario R Tredici. 2009. “Microalgae for oil: strain selection, induction of lipid synthesis and outdoor mass cultivation in a low-cost photobioreactor.” *Biotechnology and bioengineering* 102 (1) (January 1): 100-12. doi:10.1002/bit.22033.

Rozendal, René A, Hubertus V M Hamelers, Gerrit J W Euverink, Sybrand J Metz, and Cees J N Buisman. 2006. “Principle and perspectives of hydrogen production through biocatalyzed electrolysis.” *International Journal of Hydrogen Energy* 31 (12) (September): 1632-1640. doi:10.1016/j.ijhydene.2005.12.006.

Sawayama, S., S. Inoue, and S. Yokoyama. 1994. “Continuous culture of hydrocarbon-rich microalga Botryococcus braunii in secondarily treated sewage.” *Applied Microbiology and Biotechnology* 41 (6) (August 1): 729-731. doi:10.1007/s002530050206.

Schink, B, and Hans G Schlegel. 1979. “The membrane-bound hydrogenase of Alcaligenes eutrophus. I. Solubilization, purification, and biochemical properties.” *Biochimica et biophysica acta* 567 (2) (April 12): 315-24.

Schneider, Klaus, and Hans G Schlegel. 1976. “Purification and Properties of Soluble Hydrogenase from Alcaligenes eutrophus H16.” *Biochimica et biophysica acta* 452 (July): 66-80.

Sheehan, John, Terri Dunahay, John R Benemann, and Paul Roessler. 1998. *A Look Back at the U . S . Department of Energy ’ s Aquatic Species Program : Biodiesel from Algae*. *Renewable Energy*. Golden, CO.

Shifrin, N.S., and S.W. Chisholm. 1981. “PHYTOPLANKTON LIPIDS: INTERSPECIFIC DIFFERENCES AND EFFECTS OF NITRATE, SILICATE AND LIGHT-DARK CYCLES1.” *Journal of phycology* 17 (4): 374–384.

Siefert, Eike, and Norbert Pfennig. 1979. “Chemoautotrophic growth of Rhodopseudomonas species with hydrogen and chemotrophic utilization of methanol and formate.” *Archives of Microbiology* 122 (2): 177–182.

Siegel, R S, and D F Ollis. 1984. “Kinetics of growth of the hydrogen-oxidizing bacterium Alcaligenes eutrophus (ATCC 17707) in chemostat culture.” *Biotechnology and bioengineering* 26 (7) (July): 764-70. doi:10.1002/bit.260260721.

von Stockar, Urs, Thomas Maskow, Jingsong Liu, Ian W Marison, and Rodrigo Patiño. 2006. “Thermodynamics of microbial growth and metabolism: an analysis of the current situation.” *Journal of biotechnology* 121 (4) (February 24): 517-33. doi:10.1016/j.jbiotec.2005.08.012.

Stouthamer, A H. 1973. “A theoretical study on the amount of ATP required for synthesis of microbial cell material.” *Antonie van Leeuwenhoek* 39 (3) (January): 545-65.

Sueoka, N, K S Chiang, and J R Kates. 1967. “Deoxyribonucleic acid replication in meiosis of Chlamydomonas reinhardi. I. Isotopic transfer experiments with a strain producing eight zoospores.” *Journal of molecular biology* 25 (1) (April 14): 47-66.

Sánchez, Ailen M, George N Bennett, and Ka-Yiu San. 2005. “Novel pathway engineering design of the anaerobic central metabolic pathway in Escherichia coli to increase succinate yield and productivity.” *Metabolic engineering* 7 (3) (May): 229-39. doi:10.1016/j.ymben.2005.03.001.

Terry, K L. 1986. “Photosynthesis in modulated light: quantitative dependence of photosynthetic enhancement on flashing rate.” *Biotechnology and bioengineering* 28 (7) (July): 988-95. doi:10.1002/bit.260280709.

Thauer, Rudolf K, Kurt Jungermann, and Karl Decker. 1977. “Energy conservation in chemotrophic anaerobic bacteria.” *Bacteriological reviews* 41 (3) (September): 809.

Tichi, M.A., W.G. Meijer, and F.R. Tabita. 2001. “Complex I and its involvement in redox homeostasis and carbon and nitrogen metabolism in Rhodobacter capsulatus.” *Journal of Bacteriology* 183 (24): 7285. doi:10.1128/JB.183.24.7285.

Tijhuis, L, Mark C M van Loosdrecht, and J J Heijnen. 1993. “A thermodynamically based correlation for maintenance gibbs energy requirements in aerobic and anaerobic chemotrophic growth.” *Biotechnology and bioengineering* 42 (4) (August 5): 509-19. doi:10.1002/bit.260420415.

U.S. Energy Information Administration. 2011. *Short-Term Energy Outlook*. *Energy*.

Van't Riet, Klaas. 1979. "Review of Measuring Methods and Results in Nonviscous Gas-Liquid Mass Transfer in Stirred Vessels." *Industrial & Engineering Chemistry Process Design and Development* 18 (3) (July): 357-364. doi:10.1021/i260071a001.

Wake, L V, and L W Hillen. 1980. "Study of a 'bloom' of the oil-rich algaBotryococcus braunii in the Darwin River Reservoir." *Biotechnology and Bioengineering* 22 (8) (August): 1637-1656. doi:10.1002/bit.260220808.

Wang, Zi Teng, Nico Ullrich, Sunjoo Joo, Sabine Waffenschmidt, and Ursula Goodenough. 2009. "Algal lipid bodies: stress induction, purification, and biochemical characterization in wild-type and starchless Chlamydomonas reinhardtii." *Eukaryotic cell* 8 (12) (December): 1856-68. doi:10.1128/EC.00272-09.

Wolf, Fred R. 1983. "Botryococcus braunii an unusual hydrocarbon-producing alga." *Applied Biochemistry and Biotechnology* 8 (3) (June): 249-260. doi:10.1007/BF02778262.

———. 1985. "Biosynthesis of unusual acyclic isoprenoids in the Alga Botryococcus braunii." *Phytochemistry* 24 (4): 733-737. doi:10.1016/S0031-9422(00)84886-4.

Wolf, Fred R, Arthur M Nonomura, and James A Bassham. 1985. "GROWTH AND BRANCHED HYDROCARBON PRODUCTION IN A STRAIN OF BOTRYOCOCCUS BRAUNII (CHLOROPHYTA) 1." *Journal of phycology* 21 (3): 388–396.

Y, Morinaga, S Yamanaka, Ayaaki Ishizaki, and Y Hirose. 1978. "Growth characteristics and cell composition of Alcaligenes eutrophus in chemostat culture." *Agricultural and biological chemistry* 42: 439-444.

Yan, Bin, and Charles E Wyman. 2008. "Pretreatment: the key to unlocking low-cost cellulosic ethanol." *Biofuels, Bioproducts, and Biorefining* 2 (1): 26-40. doi:10.002/bbb.49.

Yoo, Chan, So-Young Jun, Jae-Yon Lee, Chi-Yong Ahn, and Hee-Mock Oh. 2010. "Selection of microalgae for lipid production under high levels carbon dioxide." *Bioresource technology* 101 Suppl (1) (January): S71-4. doi:10.1016/j.biortech.2009.03.030.

Zannoni, Davide. 1995. Aerobic and anaerobic electron transport chains in anoxygenic phototrophic bacteria. In *Anoxygenic Photosynthetic Bacteria*, ed. R E Blankenship, M T Madigan, and C E Bauer, 949-971. New York City: Kluwer Academic Publishers.

Zannoni, Davide, B Schoepp-Cothenet, and Jonathan Hosler. 2008. Respiration and Respiratory Complexes. In *The Purple Phototrophic Bacteria*, ed. C Neil Hunter, Fevzi Daldal, Marion C Thurnauer, and J Thomas Beatty, 537–561. Dordrecht: Springer.